

Electronic Thesis and Dissertation Repository

7-10-2018 11:00 AM

OFDM System with g-CPFSK Mapper: Properties and Performance

Emammer K.H Shafter, *The University of Western Ontario*

Supervisor: Raveendra Rao, *The University of Western Ontario*

A thesis submitted in partial fulfillment of the requirements for the Doctor of Philosophy degree in Electrical and Computer Engineering

© Emammer K.H Shafter 2018

Follow this and additional works at: <https://ir.lib.uwo.ca/etd>

Recommended Citation

Shafter, Emammer K.H, "OFDM System with g-CPFSK Mapper: Properties and Performance" (2018). *Electronic Thesis and Dissertation Repository*. 5451.
<https://ir.lib.uwo.ca/etd/5451>

This Dissertation/Thesis is brought to you for free and open access by Scholarship@Western. It has been accepted for inclusion in Electronic Thesis and Dissertation Repository by an authorized administrator of Scholarship@Western. For more information, please contact wlsadmin@uwo.ca.

Abstract

Orthogonal Frequency Division Multiplexing (OFDM) system with a generalized Continuous Phase Frequency Shift Keying (g-CPFSK) mapper is considered which is used to introduce systematic correlation among the transmitted OFDM symbols. The correlation thus introduced is exploited at the receiver to enhance the physical layer performance of the system by using multiple-symbol observation detector. Three subclasses of g-CPFSK mapper, single- h CPFSK, multi- h CPFSK, and asymmetric multi- h CPFSK mappers, are considered; although the class of g-CPFSK mapper comprises of a large class of mappers. The resulting OFDM signals and their properties are examined. The Peak-to-Average Power Ratio (PAPR) characteristics of these signals in conjunction with three PAPR reduction techniques, namely, Selective Mapping (SLM), Partial Transmit Sequence (PTS), and Clipping and Filtering (CF) are also investigated. Maximum Likelihood (ML) multiple-symbol detection of OFDM signals in AWGN is addressed and the structure of the optimum detector/demapper is derived using the criterion of minimum probability of Bit Error Rate (BER). Closed-form expression for BER of this detector is derived in terms of high-SNR upper and lower bounds. It is noted that BER is a function of: i) E_b/N_o , Signal-to-Noise Ratio (SNR); ii) parameters of the g-CPFSK mapper; iii) n , observation length of the receiver; and iv) M , number of levels used in the mapper. Finally, the performance of OFDM system with g-CPFSK mapper is evaluated over non-frequency selective Rayleigh and Nakagami- m fading channels.

It is shown that OFDM system with single- h and multi- h CPFSK mappers in conjunction with PTS technique can be designed to achieve PAPR reductions of 6.1 dB and 3.5 dB, respectively, relative to corresponding OFDM system with conventional BPSK mapper. However, when SLM technique is used, PAPR reductions of 1.6 dB and 1 dB,

respectively, can be achieved. Asymmetric multi- h and multi- h CPFSK mappers in conjunction with CF technique can be designed to realize PAPR reductions of 4.1 dB and 2.5 dB, respectively, with 25% clipping. Optimum sets of mapper parameters for single- h , multi- h and asymmetric multi- h CPFSK mappers are determined that minimize BER of the system. It is observed that the optimum asymmetric multi- h and multi- h CPFSK mappers outperform BPSK mapper by nearly 2.2 dB and 1.4 dB, respectively, when 4-symbol observation length detector is used. However, it is noted that the complexity of the detector increases as a function of observation length and the type of mapper used. Closed-form expressions for BER performance of OFDM system with g-CPFSK mapper are derived over Rayleigh and Nakagami- m frequency non-selective slowly fading channels and the penalty in SNR that must be paid as a consequence of the fading is assessed and illustrated.

Acknowledgements



“O Allah, to You is praise as befits the Glory of Your Face and the greatness of your Might.” All the praises, and foremost thanks are due to Allah for helping me in completing my PhD study. Without His guidance and blessings, nothing is possible. If I would count up the favours of Allah, never would I be able to number them. Prayers and peace of Allah be upon the noble Prophet Mohammad and upon his family and companions, the honorable followers.

I would like to express my deep appreciation to my thesis supervisor Dr. Raveendra Rao. His office door is always open for discussion, encouragement, insightful guidance, consistent support, invaluable advice, and constructive criticism. I appreciate his time and ideas that have helped me to be highly productive. With his involvement and patience, I have been able to write my Ph.D thesis successfully.

I would also like to show my sincere gratitude and deep thanks to my parents, my wife, my siblings and my children. Their dua’a, support, encouragement, smile, and countless sacrifices are the basis of my continuing personal development. The inexhaustible kindness and love I have received are invaluable. They deserve all the credits.

I am grateful to my late uncle Mr. Rahel Shafter for his love and support.

Acknowledgements are due to the Ministry of Education. Libya for providing me the necessary financial assistance throughout my stay at Western.

Although I cannot name them all, I thank many colleagues and the friends with whom I had the pleasure to work beside over the years.

I would like to express my gratitude to my mother whose upbringing and prayers have played a major role in making me what I am Today. As a token of appreciation I dedicate this work to her.

Emammer Shafter

Table of Contents

Abstract	i
Acknowledgements	iii
List of Tables	vii
List of Figures	ix
List of Abbreviations	xiv
1 Introduction to Thesis	1
1.1 Introduction	1
1.2 Literature Survey and Motivation	4
1.3 Objectives	8
1.4 Organization	10
1.5 Conclusions	11
2 Fundamentals of OFDM System	12
2.1 Introduction	12
2.2 Baseband OFDM System	12
2.2.1 Transmitter	13
2.2.2 Channel	16
2.2.3 Receiver	20
2.3 Cyclic Prefix	20
2.4 PAPR Statistics of OFDM Signals	24
2.4.1 Definition of PAPR	24
2.4.2 Complementary Cumulative Distribution Function	27
2.4.3 Impact of PAPR on System Performance	28
2.4.4 PAPR Reduction Techniques	30
2.5 Conclusions	35
3 OFDM System with g-CPFSK Mapper	36
3.1 Introduction	36
3.2 Description of g-CPFSK Mapper	36
3.3 Single- h CPFSK Mapper	38
3.3.1 Multi- h CPFSK Mapper	40
3.3.2 Asymmetric multi- h CPFSK Mapper	44
3.4 Conclusions	48

4	PAPR Reduction using SLM Technique for g-CPFSK Mapper	49
4.1	Introduction	49
4.2	SLM Technique and g-CPFSK Mapper	50
4.3	Numerical Results and Discussion	52
4.3.1	Single- h CPFSK Mapper	54
4.3.2	Multi- h CPFSK Mapper	62
4.3.3	Asymmetric multi- h CPFSK Mapper	62
4.4	Conclusions	65
5	PAPR Reduction using PTS Technique for OFDM System with g-CPFSK Mapper	70
5.1	Introduction	70
5.2	PTS Technique and g-CPFSK Mapper	70
5.3	Numerical Results and Discussion	74
5.3.1	Single- h CPFSK Mapper	75
5.3.2	Multi- h -CPFSK Mapper	78
5.3.3	Asymmetric Multi- h -CPFSK Mapper	81
5.4	Conclusions	84
6	PAPR Reduction using CF Technique for OFDM System with g-CPFSK Mapper	87
6.1	Introduction	87
6.2	CF Technique and g-CPFSK Mapper	87
6.3	Numerical Results and Discussion	89
6.3.1	Single- h CPFSK Mapper	89
6.3.2	Multi- h CPFSK Mapper	95
6.3.3	Asymmetric multi- h CPFSK Mapper	101
6.4	Conclusions	104
7	Performance of OFDM System with g-CPFSK Mapper in AWGN Channel	105
7.1	Introduction	105
7.2	Structure and Performance of Receiver	105
7.3	Maximum Likelihood g-CPFSK Demapper	107
7.4	Numerical Results and Analysis	110
7.5	Conclusions	113

8	Performance of OFDM System with g-CPFSK Mapper Over Fading Channels	114
8.1	Introduction	114
8.2	Fading Channel Models	114
8.3	Error Rate Expressions for OFDM System with g-CPFSK mapper over Fading Channels	115
8.3.1	Rayleigh Fading Channel	115
8.3.2	Nakagami- m Fading Channel	116
8.4	Numerical Results and Discussion	116
8.5	Conclusions	119
9	Concluding Remarks and Suggestions for Further Research	121
9.1	Introduction	121
9.2	Summary of contributions	121
9.3	Suggestions for Further Research	123
	Curriculum Vitae	133

List of Tables

Section	Page
2.1 Input and output for BPSK mapper (k=1 and M=2)	14
2.2 Input and output for QPSK mapper (k=2 and M=4)	14
3.1 Number of possible phase states for single- h CPFSK mapper for $h = \frac{1}{2}$, $h = \frac{2}{3}$, and $h = \frac{1}{4}$	39
3.2 h values as a function of symbol i in binary asymmetric multi- h CPFSK mapper using (3.11)	45
3.3 h values as a function of symbol i in binary asymmetric multi- h CPFSK mapper using (3.11)	45
3.4 h values as a function of symbol i in binary asymmetric multi- h CPFSK mapper using (3.11) [S-type]	47
3.5 h values as a function of symbol i in binary asymmetric multi- h CPFSK mapper using (3.14) [A-type]	47
4.1 Phase sequences $B^{(1)}, B^{(2)}, \dots, B^{(16)}$ for single- h CPFSK mapper ($h = \frac{1}{2}$) with $b_{u,k} \in \{e^{j0}, e^{j\pi/2}, e^{j\pi}, e^{j3\pi/2}\}$	54
4.2 Phase sequences $B^{(1)}, B^{(2)}, \dots, B^{(16)}$ for single- h CPFSK mapper ($h = \frac{2}{3}$) with $b_{u,k} \in \{e^{j0}, e^{j\pi/3}, e^{j4\pi/3}\}$	55
4.3 Comparison of PAPR performance of single- h CPFSK mapper ($h = \frac{1}{2}$) as a function of number of subcarriers	56
4.4 Comparison of PAPR performance of single- h CPFSK mapper ($h = \frac{2}{3}$) as a function of number of subcarriers	59
4.5 Phase sequences $B^{(1)}, B^{(2)}, \dots, B^{(u)}$ for multi- h CPFSK mapper $\{2/4, 3/4\}$ with $b_{u,k} \in \{e^{j0}, e^{j\pi/4}, e^{j\pi/2}, e^{j3\pi/4}, e^{j\pi}, e^{j5\pi/4}, e^{j3\pi/2}, e^{j7\pi/4}\}$	62
4.6 Comparison of PAPR performance of multi- h CPFSK mapper ($\{\frac{2}{4}, \frac{3}{4}\}$) as a function of number of subcarriers	64
4.7 Phase sequences $B^{(1)}, B^{(2)}, \dots, B^{(u)}$ for asy multi- h CPFSK mapper $H_{+i} =$ $\{\frac{2}{4}, \frac{3}{4}\}$ and $H_{-i} = \{\frac{3}{4}, \frac{2}{4}\}$	66
4.8 Comparison of PAPR performance of asymmetric multi- h CPFSK mapper ($H_{+i} = \{\frac{2}{4}, \frac{3}{4}\}$ and $H_{-i} = \{\frac{3}{4}, \frac{2}{4}\}$) as a function of number of subcarriers	66
4.9 Best phase sequences that minimize PAPR	66
4.10 Phase sequences $B^{(1)}, B^{(2)}, \dots, B^{(16)}$ for BPSK mapper with $b_{u,k} \in \{e^{j0}, e^{j\pi}\}$ 69	
5.1 Best phase rotating vectors that minimize PAPR	76

List of Tables

5.2	Comparison of PAPR performance of single- h CPFSK ($h = \frac{1}{2}$) mapper as a function of number of subcarriers	77
5.3	Comparison of PAPR performance of single- h CPFSK ($h = \frac{2}{3}$) mapper as a function of number of subcarriers	77
5.4	Comparison of PAPR performance of multi- h CPFSK mapper ($\{\frac{2}{4}, \frac{3}{4}\}$) as a function of number of subcarriers	81
5.5	Comparison of PAPR performance of asymmetric multi- h CPFSK mapper ($H_{+i} = \{\frac{2}{4}, \frac{3}{4}\}$ and $H_{-i} = \{\frac{3}{4}, \frac{2}{4}\}$) as a function of number of subcarriers	84
6.1	PAPR performance of single- h CPFSK ($\frac{1}{2}$) and BPSK mappers with and without CF technique ($N = 128, CR = 0.25$)	90
6.2	PAPR performance of multi- h CPFSK $\{\frac{2}{4}, \frac{3}{4}\}$ and BPSK mappers with and without CF technique ($N = 128, CR = 0.25$)	101
6.3	PAPR performance of asymmetric multi- h CPFSK and BPSK mappers with and without CF technique ($N = 128, CR = 0.25$)	102

List of Figures

Section	Page
1.1 Simplified block diagram of OFDM system: (a) Transmitter (b) Receiver	4
2.1 OFDM system diagram	12
2.2 Signal-space diagrams for (a) BPSK and (b) QPSK mappers	13
2.3 Discrete-time complex signal at the output for an arbitrary signal mapper	14
2.4 The additive noise channel	16
2.5 Probability density function for Rayleigh random variable for various values of σ	19
2.6 Probability density function for Nakagami- m random variable with $\Omega = 1$ for various values of m	19
2.7 OFDM signal with Cyclic Prefix (CP)	21
2.8 OFDM signal ($N = 16$) for the data sequence $[C_0, C_1, \dots, C_{15}]$	25
2.9 OFDM signal ($N = 16$) for the data sequence $[C_0, C_1, \dots, C_{15}]$	26
2.10 OFDM signal ($N = 16$) for the data sequence $[C_0, C_1, \dots, C_{15}]$	26
2.11 CCDFs of PAPR of OFDM signals for $N = 16, 32, 64, 128,$ and 256 for BPSK mapper and an oversampling factor $L = 4$	29
2.12 Transfer function of typical power amplifier.	30
2.13 Block diagram of the SLM technique	31
2.14 Block diagram of the PTS technique	33
3.1 Block diagram of OFDM system with g-CPFSK mapper (Transmitter) .	36
3.2 Phase constellation diagrams for binary single- h CPFSK mapper: (a) $h = 1/2$, (b) $h = 1/4$, and (c) $h = 2/3$	40
3.3 State trellis diagram for binary single- h CPFSK mapper for $h = 1/2$. $a_{j,q} = -1$ (dashed) and $a_{j,q} = +1$ (solid)	40
3.4 State trellis diagram for binary single- h CPFSK mapper for $h = 1/4$. $a_{j,q} = -1$ (dashed) and $a_{j,q} = +1$ (solid)	41
3.5 State diagram for binary single- h CPFSK mapper for $h = 1/2$	41
3.6 State diagram for binary single- h CPFSK mapper for $h = 2/3$. $a_{j,q} = -1$ (dashed) and $a_{j,q} = +1$ (solid)	41
3.7 State diagram for binary single- h CPFSK mapper for $h = 1/4$. $a_{j,q} = -1$ (dashed) and $a_{j,q} = +1$ (solid)	42
3.8 Path through the phase trellis as a function of symbol time for binary single- h CPFSK mapper for $h = 1/2$ for an arbitrary data sequence $[+1, -1, -1, +1]$. $a_{j,q} = -1$ (dashed) and $a_{j,q} = +1$ (solid)	42
3.9 Path through the phase trellis as a function of symbol time for binary single- h CPFSK mapper for $h = 1/4$ for an arbitrary data sequence $[+1, -1, -1, +1]$. $a_{j,q} = -1$ (dashed) and $a_{j,q} = +1$ (solid)	43

List of Tables

3.10	Phase transitions as a function of symbol time for binary single- h CPFSK mapper for $h = 2/3$ for an arbitrary data sequence $[+1, -1, -1, +1]$. $a_{j,q} = -1$ (dashed) and $a_{j,q} = +1$ (solid)	43
3.11	Phase tree for binary multi- h CPFSK mapper for $H_2 = \{1/4, 2/3\}$. $a_{j,q} = -1$ (dashed) and $a_{j,q} = +1$ (solid)	44
3.12	Phase tree for asy multi- h CPFSK mapper for $H_{2-} = \{1/4, 2/3\}$, $H_{2+} = \{2/3, 1/4\}$. $a_{j,q} = -1$ (dashed) and $a_{j,q} = +1$ (solid)	46
3.13	Phase trellises for: (a) S-type and (b) A-type mappers. $a_{j,q} = -1$ (dashed) and $a_{j,q} = +1$ (solid)	47
4.1	Block diagram of the SLM technique for an OFDM system with g-CPFSK mapper	51
4.2	Flow-chart for computation of CCDFs of PAPR using SLM technique	53
4.3	CCDFs of PAPR of single- h CPFSK mapper ($N = 64$) without SLM technique : (a) $h = \frac{1}{5}$; (b) $h = \frac{1}{3}$; (c) $h = \frac{1}{2}$; and (d) $h = \frac{4}{5}$	55
4.4	CCDFs of PAPR of an OFDM system with single- h CPFSK mapper ($h = \frac{1}{2}$) with and without SLM technique ($N=64$)	56
4.5	CCDFs of PAPR of an OFDM system with single- h CPFSK mapper ($h = \frac{1}{2}$) with and without SLM technique, ($N = 128$)	57
4.6	CCDFs of PAPR of an OFDM system with single- h CPFSK mapper ($h = \frac{1}{2}$) with and without SLM technique, ($N = 256$)	57
4.7	CCDFs of PAPR of an OFDM with single- h CPFSK mapper ($h = \frac{1}{2}$) with and without SLM technique, ($N = 512$)	58
4.8	CCDFs of PAPR of an OFDM system with single- h CPFSK mapper ($h = \frac{1}{2}$) as a function of number of subcarriers ($N=64, 128, 256,$ and 512) without SLM technique	58
4.9	CCDFs of PAPR of an OFDM system with single- h CPFSK mapper ($h = \frac{1}{2}$) as a function of number of subcarriers ($N=64, 128, 256,$ and 512) with SLM technique	59
4.10	CCDFs of PAPR of an OFDM with single- h CPFSK mapper ($h = \frac{2}{3}$) with and without SLM technique, ($N = 64$)	60
4.11	CCDFs of PAPR of an OFDM with single- h CPFSK mapper ($h = \frac{2}{3}$) with and without SLM technique, ($N = 128$)	60
4.12	CCDFs of PAPR of an OFDM with single- h CPFSK mapper ($h = \frac{2}{3}$) with and without SLM technique, ($N = 256$)	61
4.13	CCDFs of PAPR of an OFDM with single- h CPFSK mapper ($h = \frac{2}{3}$) with and without SLM technique, ($N = 512$)	61
4.14	CCDFs of PAPR of an OFDM system with multi- h -CPFSK mapper ($\{\frac{2}{4}, \frac{3}{4}\}$), with SLM technique ($N = 64$)	63
4.15	CCDFs of PAPR of an OFDM system with multi- h -CPFSK mapper ($\{\frac{2}{4}, \frac{3}{4}\}$) with SLM technique ($N = 128$)	63
4.16	CCDFs of PAPR of an OFDM system with multi- h -CPFSK mapper with ($\{\frac{2}{4}, \frac{3}{4}\}$) with SLM technique ($N = 256$)	64
4.17	CCDFs of PAPR of an OFDM system with multi- h -CPFSK mapper ($\{\frac{2}{4}, \frac{3}{4}\}$) with SLM technique ($N = 512$)	65

List of Tables

4.18	CCDFs of PAPR of an OFDM system with asymmetric multi- h -CPFSK mapper ($H_{+i} = \{\frac{2}{4}, \frac{3}{4}\}$ and $H_{-i} = \{\frac{3}{4}, \frac{2}{4}\}$) with SLM technique ($N = 64$)	67
4.19	CCDFs of PAPR of an OFDM system with asymmetric multi- h -CPFSK mapper ($H_{+i} = \{\frac{2}{4}, \frac{3}{4}\}$ and $H_{-i} = \{\frac{1}{4}, \frac{2}{3}\}$) with SLM technique ($N = 128$)	67
4.20	CCDFs of PAPR of an OFDM system with asymmetric multi- h -CPFSK mapper ($H_{+i} = \{\frac{2}{4}, \frac{3}{4}\}$ and $H_{-i} = \{\frac{3}{4}, \frac{2}{4}\}$) with SLM technique ($N = 256$)	68
4.21	CCDFs of PAPR of an OFDM system with asymmetric multi- h -CPFSK mapper ($H_{+i} = \{\frac{2}{4}, \frac{3}{4}\}$ and $H_{-i} = \{\frac{3}{4}, \frac{2}{4}\}$) with SLM technique ($N = 512$)	69
5.1	Block diagram of OFDM system with g-CPFSK mapper and PTS technique	71
5.2	Flow-chart for computation CCDFs of PAPR using PTS technique . . .	72
5.3	CCDFs of PAPR of an OFDM system with single- h CPFSK mapper ($h = \frac{1}{2}$) with and without PTS technique ($N = 64$)	75
5.4	CCDFs of PAPR of an OFDM system with single- h CPFSK mapper ($h = \frac{1}{2}$) with and without PTS technique ($N = 128$)	78
5.5	CCDFs of PAPR of an OFDM system with single- h CPFSK mapper ($h = \frac{1}{2}$) with and without PTS technique ($N = 256$)	78
5.6	CCDFs of PAPR of an OFDM system with single- h CPFSK mapper ($h = \frac{1}{2}$) with and without PTS technique ($N = 512$)	79
5.7	CCDFs of PAPR of an OFDM with single- h CPFSK mapper ($h = \frac{2}{3}$) with and without PTS technique, ($N = 64$)	79
5.8	CCDFs of PAPR of an OFDM with single- h CPFSK mapper ($h = \frac{2}{3}$) with and without PTS technique, ($N = 128$)	80
5.9	CCDFs of PAPR of an OFDM with single- h CPFSK mapper ($h = \frac{2}{3}$) with and without PTS technique, ($N = 256$)	80
5.10	CCDFs of PAPR of an OFDM with single- h CPFSK mapper ($h = \frac{2}{3}$) with and without PTS technique, ($N = 512$)	81
5.11	CCDFs of PAPR of an OFDM system with multi- h CPFSK mapper ($\{\frac{2}{4}, \frac{3}{4}\}$) with PTS technique ($N = 64$)	82
5.12	CCDFs of PAPR of an OFDM system with multi- h CPFSK mapper ($\{\frac{2}{4}, \frac{3}{4}\}$) with PTS technique ($N = 128$)	82
5.13	CCDFs of PAPR of an OFDM system with multi- h CPFSK mapper ($\{\frac{2}{4}, \frac{3}{4}\}$) with PTS technique ($N = 256$)	83
5.14	CCDFs of PAPR of an OFDM system with multi- h CPFSK mapper ($\{\frac{2}{4}, \frac{3}{4}\}$) with PTS technique ($N = 512$)	83
5.15	CCDFs of PAPR of an OFDM system with asymmetric multi- h CPFSK mapper ($H_{+i} = \{\frac{2}{4}, \frac{3}{4}\}$ and $H_{-i} = \{\frac{3}{4}, \frac{2}{4}\}$) with PTS technique ($N = 64$)	84
5.16	CCDFs of PAPR of an OFDM system with asymmetric multi- h CPFSK mapper ($H_{+i} = \{\frac{2}{4}, \frac{3}{4}\}$ and $H_{-i} = \{\frac{3}{4}, \frac{2}{4}\}$) with PTS technique ($N = 128$)	85
5.17	CCDFs of PAPR of an OFDM system with asymmetric multi- h CPFSK mapper ($H_{+i} = \{\frac{2}{4}, \frac{3}{4}\}$ and $H_{-i} = \{\frac{3}{4}, \frac{2}{4}\}$) with PTS technique ($N = 256$)	85
5.18	CCDFs of PAPR of an OFDM system with asymmetric multi- h CPFSK mapper ($H_{+i} = \{\frac{2}{4}, \frac{3}{4}\}$ and $H_{-i} = \{\frac{3}{4}, \frac{2}{4}\}$) with PTS technique ($N = 512$)	86
6.1	Block diagram of the repeated CF technique	89

List of Tables

6.2	Flow-chart for finding an OFDM signal with a specific value of PAPR using repeated CF technique	90
6.3	CCDFs of PAPR of an OFDM system with single- h CPFSK mapper ($h = \frac{1}{2}$) with and without CF technique ($N = 64, CR = 0.25$)	91
6.4	CCDFs of PAPR of an OFDM system with single- h CPFSK mapper ($h = \frac{1}{2}$) with and without CF technique ($N = 128, CR = 0.25$)	91
6.5	CCDFs of PAPR of an OFDM system with single- h CPFSK mapper ($h = \frac{1}{2}$) with and without CF technique ($N = 256, CR = 0.25$)	92
6.6	CCDFs of PAPR of an OFDM system with single- h CPFSK mapper ($h = \frac{1}{2}$) with and without CF technique ($N = 512, CR = 0.25$)	92
6.7	CCDFs of PAPR of an OFDM system with single- h CPFSK mapper ($h = \frac{2}{3}$) with and without CF technique ($N = 64, CR = 0.25$)	93
6.8	CCDFs of PAPR of an OFDM system with single- h CPFSK mapper ($h = \frac{2}{3}$) with and without CF technique ($N = 128, CR = 0.25$)	93
6.9	CCDFs of PAPR of an OFDM system with single- h CPFSK mapper ($h = \frac{2}{3}$) with and without CF technique ($N = 256, CR = 0.25$)	94
6.10	CCDFs of PAPR of an OFDM system with single- h CPFSK mapper ($h = \frac{2}{3}$) with and without CF technique ($N = 512, CR = 0.25$)	94
6.11	CCDFs of PAPR of an OFDM system with BPSK mapper and repeated CF technique ($N = 64, CR = 0.25$)	95
6.12	CCDFs of PAPR of an OFDM system with BPSK mapper and repeated CF technique ($N = 128, CR = 0.25$)	96
6.13	CCDFs of PAPR of an OFDM system with BPSK mapper and repeated CF technique ($N = 256, CR = 0.25$)	96
6.14	CCDFs of PAPR of an OFDM system with BPSK mapper and repeated CF technique ($N = 512, CR = 0.25$)	97
6.15	CCDFs of PAPR of an OFDM system with single- h CPFSK mapper ($h = \frac{1}{2}$) and repeated CF technique ($N = 64, CR = 0.25$)	97
6.16	CCDFs of PAPR of an OFDM system with single- h CPFSK mapper ($h = \frac{1}{2}$) and repeated CF technique ($N = 128, CR = 0.25$)	98
6.17	CCDFs of PAPR of an OFDM system with single- h CPFSK mapper ($h = \frac{1}{2}$) and repeated CF technique ($N = 256, CR = 0.25$)	98
6.18	CCDFs of PAPR of an OFDM system with single- h CPFSK mapper ($h = \frac{1}{2}$) and repeated CF technique ($N = 512, CR = 0.25$)	99
6.19	CCDFs of PAPR of an OFDM system with multi- h CPFSK mapper ($\{\frac{2}{4}, \frac{3}{4}\}$) with and without CF technique ($N = 64, CR = 0.25$)	99
6.20	CCDFs of PAPR of an OFDM system with multi- h CPFSK mapper ($\{\frac{2}{4}, \frac{3}{4}\}$) with and without CF technique ($N = 128, CR = 0.25$)	100
6.21	CCDFs of PAPR of an OFDM system with multi- h CPFSK mapper ($\{\frac{2}{4}, \frac{3}{4}\}$) with and without CF technique ($N = 256, CR = 0.25$)	100
6.22	CCDFs of PAPR of an OFDM system with multi- h CPFSK mapper ($\{\frac{2}{4}, \frac{3}{4}\}$) with and without CF technique ($N = 512, CR = 0.25$)	101

6.23	CCDFs of PAPR of an OFDM system with asymmetric multi- h CPFSK mapper ($H_{+i} = \{\frac{2}{4}, \frac{3}{4}\}$ and $H_{-i} = \{\frac{3}{4}, \frac{2}{4}\}$) with CF technique ($N = 64, CR = 0.25$)	102
6.24	CCDFs of PAPR of an OFDM system with asymmetric multi- h CPFSK mapper ($H_{+i} = \{\frac{2}{4}, \frac{3}{4}\}$ and $H_{-i} = \{\frac{3}{4}, \frac{2}{4}\}$) with CF technique ($N = 128, CR = 0.25$)	103
6.25	CCDFs of PAPR of an OFDM system with asymmetric multi- h CPFSK mapper ($H_{+i} = \{\frac{2}{4}, \frac{3}{4}\}$ and $H_{-i} = \{\frac{3}{4}, \frac{2}{4}\}$) with CF technique ($N = 256, CR = 0.25$)	103
6.26	CCDFs of PAPR of an OFDM system with asymmetric multi- h CPFSK mapper ($H_{+i} = \{\frac{2}{4}, \frac{3}{4}\}$ and $H_{-i} = \{\frac{3}{4}, \frac{2}{4}\}$) with CF technique ($N = 512, CR = 0.25$)	104
7.1	Block diagram of structure of receiver in an OFDM system with g-CPFSK mapper	106
7.2	Structure of optimum and high-SNR suboptimum g-CPFSK demapper	109
7.3	BER performance of single- h CPFSK mapper ($h = 0.715$) over AWGN for $n = 2, 3$	111
7.4	BER performance of multi- h CPFSK demapper ($H_2 = \{0.77, 0.62\}$) over AWGN for $n = 2, 3$	111
7.5	BER performance of asy multi- h CPFSK demapper ($H_3 = \{6/8, 4/8, 5/8\}$, A-type) over AWGN for $n = 4$ and $n = 6$	112
7.6	Probability of error as a function of observation length of receiver for single- h CPFSK demapper, n , at $E_b/N_o = 6, 8$, and 10 dB.	113
8.1	BER performance of OFDM system with single- h CPFSK ($h = 0.715$) over Rayleigh and Nakagami- m for $n = 2, 4$	117
8.2	BER performance of OFDM system with multi- h CPFSK mapper ($H_2 = \{0.77, 0.62\}$) over Rayleigh and Nakagami- m channel for $n = 2, 3$	117
8.3	BER versus m for OFDM system with multi- h CPFSK $H_2 = \{0.77, 0.62\}$ mapper as a function of SNR	118
8.4	BER performance of OFDM system with asymmetric multi- h CPFSK ($H_3 = \{6/8, 4/8, 5/8\}$, A-type) mapper over Rayleigh and Nakagami- m channels for $n = 2$	118
8.5	BER performance of OFDM system with multi- h $H_2 = \{0.77, 0.62\}$ and asy multi- h ($H_3 = \{6/8, 4/8, 5/8\}$, A-type) CPFSK mappers over Rayleigh and Nakagami- m for $n = 4$	119
8.6	BER performance of OFDM system with multi- h CPFSK $H_2 = \{0.77, 0.62\}$ and asymmetric multi- h CPFSK ($H_3 = \{6/8, 4/8, 5/8\}$, A-type) mappers over Rayleigh and Nakagami- m channels for $n = 6$	120
9.1	Conceptual model of smart grid.	123

List of Abbreviations

AWGN	Additive White Gaussian Noise
ADC	Analog-to-Digital Converter
BER	Bit Error Rate
CF	Clipping and Filtering
BPSK	Binary Phase Shift Keying
CP	Cyclic Prefix
CPM	Continuous Phase Modulation
CCDF	Complementary Cumulative Distribution Function
CPFSK	Continuous Phase Frequency Shift Keying
DAC	Digital-to-Analog Converter
FFT	Fast Fourier Transform
ICI	Interchannel Interference
i.i.d	independent and identically distributed
IFFT	Inverse Fast Fourier Transform
ISI	Intersymbol Interference
LOS	Line of Sight
LRT	Likelihood Ratio Test
PAPR	Peak-to-Average Power Ratio
PDF	Probability Density Function
PSD	Power Spectral Density
PSK	Phase Shift Keying
PTS	Partial transmit Sequence
QPSK	Quadrature Phase Shift Keying

OFDM	Orthogonal Frequency Division Multiplexing
SER	Symbol Error Rate
SLM	Selective Mapping
SNR	Signal to Noise Ratio

Chapter 1

Introduction to Thesis

1.1 Introduction

Communication has been one of the most important needs of the human race throughout recorded history. Humans have always found ways to communicate, over space and time. A particularly good natural resource for communication is electricity for its speed and ability to be controlled using devices like capacitors, microprocessors, and batteries. From the early inventions such as Morse's telegraph, Bell's telephone, Edison's phonograph, and Marconi's radio, communication technology has advanced considerably to include global telephone networks, satellite communications, and storage systems. Also, with the rise of the Internet and digital computers, digital communication has become all the more important in the recent years. In particular, wireless digital communications has become one of the most active areas of technology development of our time to provide high data rate access and mobility. One of the challenges in designing such a wireless system is to overcome the effects of the wireless channel, which is typically characterized as having multiple transmission paths and as being time-varying in character.

In a typical digital communication system, bits are mapped to k -bit data symbol. In a conventional single-carrier system, these symbols are transmitted sequentially. The transmitted waveform in such a system can be written as

$$s(t) = \sum_i a_i g(t - iT_s) \quad (1.1)$$

where $T_s = kT_b$ is the symbol duration with T_b the bit duration, $\{a_i\}$ represents data symbols with a_i taking one of the 2^k possible symbols, and $g(t)$ is the transmit pulse shape. For time-dispersive channels, interference is caused from symbol to symbol. The channel is represented by its time-variant impulse response $h(\tau, t)$, where τ is the propagation delay variable [1]. The received signal can be then expressed mathematically

as

$$\begin{aligned} r(t) &= s(t) * h(\tau, t) + n(t) \\ &= \int_{-\infty}^{\infty} h(\tau, t) s(\tau, t) d\tau + n(t) \end{aligned} \tag{1.2}$$

where $*$ represents the linear convolution operator and $n(t)$ is the Additive White Gaussian noise (AWGN). The severity of Intersymbol Interference (ISI) depends on the symbol duration T_s relative to the channel's maximum propagation delay τ_{max} . The severe ISI must be controlled at the receiver in order to achieve reliable communication.

The traditional approach to combating ISI is with time-domain equalizer and also the knowledge of the channel is essential. A variety of equalizers ranging in complexity and cost are available and so are techniques for estimation of the channel [27], [3], [4]. The ML receiver, although highly effective, but is impractical due to its enormous complexity. Linear equalizers on the other hand are much simpler from the viewpoint of implementation, but perform poorer compared to ML receiver. Nonlinear Decision Feedback Equalizers (DFEs) have complexity comparable to linear equalizers and provide better performance than these equalizers. Since all these techniques require Channel State Information (CSI), training sequences are transmitted for estimating the channel at receiver and by comparing the received signal to what was transmitted, an estimate of the channel impulse response, $h(\tau, t)$, is made. Again, there exist various algorithms for channel estimation such as Least-Mean-Square (LMS), Recursive Least-Square (RLS), Kalman Filtering etc. While LMS algorithm is the most stable and the least complex, it suffers from slow convergence rate. On the other hand, RLS algorithm provides fast convergence but has higher complexity and can be unstable as well.

In order to meet the growing demand of data rate, approaches alternative to single-carrier system have been considered. One such approach is a multicarrier modulation technique known as Orthogonal Frequency Division Multiplexing (OFDM). This technique is attractive for a number of reasons: i) it has high spectral efficiency since the subcarriers overlap in frequency and adaptive bit loading techniques can be employed; ii) the implementation of the system is simplified because the baseband modulator and demodulator are simply IFFT and FFT operations; and iii) ISI is easy to mitigate by employing a cyclic guard interval. OFDM has been implemented in both wireline and wireless applications. International standards that use OFDM for high-speed wireless

communications are IEEE 802.11, IEEE 802.16, IEEE 802.20, and European Telecommunications Standards Institute (ETSI) Broadcast Radio Access Network (BRAN) etc. Furthermore, OFDM has been implemented in wireline applications such as digital audio and video broadcasting (DAB and DVB), digital subscriber lines (DSL), and in-band on-channel (IBOC) broadcasting. OFDM is also being developed for ultra-wideband (UWB) systems, cellular systems, wireline metropolitan area networks (MANs) under the IEEE 802.16 (WiMax) standard and for wireline systems such as tower line communication (TLC).

OFDM is not without its disadvantages. The first is its sensitivity to imperfect frequency synchronization which is common for mobile applications. This sensitivity arises from the close subcarrier spacing in the system. If the frequency synthesizer at the receiver is misaligned then the subcarriers are not orthogonal and therefore interfere with one another. This intercarrier interference (ICI) causes ISI and can lead to high irreducible error floors. The second disadvantage with OFDM is its high Peak-to-Average Power Ratio (PAPR). When high PAPR signals are transmitted through non-linear power amplifiers severe signal distortion will result. Therefore, amplifiers with large linear range are required, which implies the need for more expensive power amplifiers. Therefore, techniques for reducing the PAPR of OFDM signals must be considered to make the system energy and cost effective. There exist pre-processing and post-processing techniques for reducing PAPR in OFDM systems. Pre-processing techniques use selective mapping, partial transmit sequences etc. and post-processing techniques typically clip OFDM signals in a way so that clipped signals can be restored at the receiver.

A simplified block diagram of an OFDM system is shown in Fig.1.1 The purpose of the mapper is to map an incoming serial binary stream of data to a stream of complex symbols. The Serial-to-Parallel (S/P) block converts the serial complex data stream into N parallel streams that are modulated onto N orthogonal subcarriers. This operation is easily implemented in discrete-time using N -point IFFT operation. By modulating the original data onto N subcarriers, OFDM increases the symbol duration by a factor of N , thereby, making the transmitted OFDM signal robust to frequency-selective fading. The parallel output from the IFFT block is then converted to a serial stream by the Parallel-to-Serial (P/S) converter and then the cyclic prefix (CP) is added to the signal and transmitted over the channel. At the receiver, first the CP is removed and the signal

is fed to S/P converter to transform the signal from serial to parallel form. The FFT operation is then carried out and the samples are equalized and are converted to serial form using the P/S converter and fed to the demapper/detector to estimate the original transmitted data. In the next Chapter, the basics of OFDM are examined in more detail.

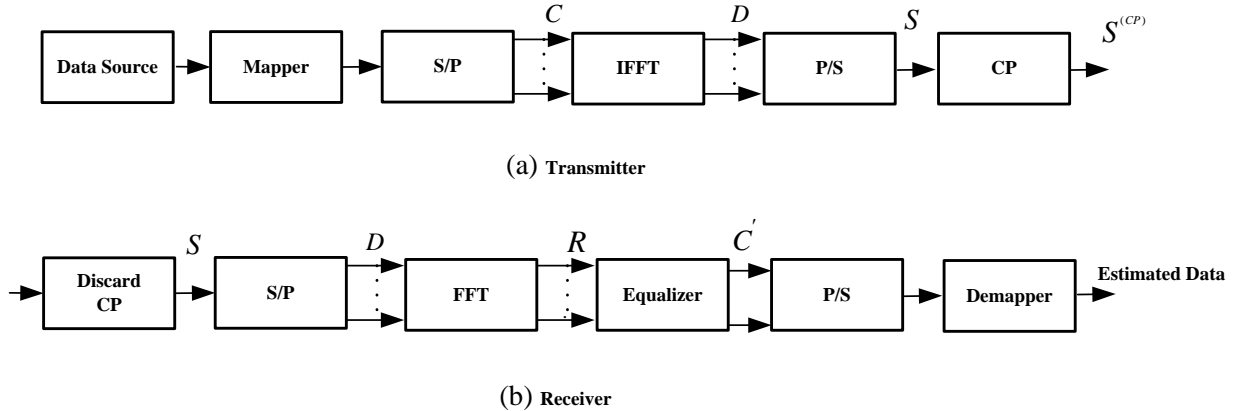


Figure 1.1: Simplified block diagram of OFDM system: (a) Transmitter (b) Receiver

1.2 Literature Survey and Motivation

In the literature OFDM systems that employ memoryless mappers such as PSK, QPSK, QAM, etc. have been proposed and investigated extensively [5], [6], [7], [8], [9], [10], [11], [12], [13]. In these systems, successive OFDM blocks are independent and uncorrelated. Thus, symbol-by-symbol detection is sufficient at the demapper for recovering data. The bit error rate performance is a function of the mapper/demapper used in an OFDM system [14],[15]. While in the literature memoryless mappers have been extensively examined, it is beneficial to consider mappers with memory in OFDM systems. By doing so, it is possible to introduce correlation among transmitted OFDM symbols. Further, if correlation is introduced in a systematic manner it is possible to exploit this at the receiver to gain advantage in terms BER performance of the system, at any arbitrary SNR. The idea of mapper with memory is derived from constant envelope CPM, a nonlinear modulation technique, used in single-carrierr system [16], [17], [18], [19], [20], [21], [22] and is widely used in satellite and mobile communications [23], [24], [25], [26], [27], [1]. CPM comprises of a wide variety of modulations including CPFSK, multi- h CPFSK, asymmetric multi- h CPFSK, correlated CPFSK etc. [28], [22], [29], [23], [30],

[31]. Two studies have introduced CPFSK mapper in an OFDM system [32], [33]. However, these studies are limited to the case of binary data transmission. It is therefore important to venture a systematic investigation of CPM mapper to understand its full potential in an OFDM system. Thus, in this thesis a generalized mapper with memory referred to as g-CPFSK is proposed in an OFDM system. The characteristics of g-CPFSK mapper is described in terms of the input M -ary data and a set of mapper parameters $\{h_1, h_2, \dots, h_k\}$. The resulting OFDM signals with memory are described, illustrated, and examined for their properties.

A major drawback of any OFDM system is its high PAPR. The ratio of the peak power and the average power of an OFDM signal is referred to as the PAPR. The high PAPR requires the transmitter's Power Amplifier (PA) to have a large linear range to be capable of accommodating the OFDM signal. But practical PAs have a limited linear range beyond which they saturate to their maximum output level. Nonlinear PA at the transmitter with limited linear range can distort the OFDM signal. This results in spectral spreading and intermodulation due to in-band and out-of-band signal interference. The out-of-band interference causes adjacent channel interference through spectral spreading and the in-band interference raises the BER of the system. Thus, efficient techniques are required that can reduce the occurrence of large OFDM signal peaks at the input of the PA to reduce the detrimental effects of nonlinear amplification without sacrificing the power efficiency of the system. In the literature, a number of techniques have been proposed to mitigate the problem of PAPR in OFDM systems such as Clipping and Filtering (CF), Coding, Tone Reservation, Tone Injection, PTS, Active Constellation Extension (ACE), and SLM [10], [34]. However, these techniques have been studied for OFDM systems in which memoryless mappers such as BPSK, QPSK, QAM etc. are used [35], [16], [36],[37]. An overview of PAPR reduction techniques can be found in [38], [10]. Among these, CF, SLM, and PTS techniques are widely used and are known to be very effective in reducing PAPR of OFDM systems. In the literature, CF technique has been extensively examined [10], [37], [46], [39], [40], [8] and in this technique the signal is clipped to a predefined level and subsequently filtered. The relatively small in-band distortion is combated using low-order signal constellation, coding [41], and/or clipping noise cancellation techniques [42]. To suppress peak regrowth due to filtering, iterative clipping and filtering (ICF) techniques can be used [39], [8]. SLM is another technique that is easy-to-implement

and introduces no distortion in the transmitted signal. However, this technique requires side information to be transmitted to the receiver and also its computational complexity increases linearly as the number of phase sequences. The SLM technique has been extensively examined in OFDM systems with memoryless mappers [5], [6], [9], [10], [11], [43], [37], [48], [44], [34], [45], [46], [47]. PTS is yet another technique that can be used to improve the PAPR statistics of OFDM signals. In this technique, the data block to be transmitted is partitioned into disjoint subblocks and the subblocks are combined using phase factors to minimize PAPR. This technique has been extensively examined in OFDM systems with memoryless mappers. [7], [9], [10], [19], [37], [48], [44], [49]. In the literature PAPR reduction techniques have been examined in conjunction with the mappers used in an OFDM system. There exist no study that clearly indicates a specific choice of PAPR reduction technique for a given arbitrary mapper, as it is too complex to analyze. Therefore, once the mapper is chosen, several PAPR reduction techniques are considered to arrive at the best technique to be used based on performance and complexity. Thus, it is also the intent of this thesis to examine the PAPR properties of an OFDM system with the proposed g-CPFSK mapper in conjunction with CF, SLM, and PTS techniques. This is carried out to establish bounds on achievable energy-efficiency of the system. Three subclasses of g-CPFSK mapper namely single- h CPFSK, multi- h CPFSK, and asymmetric multi- h CPFSK mappers are considered in conjunction with CF, SLM, and PTS techniques.

In an OFDM system, BER, defined as the ratio of the number of erroneous bits to the total number of bits received, is an important parameter that defines the reliability of the system. Therefore, it is important to estimate BER performance and it is, in general, is a function of mapper/demapper used in the system and also is a function of the nature and characteristic of the communication channel. In the literature, BER performance of OFDM systems with memoryless mappers such as BPSK [50], [51], [17], [16], QPSK [52], [50], [51], and QAM [50], [17] are available and are well illustrated. However, such an effort for an OFDM system with mapper with memory is not available. Thus, in this thesis, BER performance of an OFDM system with the proposed g-CPFSK mapper is considered. The memory inherent in the g-CPFSK mapper permits multiple-symbol observation demapper in the OFDM receiver. Thus, the demapper design problem is addressed. This problem consists of observing n OFDM symbols in the presence of AWGN

and arriving at an optimum decision on the first OFDM symbol transmitted. This is the composite hypothesis testing problem [53] and the solution is the Likelihood Ratio Test (LRT). Using this, a canonical structure of the optimum g-CPFSK demapper is derived and presented. The error probability performance of OFDM system with g-CPFSK a demapper is very complex to analyse and, thus, tight BER bounds are derived. It is observed that these bounds are functions of $\frac{E_b}{N_0}$, SNR, n , the observation length of the demapper, $\{h_1, h_2, \dots, h_k\}$, the set of mapper parameters, and M , the number of amplitude levels of the mapper. These bounds are then minimized to determine optimum parameters of single- h CPFSK, multi- h CPFSK, and asymmetric multi- h CPFSK mappers. A comparison of BER performance of the proposed OFDM system with g-CPFSK mapper with conventional OFDM system with memoryless mappers is also presented.

In a wireless communication system, the received signal quality degrades even without the presence of AWGN. This degradation is referred to as fading and the communication channels that exhibit this phenomenon are referred to as fading channels [51], [14], [54], [16], [17]. The fading can be caused due to i) natural weather disturbances such as rain-fall, snow, fog, hail etc.; ii) man-made disturbances, such as ignition [51]; iii) multiple transmission paths between transmitter and receiver; and iv) irregular earth surfaces and terrains. The fading, in general, refers to the received signal's random fluctuations as a function of time. The end-to-end system design, therefore, must incorporate techniques to mitigate the effects of fading and penalty in SNR that must be increased as consequences fading must be assessed. When the impulse response of the fading channel is modeled as a zero-mean complex-valued Gaussian process [55], its envelope at any instant is Rayleigh-distributed. In this case, the channel is referred to as a Rayleigh fading channel [54]. The Rayleigh distribution is often used to model the statistics of signals received over radio channels. The distribution is related to the Central Chi-Square distribution [56], [57]. When there exists a dominant line of sight path in the medium between transmitter and receiver, or in other words there are fixed scatters in the medium, the envelope has Rice distribution [51], [15] and the channel is referred to as Rician fading channel. Another distribution function used to model the envelope of fading signals is the Nakagami- m distribution. This distribution is often used to model signal fading over wireless communication channel and it represents a wide class of distributions [51]. In the literature, OFDM systems with memoryless mappers have been extensively exam-

ined over Rayleigh, Rice, and Nakagami- m fading channels, generally, using simulation techniques [51], [15], [55]. However, analytical work for estimating BER performance of OFDM systems over fading channel is not available. In this thesis, therefore, analytical framework for estimating BER performance of an OFDM system with the proposed g-CPFSK mapper over fading channels is provided. Closed-form expressions for BER over Rayleigh and Nakagami- m fading channels have been derived for single- h CPFSK, multi- h CPFSK, and asymmetric multi- h CPFSK mappers in an OFDM system. The numerical results are compared with the performance of OFDM system with conventional memoryless mappers. In the thesis by appropriately choosing the parameters of g-CPFSK mapper, performance of the OFDM system is also optimized.

1.3 Objectives

The objectives of this thesis are mentioned below:

1. In an OFDM system, mapper plays an important role and dictates the performance of the system. A generalized CPFSK (g-CPFSK) mapper is proposed to introduce correlation among transmitted OFDM symbols. It is shown that the mapper can be described as a discrete-time finite-state machine. Although g-CPFSK mapper represents a wide variety of mappers, in this thesis three subclasses namely single- h CPFSK, multi- h CPFSK, and asymmetric multi- h CPFSK mappers are considered. The resulting OFDM signals and their properties are described. Several examples are given and illustrated as well.
2. The energy efficiency of OFDM systems depends on the efficiency of High-Power Amplifier (HPA) in them. In this context, PAPR of OFDM signals is directly related to the energy efficiency of the system. An investigation of PAPR properties of OFDM system with g-CPFSK mapper is carried out. In particular, PAPR properties of OFDM system with single- h CPFSK, multi- h CPFSK, and asymmetric multi- h CPFSK mappers are investigated. Furthermore, these mappers with SLM, PTS, and CF techniques are considered for mitigation of PAPR. A comparison of

PAPR reductions relative to conventional memoryless mappers in an OFDM system is also provided. Suggestions are offered for design of energy efficient OFDM systems, as a function of parameters of mappers.

3. One of the important features of OFDM system with g-CPFSK mapper is that the transmitted signals have memory. This permits multiple symbols detection at the receiver. In this thesis, ML detection of received OFDM signal corrupted by AWGN is addressed. The detection problem consists of observing the received signal over n OFDM symbols and arriving at an optimum decision on the data transmitted during the first symbol. The structure of the maximum likelihood OFDM detector is derived based on the criterion of minimum probability of BER. The receiver structure is illustrated and is examined for its complexity for each of three mappers proposed in the thesis.
4. The performance of the optimum OFDM detector with g-CPFSK mapper is complex to analyze analytically. Therefore, suboptimum detectors are considered to bound the performance of the optimum detector. High-SNR upper and lower bounds are derived to approximate the performance of the optimum receiver and are illustrated for single- h CPFSK, multi- h CPFSK, and asymmetric multi- h CPFSK mappers in an OFDM system. It is shown that the BER bounds are functions of : i) E_b/N_0 , ii) characteristics of the mapper, iii) n , observation length of OFDM detector, and iv) M , number of amplitude levels of mapper. Optimum parameters of mappers that minimize BER are also determined.
5. Analytical framework for assessing BER performance of an OFDM system with g-CPFSK mapper over fading channels is provided. Closed-form expressions for BER over Rayleigh and Nakagami- m fading channels are derived and illustrated.

1.4 Organization

In Chapter 2, fundamentals of an OFDM system are provided, particularly, with reference to the problems addressed in the thesis. The functions of various sub-blocks of the system and their mathematical descriptions are given. Specifically, the concept of cyclic prefix in an OFDM system, PAPR reduction technique relevant to the thesis, and statistical descriptions of channel are provided.

In Chapter 3, the proposed g-CPFSK mapper is explained. The output of the mapper is described in terms of its parameters and input data. These subclasses of g-CPFSK mapper, single- h CPFSK, multi- h CPFSK, and asymmetric multi- h CPFSK mappers, are explained and illustrated. Signal-space properties of these mappers and mathematical descriptions of resulting OFDM signals are given.

In Chapter 4, SLM technique is introduced for PAPR reduction in an OFDM system with the proposed g-CPFSK mapper. The PAPR properties of this system with and without SLM technique are presented. A simplified method is suggested for the search of phase sequences in SLM technique that minimize the PAPR of transmitted OFDM symbols.

The PTS technique for PAPR reduction in an OFDM system with g-CPFSK mapper is described in Chapter 5 and possible reductions in PAPR of g-CPFSK mapper are assessed with and without PTS technique. A simplified method for finding best phase rotating vectors that minimize PAPR is explained.

The CF technique for PAPR reduction for an OFDM system with g-CPFSK mapper is explained in Chapter 6. The technique of repeated application of CF technique in such a system for achieving a specified level of PAPR is explained.

In Chapter 7, the problem of maximum likelihood demapper design for detection of OFDM g-CPFSK signals in AWGN is addressed. Optimum demapper structure is derived and its BER performance is evaluated using upper and lower bounds. BER performances are determined for single- h CPFSK, multi- h CPFSK, and asymmetric multi- h CPFSK demappers in an OFDM system as a function of mapper parameters.

In Chapter 8, the performance of OFDM system with g-CPFSK mapper over fading channels is considered. Rayleigh and Nakagami- m fading channels are considered. and

analytical and simulation results are presented for BER performance of OFDM system with g-CPFSK mapper.

In Chapter 9, contributions of this thesis and the conclusions from the results obtained are summarized. Based on the results of this thesis suggestions are offered for design of an OFDM system with g-CPFSK mapper. Also, areas for further research are outlined in the light of the work presented in the thesis.

1.5 Conclusions

An introduction to the thesis is provided with emphasis on the literature survey and the motivations for the problems addressed in the thesis. The primary objectives of the thesis are outlined. Also, the organization of the thesis is given.

Chapter 2

Fundamentals of OFDM System

2.1 Introduction

In this Chapter, the basic properties of OFDM are given. Section 2.2 provides a description of a typical OFDM system. The concept of cyclic prefix is described in Section 2.3. The PAPR statistics and PAPR mitigation techniques that are relevant to the thesis are described in Section 2.4. The Chapter is concluded in Section 2.5.

2.2 Baseband OFDM System

The block diagram of a typical OFDM system is shown in Fig.2.1. The three subblocks namely (a) transmitter, (b) channel, and (c) receiver are explained next.

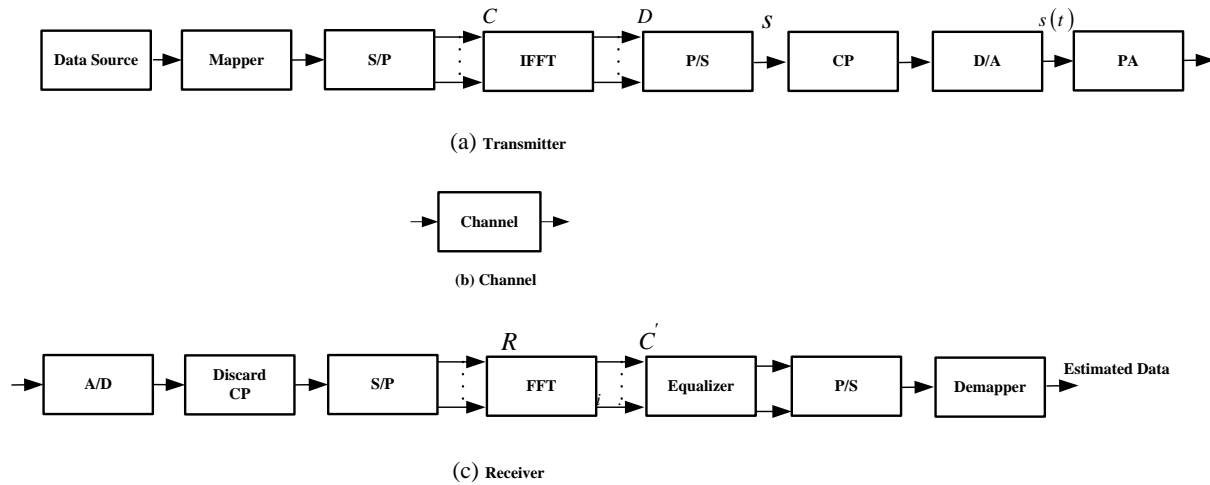


Figure 2.1: OFDM system diagram

2.2.1 Transmitter

The data source is assumed to be a sequence of binary digits $\{a_0, a_1, a_2, \dots\}$ where $a_i, i = 0, 1, \dots$, is either a 0 or a 1 with $P(a_i = 0) = P(a_i = 1) = 1/2$. The bit duration is assumed to be equal to T_b sec and the corresponding data rate is thus equal to $R = \frac{1}{T_b}$ bps. The output of the data source is grouped into blocks of k bits and each block is mapped to one of $M = 2^k$ complex data by the mapper. Such a mapper is referred to as a memoryless mapper, as its current output is a function of only the current input. Some of the commonly used mappers are BPSK, QPSK, and QAM. The signal-space diagrams for BPSK and QPSK mappers are shown in Fig. 2.2 For the case of BPSK mapper, $k = 1$ and hence $M = 2$. The mapper maps incoming bit '0' to -1 V and bit '1' to +1 V.

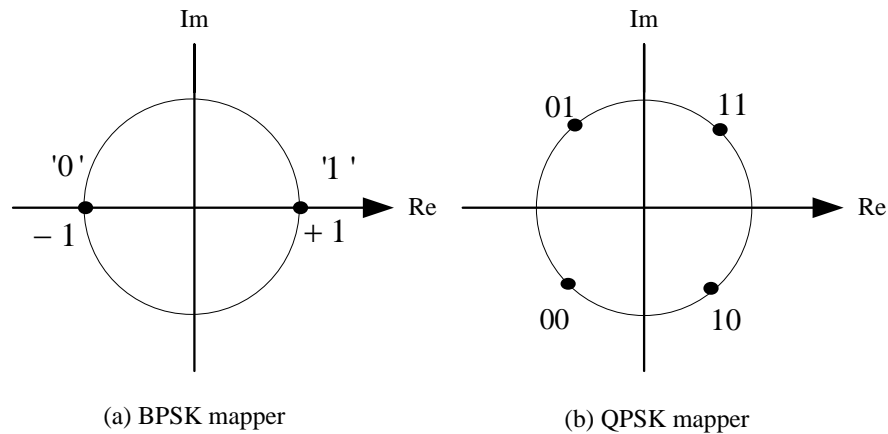


Figure 2.2: Signal-space diagrams for (a) BPSK and (b) QPSK mappers

For the QPSK mapper, $k = 2$ and $M = 4$. The mapper uses the following rule:

$$\left. \begin{aligned} '00' &\rightarrow \frac{-1}{\sqrt{2}} - j\frac{1}{\sqrt{2}} \\ '01' &\rightarrow \frac{-1}{\sqrt{2}} + j\frac{1}{\sqrt{2}} \\ '10' &\rightarrow \frac{+1}{\sqrt{2}} - j\frac{1}{\sqrt{2}} \\ '11' &\rightarrow \frac{+1}{\sqrt{2}} + j\frac{1}{\sqrt{2}} \end{aligned} \right\} \quad (2.1)$$

The output of the signal mapper, in general, can be thought of as a discrete-time complex signal, which is shown in Fig. 2.3 for an arbitrary signal mapper. For example, the input and output for BPSK and QPSK mappers are shown in Tables 3.2 and 2.2 respectively.

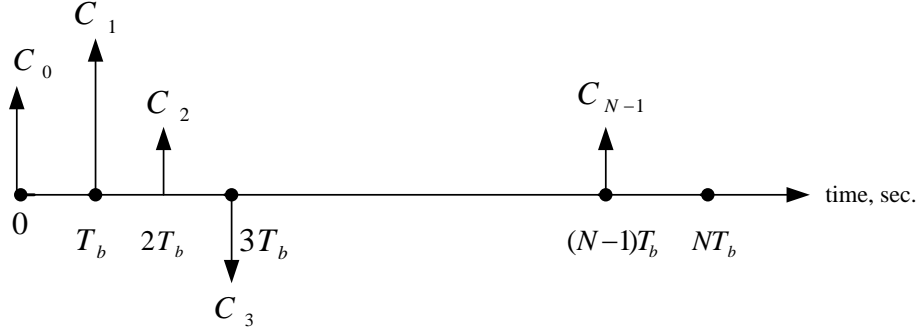


Figure 2.3: Discrete-time complex signal at the output for an arbitrary signal mapper

Table 2.1: Input and output for BPSK mapper (k=1 and M=2)

Input	$a_0 = 0$	$a_1 = 1$	$a_2 = 1$	\cdots	$a_{N-1} = 0$
Output	$C_0 = -1$	$C_1 = +1$	$C_2 = +1$	\cdots	$C_{N-1} = -1$

Table 2.2: Input and output for QPSK mapper (k=2 and M=4)

Input	$a_0a_1 = 01$	$a_2a_3 = 11$	$a_4a_5 = 00$	\cdots	$a_{2N-2}a_{2N-1} = 00$
Output	$C_0 = \frac{-1}{\sqrt{2}} + j\frac{1}{\sqrt{2}}$	$C_1 = \frac{+1}{\sqrt{2}} + j\frac{1}{\sqrt{2}}$	$C_2 = \frac{-1}{\sqrt{2}} - j\frac{1}{\sqrt{2}}$	\cdots	$C_{N-1} = \frac{-1}{\sqrt{2}} - j\frac{1}{\sqrt{2}}$

The S/P converter accepts a block of N complex data and converts it to a block of N parallel data. It is noted that the S/P converter enhances the duration of each parallel data by a factor of N . The output of this block can be written as a vector of N complex numbers given by:

$$C = [C_0, C_1, \cdots, C_{N-1}] \quad (2.2)$$

This discrete signal representing the data is fed to an N -point IFFT block to obtain:

$$D = [D_0, D_1, \cdots, D_{N-1}] \quad (2.3)$$

The relationship between (2.2) and (2.3) is given by [58]

$$D_n = \sum_{k=0}^{N-1} C_k e^{j\frac{2\pi}{N}nk}, \quad n = 0, 1, \cdots, N-1 \quad (2.4)$$

The parallel signal from the IFFT block is then converted to serial signal by the S/P

converter and fed to D/A block to obtain

$$s(t) = \sum_{k=0}^{N-1} C_k e^{j2\pi f_k t}, \quad 0 \leq t \leq NT_b \quad (2.5)$$

where $f_k = \frac{k}{NT_s}$ and $t = nT_b$. It is noted that T_b is the duration of bit from the data source, f_k is the frequency of the k -th subcarrier. The OFDM symbol duration is denoted by T_s . For a BPSK mapper used in the system $T_s = NT_b$ and for a QPSK mapper $T_s = NkT_b$. It is noted that $[C_0, C_1, \dots, C_{N-1}]$ represents a block of N data symbols and the complex sinusoids $\{e^{j2\pi f_k t}, k = 0, 1, \dots, N-1\}$ are referred to as the subcarriers of OFDM system and are orthogonal to each other. That is,

$$\frac{1}{T_s} \int_0^{T_s} \left(e^{j2\pi f_i t} \right)^* \left(e^{j2\pi f_m t} \right) dt = \begin{cases} 1, & f_i = f_m \\ 0, & f_i \neq f_m \end{cases} \quad (2.6)$$

It can be shown that the discrete sequence $D = [D_0, D_1, \dots, D_{N-1}]$ can be obtained by sampling $s(t)$ at times $t = nT_b$, $n = 0, 1, \dots, N-1$. That is,

$$s(nT_b) = D_n = \sum_{k=0}^{N-1} C_k e^{j2\pi f_k nT_b} \quad (2.7)$$

The continuous-time complex modulating signal given by (2.5) can be written as

$$s(t) = s_I(t) + js_Q(t) \quad (2.8)$$

where

$$s_I(t) = \text{Re} \{s(t)\} \quad (2.9)$$

and

$$s_Q(t) = \text{Im} \{s(t)\} \quad (2.10)$$

The signals $s_I(t)$ and $s_Q(t)$ can be written as:

$$s_I(t) = \sum_{k=0}^{N-1} (a_k \cos 2\pi f_k t - b_k \sin 2\pi f_k t) \quad (2.11)$$

and

$$s_Q(t) = \sum_{k=0}^{N-1} (a_k \sin 2\pi f_k t - b_m \cos 2\pi f_k t) \quad (2.12)$$

where $C_k = a_k + jb_k$. The modulating signal given by (2.8) is carrier modulated and transmitted, after power amplification, by the antenna over the communication channel.

2.2.2 Channel

In the design of an OFDM system for transmitting data through physical channel, two mathematical models that reflect important characteristics of transmission medium are considered; i) the additive noise channel and ii) frequency non-selective fading channel. These are described next.

A. The Additive Noise Channel

The most commonly used mathematical model of a communication channel is the additive noise channel. This is illustrated in Fig. 2.4.

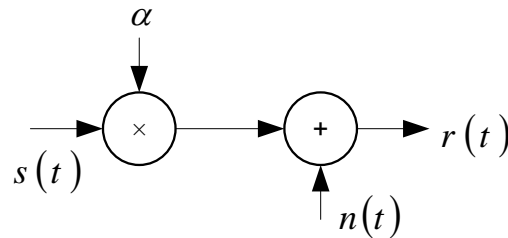


Figure 2.4: The additive noise channel

In this model, the transmitted OFDM signal $s(t)$ is corrupted by an additive random noise process $n(t)$. The additive noise process may result from electronic components and amplifiers at the receiver or from interference encountered in transmission. This type of noise is statistically characterized as Gaussian noise process. Hence, it is termed as the additive Gaussian noise channel. The received OFDM signal can be written as

$$r(t) = \alpha s(t) + n(t) \quad (2.13)$$

where α is the attenuation factor, $s(t)$ is the transmitted OFDM signal and $n(t)$ is the AWGN. The amplitude probability density of $n(t)$ is given by:

$$p_N(n) = \frac{1}{\sqrt{2\pi}\sigma} e^{-(n-\mu)^2/2\sigma^2} \quad (2.14)$$

where μ is the mean and σ^2 is the variance of the noise. The two-sided PSD of the noise is assumed to be $N_0/2$ watts/Hz.

B. Frequency Non-Selective Fading Channel

The received OFDM signal over a frequency non-selective fading channel can be modelled as

$$r(t) = \int_{-\infty}^{\infty} h(\tau) s(t - \tau) d\tau + n(t) \quad (2.15)$$

where $s(t)$ is the transmitted OFDM signal, $n(t)$ is AWGN and $h(t)$ is the impulse response of the channel and is given by

$$h(t) = \alpha e^{j\phi_0} \delta(t) \quad (2.16)$$

Using (2.16) in (2.15), the received signal can be written as

$$r(t) = \alpha e^{j\phi_0} s(t) + n(t) \quad (2.17)$$

where α and ϕ are the channel amplitude and phase, respectively. In the frequency domain, the channel is described by $H(f) = \mathcal{F}[h(t)] = \alpha e^{j\phi_0}$ denoting that it is constant at all frequencies and hence the channel is frequency non-selective. Such a channel is referred to as flat-fading channel. The channel amplitude is treated as a random quantity. When it is a zero-mean complex-valued Gaussian process, its envelope is Rayleigh distributed. The probability density function of the Rayleigh distributed random variable X is given by

$$p_X(x; \sigma) = \frac{x}{\sigma^2} e^{-x^2/2\sigma^2} \quad x \geq 0 \quad (2.18)$$

The corresponding distribution is given by

$$F_X(x; \sigma) = \int_0^x \frac{u}{\sigma^2} e^{-u^2/2\sigma^2} du = 1 - e^{-x^2/2\sigma^2}, \quad x \geq 0 \quad (2.19)$$

The moments of X are:

$$E \{X^k\} = (2\sigma^2)^{k/2} \Gamma \left(1 + \frac{k}{2}\right) \quad (2.20)$$

The variance is given by

$$\sigma_x^2 = \left(2 - \frac{\pi}{2}\right) \sigma^2 \quad (2.21)$$

The quantity σ is referred to as the scale parameter of the distribution.

Another probability distribution function that is widely used to model the envelope of fading channels is the Nakagami- m distribution. The corresponding density function is given by

$$p_X(x; m, \Omega) = \frac{2^m m}{\Gamma(m) \Omega^m} x^{2m-1} \exp\left(-\frac{m}{\Omega} x^2\right), \quad x \geq 0, \quad m \geq \frac{1}{2}, \quad \Omega > 0 \quad (2.22)$$

where Ω is defined as

$$\Omega = E \{X^2\} \quad (2.23)$$

and the parameter m represents the ratio of moments, called as the fading figure, and is given by

$$m = \frac{\Omega^2}{E \{(X^2 - \Omega)^2\}}, \quad m \geq \frac{1}{2} \quad (2.24)$$

The n -th moment of X is given by

$$E \{X^n\} = \frac{\Gamma(m + \frac{n}{2})}{\Gamma(m)} \left(\frac{\Omega}{m}\right)^{n/2} \quad (2.25)$$

It is noted that for $m = 1$, the density reduces to the well-known Rayleigh density function. For $\frac{1}{2} \leq m \leq 1$, density functions that have larger tails than Rayleigh density are obtained. For $m > 1$, densities that decay faster than the Rayleigh density are obtained.

In this thesis, Rayleigh and Nakagami- m densities are used to estimate the performance of OFDM system with g-CPFSK mapper and these densities are shown in Figs. 2.5 and 2.6, respectively.

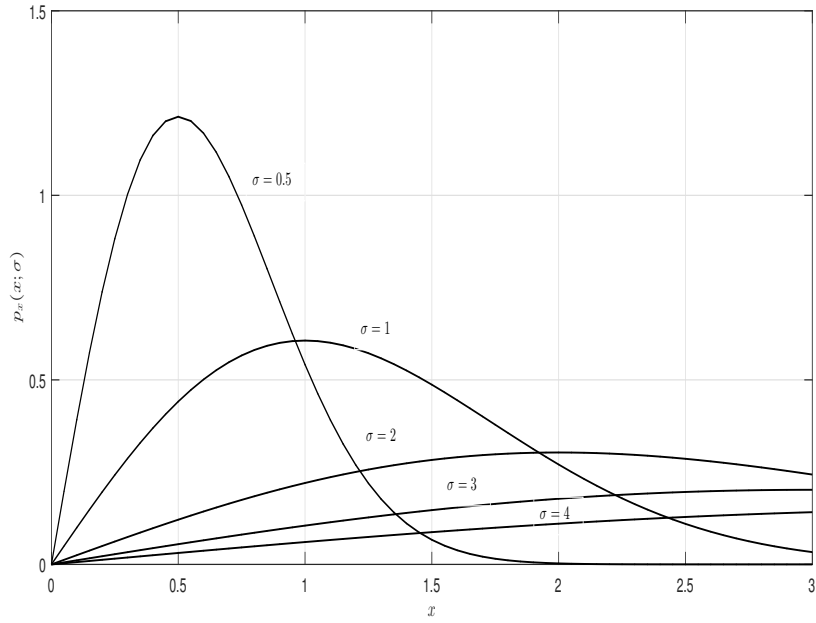


Figure 2.5: Probability density function for Rayleigh random variable for various values of σ

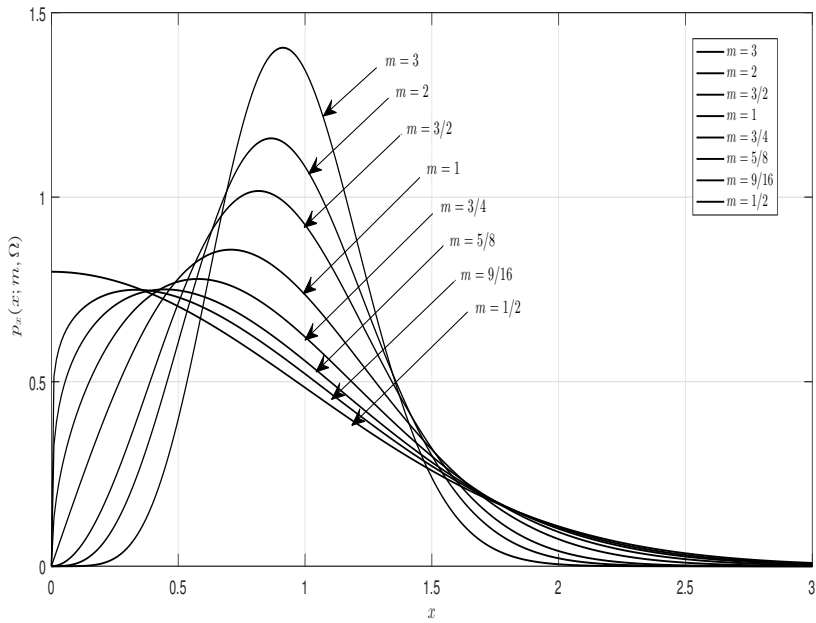


Figure 2.6: Probability density function for Nakagami- m random variable with $\Omega = 1$ for various values of m

2.2.3 Receiver

At the receiver, the received signal $s(t)$ is sampled to obtain discrete-time sequence. That is,

$$s(t) \Big|_{t=\frac{nT_s}{N}=nT_b} = \sum_{k=0}^{N-1} C_k e^{j2\pi f_k n T_b}, \quad n = 0, 1, \dots, N-1 \quad (2.26)$$

where $[s(0), s(T_b), s(2T_b), \dots, s((N-1)T_b)]$ is the IFFT of the information symbol $[C_0, C_1, \dots, C_{N-1}]$. This operation is carried out by the A/D converter. The S/P converter converts this serial vector to parallel form. It is then fed to the FFT block to obtain

$$C_k = \frac{1}{N} \sum_{n=0}^{N-1} s[nT_b] e^{-j2\frac{\pi kn}{N}}, \quad k = 0, 1, \dots, N-1 \quad (2.27)$$

Performing IFFT at the transmitter and FFT at the receiver for modulation and demodulation, respectively, is much simpler than performing modulation and demodulation in continuous-time domain using N orthogonally tuned oscillators. It is noted that the signal processing done using software makes OFDM system highly suitable for Software Defined Radio [59]. The output of FFT block is fed to the demapper, after converting parallel samples to serial form, for recovering of data transmitted by the data source.

2.3 Cyclic Prefix

The use of guard interval ensures ISI-free operation in an OFDM system. This can be achieved as long as a cyclic prefix is transmitted with an OFDM symbol interval. Consider the OFDM signal over one symbol interval:

$$s(t) = \sum_{k=0}^{N-1} C_k e^{j2\pi f_k t}, \quad 0 \leq t \leq T_s \quad (2.28)$$

where C_0, \dots, C_{N-1} are the data symbols and $e^{j2\pi f_k t}, k = 0, 1, \dots, N-1$ are the N subcarriers. The guard interval is defined over $-T_g \leq t < 0$, where T_g is the duration of the guard intervals as shown in Fig. 2.7.

To transmit a cyclic prefix, the last T_g s of the block is transmitted during the guard interval:

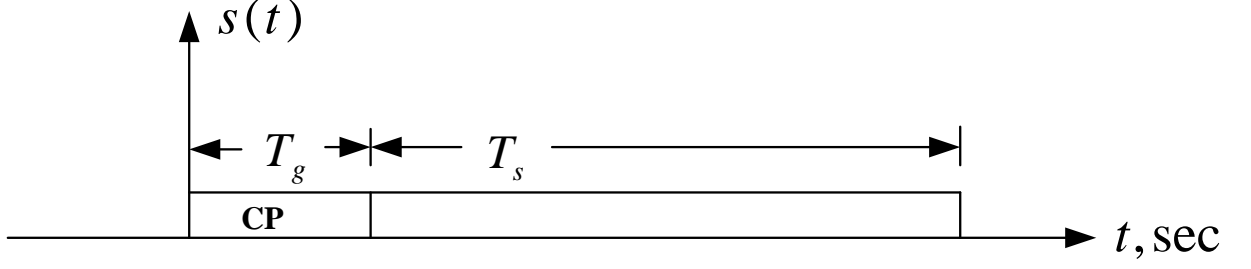


Figure 2.7: OFDM signal with Cyclic Prefix (CP)

$$s(t) = \sum_{k=0}^{N-1} C_k e^{j2\pi f_k(t+T_s)} = \sum_{k=0}^{N-1} C_k e^{j2\pi f_k t} e^{j2\pi k} = \sum_{k=0}^{N-1} C_k e^{j2\pi f_k t}, \quad (2.29)$$

$-T_g \leq t < 0$. It is noted that the above simplification is possible due to the periodicity of the signal. Thus the OFDM signal having a guard interval with cyclic prefix is given by

$$s(t) = \sum_{k=0}^{N-1} c_k e^{j2\pi f_k t}, \quad -T_g \leq t < T_s \quad (2.30)$$

The received signal can be written as:

$$\begin{aligned} r(t) &= s(t) * h(t) + n(t), \quad -T_g \leq t < T_s \\ &= \int_{-\infty}^{\infty} h(\tau) s(t - \tau) d\tau + n(t) \\ &= \int_0^{\tau_{max}} h(\tau) s(t - \tau) d\tau + n(t) \end{aligned} \quad (2.31)$$

where $h(t)$ is the time-invariant channel impulse response and $n(t)$ is the additive noise. The bounds of integration are simplified by assuming the channel is causal [$h(t) = 0$ for $t < 0$] and the maximum propagation delay τ_{max} [$h(t) = 0$ for $t > \tau_{max}$]. The received signal during the guard interval, refers interference from the previous block and is ignored and $r(t)$ during $0 \leq t < T_s$ is processed. An estimate of the p -th data symbol is made

by correlating $r(t)$ with the p -th subcarrier. That is

$$\hat{C}_p = \frac{1}{T_s} \int_0^{T_s} r(t) \left[e^{j2\pi f_p t} \right]^* dt, \quad (2.32)$$

By expanding (2.32), we get

$$\begin{aligned} \hat{C}_p &= \frac{1}{T_s} \int_0^{T_s} r(t) e^{-j2\pi f_p t} dt \\ &= \frac{1}{T_s} \int_0^{T_s} \left[\int_0^{\tau_{max}} h(\tau) \sum_{k=0}^{N-1} C_k e^{j2\pi f_k (t-\tau)} dt \right] e^{-j2\pi f_p t} dt + N_p \\ &= \frac{1}{T_s} \sum_{k=0}^{N-1} C_k \int_0^{\tau_{max}} h(\tau) e^{-j2\pi f_k \tau} dt \int_0^{T_s} e^{j2\pi t (f_k - f_p)} dt + N_p \end{aligned} \quad (2.33)$$

where

$$N_p = \frac{1}{T_s} \int_0^{T_s} n(t) e^{-j2\pi f_p t} dt. \quad (2.34)$$

Using the following observation,

$$\frac{1}{T_s} \int_0^{T_s} e^{j2\pi t (f_k - f_p)} dt = \begin{cases} 1, & k = p \\ 0, & k \neq p \end{cases} \quad (2.35)$$

equation (2.33) becomes

$$\hat{C}_p = C_p H[p] + N_p, \quad (2.36)$$

where

$$H[p] = \int_0^{\tau_{max}} h(\tau) e^{-j2\pi f_p \tau} d\tau, \quad (2.37)$$

which is $\mathcal{F}[h(t)]$ evaluated at $f = f_p$. This shows that the N received data symbols $[\hat{C}_0, \hat{C}_1, \dots, \hat{C}_{N-1}]$ are equal to the transmitted symbols $[C_0, C_1, \dots, C_{N-1}]$ scaled by the complex-valued channel gains $[H[0], H[1], \dots, H[N-1]]$. Thus, ISI is avoided since the k -th symbol isn't impacted by the $N-1$ other symbols. Therefore, using the guard

interval with cyclic prefix results in ISI-free operation. It can also be shown that by transmitting a signal other than the cyclic prefix during the guard interval results in ISI. Assume that the transmitted signal is

$$s(t) = \begin{cases} b(t), & -T_g \leq t < 0, \\ \sum_{k=0}^{N-1} C_k e^{j2\pi f_k t}, & 0 \leq t < T_s, \end{cases} \quad (2.38)$$

where $b(t) \neq \sum_{k=0}^{N-1} a_k e^{j2\pi f_k t}$. The estimate of the p -th data symbols is given by:

$$\begin{aligned} \hat{C}_p &= \frac{1}{T_s} \int_0^{T_s} r(t) e^{-j2\pi f_p t} dt \\ &= \frac{1}{T_s} \int_0^{T_s} \left[\int_0^{\tau_{max}} h(\tau) s(t - \tau) d\tau \right] e^{-j2\pi f_p t} dt + N_p \\ &= A_p + B_p + N_p. \end{aligned} \quad (2.39)$$

The regions of integration are separated into two segments, $[0, T_g]$ and $[T_g, T_s]$:

$$A_p = \frac{1}{T_s} \int_0^{T_g} \int_0^{\tau_{max}} h(\tau) s(t - \tau) e^{-j2\pi f_p t} d\tau dt, \quad (2.40)$$

and

$$B_p = \frac{1}{T_s} \int_{T_g}^{T_s} \int_0^{\tau_{max}} h(\tau) s(t - \tau) e^{-j2\pi f_p t} d\tau dt. \quad (2.41)$$

It is noted that A_p is a non-zero offset term and is a function of $b(t)$. For the second term, $t - \tau > 0$, therefore

$$\begin{aligned} B_p &= \frac{1}{T_s} \int_{T_g}^{T_s} \left[\int_0^{\tau_{max}} h(\tau) \sum_{k=0}^{N-1} C_k e^{j2\pi f_k (t - \tau)} d\tau \right] e^{-j2\pi f_p t} dt, \\ &= \frac{1}{T_s} \sum_{k=0}^{N-1} C_k \int_0^{\tau_{max}} h(\tau) e^{-j2\pi f_k \tau} d\tau \int_{T_g}^{T_s} e^{j2\pi t (f_k - f_p)} dt. \end{aligned} \quad (2.42)$$

The orthogonality condition in (2.35) is not applicable to (2.42), as regions of integration are different. The estimated data symbol can be expressed as

$$\hat{C}_p = C_p H_p K + N_p + ICI, \quad (2.43)$$

where $K = (T_s - T_g)/T_s$, and the interference term is

$$ICI = A_p + \frac{1}{T_s} \sum_{k \neq p} H[k] \int_{t_g}^{T_s} C_k e^{j2\pi t(f_k - f_p)} dt. \quad (2.44)$$

The quantity ICI in (2.44) represents the intercarrier interference. When the subcarriers are no longer orthogonal such an interference occurs. Such an interference can also result due to imperfect frequency synchronization. Therefore, ICI can manifest itself in more than one way, and when it does the data symbols interfere with one another resulting in ISI.

2.4 PAPR Statistics of OFDM Signals

2.4.1 Definition of PAPR

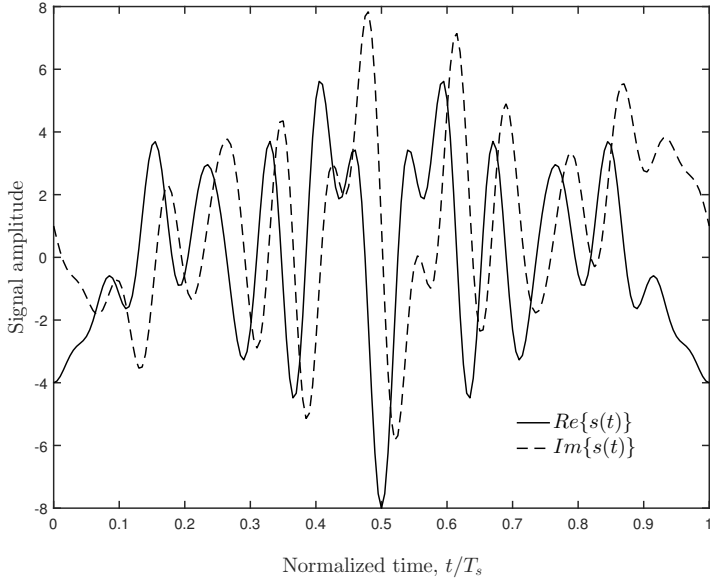
The complex baseband representation of an OFDM signal consisting of N subcarriers is given by (2.5). The signal can be thought of as the sum of independent signals modulated onto subchannels of equal bandwidth. That is,

$$s(t) = \sum_{k=0}^{N-1} C_k e^{j2\pi k \Delta f t}, \quad 0 \leq t \leq T_s \quad (2.45)$$

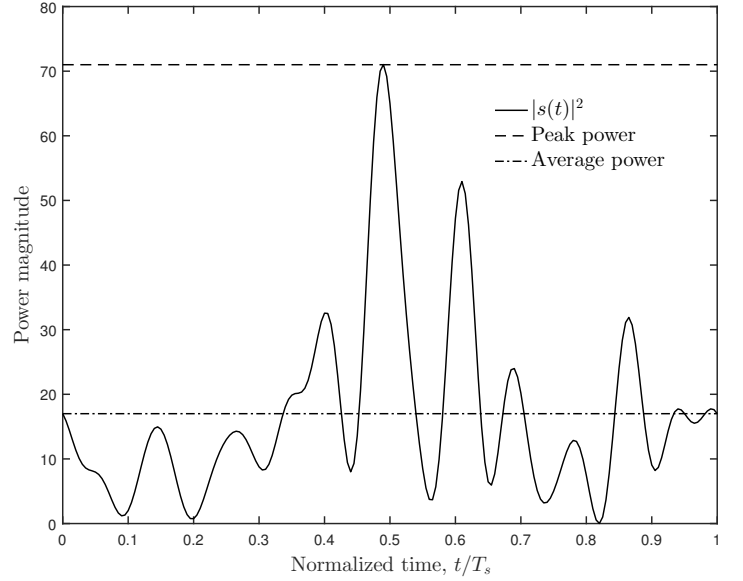
where $j = \sqrt{-1}$, $\Delta f = \frac{1}{T_s} = \frac{1}{NT_b}$ is the subcarrier spacing, and $T_s = NT_b$ is the OFDM symbol duration. Using (2.8)-(2.10), the instantaneous signal power can be written as:

$$|s(t)|^2 = s_I^2(t) + s_Q^2(t) \quad (2.46)$$

where $s_I(t)$ and $s_Q(t)$ are given by (2.11) and (2.12), respectively. In Figs. 2.8 (a), 2.9 (a), and 2.10 (a), $s_I(t)$ and $s_Q(t)$ are plotted for OFDM signals, for these different sets



(a) Signal amplitude.



(b) Signal power.

Figure 2.8: OFDM signal ($N = 16$) for the data sequence $[C_0, C_1, \dots, C_{15}]$

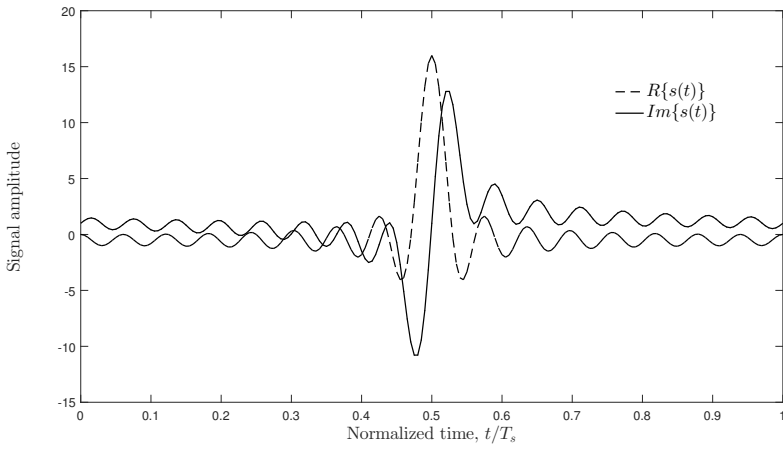
of $\{C_k\}$, with BPSK mapper for $N = 16$ subcarriers. The corresponding instantaneous signal power of OFDM signals given by (2.46) and their average powers are plotted in Figs. 2.8 (b), 2.9 (b), and 2.10 (b) for the same three different data sequences. The ratio of peak power and its average power of the signal shown in Fig. 2.8 is $71/17 = 4.2$. Typically, the PAPR is expressed in decibels. That is,

$$PAPR_{dB} = 10 \log_{10} PAPR \quad (2.47)$$

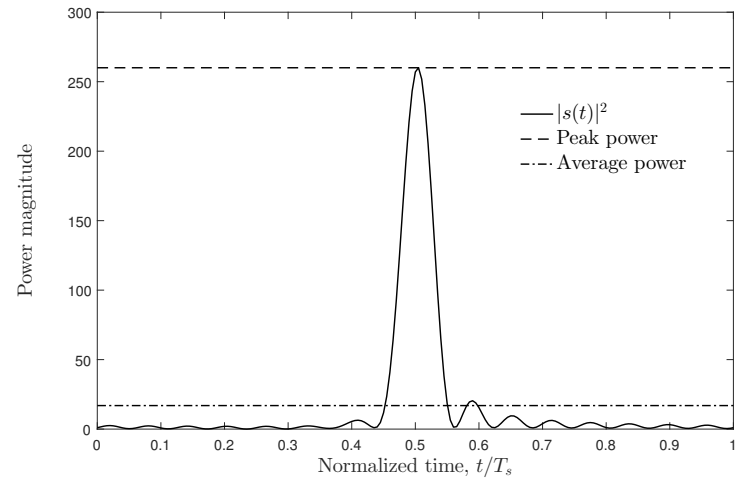
For the example shown in Fig. 2.8, the PAPR in decibels is equal to $10 \log_{10} 4.2 \approx 6.2dB$. It is observed from Figs. 2.8 - 2.10 that PAPR is a function of: i) number of subcarriers, N ; ii) the data sequence, $[C_0, C_1, \dots, C_{N-1}]$ and iii) the mapper used in the system. Since the data sequence is a random quantity, PAPR is also a random variable. The PAPR of the transmitted OFDM signal $s(t)$ is thus defined as

$$PAPR = \frac{\max_{0 \leq t \leq T_s} \{|s(t)|^2\}}{\frac{1}{T_s} \int_0^{T_s} |s(t)|^2 dt} \quad (2.48)$$

The computation of PAPR using (2.48) can be approximated by using equidistant samples

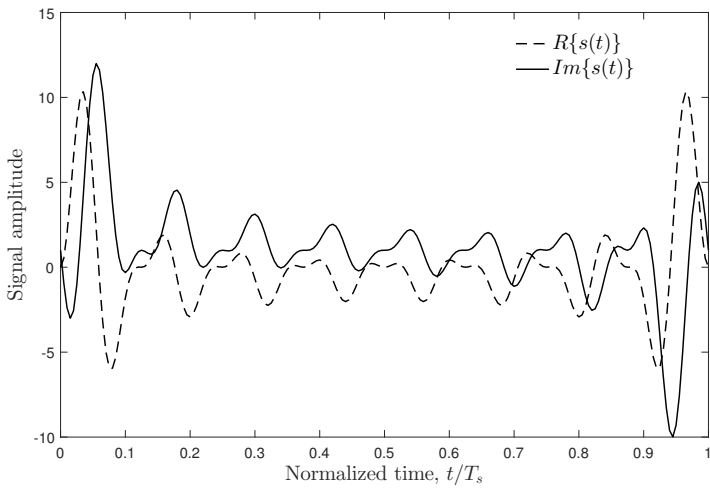


(a) Signal amplitude.

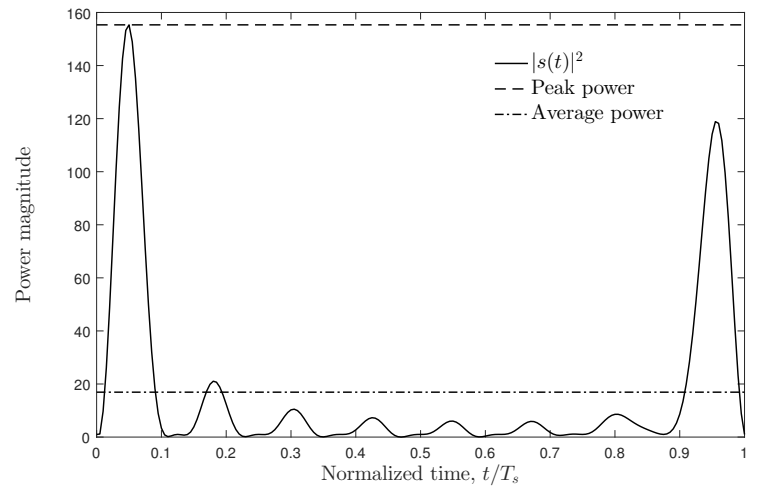


(b) Signal power.

Figure 2.9: OFDM signal ($N = 16$) for the data sequence $[C_0, C_1, \dots, C_{15}]$



(a) Signal amplitude.



(b) Signal power.

Figure 2.10: OFDM signal ($N = 16$) for the data sequence $[C_0, C_1, \dots, C_{15}]$

of $s(t)$. The reasons for using this approach for computation of PAPR are: i) most systems are implemented in discrete-time; ii) computation of PAPR in continuous-time is too complex as closed-form expression is difficult to arrive at; and iii) when an oversampling rate of four times that of Nyquist rate is used, it closely approximates continuous-time PAPR given by (2.48). Therefore, the approach used in this thesis is that of discrete-time approximation of continuous-time PAPR. When Nyquist rate of sampling is used, it is observed that

$$s(nT_b) = D_n = \sum_{k=0}^{N-1} C_k e^{j2\pi \frac{kn}{N}}, \quad n = 0, 1, \dots, N-1 \quad (2.49)$$

Using (2.49), the PAPR of the OFDM signal $s(t)$ is given by

$$PAPR = \frac{\max \left\{ |D_n|^2, n = 0, 1, \dots, N-1 \right\}}{\frac{1}{N} \sum_{n=0}^{N-1} |D_n|^2} \quad (2.50)$$

When the sampling rate is L times that of the Nyquist rate, the samples of $s(t)$ are given by

$$s\left(\frac{nT_b}{L}\right) = D_n = \sum_{k=0}^{N-1} C_k e^{j2\pi \frac{kn}{NL}}, \quad n = 0, 1, \dots, NL-1 \quad (2.51)$$

It is noted that the vector $[D_0, D_1, \dots, D_{NL-1}]$ can be viewed as the IFFT of data vector $[C_0, C_1, \dots, C_{N-1}]$ with $(L-1)N$ padded zeros. Thus, the PAPR computed using L times oversampled continuous-time signal is given by

$$PAPR = \frac{\max \left\{ |D_n|^2, n = 0, 1, \dots, NL-1 \right\}}{\frac{1}{NL} \sum_{n=0}^{NL-1} |D_n|^2} \quad (2.52)$$

In the thesis (2.52) is used for computation of PAPR of OFDM signals with $L = 4$.

2.4.2 Complementary Cumulative Distribution Function

The PAPR given by (2.52) is a random variable and is typically expressed in decibels using (2.47). The Cumulative Distribution Function (CDF) can be used to understand the statistical properties of PAPR. However, in the literature, the Complementary Cumulative Distribution Function (CCDF) is commonly used instead of CDF and denotes

the probability that the PAPR of a data block exceeds a given threshold value of PAPR, denoted as $PAPR_0$. The CCDF is used to measure the PAPR performance for a given arbitrary mapper in an OFDM system. Also, it is used to measure performance of PAPR reduction techniques. An approximate expression for the PAPR of an OFDM signal with large number of subcarriers can be derived by noting that the real and imaginary parts of $s(t)$ given by (2.11) and (2.12), respectively, are Gaussian distributed by virtue of Central Limit Theorem (CLT), with mean equal to zero and variance of $1/2$. Hence, the magnitude of $s(t)$ is Rayleigh distributed and its power is Central Chi-square distributed with two degrees of freedom. Thus, the CDF of the magnitude of signal sample is given by

$$P_{PAPR}(PAPR) = 1 - \exp(-PAPR) \quad (2.53)$$

The corresponding CCDF of PAPR of a data block with Nyquist rate of sampling can be shown to be given by

$$P_r(PAPR > PAPR_0) = 1 - P_r(PAPR \leq PAPR_0) \quad (2.54)$$

Using (2.53) in (2.54), we get

$$P_r(PAPR > PAPR_0) = 1 - (1 - \exp(-PAPR_0))^N \quad (2.55)$$

The expression in (2.55) assumes that the N time-domain samples of $s(t)$ are independent and uncorrelated and N is large. It is noted that the CCDF given by (2.55) is not accurate when: i) the number of subcarriers, N , is small and ii) the signal is oversampled. In Fig. 2.11 are shown CCDFs of OFDM signal for $N = 16, 32, 64$, and 128 for BPSK mapper with an oversampling factor $L = 4$.

2.4.3 Impact of PAPR on System Performance

The high PAPR associated with OFDM signals requires system components with large linear range capable of accommodating the entire signal in order to avoid nonlinear distortion and hence degradation of system performance. One of the nonlinear devices in an OFDM system is the Power Amplifier (PA) at the transmitter. The input-output

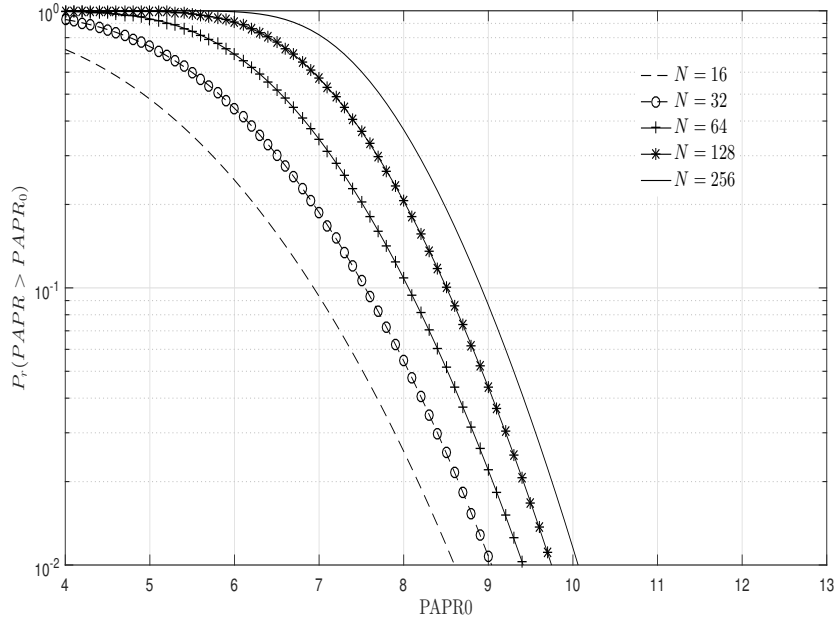


Figure 2.11: CCDFs of PAPR of OFDM signals for $N = 16, 32, 64, 128,$ and 256 for BPSK mapper and an oversampling factor $L = 4$.

characteristic of a typical PA is shown in Fig. 2.12. Ideally, the output of power amplifier is equal to the input times a gain factor. However, in reality the PA has a limited linear range, beyond which it saturates to a maximum output level as shown in Fig. 2.12. In the linear region the curve matches the ideal characteristic of PA, but as the input power level increases the PA saturates. The most efficient operating point is at the PA's saturation point (shown as the 'Optimum' point in Fig. 2.12), but for OFDM signal with large PAPR, the operating point must shift to the left (shown as the 'Actual' point in Fig. 2.12) for linear amplification of the signal. Thus, the average input power is reduced and as a consequence Input Power backOff (IBO) is required. In order to keep the peak power of the input signal less than or equal to the saturation input power level, the IBO must be chosen to be at least equal to the PAPR of the OFDM signal. For example, for the signal shown in Fig. 2.8, the required IBO is equal to 6.2 dB. This essentially reduces the efficiency of the PA and is detrimental to the operation of mobile devices using battery-powered energy sources. Hence, it is necessary to adopt some PAPR reduction techniques for the OFDM signal before applying it to a nonlinear device such as the power amplifier.

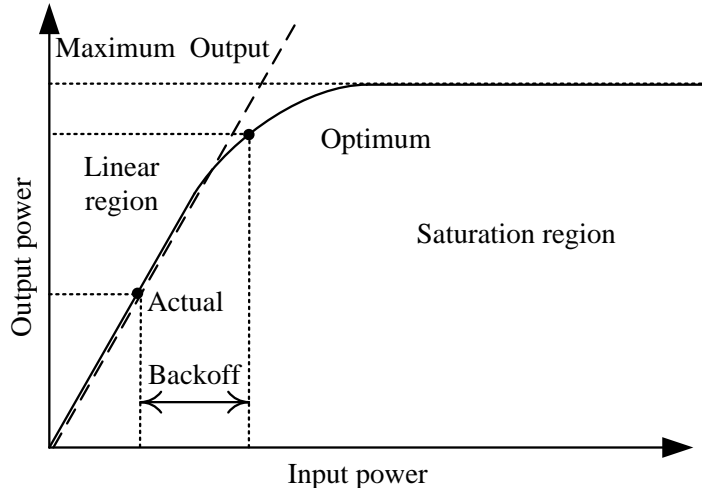


Figure 2.12: Transfer function of typical power amplifier.

2.4.4 PAPR Reduction Techniques

In this Section three PAPR reduction techniques are briefly described. These techniques will be used in the thesis for OFDM systems with g-CPFSK mapper.

2.4.4.1 Clipping and Filtering (CF) Technique

The simplest technique for PAPR reduction is amplitude clipping [60] which limits the peak envelope of the OFDM signal to a predetermined value or otherwise passes the signal unaltered [61]. The OFDM signal given by (2.5) is, in general, complex. The output of the amplitude clipper, thus, can be written as:

$$B(x) = \begin{cases} x, & |x| \leq A \\ Ae^{j\phi(x)}, & |x| > A, \end{cases} \quad (2.56)$$

where $|x|$ and $\phi(x)$ are the magnitude and phase of x , respectively. The input x to the clipper is the sampled value of $s(t)$ given by $x = s(t_i), i = 0, 1, \dots, LN - 1$. The distortion caused by amplitude clipping is a source of noise and falls both in-band and out-of-band of the signal. The distortion caused by in-band noise cannot be reduced by filtering and results in an error performance degradation. The out-of-band radiation reduces the spectral efficiency of the system. Filtering after clipping can be used to reduce out-of-band radiation but may cause the output signal level exceed the clipping level at

some points. To reduce overall peak regrowth, a repeated clipping-and-filtering operation can be used [8], [39]. Another way to compensate for the performance degradation from clipping is to reconstruct the clipped samples based on samples obtained using oversampled signals. In [62] oversampled signal reconstruction is used to compensate for signal-to-noise ratio (SNR) degradation due to clipping for low values of clipping threshold. The clipping ratio, CR , is termed as a ratio of the clipping level to the root mean square of the clipped signal. the the optimum value of clipping ratio used in this technique is $CR = 0.25$. Next, clipping is followed by filtering to mitigate out-of-band power, which causes some peak regrowth.

2.4.4.2 Selective Mapping (SLM) Technique

In the SLM technique, at the transmitter a set of sufficiently different candidate data blocks, all representing the original data block $C = [C_0, C_1, \dots, C_{N-1}]$ are generated, and the most favourable among these is selected for transmission [46], [63]. The block diagram of the SLM technique is shown in Fig. 2.13.

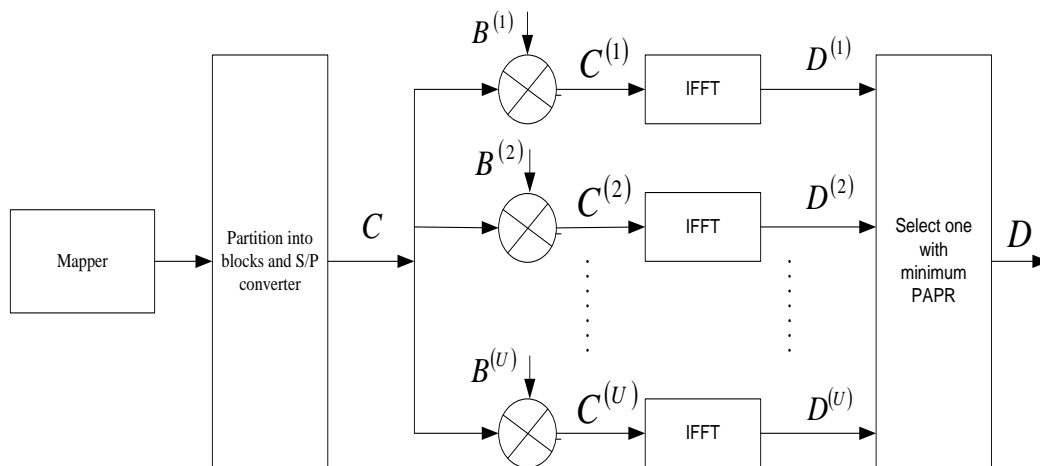


Figure 2.13: Block diagram of the SLM technique

The data block $C = [C_0, C_1, \dots, C_{N-1}]$ is multiplied by U different phase sequences, each of length N , $B^{(u)} = [b_{u,0}, b_{u,1}, \dots, b_{u,N-1}]^T$, $u = 1, 2, \dots, U$, resulting in U modified data blocks $C^{(1)}, C^{(2)}, \dots, C^{(U)}$. The phase sequence $B^{(1)}$ is set to as all-one vector of length N . Thus, the modified data block for the u -th phase sequence is given by

$C^{(u)} = [C_0 b_{u,0}, C_1 b_{u,1}, \dots, C_{N-1} b_{u,N-1}]$, $u = 1, 2, \dots, U$. These are then fed to IFFT blocks to obtain $D^{(u)} = [D_0^{(u)}, D_1^{(u)} \dots, D_{N-1}^{(u)}]$, $u = 1, 2, \dots, U$, where

$$D_k^{(u)} = \sum_{n=0}^{N-1} C_n b_{u,n} e^{j2\pi \frac{kn}{N}}, k = 0, 1, \dots, N-1, \quad (2.57)$$

The PAPR of each of the modified data blocks $C^{(u)}$ is then computed. Among the modified data blocks $C^{(u)}$, $u = 1, 2, \dots, U$, the one with the lowest PAPR, say $C^{(k)}$, is selected for transmission. The transmitted signal can be written as:

$$s^{(k)}(t) = \sum_{n=0}^{N-1} C_n b_{k,n} e^{j2\pi f_k t}, 0 \leq t \leq NT_b \quad (2.58)$$

Information about the selected phase sequence k should be transmitted to the receiver as side information. At the receiver, the reverse operation is performed to recover the original data block. For implementation, the SLM technique needs U IFFT operations, and the number of required side information bits to be transmitted is $\log_2 U$ for each data block. This approach is applicable with all types of mapper and any number of subcarriers. The amount of PAPR reduction for SLM depends on the number of phase sequences U and the design of the phase sequences. An example of the SLM technique for an OFDM system with BPSK mapper and eight subcarriers is given below. Let the number of phase sequences be $U = 4$ and data block to be transmitted be $C = [1, 1, -1, 1, 1, 1, -1, 1, -1]$ whose PAPR before applying SLM is 6.5 dB. Suppose the four phase sequence be $B^{(1)} = [1, 1, 1, 1, 1, 1, 1, 1]$, $B^{(2)} = [-1, -1, 1, 1, 1, 1, 1, -1]$, $B^{(3)} = [-1, 1, -1, 1, -1, 1, 1, 1]$, and $B^{(4)} = [1, 1, -1, 1, 1, -1, 1, 1]$. Among the four modified data blocks $C^{(u)}$, $u = 1, 2, 3, 4$, $C^{(2)}$, has the lowest PAPR of 3.0 dB. Hence, $C^{(2)}$ is selected and transmitted to the receiver. For this data block, the PAPR is reduced from 6.5 to 3.0 dB, resulting in a 3.5 dB reduction. In this case, the number of IFFT operations is 4 and the amount of side information is $\log_2 4 = 2$ bits. The amount of PAPR reduction may vary from data block to data block, but PAPR reduction is possible for all data blocks. The complexity of this technique is a function of U and must be chosen appropriately.

2.4.4.3 Partial Transmit Sequence (PTS) Technique

In this technique, an input data block of N symbols is partitioned into disjoint subblocks. The subcarriers in each subblock are weighted by a phase factor for that subblock. The phase factors are selected such that the PAPR of the combined signal is minimized. Fig. 2.14. shows the block diagram of the PTS technique.

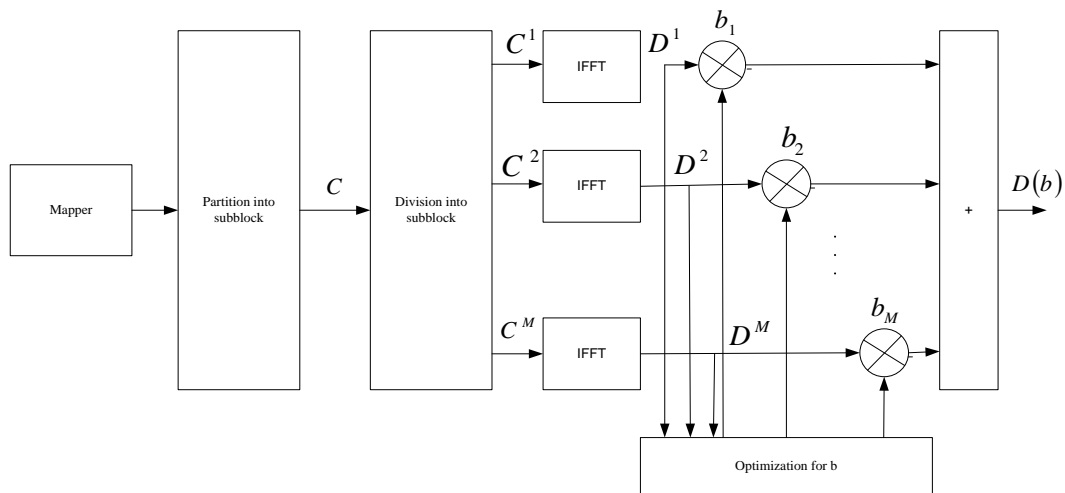


Figure 2.14: Block diagram of the PTS technique

In the PTS technique [64], [65] input data block $C = [C_0, C_1, \dots, C_{N-1}]$ is partitioned into M disjoint subblocks $C^m = [C_{m,0}, C_{m,1}, \dots, C_{m,N-1}]$, $m = 1, 2, \dots, M$, such that $\sum_{m=1}^M C^m = C$ and the subblocks are then combined to minimize the PAPR in the time-domain. The L -times oversampled time domain signals $D^m = [D_{m,0}, D_{m,1}, \dots, D_{m,N-1}]$, $m = 1, 2, \dots, M$, are obtained by taking an IFFT of length NL on C^m concatenated with $(L-1)N$ zeros, that is, $C^m = [C_{m,0}, C_{m,1}, \dots, C_{m,N-1}, 0, 0, \dots, 0]$. These D^m s are called the partial transmit sequences. Complex phase factors $b_m = e^{j\phi_m}$, $m = 1, 2, \dots, M$, are then introduced to combine these sequences. The set of phase factors is denoted as a vector $b = [b_1, b_2, \dots, b_M]$. The time domain signal after combining is given by

$$D(b) = \sum_{m=1}^M D^m b_m, \quad (2.59)$$

where $D^m = \text{IFFT}\{C^m\}$. The objective is to find b that minimizes the PAPR. In general, the selection of the phase factors is limited to a set with a finite number of elements to reduce the search complexity. The set of allowed phase factors is written

as $\left\{ e^{j\frac{2\pi l}{W}}, l = 0, 1, \dots, (W - 1) \right\}$, where W is the number of allowed phase factors. In addition, we can set $b_1 = 1$ without any loss of performance. So, we should perform an exhaustive search for $(M - 1)$ phase factors. Hence, W^{M-1} sets of phase factors are searched to find the optimum set of phase factors. The search complexity increases exponentially with the number of subblocks M . PTS needs M IFFT operations for each data block, and the number of required side information bits is $\lceil \log_2 W^{M-1} \rceil$, where $\lceil y \rceil$ denotes the smallest integer that does not exceed y . The amount of PAPR reduction depends on the number of subblocks M and the number of allowed phase factors W . Another factor that may affect the PAPR reduction performance in PTS is the subblock partitioning, which is the method of division of the subcarriers into multiple disjoint subblocks. There are three kinds of subblock partitioning schemes: adjacent, interleaved, and pseudo-random partitioning [65]. Among them, pseudo-random partitioning has been found to be the best choice. The PTS technique works for an arbitrary number of subcarriers and any mapping scheme in an OFDM system. To reduce the search complexity, various techniques have been suggested. In [66], iterations for updating the set of phase factors are stopped once the PAPR drops below a preset threshold. An example of the PTS technique is given next.

Consider an OFDM system with eight subcarriers ($N = 8$) that are divided into four subblocks ($M = 4$). The phase factors are selected from the set $\left\{ e^{j\frac{2\pi l}{2}}, l = 0, 1 \right\} = \{+1, -1\}$. It is noted that number of those factors $W = 2$. The adjacent subblock partitioning for a data block $C = [1, -1, 1, -1, 1, -1, -1, -1]$ of length 8 are $C^1 = [1, -1, 0, 0, 0, 0, 0, 0]$, $C^2 = [0, 0, 1, -1, 0, 0, 0, 0]$, $C^3 = [0, 0, 0, 0, 1, -1, 0, 0]$, and $C^4 = [0, 0, 0, 0, 0, 0, -1, -1]$. The original data block C has a PAPR of 6.5 dB. There are $8 (= 2^{4-1})$ ways to combine the subblocks with fixed $b_1 = 1$. Among them $[b_1, b_2, b_3, b_4] = [1, -1, -1, -1]$ achieves the lowest PAPR. The modified data block will be $C' = \sum_{m=1}^M b_m C^m = [1, -1, -1, 1, -1, 1, 1, 1]$ whose PAPR is 2.2 dB, resulting in a 4.3 dB reduction. In this case, the number of required IFFT operations is 4 and the amount of side information required to be transmitted is 3 bits. This side information must be transmitted to the receiver to recover the original data block. One way to do this is to transmit these side information bits with a separate channel other than the data channel. It is also possible to include the side information within the data block; however, this results in data rate loss.

2.5 Conclusions

In this Chapter, fundamentals of an OFDM system relevant to the thesis are presented. In particular, a system block diagram consisting of transmitter, channel, and receiver is presented and explained. The concepts of Cyclic Prefix and PAPR are sketched in details. Also, three PAPR reduction techniques are explained with examples. Statistical descriptions of channel models used in the thesis are given.

Chapter 3

OFDM System with g-CPFSK Mapper

3.1 Introduction

In this Chapter, a class of mapper called g-CPFSK mapper that permits systematic correlation among transmitted OFDM symbols is introduced. The output of such a mapper is described in terms of input data and a set of parameters $H_K = \{h_1, h_2, \dots, h_k\}$ of the mapper. Three subclasses of g-CPFSK mapper namely single- h CPFSK, multi- h CPFSK, and asymmetric multi- h CPFSK mappers are identified, based on the manner in which H_K is used, described, and illustrated. These mappers are examined for their properties using state, trellis, and tree diagrams. The resulting OFDM signals are mathematically described.

3.2 Description of g-CPFSK Mapper

Consider the block diagram shown in Fig. 3.1 The serial bit stream $a_i (\pm 1), i = 1, 2, \dots$

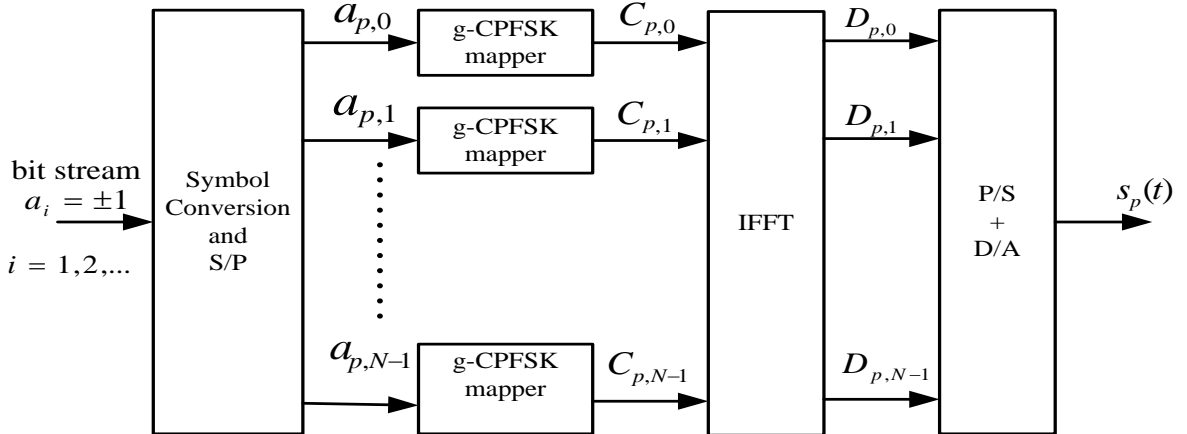


Figure 3.1: Block diagram of OFDM system with g-CPFSK mapper (Transmitter)

with bit duration of T_b seconds is converted into blocks of N symbols $[a_{p,0}, a_{p,1}, \dots, a_{p,N-1}]$, $p =$

$1, 2, \dots$, where p denotes the OFDM symbol number. The symbols entering g-CPFSK mappers during the first n OFDM symbols can be written as:

$$\begin{bmatrix} a_{1,0} & a_{2,0} & a_{3,0} & \cdots & a_{n,0} \\ a_{1,1} & a_{2,1} & a_{3,1} & \cdots & a_{n,1} \\ \vdots & \vdots & \vdots & \cdots & \vdots \\ a_{1,N-1} & a_{2,N-1} & a_{3,N-1} & \cdots & a_{n,N-1} \end{bmatrix} \quad (3.1)$$

For binary 2-ary g-CPFSK mapper, the elements of the matrix in (3.4) take values ± 1 and, in general, for M-ary g-CPFSK mapper, the elements in (3.4) can take values $\pm 1, \pm 3, \dots, \pm (M - 1)$. The g-CPFSK mapper transforms the incoming data $a_{p,q}$, $p = 1, 2, \dots, q = 0, 1, \dots, N - 1$ into complex numbers $C_{p,q}$ given by

$$C_{p,q} = \exp(j\theta_{p,q}) \quad (3.2)$$

where

$$\theta_{j,q} = \begin{cases} a_{j,q}\pi h_{[j]} + \pi \sum_{l=1}^{j-1} h_{[l]} a_{l,q}, & j > 1 \\ a_{1,q}\pi h_{[1]}, & j = 1 \end{cases} \quad (3.3)$$

and $1 \leq j \leq n$, where $h_{[j]}$ denotes the value of h used during the $j - th$ symbol interval from the set $H_K = \{h_1, h_2, \dots, h_k\}$. The manner in which $h_{[j]}$ s are chosen results in three subclasses of g-CPFSK mapper. It is noted that in response to data in (3.4). The phases $\theta_{p,q}$ are given by

$$\begin{bmatrix} \theta_{1,0} & \theta_{2,0} & \theta_{3,0} & \cdots & \theta_{n,0} \\ \theta_{1,1} & \theta_{2,1} & \theta_{3,1} & \cdots & \theta_{n,1} \\ \vdots & \vdots & \vdots & \cdots & \vdots \\ \theta_{1,N-1} & \theta_{2,N-1} & \theta_{3,N-1} & \cdots & \theta_{n,N-1} \end{bmatrix} \quad (3.4)$$

For example, along the subcarrier '0' the phases are given by:

$$\begin{aligned}
\theta_{1,0} &= a_{1,0}\pi h_{[1]}, \quad 0 \leq t \leq T \\
\theta_{2,0} &= a_{2,0}\pi h_{[2]} + a_{1,0}\pi h_{[1]}, \quad T \leq t \leq 2T \\
\theta_{3,0} &= a_{3,0}\pi h_{[3]} + a_{2,0}\pi h_{[2]} + a_{1,0}\pi h_{[1]}, \quad 2T \leq t \leq 3T \\
&\vdots \\
\theta_{i,0} &= a_{i,0}\pi h_{[i]} + \pi \sum_{l=1}^{i-1} a_{l,0}h_l, \quad (i-1)T \leq t \leq iT
\end{aligned}$$

where T is the OFDM symbol duration. For binary g-CPFSK mapper $T = NT_b$ and for M-ary CPFSK mapper $T = (\log_2 M) NT_b$, where N denotes the number of subcarriers in the system. It is observed that along subcarrier '0', the phase during the i -th symbol is a function of data during that symbol $a_{i,0}$ and also the data during the past $(i-1)$ symbols given by $a_{1,0}, a_{2,0}, \dots, a_{i-1,0}$. Using (3.3) in (3.2), the complex numbers produced by the g-CPFSK mappers are given by:

$$\begin{bmatrix} C_{1,0} & C_{2,0} & C_{3,0} & \cdots & C_{n,0} \\ C_{1,1} & C_{2,1} & C_{3,1} & \cdots & C_{n,1} \\ \vdots & \vdots & \vdots & \cdots & \vdots \\ C_{1,N-1} & C_{2,N-1} & C_{3,N-1} & \cdots & C_{n,N-1} \end{bmatrix} \quad (3.5)$$

Where each column in the matrix denotes the set of complex numbers fed parallelly to IFFT block during each symbol interval. The resulting transmitted OFDM signal after P/S conversion and ADC can be written as:

$$s(t) = \sum_{p=1}^n \sum_{q=0}^{N-1} C_{p,q} e^{j2\pi f_q t}, \quad 0 < t < nT. \quad (3.6)$$

The three subclasses of g-CPFSK mapper are explained next.

3.3 Single- h CPFSK Mapper

In the case of binary single- h CPFSK mapper a single value of $h = h_{[1]} = h_{[2]} = \dots$ is chosen, which implies that for every OFDM symbol, the value of h used is the same.

Therefore (3.3) becomes

$$\theta_{j,q} = \begin{cases} a_{j,q}\pi h + \pi h \sum_{l=1}^{j-1} a_{l,q}, & j > 1 \\ a_{1,q}\pi h, & j = 1 \end{cases} \quad (3.7)$$

The choice of h determines the number of phase states in the mapper. Consider the symbols along the $k - th$ subcarrier, $a_{1,k}, a_{2,k}, \dots, a_{n,k}$, where $a_{i,k} = \pm 1$ for $i = 1, 2, \dots, n$. The number of possible phase states for $\theta_{j,q}$ are given by (3.7). For example, when $h = \frac{1}{2}, \frac{2}{3}$, and $\frac{1}{4}$ the number of phases would be 4, 3, and 8, respectively, since phase is modulo 2π . When the parameter h used in the single- h CPFSK mapper is a ratio of two integers P and Q , i.e, $h = P/Q$, where P and Q are integers, the number of phase states of $\theta_{j,q}$ for the case of P even is be given by the set:

$$\left\{ 0, \frac{\pi P}{Q}, \frac{2\pi P}{Q}, \dots, \frac{(Q-1)\pi P}{Q} \right\} \quad (3.8)$$

and for the case of P odd it is given by the set:

$$\left\{ 0, \frac{\pi P}{Q}, \frac{2\pi P}{Q}, \dots, \frac{(2Q-1)\pi P}{Q} \right\} \quad (3.9)$$

Thus, there are Q terminal phase states when P is even and $2Q$ states when P is odd. Fig 3.2 shows the phase constellation diagrams for single- h CPFSK mappers for $h = 1/2, 1/4$ and $2/3$. Table 3.1. shows the possible phase states for these values of h .

Table 3.1: Number of possible phase states for single- h CPFSK mapper for $h = \frac{1}{2}$, $h = \frac{2}{3}$, and $h = \frac{1}{4}$

$h = \frac{P}{Q}$	$\theta_{j,q}$
$\frac{1}{2}$	$0, \frac{\pi}{2}, \pi, \frac{3\pi}{2}$
$\frac{2}{3}$	$0, \frac{2\pi}{3}, \frac{4\pi}{3}$
$\frac{1}{4}$	$0, \frac{\pi}{4}, \frac{\pi}{2}, \frac{3\pi}{4}, \pi, \frac{5\pi}{4}, \frac{3\pi}{2}, \frac{7\pi}{4}$

The state trellis diagram for binary single- h CPFSK mapper for $h = \frac{1}{2}$ is shown in Fig. 3.3. It is noted that the phase transitions from one state to another are not true phase transitions but they represent phase transitions from one terminal state to another. In Fig. 3.4 is shown the state trellis diagram for binary single- h CPFSK mapper for $h = \frac{1}{4}$. An alternative representation to the state trellis is state diagram which illustrates the

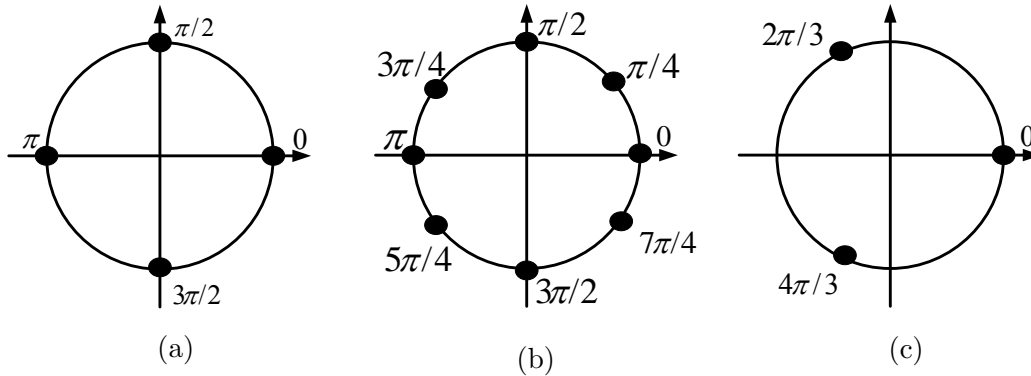


Figure 3.2: Phase constellation diagrams for binary single- h CPFSK mapper: (a) $h = 1/2$, (b) $h = 1/4$, and (c) $h = 2/3$.

possible phase transitions from one state to another. In Figs. 3.5, 3.6, and 3.7 are shown state diagrams for binary single- h CPFSK mapper for $h = \frac{1}{2}$, $h = \frac{2}{3}$, and $h = \frac{1}{4}$, respectively. Figs. 3.8 to 3.10 show paths through phase trellis as a function of symbol time for binary single- h CPFSK mapper for an arbitrary data sequence $[+1, -1, -1, +1]$ for $h = \frac{1}{2}, \frac{1}{4}$ and $\frac{2}{3}$, respectively.

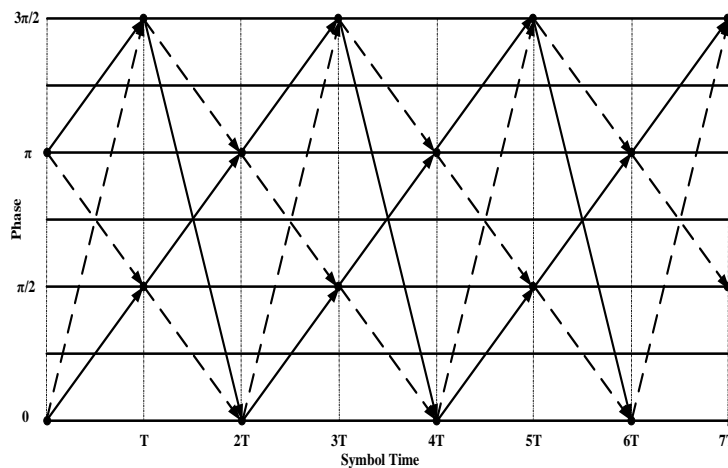


Figure 3.3: State trellis diagram for binary single- h CPFSK mapper for $h = 1/2$. $a_{j,q} = -1$ (dashed) and $a_{j,q} = +1$ (solid)

3.3.1 Multi- h CPFSK Mapper

In the case of single- h CPFSK mapper, the parameter h is the same for all symbols. However, when h is varied from symbol to symbol one obtains a class of mappers referred

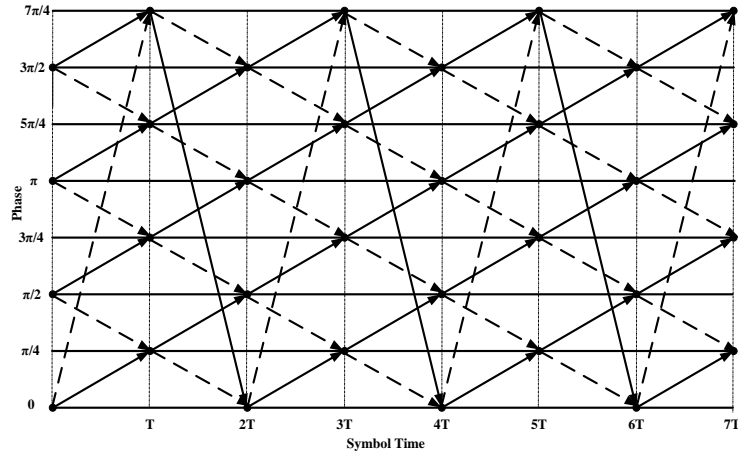


Figure 3.4: State trellis diagram for binary single- h CPFSK mapper for $h = 1/4$. $a_{j,q} = -1$ (dashed) and $a_{j,q} = +1$ (solid)

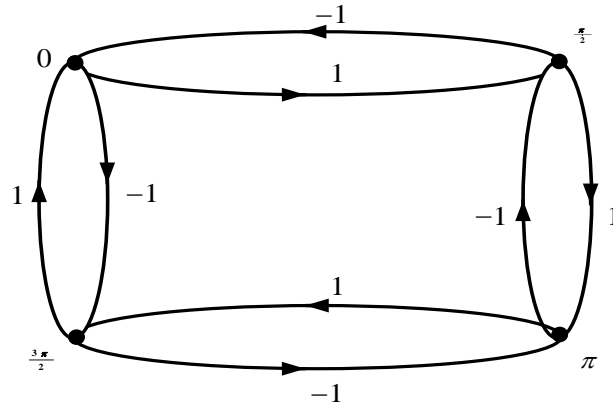


Figure 3.5: State diagram for binary single- h CPFSK mapper for $h = 1/2$.

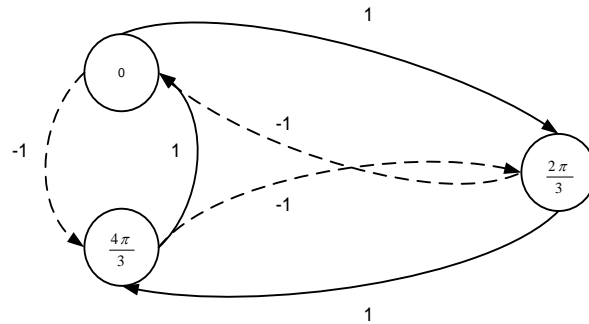


Figure 3.6: State diagram for binary single- h CPFSK mapper for $h = 2/3$. $a_{j,q} = -1$ (dashed) and $a_{j,q} = +1$ (solid)

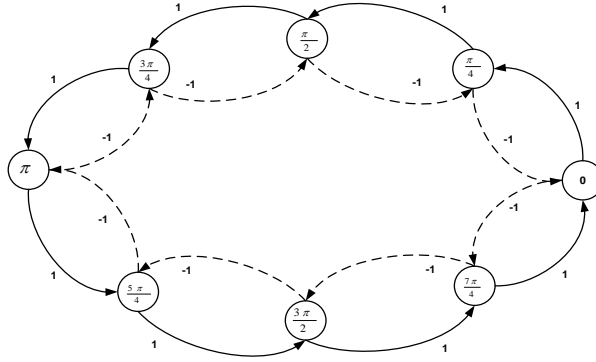


Figure 3.7: State diagram for binary single- h CPFSK mapper for $h = 1/4$. $a_{j,q} = -1$ (dashed) and $a_{j,q} = +1$ (solid)

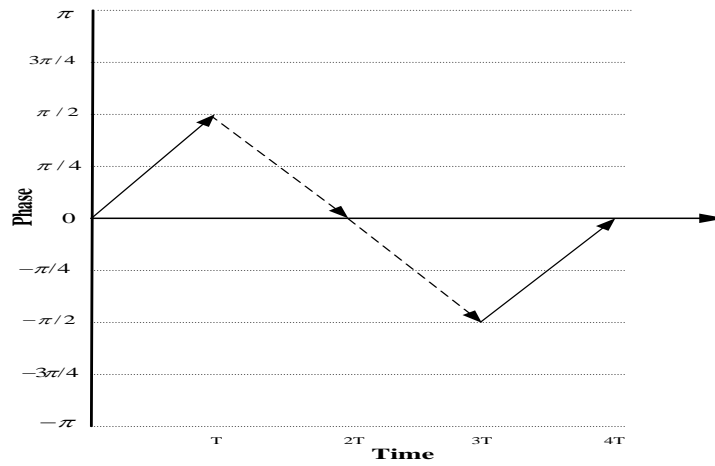


Figure 3.8: Path through the phase trellis as a function of symbol time for binary single- h CPFSK mapper for $h = 1/2$ for an arbitrary data sequence $[+1, -1, -1, +1]$. $a_{j,q} = -1$ (dashed) and $a_{j,q} = +1$ (solid)

to as multi- h CPFSK mapper. The complexity of this class of mappers depend on the set H_K employed. In multi- h CPFSK mapper, h is cyclicly chosen from set $H_K = \{h_1, h_2, \dots, h_K\}$, where K denotes the number of h values. The modulation index used in the first symbol is $h_{[1]} = h_1$, in the second symbol it is $h_{[2]} = h_2$ and so on until $h_{[K]} = h_K$ during the $K - th$ symbol. In the $(K + 1) - th$ symbol the modulation index used is $h_{[K+1]} = h_1$ and so on until $h_{[K+K]} = h_K$. That is

$$h_{[i]} = h_{[i+K]} = h_{[i+2K]} = \dots \quad (3.10)$$

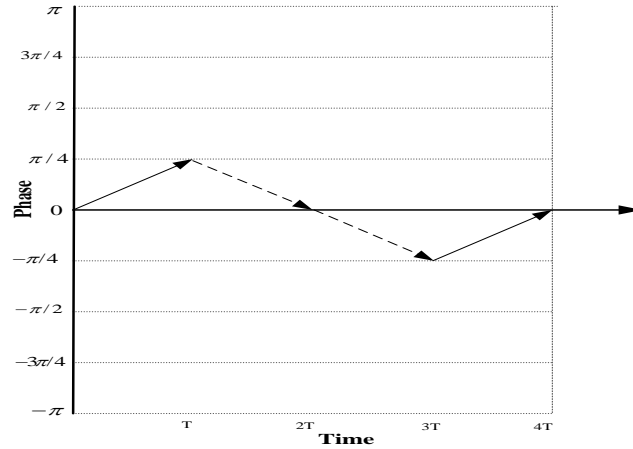


Figure 3.9: Path through the phase trellis as a function of symbol time for binary single- h CPFSK mapper for $h = 1/4$ for an arbitrary data sequence $[+1, -1, -1, +1]$. $a_{j,q} = -1$ (dashed) and $a_{j,q} = +1$ (solid)

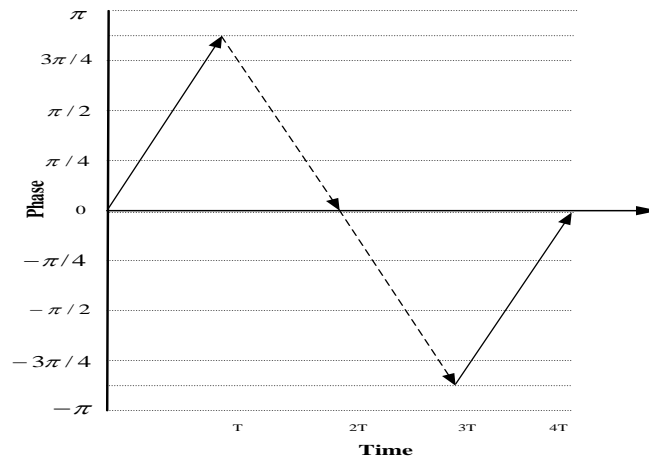


Figure 3.10: Phase transitions as a function of symbol time for binary single- h CPFSK mapper for $h = 2/3$ for an arbitrary data sequence $[+1, -1, -1, +1]$. $a_{j,q} = -1$ (dashed) and $a_{j,q} = +1$ (solid)

The binary multi- h CPFSK mapper transforms incoming data $a_{p,q}, p = 1, 2, \dots, q = 0, 1, \dots, N - 1$ into complex numbers given by (3.2) using (3.3). Since in the generation of $\theta_{j,q}$ the h values are chosen cyclically from $H_K = \{h_1, h_2, \dots, h_K\}$, the choice of $h_i, 1 \leq i \leq K$, plays an important role in restricting the number of terminal phase states of the mapper. When h_i s are chosen rational, a periodic phase trellis with period K can be obtained. Furthermore, when h_i s are restricted to be ratios of integers having common denominator, the phase trellis associated with $H_K = \left\{ \frac{l_1}{Q}, \frac{l_2}{Q}, \dots, \frac{l_K}{Q} \right\}$ is composed of

transitions among $2Q$ phase values $\frac{n\pi}{Q}, n = 0, 1, \dots, 2Q - 1$. The number of phases reflect upon the complexity of demapper at the receiver and hence l_i and Q are chosen small. Further, by choosing $H_K = \{h_1, h_2, \dots, h_K\}$ such that no two subsets have the same sum modulo 1, it is possible to attain maximum possible constraint length for a given K . From the viewpoint of demapper implementation K and Q should be chosen small, typically $K \leq 4$ and $Q \leq 16$. A detailed description of multi- h phase codes can be found in [67]. For examples $H_2 = \{3/4, 2/4\}$ satisfies the subset condition and $H_3 = \{3/4, 2/4, 1/4\}$ doesn't satisfy the subset condition. Fig. 3.11 shows the the phase tree for binary multi- h CPFSK mapper for $H_2 = \{1/4, 2/3\}$.

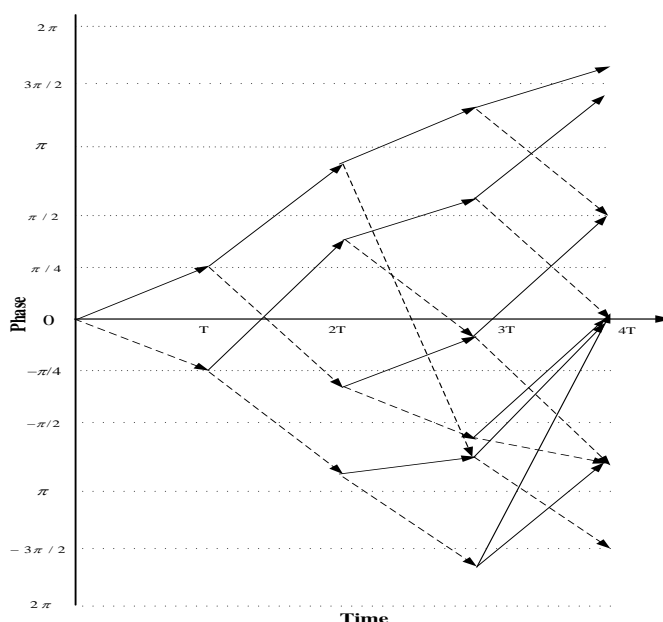


Figure 3.11: Phase tree for binary multi- h CPFSK mapper for $H_2 = \{1/4, 2/3\}$. $a_{j,q} = -1$ (dashed) and $a_{j,q} = +1$ (solid)

It is noted that in multi- h CPFSK mapper the phase trellis is always symmetrical and the separation between two possible paths in the phase trellis for multi- h CPFSK mapper is greater than that for single- h CPFSK mapper. Consequently, a demapper that bases its decision on a larger observation length can yield improved performance.

3.3.2 Asymmetric multi- h CPFSK Mapper

In multi- h CPFSK mapper the h values the set H_K are cyclically chosen independent of the input data $a_{k,p} = \pm 1$. That is the value of h chosen from the set $H_K =$

$\{h_1, h_2, \dots, h_K\}$ during a symbol interval is the same regardless of whether input data $a_{k,p} = \pm 1$. However, in the case of asymmetric multi- h CPFSK mapper, the choice of h during a symbol interval is a function of input data $a_{k,p}$ and hence asymmetric. That is, the set of h values used when input $a_{k,p} = +1$ is different from the set of h values used when the input data $a_{k,p} = -1$. In order to illustrate this concept, consider $H_K = \{h_1, h_2, \dots, h_K\} = \left\{ \frac{l_1}{Q}, \frac{l_2}{Q}, \dots, \frac{l_K}{Q} \right\}$ to be the set of h_i ($0 < h_i < 1, i = 1, 2, \dots, K$) values used by the asymmetric multi- h CPFSK mapper. Using H_K two sets H_{+K} and H_{-K} are constructed, each with K values of h from the set H_K . The value of h used during i -th symbol is either from H_{+K} or from H_{-K} depending on whether input data $a_{k,p} = +1$ or $a_{k,p} = -1$, respectively. The sets H_{+K} and H_{-K} are derived from the same set H_K for simplicity. For example, let $H_2 = \{h_1, h_2\}$. Then, there are two ways in which H_{2+} and H_{2-} can be chosen. They are:

$$H_{2+} = \{h_1, h_2\} \text{ and } H_{2-} = \{h_2, h_1\} \quad (3.11)$$

$$H_{2+} = \{h_2, h_1\} \text{ and } H_{2-} = \{h_1, h_2\} \quad (3.12)$$

If (3.11) is employed, the h values during symbol i ($1 \leq i \leq n$) are as given in Table 3.2 and if (3.12) is used, h values during symbol i are as given in Table 3.3. It is noted that h_{+i} and h_{-i} denote value of h used during i -th symbol accordingly as $a_{k,p} = +1$ and $a_{k,p} = -1$, respectively.

Table 3.2: h values as a function of symbol i in binary asymmetric multi- h CPFSK mapper using (3.11)

Symbol, i	1	2	3	4	...
h_{+i}	h_1	h_2	h_1	h_2	...
h_{-i}	h_2	h_1	h_2	h_1	...

Table 3.3: h values as a function of symbol i in binary asymmetric multi- h CPFSK mapper using (3.12)

Symbol, i	1	2	3	4	...
h_{+i}	h_2	h_1	h_2	h_1	...
h_{-i}	h_1	h_2	h_1	h_2	...

Both (3.11) and (3.12) result in the same steady-state phase trellis and this type of selection is referred to as A-type selection. If $H_{2+} = \{h_1, h_2\}$ and $H_{2-} = \{h_1, h_2\}$ or $H_{2+} = \{h_2, h_1\}$ and $H_{2-} = \{h_2, h_1\}$ then we get S-type selection. It is noted that S-type selection results in multi- h CPFSK mapper described in Section 3.4. Fig. 3.12 shows the phase tree for binary asymmetric multi- h CPFSK mapper for $H_2 = \left\{\frac{1}{4}, \frac{2}{3}\right\}$ with $H_{2+} = \left\{\frac{2}{3}, \frac{1}{4}\right\}$ and $H_{2-} = \left\{\frac{1}{4}, \frac{2}{3}\right\}$.

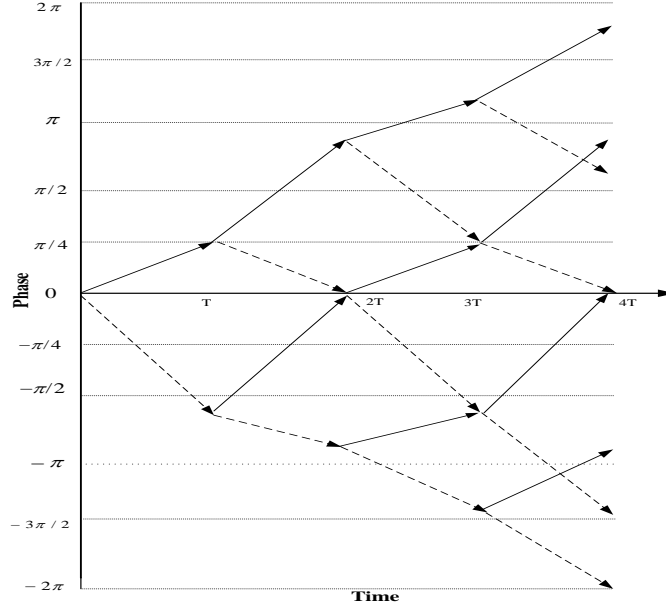


Figure 3.12: Phase tree for asy multi- h CPFSK mapper for $H_{2-} = \{1/4, 2/3\}$, $H_{2+} = \{2/3, 1/4\}$. $a_{j,q} = -1$ (dashed) and $a_{j,q} = +1$ (solid)

Next, consider $H_3 = \{h_1, h_2, h_3\}$ to be the set of h values in the asymmetric multi- h CPFSK mapper. The S-type mapper can be accomplished by choosing:

$$H_{3+} = \{h_1, h_2, h_3\} \text{ and } H_{3-} = \{h_1, h_2, h_3\}, \quad (3.13)$$

which results in the multi- h CPFSK mapper discussed in Section 3.4. The h values used during symbol i are shown in Table 3.4.

A simple way to introduce asymmetry in mapper is to use one symbol shift in H_{3-} relative to H_{3+} . That is

$$H_{3+} = \{h_1, h_2, h_3\} \text{ and } H_{3-} = \{h_2, h_3, h_1\}, \quad (3.14)$$

Table 3.4: h values as a function of symbol i in binary asymmetric multi- h CPFSK mapper using (3.11) [S-type]

Symbol, i	1	2	3	4	...
h_{+i}	h_2	h_1	h_2	h_1	...
h_{-i}	h_1	h_2	h_1	h_2	...

The h values used as a function of symbol i is given by Table 3.5. The selection given by (3.14) results in A-type mapper. An example of phase trellis of S-type and A-type mapper for $H_{3+} = \{h_1, h_2, h_3\} = \{6/8, 4/8, 5/8\}$ are shown in Fig. 3.13. Another way of obtaining A-type mappers For H_3 is:

Table 3.5: h values as a function of symbol i in binary asymmetric multi- h CPFSK mapper using (3.14) [A-type]

Symbol, i	1	2	3	4	...
h_{+i}	h_1	h_2	h_3	h_1	...
h_{-i}	h_2	h_3	h_1	h_2	...

$$H_{3+} = \{h_1, h_2, h_3\} \text{ and } H_{3-} = \{h_3, h_1, h_2\},$$

It is observed that these exist no simple method to design asymmetric multi- h CPFSK mapper for a given arbitrary value of K

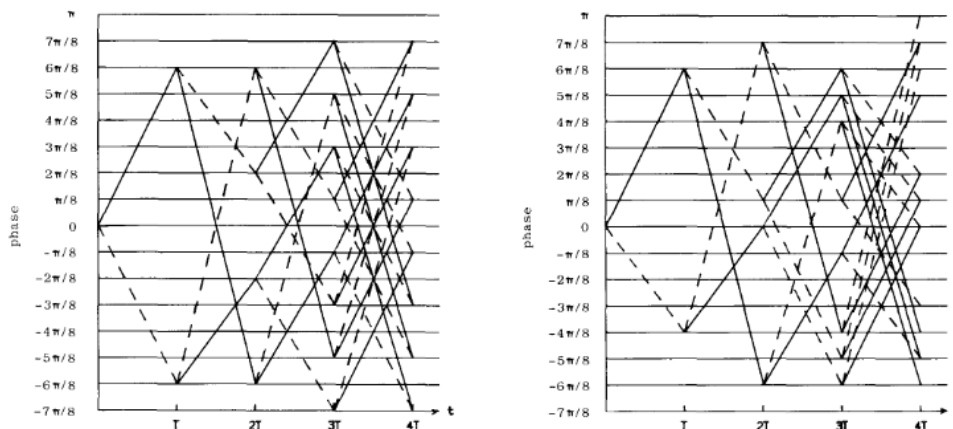


Figure 3.13: Phase trellises for: (a) S-type and (b) A-type mappers. $a_{j,q} = -1$ (dashed) and $a_{j,q} = +1$ (solid)

3.4 Conclusions

In this Chapter a class of generalized-CPFSK (g-CPFSK) mapper is introduced that can be used for generation of correlated OFDM signals. In general, the output of a g-CPFSK mapper is a function of the input data and a set of parameters $H_K = \{h_1, h_2, \dots, h_K\}$. The manner in which H_K is used gives rise to three subclasses of g-CPFSK mapper: i) Single- h CPFSK mapper; ii) Multi- h CPFSK mapper; and iii) Asymmetric multi- h CPFSK mapper. These mappers are described using examples and using state, trellis and tree diagrams. By appropriately choosing h_i ($1 \leq i \leq K$) in H_K , it is possible to obtain periodic phase trellis. Also, a general expression is developed for the transmitted signal in an OFDM system with g-CPFSK mapper. Examples are given for each of the three subclass of mappers.

Chapter 4

PAPR Reduction using SLM Technique for OFDM System with g-CPFSK Mapper^{1,2}

4.1 Introduction

In this Chapter, an OFDM system with g-CPFSK mapper is examined for PAPR properties with SLM technique. The ability of the system to reduce PAPR is assessed as a function of parameters of the mapper and the number of subcarriers in the system. Firstly, three subclasses of g-CPFSK mapper, namely, single- h CPFSK, multi- h CPFSK, and asymmetric multi- h CPFSK mappers are considered and their PAPR performances are assessed. These mappers in the OFDM system with SLM technique are considered and their PAPR performances are examined. A comparison of the PAPR reduction capability of g-CPFSK mapper relative to memoryless BPSK mapper in an OFDM system is presented.

-
1. E. Shafter, and R K. Rao, "PAPR Reduction using CPFSK Mappers and SLM in OFDM Systems," Lecture Notes in Engineering and Computer Science: Proceedings of The World Congress on Engineering and Computer Science (WCECS), San Francisco, USA, pp. 663-667, Oct. 2015.
 2. E. Shafter, and R K. Rao. "A Comparison between SLM, PTS, and CF Schemes for the Reduction of PAPR of OFDM System with CPFSK Mappers," IAENG International Journal of Computer Science 43.2, 2016.

4.2 SLM Technique and g-CPFSK Mapper

The block diagram of SLM technique for an OFDM system with g-CPFSK mapper is shown in Fig. 4.1. The data stream from the g-CPFSK mapper in Fig. 4.1 can be represented as

$$C_p = [C_{p,0}, C_{p,1}, \dots, C_{p,N-1}] \quad (4.1)$$

In SLM technique each data block is multiplied by U different phase sequences of length N given by $B^{(u)} = [b_{u,0}, b_{u,1}, \dots, b_{u,N-1}]$, $u = 1, 2, \dots, U$, resulting in U modified data blocks $C_p^{(u)}$, $u = 1, 2, \dots, U$. The modified data blocks are given by:

$$\begin{aligned} C_p^{(1)} &= [C_{p,0} b_{1,0}, C_{p,1} b_{1,1}, \dots, C_{p,N-1} b_{1,N-1}] \\ C_p^{(2)} &= [C_{p,0} b_{2,0}, C_{p,1} b_{2,1}, \dots, C_{p,N-1} b_{2,N-1}] \\ &\vdots \\ C_p^{(U)} &= [C_{p,0} b_{U,0}, C_{p,1} b_{U,1}, \dots, C_{p,N-1} b_{U,N-1}] \end{aligned} \quad (4.2)$$

The outputs of U IFFT blocks in Fig. 4.1 for U modified data sequences are given by:

$$[D_p^{(1)}, D_p^{(2)}, \dots, D_p^{(U)}] \quad (4.3)$$

where

$$D_p^{(u)} = [D_{p,0}^{(u)}, D_{p,1}^{(u)}, \dots, D_{p,N-1}^{(u)}] \quad (4.4)$$

and

$$D_{p,k}^{(u)} = \frac{1}{\sqrt{N}} \sum_{n=0}^{N-1} C_{p,n} b_{u,n} e^{j2\pi kn/N}, k = 0, 1, \dots, N-1. \quad (4.5)$$

The L -times oversampled time-domain OFDM signal $S_p^{(u)}(t)$ can be written as

$$S_p^{(u)}\left(\frac{kT}{L}\right) = \frac{1}{\sqrt{NL}} \sum_{n=0}^{N-1} C_{p,n} b_{u,n} e^{j2\pi kn/NL}, u = 1, 2, \dots, U, k = 0, 1, \dots, NL-1 \quad (4.6)$$

and is used to compute PAPR. That is, the PAPR for each $S_p^{(1)}(t), S_p^{(2)}(t), \dots, S_p^{(U)}(t)$ signal is computed in discrete-time using (4.6) and the one with the minimum value is chosen for transmission. That is,

$$\min_{1 \leq u \leq U} \text{PAPR}\{S_p^{(u)}(t)\} \quad (4.7)$$

If $u = \lambda$ (say) is the one that results in minimum PAPR, the phase sequence corresponding to this value of λ needs to be communicated to the receiver or equivalently $\lceil \log_2 U \rceil$ bits of side information needs to be sent to the receiver.

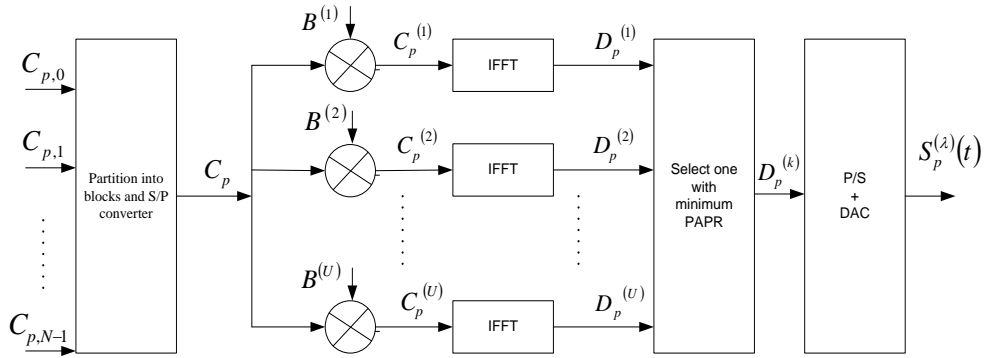


Figure 4.1: Block diagram of the SLM technique for an OFDM system with g-CPFSK mapper

The number of phase sequences U to be considered in the computation of (4.7) is a function of the number of phase states in g-CPFSK mapper used in the OFDM system and the number of subcarriers, N , of the system. Let the number of phase states be \mathfrak{H} , then the number of phase sequences is given by:

$$U = \mathfrak{H}^N \quad (4.8)$$

In order to illustrate the complexity involved in the computation of (4.7), consider a single- h CPFSK mapper with $h = 1/2$. The number of possible phase states for this mapper is $\mathfrak{H} = 4$ and the phase states are $\{0, \pi/2, \pi, 3\pi/2\}$ or equivalently $b_{u,k} \in \{e^{j0}, e^{j\pi/2}, e^{j\pi}, e^{j3\pi/2}\} = \{+1, j, -1, -j\}$. Thus, for an OFDM system with $N = 128$ subcarriers, one needs to consider $U = 4^{128}$ phase sequences before transmission of each OFDM symbol and also $\lceil \log_2 4^{128} \rceil = 256$ bits of side information needs to be sent to the receiver. Obviously, this is too complex to be of any practical value in OFDM sys-

tems. Therefore, methods are required that restrict the value of U to be practical and yet provide reasonable reductions in PAPR values. In this thesis, a method is suggested to achieve this objective. The value of U is set equal to 16 regardless of the number of subcarriers, N , used in the OFDM system with g-CPFSK mapper. The initial matrix of phase sequences can be written in matrix form as:

$$B = \begin{bmatrix} B^{(1)} \\ B^{(2)} \\ \vdots \\ B^{(16)} \end{bmatrix} = \begin{bmatrix} b_{1,0} & b_{1,1} & \cdots & b_{1,15} \\ b_{2,0} & b_{2,1} & \cdots & b_{2,15} \\ \vdots & \vdots & & \vdots \\ b_{16,0} & b_{16,1} & \cdots & b_{16,15} \end{bmatrix} = b \quad (4.9)$$

where $b_{1,k}, k = 0, 1, \dots, 15, = e^{j0} = 1$ and $b_{l,k}, l = 2, 3, \dots, 16$ and $k = 0, 1, \dots, 15$, are randomly chosen from the set of possible phase values for a given g-CPFSK mapper used in the OFDM system. For example, for the single- h CPFSK mapper with $h = 1/2$, the set of possible phase values is given by $\{e^{j0}, e^{j\pi/2}, e^{j\pi}, e^{j3\pi/2}\} = \{+1, +j, -1, -j\}$. The first phase sequence $B^{(1)} = [b_{1,0}, b_{1,1}, \dots, b_{1,15}] = [+1, +1, \dots, +1]$ is always chosen as this phase sequence as the modified data sequence corresponding this phase sequence represents the original unmodified data sequence, as the objective in SLM is to find a modified sequence that results in a PAPR smaller than that of the original unmodified sequence. Once the $B^{(u)}, u = 1, 2, \dots, 16$, phase sequences are chosen it can be applied to OFDM system with arbitrary number of subcarriers, N . For example, if $N = 64$, the 16 phase sequences can be expressed by the matrix:

$$B = \begin{bmatrix} b & \vdots & b & \vdots & b & \vdots & b \end{bmatrix} \quad (4.10)$$

In the thesis (4.7) is determined for single- h CPFSK, multi- h CPFSK, and asymmetric multi- h CPFSK mappers in an OFDM system as a function of number of subcarriers N . Numerical results are presented in the next Section.

4.3 Numerical Results and Discussion

In this Section numerical results are presented using CCDFs of PAPR of OFDM system with g-CPFSK mapper with and without SLM technique, as a function of number of

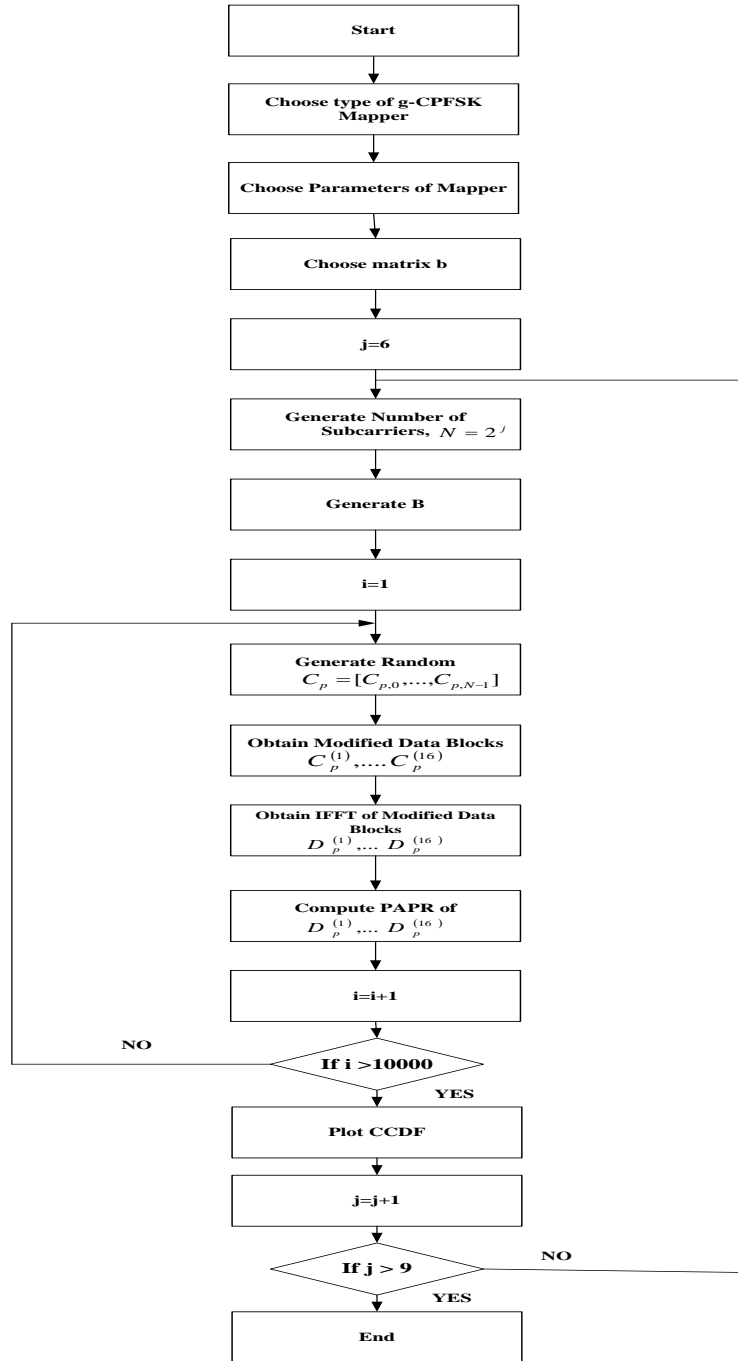


Figure 4.2: Flow-chart for computation of CCDFs of PAPR using SLM technique

subcarriers ($N=64, 128, 256, 512$). In the computation of PAPR, an oversampling factor $L = 4$ is used and simulation results have been obtained using MATLAB. For each CCDF plot 10,000 random OFDM symbols are considered. Fig. 4.2 shows the flow-chart used for computation of (4.7).

Table 4.1: Phase sequences $B^{(1)}, B^{(2)}, \dots, B^{(16)}$ for single- h CPFSK mapper ($h = \frac{1}{2}$) with $b_{u,k} \in \{e^{j0}, e^{j\pi/2}, e^{j\pi}, e^{j3\pi/2}\}$

$B^{(u)}$	$b_{u,0}$	$b_{u,1}$	$b_{u,2}$	$b_{u,3}$	$b_{u,4}$	$b_{u,5}$	$b_{u,6}$	$b_{u,7}$	$b_{u,8}$	$b_{u,9}$	$b_{u,10}$	$b_{u,11}$	$b_{u,12}$	$b_{u,13}$	$b_{u,14}$	$b_{u,15}$
$B^{(1)}$	+1	+1	+1	+1	+1	+1	+1	+1	+1	+1	+1	+1	+1	+1	+1	+1
$B^{(2)}$	e^{j0}	$e^{j\pi/2}$	$e^{j\pi/2}$	$e^{j\pi}$	$e^{j\pi}$	$e^{j\pi/2}$	e^{j0}	e^{j0}	e^{j0}	$e^{j3\pi/2}$	$e^{j\pi/2}$	e^{j0}	$e^{j\pi}$	e^{j0}	e^{j0}	$e^{j3\pi/2}$
$B^{(3)}$	$e^{j\pi/2}$	$e^{j\pi/2}$	$e^{j\pi/2}$	$e^{j\pi}$	$e^{j\pi}$	e^{j0}	$e^{j3\pi/2}$	e^{j0}	$e^{j\pi/2}$	e^{j0}	$e^{j\pi}$	$e^{j\pi}$	e^{j0}	$e^{j\pi}$	e^{j0}	$e^{j\pi}$
$B^{(4)}$	e^{j0}	e^{j0}	e^{j0}	e^{j0}	$e^{j\pi}$	$e^{j\pi}$	$e^{j\pi/2}$	e^{j0}	$e^{j3\pi/2}$	$e^{j\pi}$	$e^{j3\pi/2}$	$e^{j\pi/2}$	$e^{j\pi/2}$	e^{j0}	e^{j0}	e^{j0}
$B^{(5)}$	e^{j0}	$e^{j\pi/2}$	e^{j0}	$e^{j\pi}$	$e^{j\pi/2}$	$e^{j3\pi/2}$	$e^{j\pi/2}$	$e^{j3\pi/2}$	$e^{j\pi}$	$e^{j\pi}$	$e^{j3\pi/2}$	e^{j0}	e^{j0}	$e^{j3\pi/2}$	e^{j0}	$e^{j\pi/2}$
$B^{(6)}$	$e^{j\pi/2}$	$e^{j\pi/2}$	$e^{j\pi}$	$e^{j\pi}$	e^{j0}	e^{j0}	$e^{j\pi/2}$	$e^{j3\pi/2}$	$e^{j3\pi/2}$	$e^{j3\pi/2}$	e^{j0}	e^{j0}	e^{j0}	e^{j0}	$e^{j\pi}$	e^{j0}
$B^{(7)}$	$e^{j\pi}$	$e^{j\pi}$	$e^{j\pi}$	$e^{j\pi}$	e^{j0}	e^{j0}	$e^{j\pi}$	e^{j0}	$e^{j\pi/2}$	$e^{j3\pi/2}$	e^{j0}	$e^{j\pi/2}$	$e^{j3\pi/2}$	$e^{j3\pi/2}$	$e^{j\pi/2}$	e^{j0}
$B^{(8)}$	e^{j0}	e^{j0}	$e^{j\pi}$	$e^{j\pi/2}$	$e^{j3\pi/2}$	$e^{j\pi/2}$	e^{j0}	e^{j0}	$e^{j\pi}$	$e^{j\pi}$	e^{j0}	$e^{j\pi}$	$e^{j\pi}$	$e^{j3\pi/2}$	$e^{j\pi/2}$	$e^{j\pi/2}$
$B^{(9)}$	$e^{j\pi/2}$	$e^{j\pi/2}$	$e^{j3\pi/2}$	$e^{j\pi}$	$e^{j\pi}$	e^{j0}	e^{j0}	e^{j0}	e^{j0}	e^{j0}	$e^{j\pi}$	$e^{j\pi}$	$e^{j3\pi/2}$	$e^{j\pi/2}$	$e^{j3\pi/2}$	e^{j0}
$B^{(10)}$	e^{j0}	$e^{j\pi}$	$e^{j\pi}$	$e^{j\pi}$	$e^{j\pi}$	$e^{j\pi/2}$	$e^{j\pi/2}$	$e^{j3\pi/2}$	e^{j0}	e^{j0}	e^{j0}	e^{j0}	$e^{j3\pi/2}$	$e^{j3\pi/2}$	$e^{j\pi/2}$	$e^{j3\pi/2}$
$B^{(11)}$	e^{j0}	$e^{j\pi}$	$e^{j\pi}$	$e^{j\pi/2}$	$e^{j\pi/2}$	$e^{j\pi/2}$	e^{j0}	e^{j0}	$e^{j\pi}$	$e^{j\pi}$	$e^{j\pi}$	$e^{j3\pi/2}$	$e^{j3\pi/2}$	$e^{j3\pi/2}$	$e^{j3\pi/2}$	$e^{j3\pi/2}$
$B^{(12)}$	$e^{j\pi/2}$	$e^{j\pi}$	$e^{j3\pi/2}$	$e^{j\pi}$	e^{j0}	$e^{j\pi}$	e^{j0}	$e^{j\pi}$	$e^{j\pi/2}$	$e^{j3\pi/2}$	$e^{j\pi/2}$	$e^{j3\pi/2}$	$e^{j\pi}$	e^{j0}	e^{j0}	e^{j0}
$B^{(13)}$	e^{j0}	e^{j0}	$e^{j\pi/2}$	$e^{j\pi/2}$	$e^{j3\pi/2}$	e^{j0}	e^{j0}	e^{j0}	$e^{j\pi/2}$	$e^{j\pi}$	$e^{j3\pi/2}$	$e^{j3\pi/2}$	$e^{j3\pi/2}$	$e^{j\pi}$	$e^{j\pi/2}$	$e^{j\pi}$
$B^{(14)}$	e^{j0}	$e^{j3\pi/2}$	e^{j0}	$e^{j3\pi/2}$	$e^{j\pi}$	e^{j0}	e^{j0}	$e^{j3\pi/2}$	$e^{j\pi}$	$e^{j\pi/2}$	$e^{j\pi}$	$e^{j3\pi/2}$	e^{j0}	e^{j0}	e^{j0}	e^{j0}
$B^{(15)}$	e^{j0}	e^{j0}	e^{j0}	$e^{j\pi}$	$e^{j\pi}$	$e^{j\pi/2}$	$e^{j3\pi/2}$	$e^{j\pi}$	$e^{j\pi/2}$	e^{j0}	$e^{j3\pi/2}$	$e^{j3\pi/2}$	$e^{j3\pi/2}$	$e^{j\pi/2}$	e^{j0}	e^{j0}
$B^{(16)}$	e^{j0}	e^{j0}	e^{j0}	$e^{j\pi}$	$e^{j\pi}$	$e^{j\pi}$	$e^{j\pi}$	$e^{j\pi/2}$	$e^{j3\pi/2}$	$e^{j3\pi/2}$	$e^{j\pi/2}$	$e^{j\pi/2}$	$e^{j3\pi/2}$	$e^{j\pi}$	$e^{j\pi}$	$e^{j3\pi/2}$

4.3.1 Single- h CPFSK Mapper

In the case of single- h CPFSK mapper the number of possible states is a function of the value of h chosen, which in turn determines the possible values $b_{u,k}$ can take. For $h = 1/2$, $b_{u,k} \in \{e^{j0}, e^{j\pi/2}, e^{j\pi}, e^{j3\pi/2}\}$. Similarly for $h = 2/3$, $b_{u,k} \in \{e^{j0}, e^{j\pi/3}, e^{j4\pi/3}\}$. In Tables 4.1 and 4.2 are shown the initial values of $B^{(1)}, B^{(2)}, \dots, B^{(16)}$ for these two values of h used in the computation of PAPR with SLM technique. The CCDFs of PAPR of an OFDM system without SLM technique for $h = \frac{1}{5}, \frac{1}{3}, \frac{1}{2}$ and $\frac{4}{5}$ are shown in Fig. 4.3. Also, shown in these plots are CCDFs of PAPR of an OFDM system with memoryless BPSK mapper. It is observed that single- h CPFSK ($h = 1/2$) mapper offers superior PAPR performance compared to the BPSK mapper. The OFDM system with single- h CPFSK mapper ($h = 1/2$) has a PAPR that exceeds 10.6 dB for less than 0.1 percent of data blocks; whereas for BPSK mapper this value is nearly 13.1 dB. The CCDFs of PAPR after applying SLM technique for single- h CPFSK $h = 1/2$ mapper are shown in Figs. 4.4 to 4.7 for $N = 64, 128, 256$, and 512. The phase sequences that resulted in minimum PAPR are $B^{(6)}, B^{(4)}, B^{(8)}$, and $B^{(5)}$ for $N = 64, 128, 256$, and 512 respectively. These sequences are given in Table 4.9. It is noted that when SLM is applied with single- h CPFSK mapper ($h = 1/2$), the PAPR reduces to 8.02 dB which is an improvement of nearly 3 dB relative to the corresponding system without SLM technique. Also, it is observed that BPSK mapper with SLM applied results in PAPR of 9.2 dB. A comparison of PAPR reductions for both BPSK and single- h CPFSK mappers with and without

Table 4.2: Phase sequences $B^{(1)}, B^{(2)}, \dots, B^{(16)}$ for single- h CPFSK mapper ($h = \frac{2}{3}$) with $b_{u,k} \in \{e^{j0}, e^{j\pi/3}, e^{j4\pi/3}\}$

$B^{(u)}$	$b_{u,0}$	$b_{u,1}$	$b_{u,2}$	$b_{u,3}$	$b_{u,4}$	$b_{u,5}$	$b_{u,6}$	$b_{u,7}$	$b_{u,8}$	$b_{u,9}$	$b_{u,10}$	$b_{u,11}$	$b_{u,12}$	$b_{u,13}$	$b_{u,14}$	$b_{u,15}$
$B^{(1)}$	+1	+1	+1	+1	+1	+1	+1	+1	+1	+1	+1	+1	+1	+1	+1	+1
$B^{(2)}$	$e^{j\pi/3}$	$e^{j\pi/3}$	e^{j0}	$e^{j\pi/3}$	e^{j0}	e^{j0}	$e^{j4\pi/3}$	e^{j0}	e^{j0}	$e^{j4\pi/3}$	$e^{j\pi/3}$	e^{j0}	e^{j0}	e^{j0}	e^{j0}	$e^{j\pi/3}$
$B^{(3)}$	$e^{j\pi/3}$	$e^{j\pi/3}$	$e^{j\pi/3}$	$e^{j\pi/3}$	e^{j0}	$e^{j4\pi/3}$	$e^{j4\pi/3}$	e^{j0}	e^{j0}	$e^{j4\pi/3}$	$e^{j\pi/3}$	e^{j0}	e^{j0}	$e^{j4\pi/3}$	e^{j0}	$e^{j4\pi/3}$
$B^{(4)}$	$e^{j4\pi/3}$	$e^{j4\pi/3}$	e^{j0}	$e^{j\pi/3}$	e^{j0}	$e^{j\pi/3}$	$e^{j\pi/3}$	e^{j0}	e^{j0}	$e^{j4\pi/3}$	$e^{j\pi/3}$	e^{j0}	$e^{j\pi/3}$	e^{j0}	$e^{j4\pi/3}$	$e^{j\pi/3}$
$B^{(5)}$	$e^{j\pi/3}$	$e^{j4\pi/3}$	e^{j0}	$e^{j4\pi/3}$	e^{j0}	$e^{j\pi/3}$	$e^{j4\pi/3}$	e^{j0}	e^{j0}	$e^{j4\pi/3}$	$e^{j\pi/3}$	$e^{j\pi/3}$	e^{j0}	$e^{j4\pi/3}$	e^{j0}	$e^{j\pi/3}$
$B^{(6)}$	$e^{j\pi/3}$	$e^{j\pi/3}$	e^{j0}	$e^{j\pi/3}$	$e^{j\pi/3}$	e^{j0}	$e^{j4\pi/3}$	e^{j0}	$e^{j4\pi/3}$	$e^{j4\pi/3}$	$e^{j\pi/3}$	$e^{j4\pi/3}$	$e^{j\pi/3}$	$e^{j\pi/3}$	$e^{j\pi/3}$	$e^{j\pi/3}$
$B^{(7)}$	e^{j0}	e^{j0}	e^{j0}	$e^{j4\pi/3}$	$e^{j\pi/3}$	$e^{j\pi/3}$	$e^{j4\pi/3}$	e^{j0}	e^{j0}	$e^{j4\pi/3}$	$e^{j\pi/3}$	$e^{j\pi/3}$	e^{j0}	e^{j0}	$e^{j4\pi/3}$	$e^{j\pi/3}$
$B^{(8)}$	$e^{j\pi/3}$	$e^{j4\pi/3}$	e^{j0}	$e^{j\pi/3}$	e^{j0}	$e^{j4\pi/3}$	$e^{j4\pi/3}$	$e^{j4\pi/3}$	$e^{j\pi/3}$	$e^{j4\pi/3}$	$e^{j\pi/3}$	e^{j0}	$e^{j\pi/3}$	e^{j0}	$e^{j4\pi/3}$	$e^{j\pi/3}$
$B^{(9)}$	$e^{j\pi/3}$	$e^{j\pi/3}$	e^{j0}	e^{j0}	e^{j0}	$e^{j\pi/3}$	$e^{j4\pi/3}$	$e^{j\pi/3}$	$e^{j\pi/3}$	$e^{j4\pi/3}$	$e^{j\pi/3}$	$e^{j4\pi/3}$	$e^{j\pi/3}$	$e^{j\pi/3}$	$e^{j\pi/3}$	$e^{j\pi/3}$
$B^{(10)}$	$e^{j\pi/3}$	e^{j0}	$e^{j\pi/3}$	$e^{j\pi/3}$	e^{j0}	$e^{j\pi/3}$	$e^{j4\pi/3}$	e^{j0}	e^{j0}	$e^{j\pi/3}$	$e^{j\pi/3}$	$e^{j\pi/3}$	$e^{j\pi/3}$	$e^{j4\pi/3}$	e^{j0}	$e^{j\pi/3}$
$B^{(11)}$	$e^{j4\pi/3}$	$e^{j4\pi/3}$	$e^{j\pi/3}$	$e^{j\pi/3}$	e^{j0}	$e^{j4\pi/3}$	$e^{j4\pi/3}$	$e^{j\pi/3}$	e^{j0}	$e^{j4\pi/3}$	$e^{j\pi/3}$	$e^{j4\pi/3}$	e^{j0}	$e^{j\pi/3}$	e^{j0}	$e^{j4\pi/3}$
$B^{(12)}$	$e^{j\pi/3}$	$e^{j4\pi/3}$	$e^{j\pi/3}$	$e^{j4\pi/3}$	e^{j0}	$e^{j4\pi/3}$	$e^{j\pi/3}$	e^{j0}	$e^{j\pi/3}$	$e^{j4\pi/3}$	$e^{j\pi/3}$	$e^{j4\pi/3}$	$e^{j4\pi/3}$	$e^{j\pi/3}$	$e^{j4\pi/3}$	$e^{j\pi/3}$
$B^{(13)}$	$e^{j\pi/3}$	$e^{j4\pi/3}$	e^{j0}	$e^{j4\pi/3}$	e^{j0}	e^{j0}	e^{j0}	e^{j0}	$e^{j\pi/3}$	$e^{j4\pi/3}$	$e^{j\pi/3}$	$e^{j\pi/3}$	e^{j0}	$e^{j4\pi/3}$	e^{j0}	$e^{j\pi/3}$
$B^{(14)}$	e^{j0}	$e^{j\pi/3}$	e^{j0}	$e^{j4\pi/3}$	e^{j0}	$e^{j\pi/3}$	$e^{j\pi/3}$	$e^{j\pi/3}$	e^{j0}	$e^{j4\pi/3}$	$e^{j\pi/3}$	$e^{j\pi/3}$	$e^{j\pi/3}$	$e^{j\pi/3}$	$e^{j\pi/3}$	$e^{j\pi/3}$
$B^{(15)}$	$e^{j\pi/3}$	e^{j0}	e^{j0}	e^{j0}	e^{j0}	$e^{j4\pi/3}$	$e^{j\pi/3}$	$e^{j\pi/3}$	$e^{j\pi/3}$	$e^{j4\pi/3}$	$e^{j\pi/3}$	$e^{j\pi/3}$	e^{j0}	e^{j0}	$e^{j4\pi/3}$	$e^{j\pi/3}$
$B^{(16)}$	$e^{j\pi/3}$	$e^{j\pi/3}$	e^{j0}	e^{j0}	e^{j0}	e^{j0}	$e^{j4\pi/3}$	$e^{j\pi/3}$	$e^{j\pi/3}$	$e^{j4\pi/3}$	$e^{j\pi/3}$	$e^{j\pi/3}$	$e^{j\pi/3}$	$e^{j\pi/3}$	$e^{j\pi/3}$	$e^{j\pi/3}$

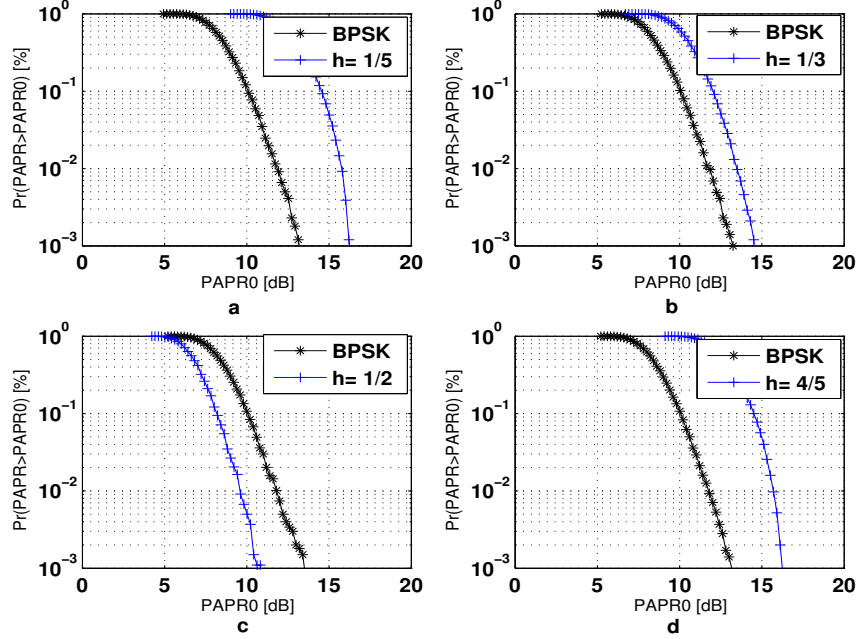


Figure 4.3: CCDFs of PAPR of single- h CPFSK mapper ($N = 64$) without SLM technique : (a) $h = \frac{1}{5}$; (b) $h = \frac{1}{3}$; (c) $h = \frac{1}{2}$; and (d) $h = \frac{4}{5}$

SLM technique is given in Table 4.3. In order to compare possible PAPR reductions as a function of number of subcarriers in an OFDM system, CCDFs of PAPR of single- h CPFSK mapper ($h = 1/2$) with and without SLM technique are plotted in Figs. 4.8 and 4.9 respectively. Also, plotted in these figures are CCDFs for BPSK mapper with and without SLM technique. The CCDFs of PAPR of an OFDM system with single-

Table 4.3: Comparison of PAPR performance of single- h CPFSK mapper ($h = \frac{1}{2}$) as a function of number of subcarriers

Number of Subcarriers	Mapper			
	BPSK		Single- h CPFSK	
	Without SLM (dB)	With SLM (dB)	Without SLM (dB)	With SLM (dB)
64	13.1	7.9	10.6	6.8
128	13.2	8.6	11.2	7.5
256	13.5	9.3	11.3	8.1
512	14.1	9.9	11.4	8.5

h CPFSK mapper ($h = 2/3$) for $N = 64, 128, 256$, and 512 , with and without SLM technique, are shown in Figs. 4.10, 4.11, 4.12, and 4.13, respectively. The best phase sequences that minimize PAPR are $B^{(11)}, B^{(4)}, B^{(8)}$, and $B^{(7)}$ for $N = 64, 128, 256$, and 512 respectively. These are listed in Table 4.9.

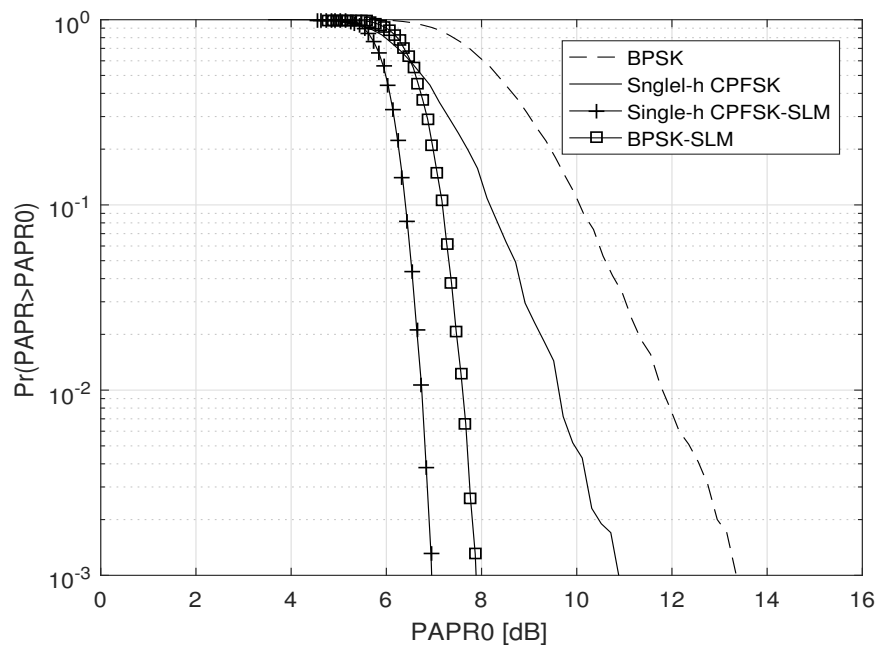


Figure 4.4: CCDFs of PAPR of an OFDM system with single- h CPFSK mapper ($h = \frac{1}{2}$) with and without SLM technique ($N=64$)

A comparison of PAPR reductions for both BPSK and single- h CPFSK ($h = 2/3$) mapper with and without SLM technique is given in Table 4.4. It is noted that PAPR, in general, increases as a function of increasing number of subcarriers in the system, for both single-

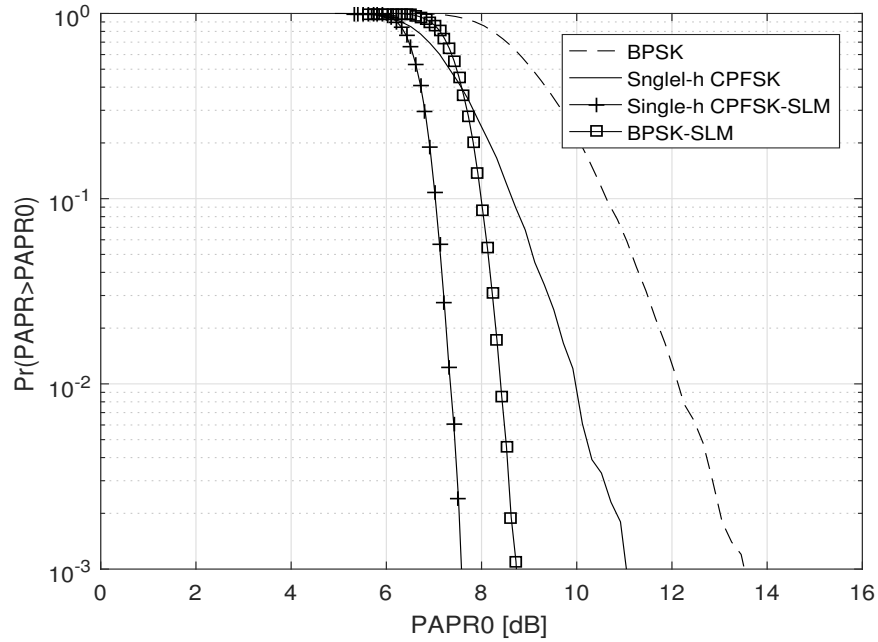


Figure 4.5: CCDFs of PAPR of an OFDM system with single- h CPFSK mapper ($h = \frac{1}{2}$) with and without SLM technique, ($N = 128$)

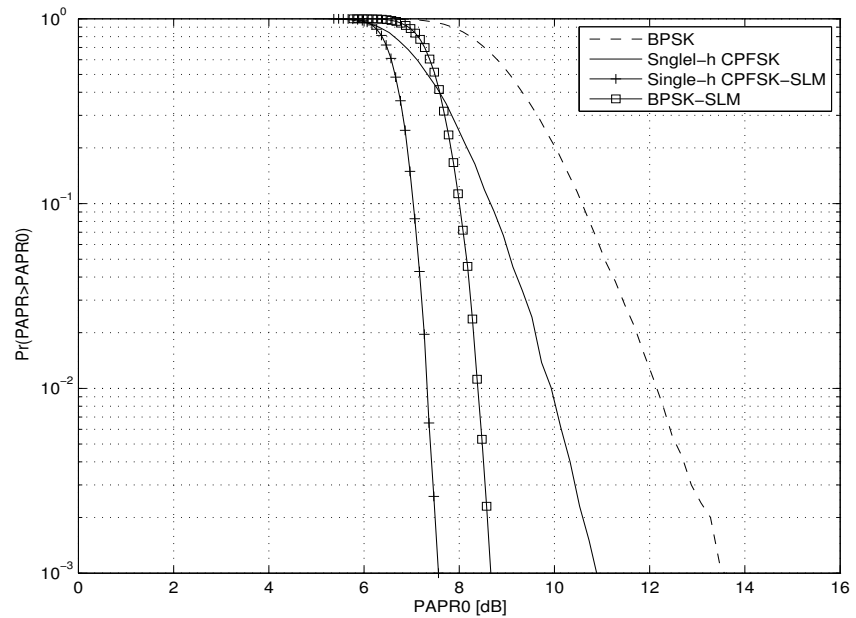


Figure 4.6: CCDFs of PAPR of an OFDM system with single- h CPFSK mapper ($h = \frac{1}{2}$) with and without SLM technique, ($N = 256$)

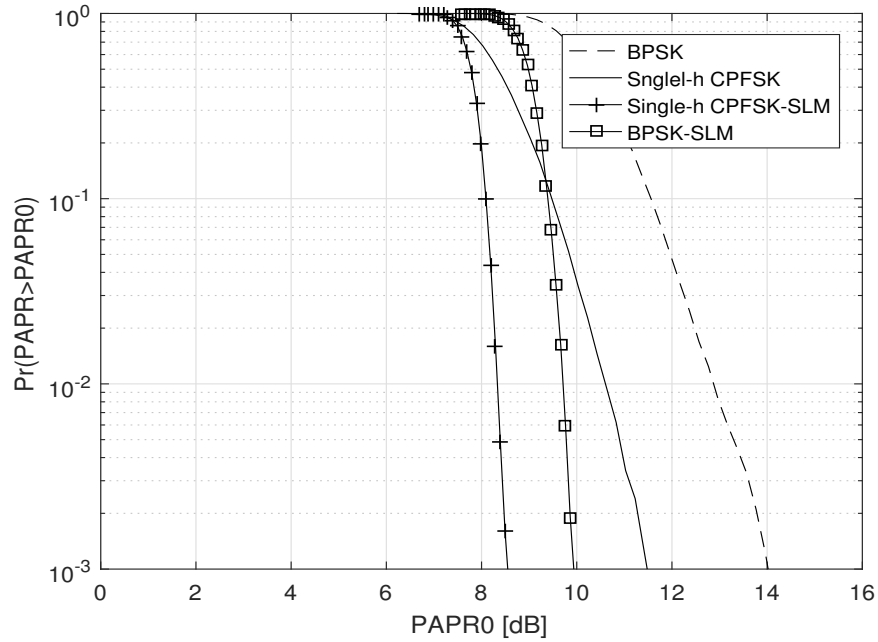


Figure 4.7: CCDFs of PAPR of an OFDM with single- h CPFSK mapper ($h = \frac{1}{2}$) with and without SLM technique, ($N = 512$)

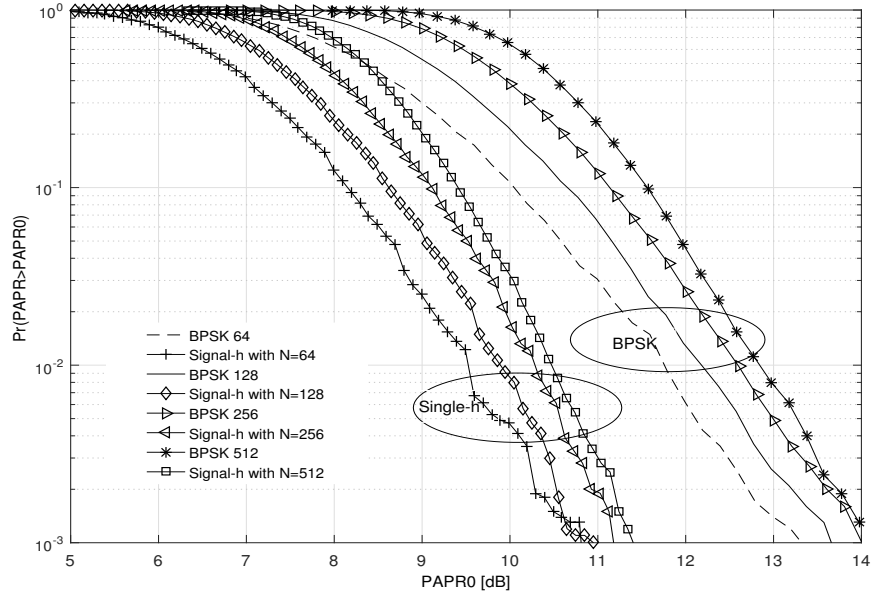


Figure 4.8: CCDFs of PAPR of an OFDM system with single- h CPFSK mapper ($h = \frac{1}{2}$) as a function of number of subcarriers ($N=64, 128, 256,$ and 512) without SLM technique

Table 4.4: Comparison of PAPR performance of single- h CPFSK mapper ($h = \frac{2}{3}$) as a function of number of subcarriers

Number of Subcarriers	Mapper			
	BPSK		Single- h CPFSK	
	Without SLM (dB)	With SLM (dB)	Without SLM (dB)	With SLM (dB)
64	13.1	7.9	13.8	7
128	13.2	8.7	14.1	7.8
256	13.5	9.2	14.9	8.0
512	14.1	9.9	15.0	8.3

h CPFSK and BPSK mappers regardless of whether SLM technique is used or not. However, for a given number of subcarriers in the system, PAPR reductions always exist with the use of SLM technique compared to the system without this technique. An overall improvement in PAPR of 3 dB can be achieved with single- h CPFSK mapper by using SLM technique relative to the same system without this technique.

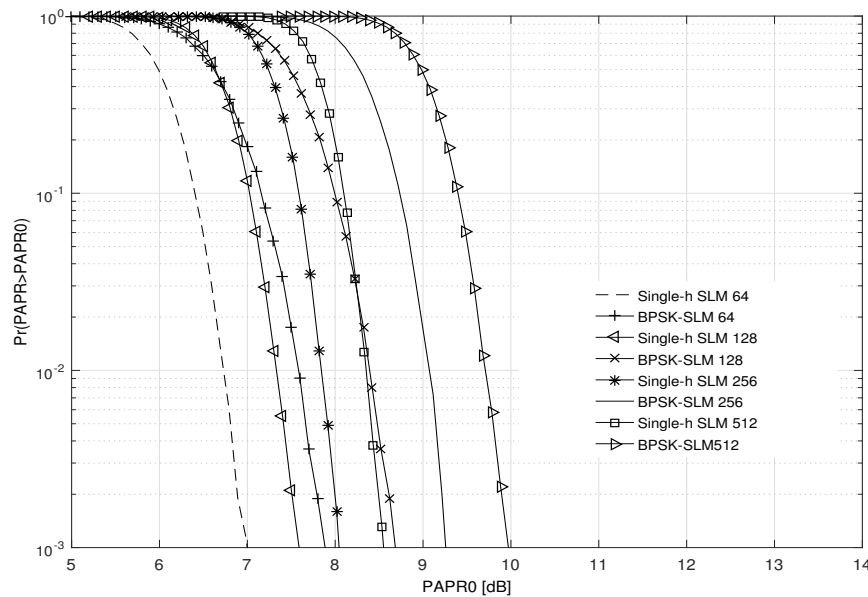


Figure 4.9: CCDFs of PAPR of an OFDM system with single- h CPFSK mapper ($h = \frac{1}{2}$) as a function of number of subcarriers ($N=64, 128, 256,$ and 512) with SLM technique

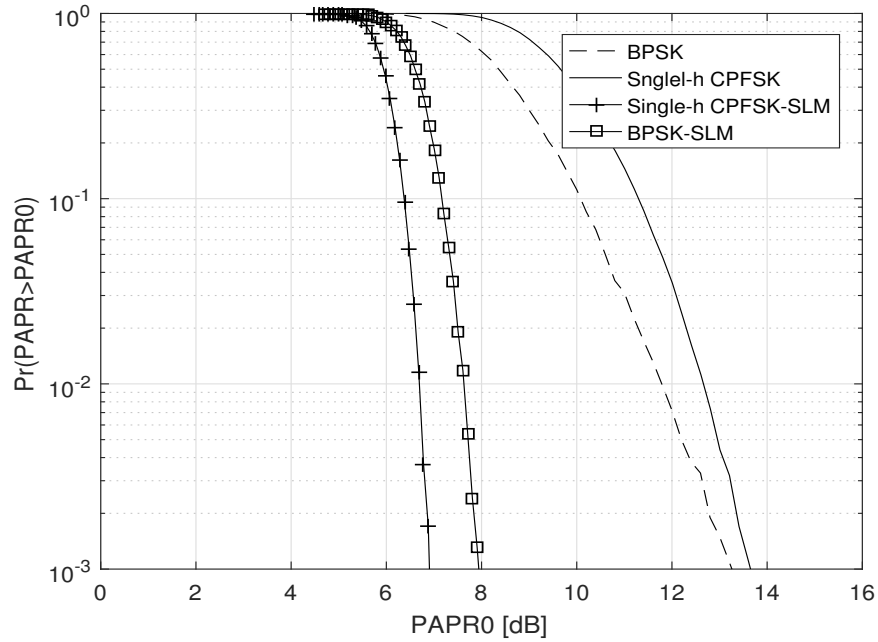


Figure 4.10: CCDFs of PAPR of an OFDM with single- h CPFSK mapper ($h = \frac{2}{3}$) with and without SLM technique, ($N = 64$)

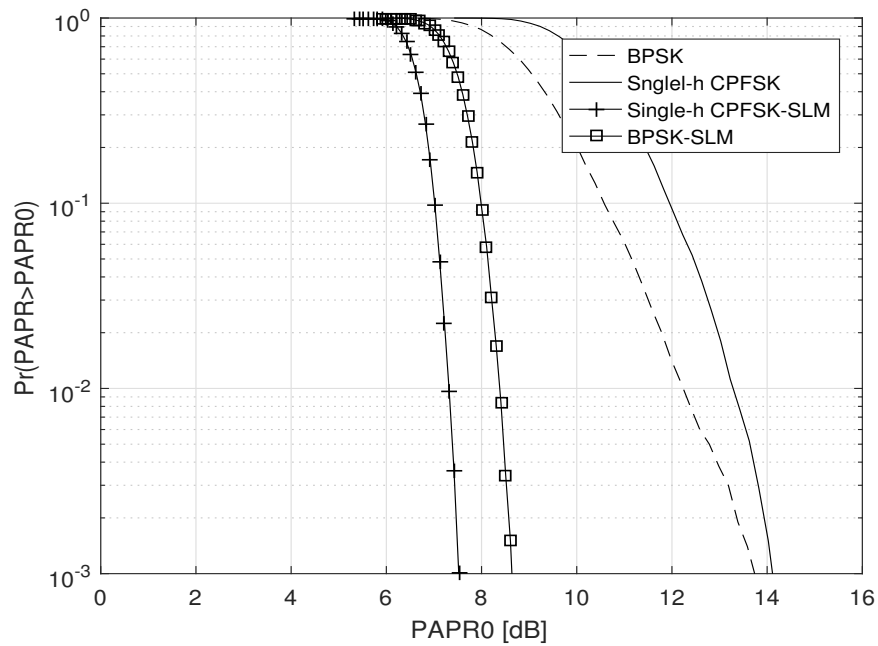


Figure 4.11: CCDFs of PAPR of an OFDM with single- h CPFSK mapper ($h = \frac{2}{3}$) with and without SLM technique, ($N = 128$)

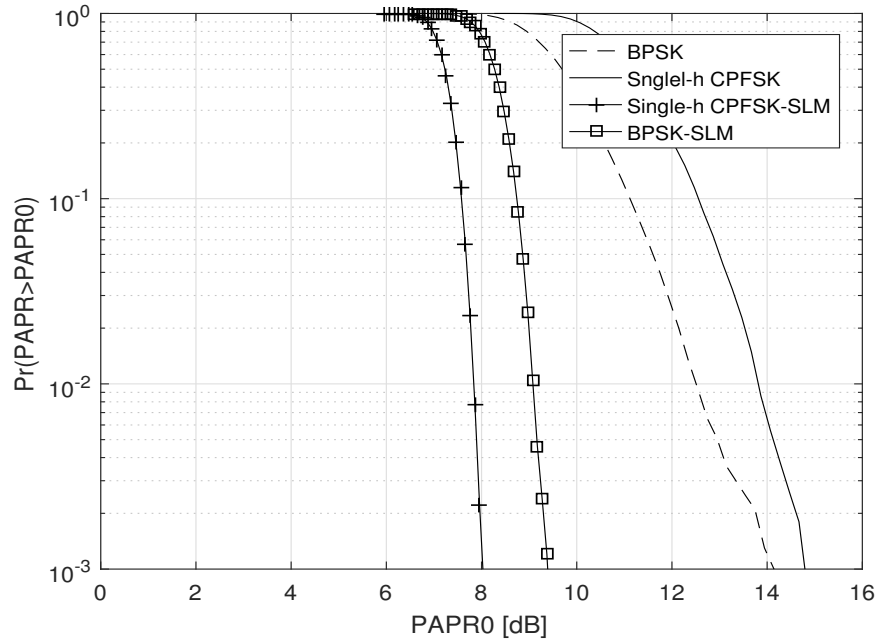


Figure 4.12: CCDFs of PAPR of an OFDM with single- h CPFSK mapper ($h = \frac{2}{3}$) with and without SLM technique, ($N = 256$)

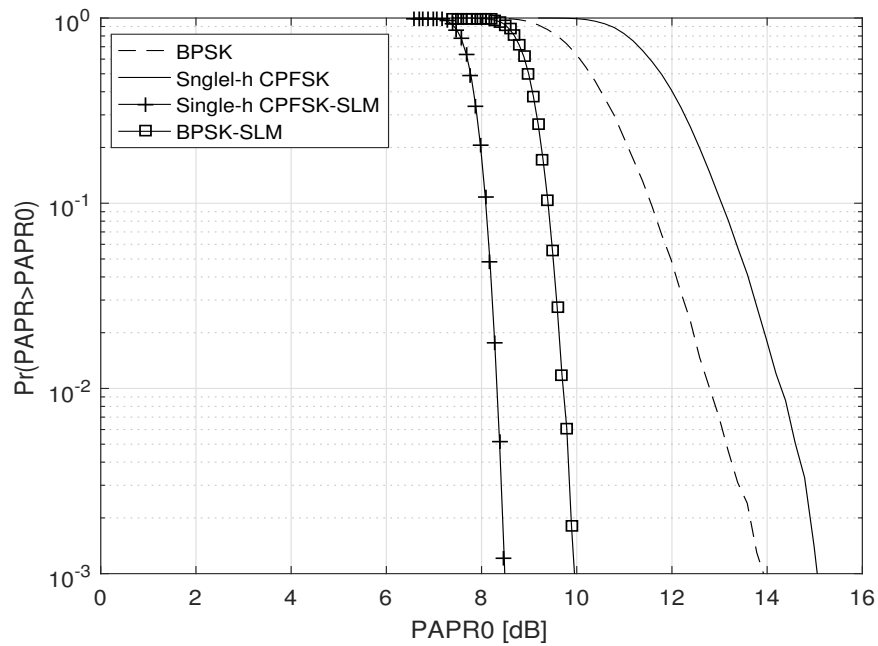


Figure 4.13: CCDFs of PAPR of an OFDM with single- h CPFSK mapper ($h = \frac{2}{3}$) with and without SLM technique, ($N = 512$)

Table 4.5: Phase sequences $B^{(1)}, B^{(2)}, \dots, B^{(u)}$ for multi- h CPFSK mapper $\{2/4, 3/4\}$ with $b_{u,k} \in \{e^{j0}, e^{j\pi/4}, e^{j\pi/2}, e^{j3\pi/4}, e^{j\pi}, e^{j5\pi/4}, e^{j3\pi/2}, e^{j7\pi/4}\}$

$B^{(u)}$	$b_{u,0}$	$b_{u,1}$	$b_{u,2}$	$b_{u,3}$	$b_{u,4}$	$b_{u,5}$	$b_{u,6}$	$b_{u,7}$	$b_{u,8}$	$b_{u,9}$	$b_{u,10}$	$b_{u,11}$	$b_{u,12}$	$b_{u,13}$	$b_{u,14}$	$b_{u,15}$
$B^{(1)}$	+1	+1	+1	+1	+1	+1	+1	+1	+1	+1	+1	+1	+1	+1	+1	+1
$B^{(2)}$	$e^{j\pi/4}$	e^{j0}	$e^{j3\pi/4}$	$e^{j3\pi/4}$	$e^{j\pi/2}$	$e^{j\pi/2}$	$e^{j\pi/2}$	$e^{j\pi}$	$e^{j\pi}$	$e^{j7\pi/4}$	$e^{j3\pi/4}$	$e^{j3\pi/4}$	e^{j0}	$e^{j3\pi/4}$	e^{j0}	$e^{j7\pi/4}$
$B^{(3)}$	$e^{j\pi/4}$	e^{j0}	$e^{j3\pi/4}$	$e^{j3\pi/4}$	$e^{j\pi/2}$	$e^{j\pi/2}$	$e^{j\pi/2}$	$e^{j\pi}$	$e^{j\pi}$	$e^{j5\pi/4}$	e^{j0}	$e^{j3\pi/4}$	$e^{j7\pi/4}$	$e^{j3\pi/2}$	$e^{j5\pi/4}$	$e^{j3\pi/4}$
$B^{(4)}$	$e^{j\pi/4}$	e^{j0}	$e^{j3\pi/4}$	$e^{j3\pi/2}$	$e^{j\pi/2}$	$e^{j\pi/2}$	$e^{j\pi/2}$	$e^{j\pi}$	$e^{j\pi}$	$e^{j7\pi/4}$	$e^{j7\pi/4}$	$e^{j3\pi/4}$	$e^{j5\pi/4}$	$e^{j3\pi/4}$	$e^{j\pi/4}$	$e^{j\pi/4}$
$B^{(5)}$	e^{j0}	e^{j0}	$e^{j3\pi/2}$	$e^{j7\pi/2}$	e^{j0}	$e^{j3\pi/2}$	$e^{j3\pi/2}$	$e^{j\pi}$	$e^{j\pi}$	$e^{j3\pi/2}$	$e^{j7\pi/4}$	e^{j0}	$e^{j7\pi/4}$	$e^{j3\pi/4}$	e^{j0}	$e^{j7\pi/4}$
$B^{(6)}$	$e^{j\pi/4}$	e^{j0}	$e^{j3\pi/4}$	$e^{j3\pi/4}$	$e^{j\pi/2}$	$e^{j\pi/2}$	$e^{j\pi/2}$	$e^{j\pi}$	$e^{j\pi}$	$e^{j3\pi/2}$	$e^{j5\pi/4}$	$e^{j3\pi/2}$	$e^{j5\pi/4}$	$e^{j5\pi/4}$	$e^{j5\pi/4}$	$e^{j3\pi/2}$
$B^{(7)}$	$e^{j\pi/4}$	e^{j0}	$e^{j3\pi/4}$	$e^{j3\pi/4}$	e^{j0}	$e^{j\pi/2}$	$e^{j\pi/2}$	$e^{j\pi}$	$e^{j\pi}$	e^{j0}	$e^{j3\pi/2}$	$e^{j\pi/2}$	$e^{j7\pi/4}$	$e^{j3\pi/4}$	$e^{j5\pi/4}$	$e^{j7\pi/4}$
$B^{(8)}$	$e^{j\pi/4}$	e^{j0}	$e^{j3\pi/4}$	$e^{j3\pi/4}$	$e^{j\pi/2}$	$e^{j\pi/2}$	$e^{j\pi/2}$	$e^{j\pi}$	$e^{j\pi}$	$e^{j3\pi/4}$	$e^{j5\pi/4}$	$e^{j3\pi/2}$	$e^{j7\pi/4}$	$e^{j3\pi/4}$	$e^{j7\pi/4}$	$e^{j\pi/4}$
$B^{(9)}$	$e^{j\pi/2}$	e^{j0}	$e^{j3\pi/4}$	$e^{j3\pi/4}$	$e^{j3\pi/2}$	$e^{j\pi/2}$	$e^{j\pi/2}$	$e^{j\pi}$	$e^{j\pi}$	$e^{j3\pi/4}$	$e^{j5\pi/4}$	$e^{j3\pi/2}$	$e^{j7\pi/4}$	$e^{j3\pi/2}$	$e^{j5\pi/4}$	$e^{j7\pi/4}$
$B^{(10)}$	$e^{j\pi/4}$	e^{j0}	$e^{j3\pi/4}$	$e^{j3\pi/4}$	$e^{j\pi/2}$	$e^{j\pi/2}$	$e^{j\pi/2}$	$e^{j\pi}$	$e^{j\pi}$	$e^{j3\pi/2}$	$e^{j5\pi/4}$	$e^{j3\pi/2}$	$e^{j7\pi/4}$	$e^{j3\pi/4}$	$e^{j5\pi/4}$	$e^{j\pi/4}$
$B^{(11)}$	$e^{j\pi/4}$	e^{j0}	$e^{j3\pi/4}$	$e^{j3\pi/4}$	$e^{j\pi/2}$	$e^{j\pi/2}$	$e^{j\pi/2}$	$e^{j\pi}$	$e^{j\pi}$	$e^{j3\pi/4}$	$e^{j5\pi/4}$	$e^{j3\pi/2}$	$e^{j7\pi/4}$	$e^{j3\pi/4}$	$e^{j5\pi/4}$	$e^{j\pi/4}$
$B^{(12)}$	$e^{j\pi/4}$	e^{j0}	$e^{j3\pi/4}$	$e^{j3\pi/4}$	$e^{j\pi/2}$	$e^{j\pi/2}$	$e^{j\pi/2}$	$e^{j\pi}$	$e^{j\pi}$	$e^{j3\pi/4}$	$e^{j7\pi/4}$	$e^{j3\pi/2}$	$e^{j5\pi/4}$	$e^{j7\pi/4}$	$e^{j\pi/4}$	$e^{j\pi/4}$
$B^{(13)}$	$e^{j\pi/4}$	e^{j0}	$e^{j3\pi/2}$	$e^{j3\pi/4}$	$e^{j3\pi/2}$	$e^{j3\pi/2}$	$e^{j\pi/2}$	$e^{j\pi}$	$e^{j\pi}$	$e^{j3\pi/4}$	$e^{j5\pi/4}$	$e^{j3\pi/2}$	$e^{j7\pi/4}$	$e^{j3\pi/4}$	$e^{j5\pi/4}$	$e^{j7\pi/4}$
$B^{(14)}$	e^{j0}	$e^{j3\pi/4}$	$e^{j6\pi/4}$	$e^{j3\pi/4}$	$e^{j\pi/2}$	$e^{j\pi/2}$	$e^{j\pi/2}$	$e^{j\pi}$	$e^{j\pi}$	$e^{j3\pi/4}$	$e^{j5\pi/4}$	$e^{j3\pi/2}$	$e^{j5\pi/4}$	$e^{j3\pi/4}$	$e^{j5\pi/4}$	$e^{j\pi/4}$
$B^{(15)}$	$e^{j\pi/4}$	e^{j0}	$e^{j5\pi/4}$	$e^{j7\pi/4}$	$e^{j\pi/2}$	$e^{j3\pi/2}$	$e^{j3\pi/2}$	$e^{j\pi}$	$e^{j\pi}$	$e^{j5\pi/4}$	e^{j0}	$e^{j3\pi/2}$	$e^{j7\pi/4}$	$e^{j5\pi/4}$	$e^{j5\pi/4}$	$e^{j5\pi/4}$
$B^{(16)}$	$e^{j\pi/4}$	$e^{j3\pi/4}$	$e^{j3\pi/4}$	$e^{j3\pi/4}$	$e^{j\pi/2}$	$e^{j\pi/2}$	$e^{j\pi/2}$	$e^{j\pi}$	$e^{j\pi}$	e^{j0}	$e^{j5\pi/4}$	$e^{j3\pi/2}$	e^{j0}	$e^{j5\pi/4}$	$e^{j5\pi/4}$	$e^{j\pi/4}$

4.3.2 Multi- h CPFSK Mapper

In order to illustrate the PAPR performance of OFDM system with multi- h CPFSK mapper, $H_2 = \{h_1, h_2\} = \left\{\frac{2}{4}, \frac{3}{4}\right\}$ is chosen. The possible phase values for this mapper is given by the set $\{0, \pi/4, \pi/2, 3\pi/4, \pi, 5\pi/4, 3\pi/2, 7\pi/4\}$ and hence the possible values are given by $\{e^{j0}, e^{j\pi/4}, e^{j\pi/2}, e^{j3\pi/4}, e^{j\pi}, e^{j5\pi/4}, e^{j3\pi/2}, e^{j7\pi/4}\}$. The initial phase sequences $B^{(u)}, u = 1, 2, \dots, 16$, are given in Table 4.5. In Figs. 4.14, 4.15, 4.16, and 4.17 are shown CCDFs of PAPR for multi- h CPFSK mapper $\left(\left\{\frac{2}{4}, \frac{3}{4}\right\}\right)$ for $N = 64, 128, 256$, and 512, respectively. A comparison of PAPR performance of this mapper relative to BPSK mapper as a function of number of subcarriers of the system is given in Table 4.6. It is observed that the amount of reduction in PAPR in the case of multi- h CPFSK mapper $\left(\left\{\frac{2}{4}, \frac{3}{4}\right\}\right)$ with the use of SLM technique relative to corresponding system without SLM technique is nearly 5 dB, for $N = 64$. Single- h CPFSK mapper ($h = 1/2$) on the other hand, provides only 3.8 dB reduction in going from without SLM technique to SLM technique in the system. In general, SLM technique is much more effective with multi- h CPFSK mapper compared to single- h CPFSK mapper.

4.3.3 Asymmetric multi- h CPFSK Mapper

In order to illustrate the PAPR performance of OFDM system with asymmetric multi- h CPFSK mapper, $H_2 = \left\{\frac{2}{4}, \frac{3}{4}\right\}$ with $H_{+i} = \left\{\frac{2}{4}, \frac{3}{4}\right\}$ and $H_{-i} = \left\{\frac{3}{4}, \frac{2}{4}\right\}$ is chosen. The possible phase values for this mapper is given by the set $\{0, \pi/4, \pi/2, 3\pi/4, \pi, 5\pi/4, 3\pi/2, 7\pi/4\}$

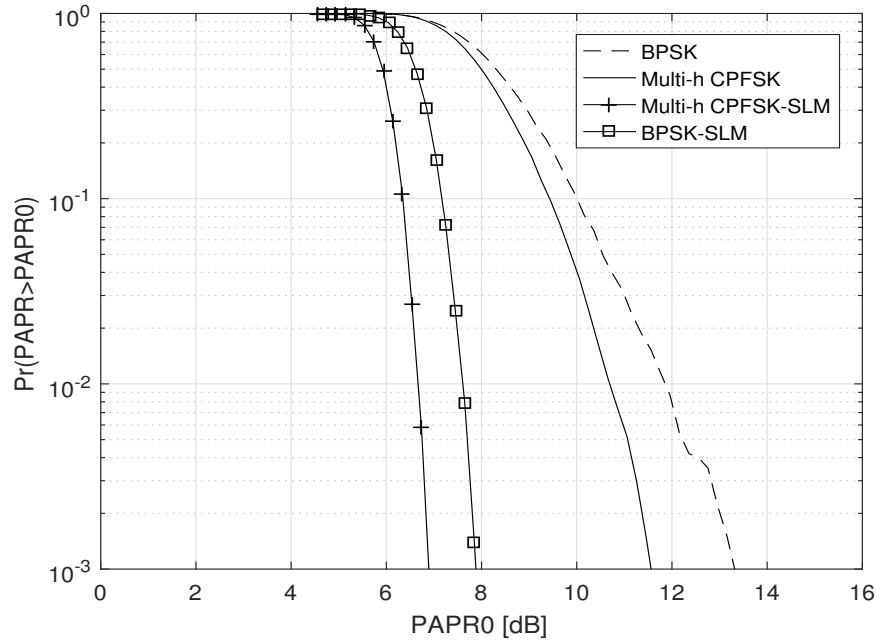


Figure 4.14: CCDFs of PAPR of an OFDM system with multi- h -CPFSK mapper $(\{\frac{2}{4}, \frac{3}{4}\})$, with SLM technique ($N = 64$)

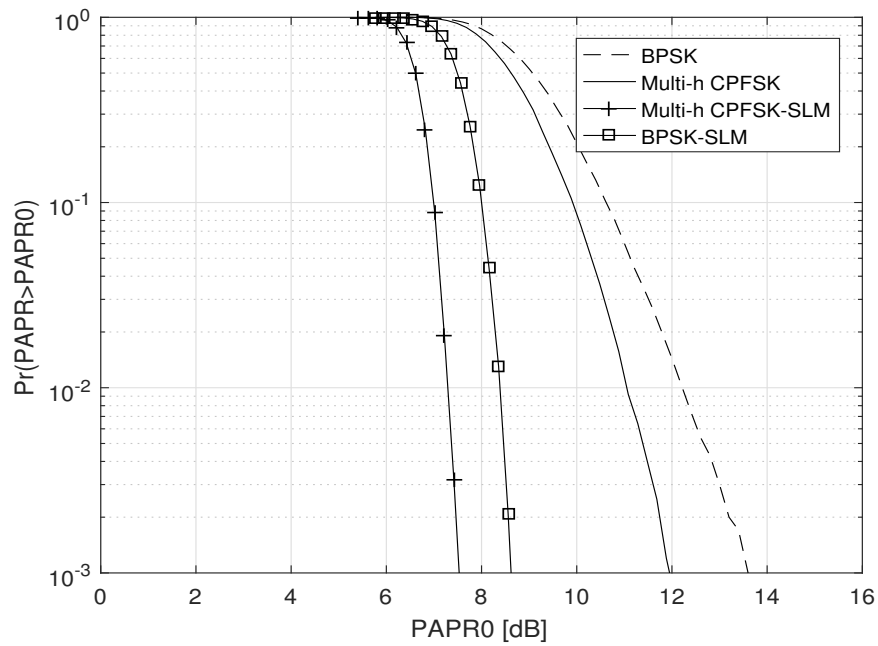


Figure 4.15: CCDFs of PAPR of an OFDM system with multi- h -CPFSK mapper $(\{\frac{2}{4}, \frac{3}{4}\})$ with SLM technique ($N = 128$)

Table 4.6: Comparison of PAPR performance of multi- h CPFSK mapper ($\{\frac{2}{4}, \frac{3}{4}\}$) as a function of number of subcarriers

Number of Subcarriers	Mapper			
	BPSK		Multi- h CPFSK	
	Without SLM (dB)	With SLM (dB)	Without SLM (dB)	With SLM (dB)
64	13.1	7.9	12.2	6.9
128	13.2	8.7	13.2	7.5
256	13.5	9.4	13.5	8.1
512	14.1	9.9	14.0	8.5

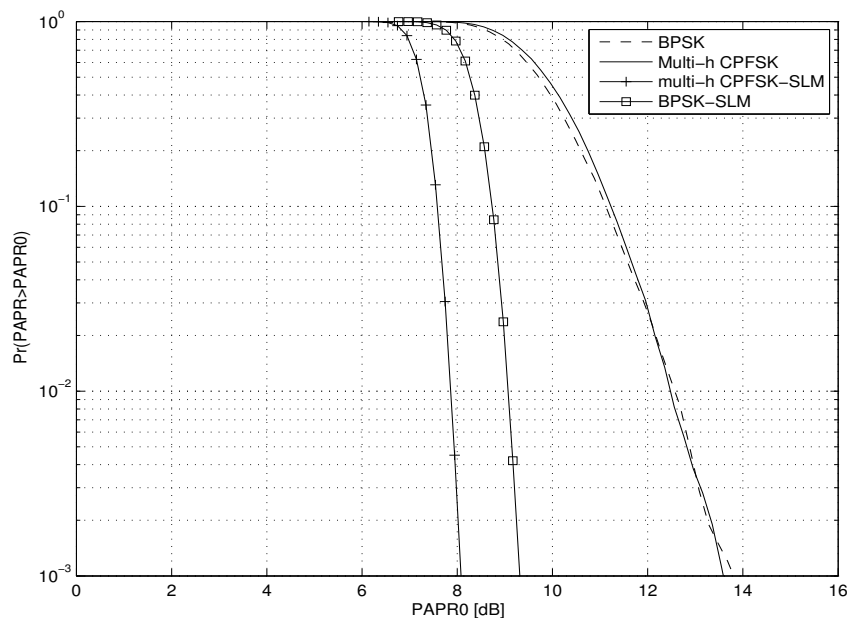


Figure 4.16: CCDFs of PAPR of an OFDM system with multi- h -CPFSK mapper with ($\{\frac{2}{4}, \frac{3}{4}\}$) with SLM technique ($N = 256$)

and hence the possible values are given by $\{e^{j0}, e^{j\pi/4}, e^{j\pi/2}, e^{j3\pi/4}, e^{j\pi}, e^{j5\pi/4}, e^{j3\pi/2}, e^{j7\pi/4}\}$.

The initial phase sequences $B^{(u)}, u = 1, 2, \dots, 16$, are given in Table 4.7. In Figs. 4.18, 4.19, 4.20, and 4.21 are shown CCDFs of PAPR for asymmetric multi- h CPFSK mapper ($H_{+i} = \{\frac{2}{4}, \frac{3}{4}\}$ and $H_{-i} = \{\frac{3}{4}, \frac{2}{4}\}$) for $N = 64, 128, 256$, and 512, respectively. A comparison of PAPR performance of this mapper relative to BPSK mapper as a function of number of subcarriers of the system is given in Table 4.8. It is observed that the amount of reduction in PAPR in the case of asymmetric multi- h CPFSK mapper ($H_{+i} = \{\frac{2}{4}, \frac{3}{4}\}$)

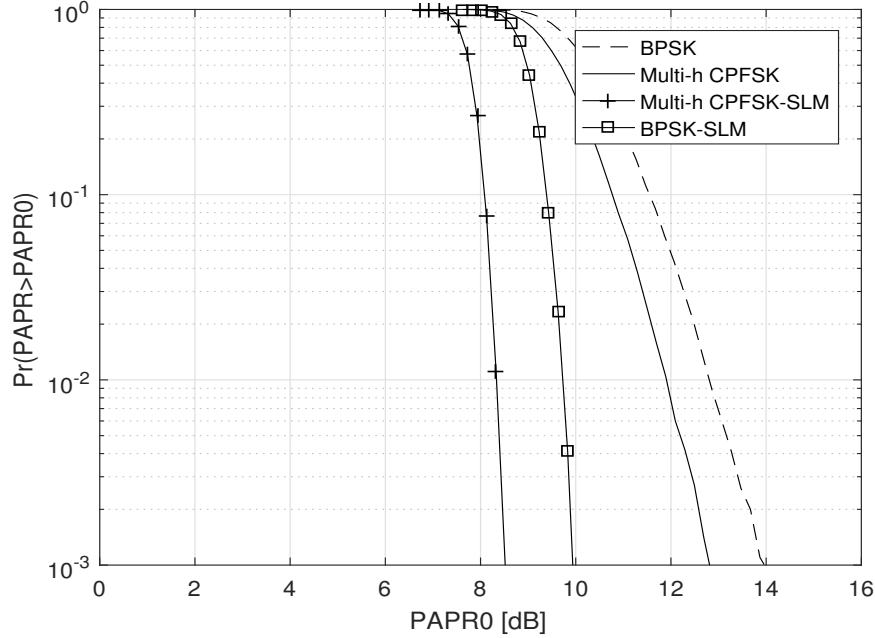


Figure 4.17: CCDFs of PAPR of an OFDM system with multi- h -CPFSK mapper $(\{\frac{2}{4}, \frac{3}{4}\})$ with SLM technique ($N = 512$)

and $H_{-i} = \{\frac{3}{4}, \frac{2}{4}\})$ with the use of SLM technique relative to corresponding system without SLM technique is nearly 4.1 dB, for $N = 64$. Single- h CPFSK mapper ($h = 1/2$) on the other hand, provides only 3.8 dB reduction in going from without SLM technique to SLM technique in the system. In general, SLM technique is much more effective with asymmetric multi- h CPFSK mapper compared to single- h CPFSK mapper.

4.4 Conclusions

In this Chapter, g-CPFSK mapper in an OFDM system is investigated for PAPR performance. Three subclasses of g-CPFSK mapper namely single- h CPFSK, multi- h CPFSK mapper and asymmetric multi- h CPFSK- are considered and their PAPR reduction ability relative to conventional BPSK mapper is assessed using extensive simulations. The gains in PAPR that are achievable by these mappers in conjunction with SLM technique in the system are determined. A method is suggested that simplifies the task of search of phase sequences in SLM technique. Also, it is noted that this method minimizes the amount of side information required to be conveyed to the receiver. It is demonstrated that SLM technique can be gainfully used in an OFDM system with g-CPFSK mapper.

Table 4.7: Phase sequences $B^{(1)}, B^{(2)}, \dots, B^{(u)}$ for asy multi- h CPFSK mapper $H_{+i} = \{\frac{2}{4}, \frac{3}{4}\}$ and $H_{-i} = \{\frac{3}{4}, \frac{2}{4}\}$

$B^{(u)}$	$b_{u,0}$	$b_{u,1}$	$b_{u,2}$	$b_{u,3}$	$b_{u,4}$	$b_{u,5}$	$b_{u,6}$	$b_{u,7}$	$b_{u,8}$	$b_{u,9}$	$b_{u,10}$	$b_{u,11}$	$b_{u,12}$	$b_{u,13}$	$b_{u,14}$	$b_{u,15}$
$B^{(1)}$	+1	+1	+1	+1	+1	+1	+1	+1	+1	+1	+1	+1	+1	+1	+1	+1
$B^{(2)}$	$e^{j3\pi/4}$	$e^{j5\pi/4}$	$e^{j3\pi/4}$	$e^{j7\pi/4}$	$e^{j\pi/2}$	$e^{j\pi/2}$	$e^{j\pi/2}$	$e^{j\pi/2}$	$e^{j\pi}$	$e^{j\pi}$	$e^{j7\pi/4}$	$e^{j3\pi/4}$	$e^{j3\pi/4}$	$e^{j5\pi/4}$	$e^{j3\pi/4}$	e^{j0}
$B^{(3)}$	$e^{j\pi}$	$e^{j7\pi/4}$	$e^{j3\pi/4}$	$e^{j\pi}$	$e^{j\pi/2}$	$e^{j\pi/2}$	$e^{j\pi/2}$	$e^{j\pi}$	$e^{j\pi}$	$e^{j7\pi/4}$	e^{j0}	$e^{j3\pi/4}$	$e^{j7\pi/4}$	$e^{j3\pi/2}$	$e^{j5\pi/4}$	$e^{j5\pi/4}$
$B^{(4)}$	$e^{j3\pi/4}$	e^{j0}	$e^{j7\pi/4}$	$e^{j3\pi/2}$	$e^{j\pi/2}$	$e^{j\pi/2}$	$e^{j\pi/2}$	$e^{j\pi}$	$e^{j\pi}$	$e^{j7\pi/4}$	$e^{j7\pi/4}$	$e^{j3\pi/4}$	$e^{j5\pi/4}$	$e^{j\pi}$	$e^{j\pi/4}$	$e^{j\pi/4}$
$B^{(5)}$	e^{j0}	$e^{j5\pi/4}$	$e^{j5\pi/2}$	$e^{j\pi}$	e^{j0}	$e^{j3\pi/2}$	$e^{j3\pi/2}$	$e^{j\pi}$	$e^{j\pi}$	$e^{j3\pi/2}$	$e^{j3\pi/2}$	e^{j0}	$e^{j7\pi/4}$	$e^{j3\pi/4}$	e^{j0}	$e^{j3\pi/4}$
$B^{(6)}$	$e^{j3\pi/4}$	e^{j0}	$e^{j3\pi/2}$	$e^{j3\pi/4}$	$e^{j\pi/2}$	$e^{j\pi/2}$	$e^{j\pi/2}$	$e^{j\pi}$	$e^{j\pi}$	$e^{j3\pi/2}$	$e^{j7\pi/4}$	$e^{j3\pi/2}$	$e^{j5\pi/4}$	$e^{j3\pi/4}$	$e^{j3\pi/4}$	$e^{j3\pi/2}$
$B^{(7)}$	$e^{j\pi}$	e^{j0}	$e^{j3\pi/4}$	$e^{j5\pi/4}$	e^{j0}	$e^{j\pi/2}$	$e^{j\pi/2}$	$e^{j\pi}$	$e^{j\pi}$	e^{j0}	$e^{j3\pi/2}$	$e^{j\pi/2}$	$e^{j7\pi/4}$	$e^{j3\pi/4}$	$e^{j5\pi/4}$	e^{j0}
$B^{(8)}$	$e^{j3\pi/2}$	e^{j0}	$e^{j3\pi/4}$	$e^{j5\pi/4}$	$e^{j\pi/2}$	$e^{j3\pi/2}$	$e^{j\pi/2}$	$e^{j\pi}$	$e^{j\pi}$	$e^{j3\pi/4}$	$e^{j5\pi/4}$	$e^{j3\pi/2}$	$e^{j7\pi/4}$	$e^{j3\pi/4}$	$e^{j7\pi/4}$	$e^{j3\pi/2}$
$B^{(9)}$	$e^{j\pi/2}$	e^{j0}	$e^{j3\pi/4}$	$e^{j5\pi/4}$	$e^{j7\pi/4}$	$e^{j\pi/2}$	$e^{j\pi/2}$	$e^{j\pi}$	$e^{j\pi}$	$e^{j3\pi/4}$	$e^{j5\pi/4}$	$e^{j3\pi/2}$	$e^{j7\pi/4}$	$e^{j3\pi/2}$	e^{j0}	$e^{j3\pi/4}$
$B^{(10)}$	$e^{j3\pi/2}$	e^{j0}	$e^{j7\pi/4}$	$e^{j5\pi/4}$	$e^{j3\pi/2}$	$e^{j\pi/2}$	$e^{j\pi/2}$	$e^{j\pi}$	$e^{j\pi}$	$e^{j3\pi/2}$	$e^{j5\pi/4}$	$e^{j3\pi/2}$	$e^{j7\pi/4}$	$e^{j3\pi/4}$	e^{j0}	$e^{j5\pi/4}$
$B^{(11)}$	$e^{j\pi/4}$	e^{j0}	$e^{j3\pi/2}$	$e^{j3\pi/4}$	$e^{j\pi/2}$	$e^{j\pi/2}$	$e^{j\pi/2}$	$e^{j\pi}$	$e^{j\pi}$	$e^{j3\pi/4}$	$e^{j5\pi/4}$	$e^{j3\pi/2}$	e^{j0}	$e^{j3\pi/4}$	$e^{j5\pi/4}$	$e^{j\pi}$
$B^{(12)}$	$e^{j\pi/2}$	$e^{j\pi/2}$	$e^{j\pi/2}$	$e^{j3\pi/4}$	$e^{j\pi/2}$	$e^{j\pi/2}$	$e^{j\pi/2}$	$e^{j\pi}$	$e^{j\pi}$	$e^{j3\pi/4}$	$e^{j\pi/2}$	$e^{j3\pi/2}$	$e^{j5\pi/4}$	$e^{j7\pi/4}$	$e^{j5\pi/4}$	$e^{j\pi/2}$
$B^{(13)}$	$e^{j3\pi/4}$	$e^{j\pi/2}$	$e^{j3\pi/2}$	$e^{j3\pi/4}$	$e^{j\pi/2}$	$e^{j3\pi/2}$	$e^{j\pi/2}$	$e^{j\pi}$	$e^{j\pi}$	$e^{j3\pi/4}$	$e^{j5\pi/4}$	$e^{j3\pi/2}$	$e^{j7\pi/4}$	$e^{j3\pi/4}$	$e^{j5\pi/4}$	$e^{j\pi/2}$
$B^{(14)}$	e^{j0}	$e^{j3\pi/2}$	$e^{j6\pi/4}$	$e^{j3\pi/2}$	$e^{j\pi/2}$	$e^{j\pi/2}$	$e^{j\pi/2}$	$e^{j\pi}$	$e^{j\pi}$	$e^{j3\pi/4}$	$e^{j5\pi/4}$	$e^{j\pi/2}$	$e^{j5\pi/4}$	$e^{j3\pi/4}$	$e^{j5\pi/4}$	$e^{j\pi/2}$
$B^{(15)}$	$e^{j3\pi/4}$	e^{j0}	$e^{j3\pi/4}$	$e^{j7\pi/4}$	$e^{j\pi/2}$	$e^{j3\pi/2}$	$e^{j\pi/2}$	$e^{j\pi}$	$e^{j\pi}$	$e^{j5\pi/4}$	e^{j0}	$e^{j3\pi/2}$	$e^{j7\pi/4}$	$e^{j5\pi/4}$	$e^{j5\pi/4}$	e^{j0}
$B^{(16)}$	$e^{j\pi/2}$	$e^{j3\pi/4}$	$e^{j3\pi/2}$	$e^{j3\pi/4}$	$e^{j3\pi/2}$	$e^{j\pi/2}$	$e^{j\pi/2}$	$e^{j\pi}$	$e^{j\pi}$	e^{j0}	$e^{j7\pi/4}$	$e^{j3\pi/2}$	e^{j0}	$e^{j3\pi/4}$	$e^{j5\pi/4}$	$e^{j5\pi/4}$

Table 4.8: Comparison of PAPR performance of asymmetric multi- h CPFSK mapper ($H_{+i} = \{\frac{2}{4}, \frac{3}{4}\}$ and $H_{-i} = \{\frac{3}{4}, \frac{2}{4}\}$) as a function of number of subcarriers

Number of Subcarriers	Mapper			
	BPSK		asy multi- h CPFSK	
	Without SLM (dB)	With SLM (dB)	Without SLM (dB)	With SLM (dB)
64	13.1	7.9	11	6.9
128	13.2	8.6	11.3	7.4
256	13.5	9.4	11.7	8.1
512	14.1	9.9	11.8	8.5

Table 4.9: Best phase sequences that minimize PAPR

N	$h = 1/2$	$h = 2/3$	multi- h	asy multi- h
64	$B^{(6)}$	$B^{(11)}$	$B^{(12)}$	$B^{(5)}$
128	$B^{(4)}$	$B^{(4)}$	$B^{(7)}$	$B^{(3)}$
256	$B^{(8)}$	$B^{(8)}$	$B^{(15)}$	$B^{(6)}$
512	$B^{(5)}$	$B^{(7)}$	$B^{(4)}$	$B^{(5)}$

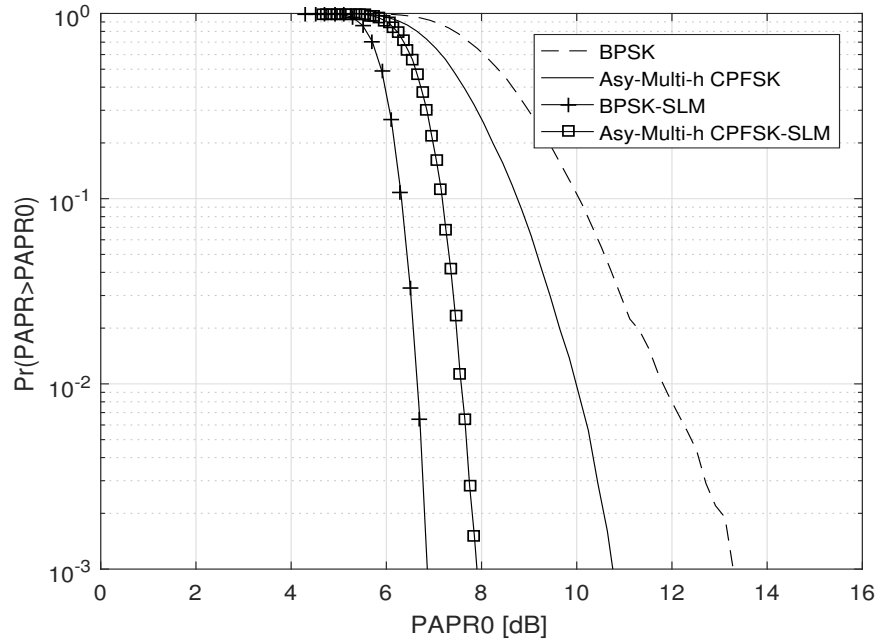


Figure 4.18: CCDFs of PAPR of an OFDM system with asymmetric multi- h -CPFSK mapper ($H_{+i} = \{\frac{2}{4}, \frac{3}{4}\}$ and $H_{-i} = \{\frac{3}{4}, \frac{2}{4}\}$) with SLM technique ($N = 64$)

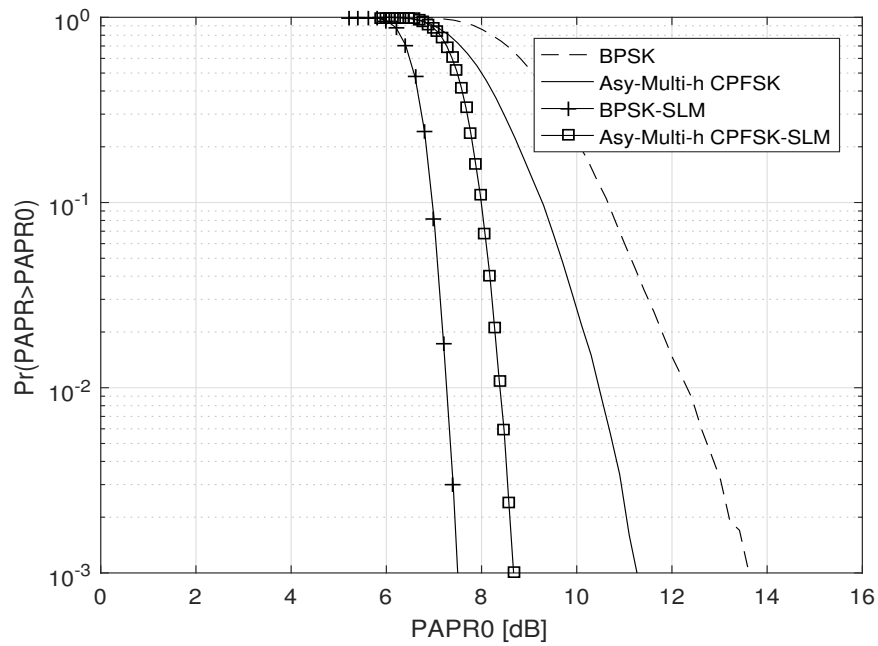


Figure 4.19: CCDFs of PAPR of an OFDM system with asymmetric multi- h -CPFSK mapper ($H_{+i} = \{\frac{2}{4}, \frac{3}{4}\}$ and $H_{-i} = \{\frac{1}{4}, \frac{2}{3}\}$) with SLM technique ($N = 128$)

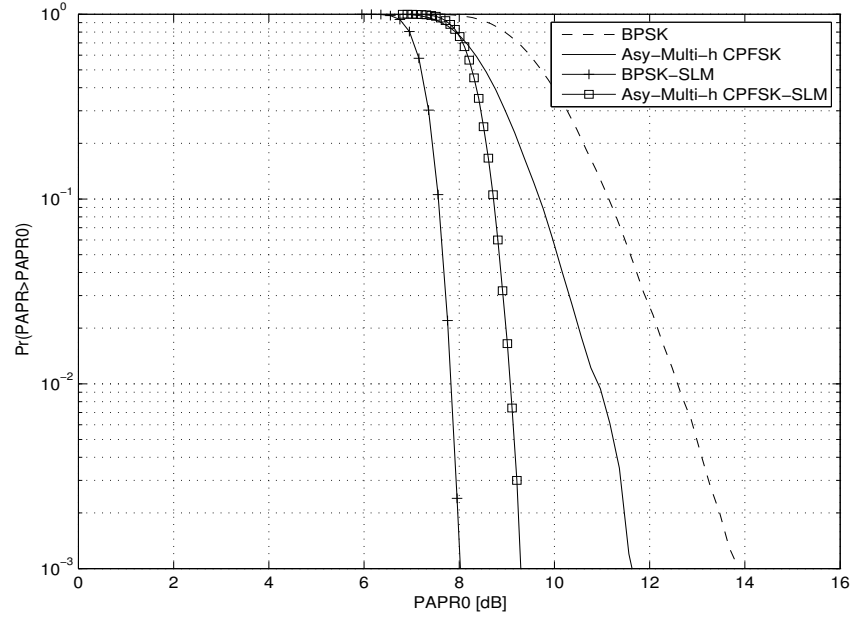


Figure 4.20: CCDFs of PAPR of an OFDM system with asymmetric multi- h -CPFSK mapper ($H_{+i} = \{\frac{2}{4}, \frac{3}{4}\}$ and $H_{-i} = \{\frac{3}{4}, \frac{2}{4}\}$) with SLM technique ($N = 256$)

Also, it is observed that PAPR reduction ability using SLM technique improves in such a system with the memory inherent.

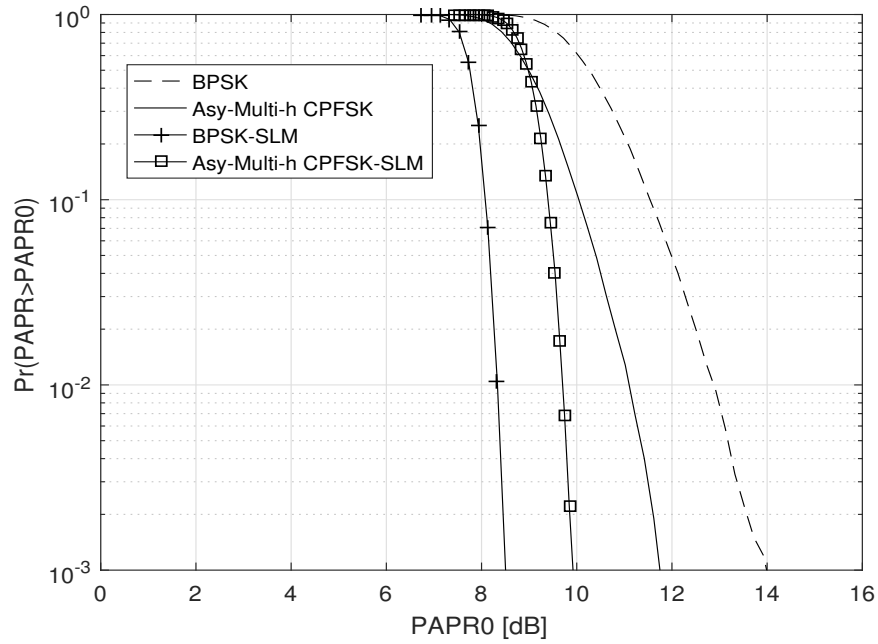


Figure 4.21: CCDFs of PAPR of an OFDM system with asymmetric multi- h -CPFSK mapper ($H_{+i} = \{\frac{2}{4}, \frac{3}{4}\}$ and $H_{-i} = \{\frac{3}{4}, \frac{2}{4}\}$) with SLM technique ($N = 512$)

Table 4.10: Phase sequences $B^{(1)}, B^{(2)}, \dots, B^{(16)}$ for BPSK mapper with $b_{u,k} \in \{e^{j0}, e^{j\pi}\}$

$B^{(u)}$	$b_{u,0}$	$b_{u,1}$	$b_{u,2}$	$b_{u,3}$	$b_{u,4}$	$b_{u,5}$	$b_{u,6}$	$b_{u,7}$	$b_{u,8}$	$b_{u,9}$	$b_{u,10}$	$b_{u,11}$	$b_{u,12}$	$b_{u,13}$	$b_{u,14}$	$b_{u,15}$
$B^{(1)}$	+1	+1	+1	+1	+1	+1	+1	+1	+1	+1	+1	+1	+1	+1	+1	+1
$B^{(2)}$	e^{j0}	e^{j0}	$e^{j\pi}$	$e^{j\pi}$	$e^{j\pi}$	e^{j0}	e^{j0}	e^{j0}	e^{j0}	$e^{j\pi}$	e^{j0}	e^{j0}	$e^{j\pi}$	e^{j0}	e^{j0}	$e^{j\pi}$
$B^{(3)}$	$e^{j\pi}$	e^{j0}	$e^{j\pi}$	$e^{j\pi}$	$e^{j\pi}$	$e^{j\pi}$	e^{j0}	e^{j0}	e^{j0}	$e^{j\pi}$	e^{j0}	e^{j0}	$e^{j\pi}$	$e^{j\pi}$	e^{j0}	$e^{j\pi}$
$B^{(4)}$	$e^{j\pi}$	$e^{j\pi}$	$e^{j\pi}$	$e^{j\pi}$	$e^{j\pi}$	e^{j0}	e^{j0}	e^{j0}	e^{j0}	$e^{j\pi}$	e^{j0}	e^{j0}	$e^{j\pi}$	e^{j0}	e^{j0}	e^{j0}
$B^{(5)}$	e^{j0}	$e^{j\pi}$	$e^{j\pi}$	$e^{j\pi}$	$e^{j\pi}$	$e^{j\pi}$	e^{j0}	e^{j0}	$e^{j\pi}$	$e^{j\pi}$	e^{j0}	e^{j0}	$e^{j\pi}$	e^{j0}	e^{j0}	e^{j0}
$B^{(6)}$	e^{j0}	$e^{j\pi}$	$e^{j\pi}$	$e^{j\pi}$	$e^{j\pi}$	$e^{j\pi}$	e^{j0}	e^{j0}	$e^{j\pi}$	$e^{j\pi}$	e^{j0}	e^{j0}	$e^{j\pi}$	e^{j0}	e^{j0}	$e^{j\pi}$
$B^{(7)}$	e^{j0}	$e^{j\pi}$	$e^{j\pi}$	$e^{j\pi}$	$e^{j\pi}$	e^{j0}	e^{j0}	$e^{j\pi}$	e^{j0}	$e^{j\pi}$	e^{j0}	$e^{j\pi}$	$e^{j\pi}$	e^{j0}	e^{j0}	$e^{j\pi}$
$B^{(8)}$	e^{j0}	e^{j0}	e^{j0}	e^{j0}	$e^{j\pi}$	e^{j0}	$e^{j\pi}$	e^{j0}	e^{j0}	$e^{j\pi}$	$e^{j\pi}$	e^{j0}	$e^{j\pi}$	e^{j0}	$e^{j\pi}$	$e^{j\pi}$
$B^{(9)}$	$e^{j\pi}$	$e^{j\pi}$	$e^{j\pi}$	$e^{j\pi}$	$e^{j\pi}$	$e^{j\pi}$	e^{j0}	e^{j0}	$e^{j\pi}$	$e^{j\pi}$	e^{j0}	e^{j0}	$e^{j\pi}$	$e^{j\pi}$	e^{j0}	$e^{j\pi}$
$B^{(10)}$	$e^{j\pi}$	e^{j0}	e^{j0}	$e^{j\pi}$	e^{j0}	e^{j0}	$e^{j\pi}$	$e^{j\pi}$	e^{j0}	$e^{j\pi}$	e^{j0}	e^{j0}	$e^{j\pi}$	e^{j0}	$e^{j\pi}$	$e^{j\pi}$
$B^{(11)}$	$e^{j\pi}$	$e^{j\pi}$	$e^{j\pi}$	$e^{j\pi}$	0	e^{j0}	e^{j0}	e^{j0}	e^{j0}	e^{j0}	e^{j0}	e^{j0}	$e^{j\pi}$	e^{j0}	$e^{j\pi}$	$e^{j\pi}$
$B^{(12)}$	$e^{j\pi}$	e^{j0}	e^{j0}	$e^{j\pi}$	e^{j0}	$e^{j\pi}$	e^{j0}	$e^{j\pi}$	e^{j0}	$e^{j\pi}$	$e^{j\pi}$	e^{j0}	$e^{j\pi}$	e^{j0}	$e^{j\pi}$	$e^{j\pi}$
$B^{(13)}$	$e^{j\pi}$	$e^{j\pi}$	$e^{j\pi}$	$e^{j\pi}$	e^{j0}	$e^{j\pi}$	e^{j0}	$e^{j\pi}$	e^{j0}	$e^{j\pi}$	$e^{j\pi}$	$e^{j\pi}$	$e^{j\pi}$	$e^{j\pi}$	$e^{j\pi}$	$e^{j\pi}$
$B^{(14)}$	$e^{j\pi}$	e^{j0}	$e^{j\pi}$	$e^{j\pi}$	$e^{j\pi}$	$e^{j\pi}$	e^{j0}	e^{j0}	$e^{j\pi}$	$e^{j\pi}$	e^{j0}	$e^{j\pi}$	$e^{j\pi}$	$e^{j\pi}$	e^{j0}	$e^{j\pi}$
$B^{(15)}$	e^{j0}	$e^{j\pi}$	$e^{j\pi}$	$e^{j\pi}$	$e^{j\pi}$	$e^{j\pi}$	e^{j0}	$e^{j\pi}$	$e^{j\pi}$	$e^{j\pi}$	e^{j0}	e^{j0}	$e^{j\pi}$	e^{j0}	$e^{j\pi}$	$e^{j\pi}$
$B^{(16)}$	e^{j0}	e^{j0}	$e^{j\pi}$	$e^{j\pi}$	e^{j0}	$e^{j\pi}$	e^{j0}	$e^{j\pi}$	$e^{j\pi}$	$e^{j\pi}$	e^{j0}	e^{j0}	$e^{j\pi}$	$e^{j\pi}$	$e^{j\pi}$	$e^{j\pi}$

Chapter 5

PAPR Reduction using PTS Technique for OFDM System with g-CPFSK Mapper^{1,2}

5.1 Introduction

In this Chapter, an OFDM system with g-CPFSK mapper is considered. The PAPR properties of such a system with PTS technique is examined. The ability of the system to reduce PAPR is assessed as a function of parameters of the mapper and the number of subcarriers in the system. Firstly, three subclasses of g-CPFSK mapper, namely, single- h CPFSK, multi- h CPFSK, and asymmetric multi- h CPFSK mappers are considered and their PAPR performances are assessed. These mappers in conjunction with PTS technique are considered and their PAPR performances are examined. A comparison of the PAPR reduction capability of g-CPFSK mapper relative to memoryless BPSK mappers in an OFDM system is presented.

5.2 PTS Technique and g-CPFSK Mapper

The idea behind the PTS technique is that the data stream generated from the g-CPFSK mapper is partitioned into disjoint subblocks. The subcarriers in each subblock are

-
1. E. Shafter, and R. K. Rao, "The Reduction of PAPR using CPM Mappers and Partial Transmit Sequence (PTS) Scheme in OFDM Systems," Lecture Notes in Engineering and Computer Science: Proceedings of The World Congress on Engineering and Computer Science, WCECS, San Francisco, USA, pp. 707-710, Oct. 2015.
 2. E. Shafter, and R. K. Rao, "A Comparison between SLM, PTS, and CF Schemes for the Reduction of PAPR of OFDM System with CPM Mappers," IAENG International Journal of Computer Science 43.2, 2016.

weighted by a phase factor for that subblock. The phase factors are selected such that the PAPR of the combined signal is minimum [16]. The block diagram of OFDM system with g-CPFSK mapper and PTS technique is shown in Fig.5.1. The data stream generated from the g-CPFSK mapper can be represented as

$$\mathbf{C}_p = [C_{p,0}, C_{p,1}, \dots, C_{p,N-1}] \quad (5.1)$$

In PTS technique \mathbf{C}_p is partitioned into M subblocks. These subblocks can be written as

$$\begin{aligned} \mathbf{C}_p^{(1)} &= [C_{p,0}, C_{p,1}, \dots, C_{p,P-1}, 0, 0, \dots, 0] \\ \mathbf{C}_p^{(2)} &= [0, 0, \dots, C_{p,P}, C_{p,P+1}, \dots, C_{p,2P-1}, 0, 0, \dots] \\ &\vdots \\ \mathbf{C}_p^{(M)} &= [0, 0, \dots, 0, \dots, C_{p,(M-1)P}, C_{p,(M-1)P+1}, \dots, C_{p,MP-1}] \end{aligned} \quad (5.2)$$

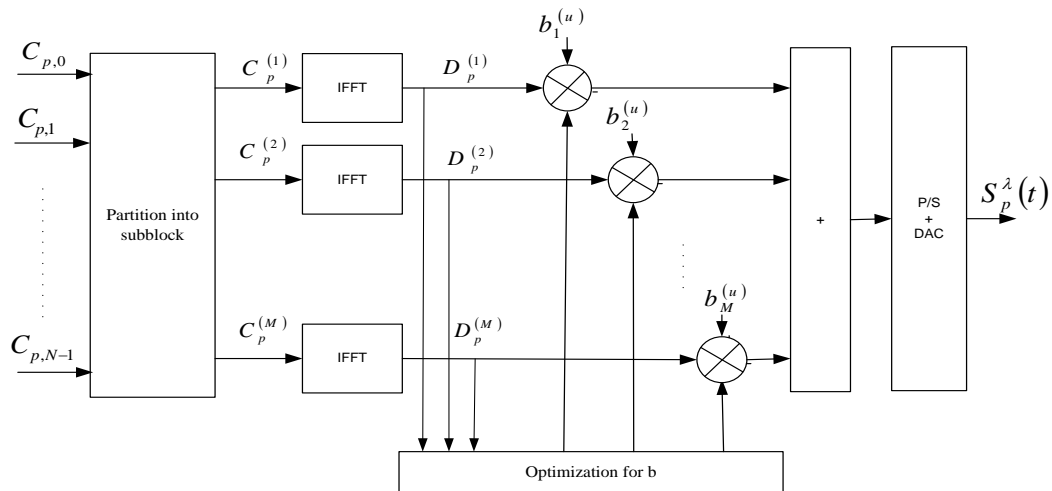


Figure 5.1: Block diagram of OFDM system with g-CPFSK mapper and PTS technique

It is noted that each of the subblocks in (5.2), $\mathbf{C}_p^{(i)}, i = 1, 2, \dots, M$, has P elements of \mathbf{C}_p given in (5.1) and rest of $(N - P)$ elements are zeros. This type of partition of \mathbf{C}_p into M subblocks is referred as adjacent partitioning. Also, it is possible to use random partitioning in which element of \mathbf{C}_p are first randomly organized and then adjacent partitioning is used. For example, consider $\mathbf{C}_p = [C_{p,0}, C_{p,1}, \dots, C_{p,7}]$ which

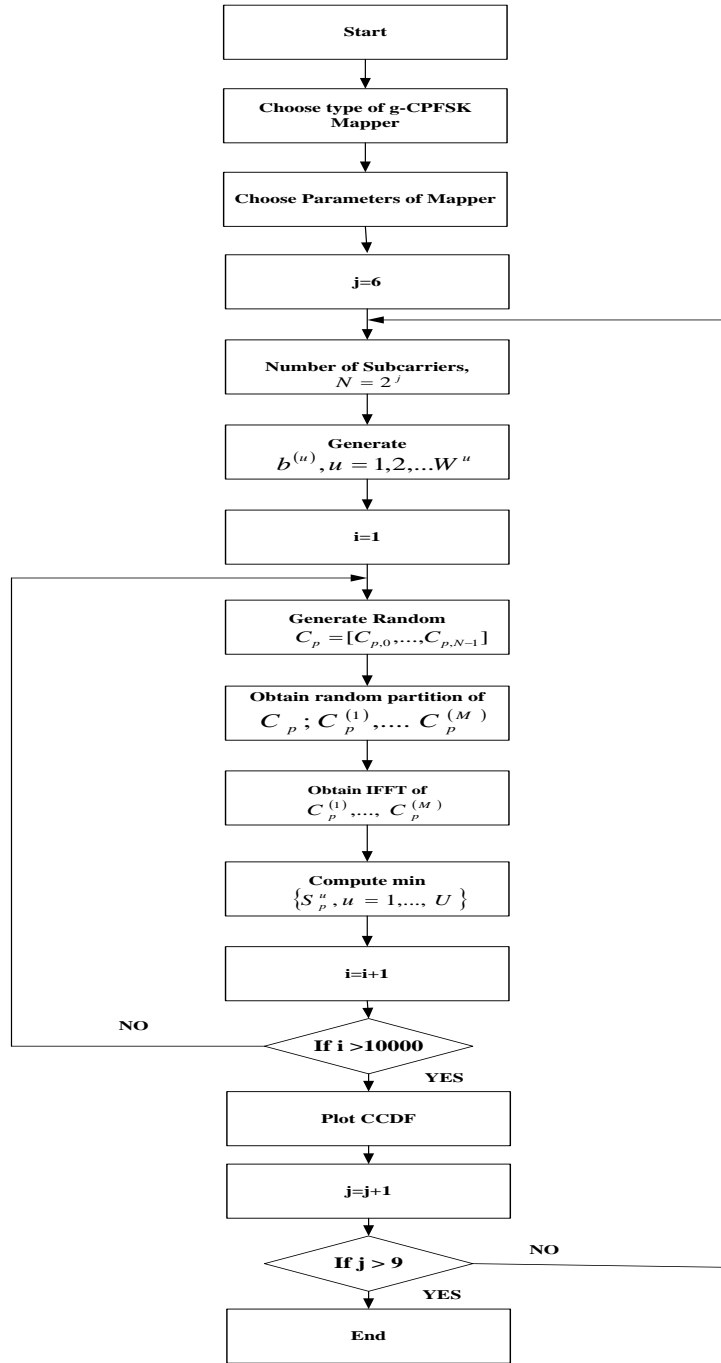


Figure 5.2: Flow-chart for computation CCDFs of PAPR using PTS technique

has 8 elements. If $M = 4$ is chosen, then there are 4 subblocks $\mathbf{C}_p^{(i)}$, $i = 1, 2, 3, 4$ possible

using adjacent partitioning and are given by:

$$\begin{aligned}
\mathbf{C}_p^{(1)} &= [C_{p,0}, C_{p,1}, 0, 0, 0, 0, 0, 0] \\
\mathbf{C}_p^{(2)} &= [0, 0, C_{p,2}, C_{p,3}, 0, 0, 0, 0] \\
\mathbf{C}_p^{(3)} &= [0, 0, 0, 0, C_{p,4}, C_{p,5}, 0, 0] \\
\mathbf{C}_p^{(4)} &= [0, 0, 0, 0, 0, 0, C_{p,6}, C_{p,7}]
\end{aligned} \tag{5.3}$$

If random partitioning is used, the elements of \mathbf{C}_p are first organized in a random manner, say, $\mathbf{C}_p = [C_{p,7}, C_{p,0}, C_{p,3}, C_{p,4}, C_{p,2}, C_{p,5}, C_{p,1}, C_{p,6}]$. Upon using adjacent partitioning, the 4 subblocks can be written as:

$$\begin{aligned}
\mathbf{C}_p^{(1)} &= [C_{p,7}, C_{p,0}, 0, 0, 0, 0, 0, 0] \\
\mathbf{C}_p^{(2)} &= [0, 0, C_{p,3}, C_{p,4}, 0, 0, 0, 0] \\
\mathbf{C}_p^{(3)} &= [0, 0, 0, 0, C_{p,2}, C_{p,5}, 0, 0] \\
\mathbf{C}_p^{(4)} &= [0, 0, 0, 0, 0, 0, C_{p,1}, C_{p,6}]
\end{aligned} \tag{5.4}$$

The number of partitioned subblocks, M , and the number of elements in each subblock is related by $P = \frac{N}{M}$, where N is the number of subcarriers. Typically $N = 2^n$, n being an integer. In PTS technique, the input symbol block \mathbf{C}_p in (5.1) is partitioned into M disjoint symbol subblocks $C_p^{(i)}$, $i = 1, 2, \dots, M$, such that

$$\mathbf{C}_p = \sum_{i=1}^M \mathbf{C}_p^{(i)} \tag{5.5}$$

The time-domain L -times oversampled, signal vector $\mathbf{S}_p^{(m)}$ is generated by applying IFFT to each $\mathbf{C}_p^{(m)}$, $m = 1, 2, \dots, M$. That is

$$S_p^{(m)}(k) = S_p^{(m)}\left(\frac{kT}{L}\right) = \frac{1}{\sqrt{N}} \sum_{n=0}^{N-1} C_{pn}^{(m)} e^{j\frac{2\pi kn}{NL}}, m = 1, 2, \dots, M; k = 0, 1, \dots, NL - 1 \tag{5.6}$$

where $C_{pn}^{(m)}$, $n = 0, 1, \dots, N - 1$ are elements of $C_p^{(m)}$. The vector $\mathbf{S}_p^{(m)}$ can be written as:

$$\mathbf{S}_p^{(m)} = [S_p^{(m)}(0), S_p^{(m)}(1), \dots, S_p^{(m)}(NL - 1)] \tag{5.7}$$

In PTS technique each $\mathbf{S}_p^{(m)}$ is independently rotated by multiplying phase rotating vector $\theta_m \epsilon \left\{ e^{j\frac{2\pi l}{W}}, l = 0, 1, \dots, W-1 \right\}$, where W is the number of phase rotating factors. It is noted that the phase-rotating factors θ_m can be expressed as a phase rotating vector $b^{(u)} = \left[b_1^{(u)}, b_2^{(u)}, \dots, b_M^{(u)} \right]$, $u = 1, 2, \dots, U$ where M is the number of subblocks of \mathbf{C}_p . Thus, using this phase rotating vector $\mathbf{b}^{(u)}$, the u^{th} OFDM signal can be written as

$$\mathbf{S}_p^u = \sum_{m=1}^M b_m^{(u)} \mathbf{S}_p^{(m)}, u = 1, 2, \dots, U$$

The objective in PTS technique is to find PAPR of $\mathbf{S}_p^u, u = 1, 2, \dots, U$ and choosing the one with minimum value. Mathematically, this can be stated as:

$$\min_{1 \leq u \leq U} PAPR\{\mathbf{S}_p^u\} \quad (5.8)$$

If $u = \lambda$, say, is the one that results in minimum PAPR, then $S_p^\lambda(t)$ is transmitted along with side information about λ . With the knowledge of λ and hence, $b^{(\lambda)} = \left[b_1^{(\lambda)}, b_2^{(\lambda)}, \dots, b_M^{(\lambda)} \right]$, \mathbf{C}_p can be recovered at the receiver. The computation of (5.8) is too high. In arriving at value of λ one needs to perform W^M computations. For example, when the number of subcarriers $N = 128$ and if number of partitions $M = 16$ and the number of phase rotating factors $W = 4$, 4^{16} computations are required before arriving at the best sequence $b^{(\lambda)} = \left[b_1^{(\lambda)}, b_2^{(\lambda)}, \dots, b_M^{(\lambda)} \right]$ that minimize (5.8).

5.3 Numerical Results and Discussion

In this Section numerical results are presented using CCDFs of PAPR of OFDM system with g-CPFSK mapper with and without PTS technique, as a function of number of subcarriers ($N = 64, 128, 256, 512$). In the computation of PAPR, an oversampling factor $L = 4$ is used and simulation results have been obtained using MATLAB. For each CCDF plot 10,000 random OFDM symbols are considered. Fig. 5.2 shows the flow-chart for computation of CCDFs of PAPR using PTS technique. Numerical results are presented for the case of $\theta_m = \left\{ e^{j0}, e^{j\pi/2}, e^{j\pi}, e^{j3\pi/2} \right\} = \{+1, +j, -1, -j\}$. Also, the number of partitions M is set equal to 8 in all computations and random partitioning technique is used. For example, if $N = 64$ and $M = 8$, then $P = 8$, number of elements in each

subblock. The phase rotating vector $b^{(u)} = [b_1^{(u)}, b_2^{(u)}, b_3^{(u)}, b_4^{(u)}, b_5^{(u)}, b_6^{(u)}, b_7^{(u)}, b_8^{(u)}]$ with $b_i^{(u)} \in \theta_m$ is used for finding $b^{(\lambda)}$ that minimize the PAPR in (5.8). Since $M = 8$ and $W = 4$, $u = 1, 2, \dots, 4096(W^M)$, where W is the number of elements in θ_m . If, on the other hand, $N = 128$ and $M = 8$, $P = 16$, number of elements in each subblock. Then the phase rotating vector $b^{(u)}$ is still the same thereby keeping the search space same. Since u can take values from 1 to 4096, the best phase rotating vectors can be identified as $b^{(\lambda)}$, $1 \leq \lambda \leq 4096$, both at the transmitter and at the receiver. For a given OFDM block, the value of λ must be conveyed to the receiver. This implies 14 bits of side information for each OFDM block.

5.3.1 Single- h CPFSK Mapper

For the case of OFDM system with single- h CPFSK mapper, CCDFs of PAPR for $h = \frac{1}{2}$ are shown in Figs. 5.3, 5.4, 5.5, and 5.8 for $N = 64, 128, 256$, and 512, respectively. The PAPR plots shown in these figures are for systems with and without PTS technique. Also, shown in these figures are PAPR plots for an OFDM system with memoryless BPSK mapper, with and without PTS technique.

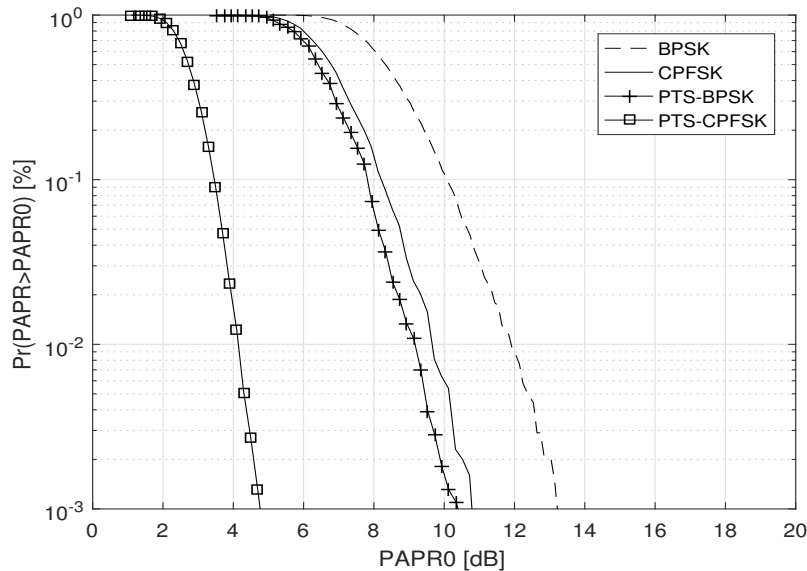


Figure 5.3: CCDFs of PAPR of an OFDM system with single- h CPFSK mapper ($h = \frac{1}{2}$) with and without PTS technique ($N = 64$)

It is observed that single- h CPFSK ($h = 1/2$) mapper offers superior PAPR performance

Table 5.1: Best phase rotating vectors that minimize PAPR

N	$h = 1/2$	$h = 2/3$	multi- h	asy multi- h
64	$b^{(201)}$	$b^{(10)}$	$b^{(87)}$	$b^{(55)}$
128	$b^{(789)}$	$b^{(114)}$	$b^{(289)}$	$b^{(98)}$
256	$b^{(1389)}$	$b^{(503)}$	$b^{(876)}$	$b^{(671)}$
512	$b^{(3200)}$	$b^{(749)}$	$b^{(1200)}$	$b^{(3290)}$

compared to the BPSK mapper. The OFDM system with single- h CPFSK ($h = 1/2$) mapper has a PAPR that exceeds 10.7 dB for less than 0.1 percent of data blocks; whereas for BPSK mapper this value is nearly 13.1 dB. The phase rotating vectors that resulted in minimum PAPR are $b^{(201)}$, $b^{(789)}$, $b^{(1389)}$, and $b^{(3200)}$ for $N = 64, 128, 256$, and 512 respectively. These sequences are given in Table 5.1. It is noted that when PTS is applied with single- h CPFSK ($h = 1/2$) mapper, the PAPR reduces to 4.8 dB which is an improvement of nearly 5.9 dB relative to the corresponding system without PTS technique. Also, it is observed that BPSK mapper with PTS applied results in PAPR of 10.3 dB. A comparison of PAPR reductions for both BPSK and single- h CPFSK mappers with and without PTS technique is given in Table 5.2. The CCDFs of PAPR of an OFDM system with single- h CPFSK ($h = 2/3$) mapper for $N = 64, 128, 256$, and 512, with and without PTS technique, are shown in Figs. 5.7, 5.8, 5.9, and 5.10, respectively. The best phase rotating vector that minimize PAPR are $b^{(10)}$, $b^{(114)}$, $b^{(503)}$, and $b^{(749)}$ for $N = 64, 128, 256$, and 512, respectively. These are listed in Table 5.1. A comparison of PAPR reductions for both BPSK and single- h CPFSK ($h = 2/3$) mapper with and without PTS technique is given in Table 5.3. It is noted that PAPR, in general, increases as a function of increasing number of subcarriers in the system, for both single- h CPFSK and BPSK mappers regardless of whether PTS technique is used or not. However, for a given number of subcarriers in the system, PAPR reductions always exist with the use of PTS technique compared to the system without this technique. An overall improvement in PAPR of 6.7 dB can be achieved with single- h CPFSK mapper by using PTS technique relative to the same system without this technique.

Table 5.2: Comparison of PAPR performance of single- h CPFSK ($h = \frac{1}{2}$) mapper as a function of number of subcarriers

Number of Subcarriers	Mapper			
	BPSK		Single- h CPFSK	
	Without PTS (dB)	With PTS (dB)	Without PTS (dB)	With PTS (dB)
64	13.1	10.3	10.7	4.8
128	13.2	10.4	10.8	5.2
256	13.5	11.0	10.9	5.3
512	14.1	11.1	11	6.0

Table 5.3: Comparison of PAPR performance of single- h CPFSK ($h = \frac{2}{3}$) mapper as a function of number of subcarriers

Number of Subcarriers	Mapper			
	BPSK		Single- h CPFSK	
	Without PTS (dB)	With PTS (dB)	Without PTS (dB)	With PTS (dB)
64	13.1	10.0	13.8	7.1
128	13.2	10.8	14.2	8.2
256	13.5	12.8	14.7	9.0
512	14.1	13.9	15.2	9.7

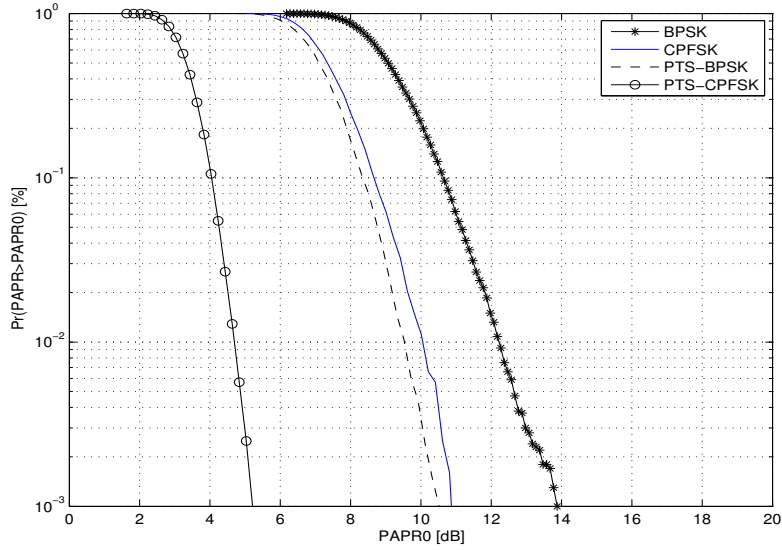


Figure 5.4: CCDFs of PAPR of an OFDM system with single- h CPFSK mapper ($h = \frac{1}{2}$) with and without PTS technique ($N = 128$)

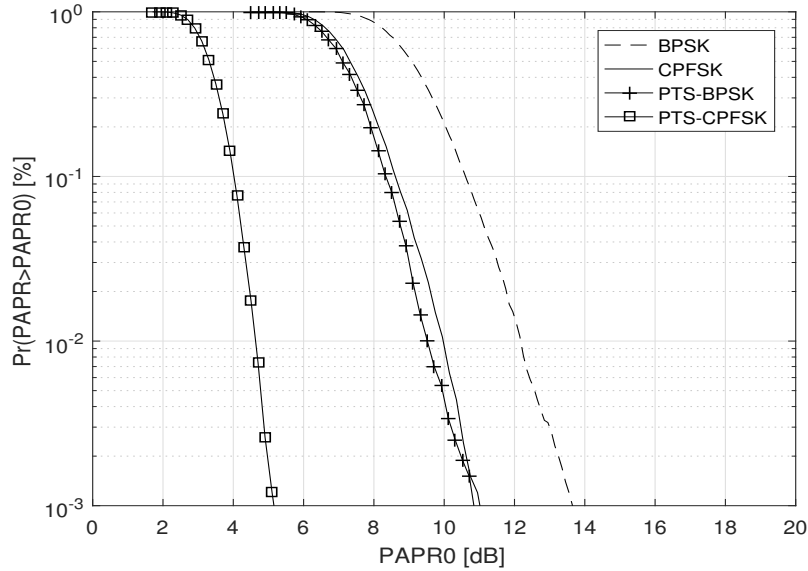


Figure 5.5: CCDFs of PAPR of an OFDM system with single- h CPFSK mapper ($h = \frac{1}{2}$) with and without PTS technique ($N = 256$)

5.3.2 Multi- h -CPFSK Mapper

To illustrate the PAPR performance of OFDM system with multi- h CPFSK mapper, $H_2 = \{h_1, h_2\} = \left\{\frac{2}{4}, \frac{3}{4}\right\}$ is chosen. In Figs. 5.11, 5.12, 5.13, and 5.14 are shown

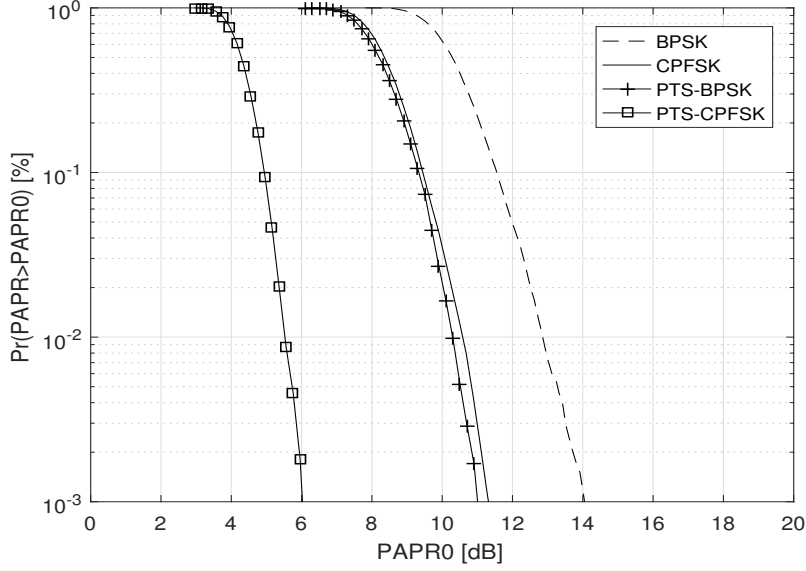


Figure 5.6: CCDFs of PAPR of an OFDM system with single- h CPFSK mapper ($h = \frac{1}{2}$) with and without PTS technique ($N = 512$)

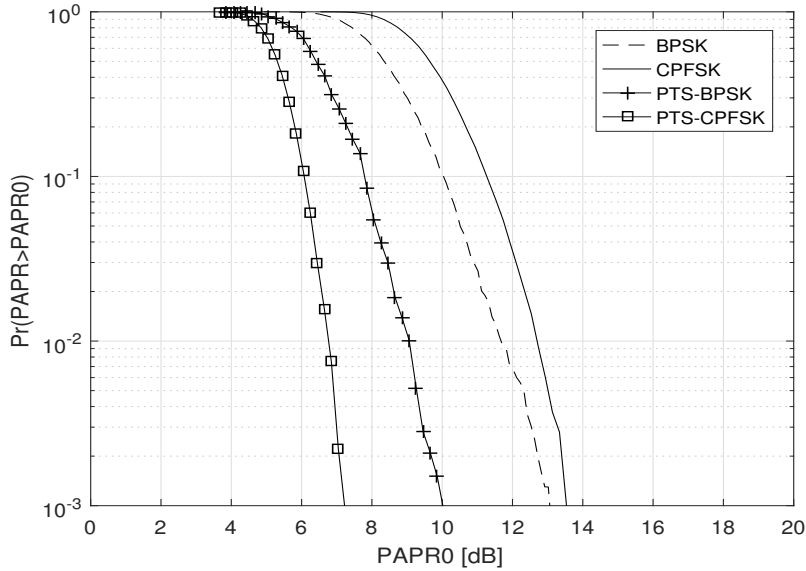


Figure 5.7: CCDFs of PAPR of an OFDM with single- h CPFSK mapper ($h = \frac{2}{3}$) with and without PTS technique, ($N = 64$)

CCDFs of PAPR for multi- h CPFSK mapper ($\{\frac{2}{4}, \frac{3}{4}\}$) for $N = 64, 128, 256,$ and $512,$ respectively. The phase rotating vectors that minimize PAPR are $b^{(87)}, b^{(289)}, b^{(876)},$ and $b^{(1200)}$ for $N = 64, 128, 256,$ and $512,$ respectively. A comparison of PAPR performance of this mapper relative to BPSK mapper as a function of number of subcarriers of the

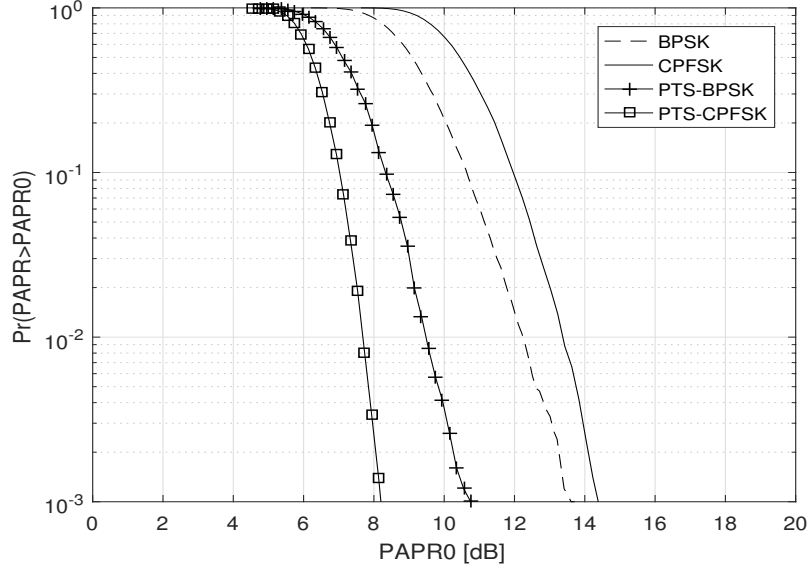


Figure 5.8: CCDFs of PAPR of an OFDM with single- h CPFSK mapper ($h = \frac{2}{3}$) with and without PTS technique, ($N = 128$)

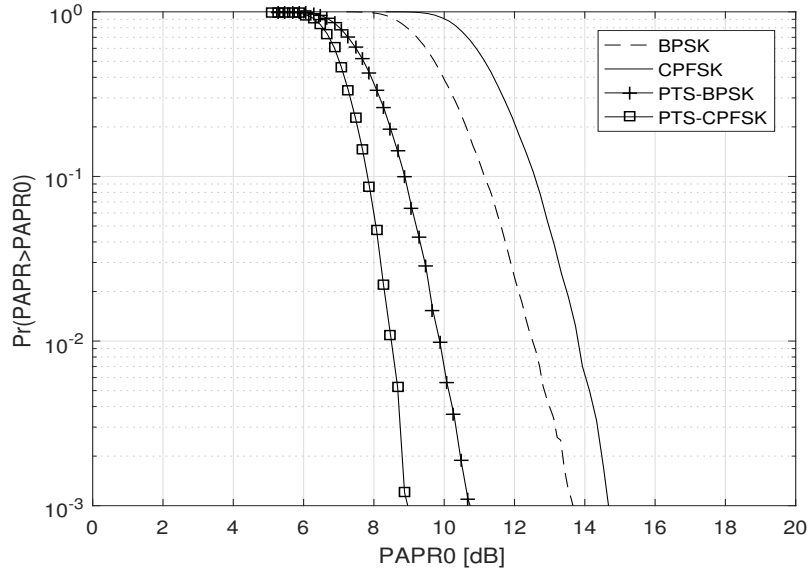


Figure 5.9: CCDFs of PAPR of an OFDM with single- h CPFSK mapper ($h = \frac{2}{3}$) with and without PTS technique, ($N = 256$)

system is given in Table 5.4. It is observed that the amount of reduction in PAPR in the case of multi- h CPFSK mapper ($\{\frac{2}{4}, \frac{3}{4}\}$) with the use of PTS technique relative to corresponding system without PTS technique is nearly 4.2 dB, for $N = 64$. Single- h CPFSK mapper ($h = 1/2$) on the other hand, provides only 2.4 dB reduction in going

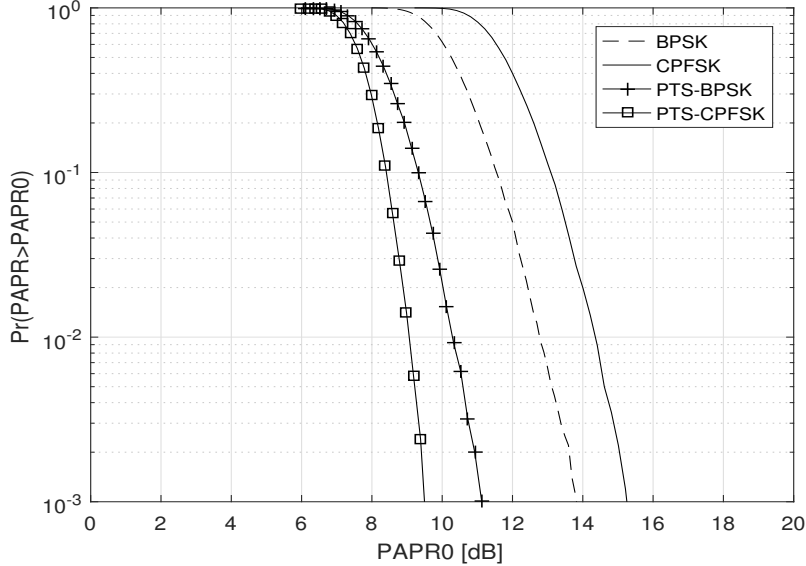


Figure 5.10: CCDFs of PAPR of an OFDM with single- h CPFSK mapper ($h = \frac{2}{3}$) with and without PTS technique, ($N = 512$)

from a system without PTS technique to a system with PTS technique in the system. In general, PTS technique is much more effective with multi- h CPFSK mapper compared to single- h CPFSK mapper.

5.3.3 Asymmetric Multi- h -CPFSK Mapper

To illustrate the PAPR performance of OFDM system with asymmetric multi- h CPFSK mapper, $H_2 = \left\{ \frac{2}{4}, \frac{3}{4} \right\}$ with $H_{+i} = \left\{ \frac{2}{4}, \frac{3}{4} \right\}$ and $H_{-i} = \left\{ \frac{3}{4}, \frac{2}{4} \right\}$ is chosen. In Figs. 5.15, 5.16, 5.17, and 5.18 are shown CCDFs of PAPR for asymmetric multi- h CPFSK mapper

Table 5.4: Comparison of PAPR performance of multi- h CPFSK mapper ($\left\{ \frac{2}{4}, \frac{3}{4} \right\}$) as a function of number of subcarriers

Number of Subcarriers	Mapper			
	BPSK		Multi- h CPFSK	
	Without PTS (dB)	With PTS (dB)	Without PTS (dB)	With PTS (dB)
64	13.1	10.0	12.2	6.2
128	13.2	10.2	13.0	7.0
256	13.5	10.8	13.3	7.8
512	14.1	11.0	13.8	8.2

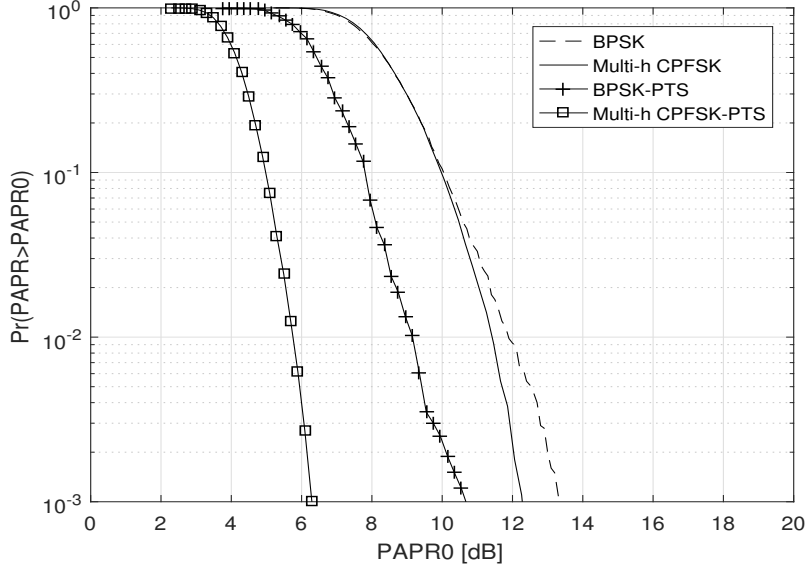


Figure 5.11: CCDFs of PAPR of an OFDM system with multi- h CPFSK mapper $(\{\frac{2}{4}, \frac{3}{4}\})$ with PTS technique ($N = 64$)

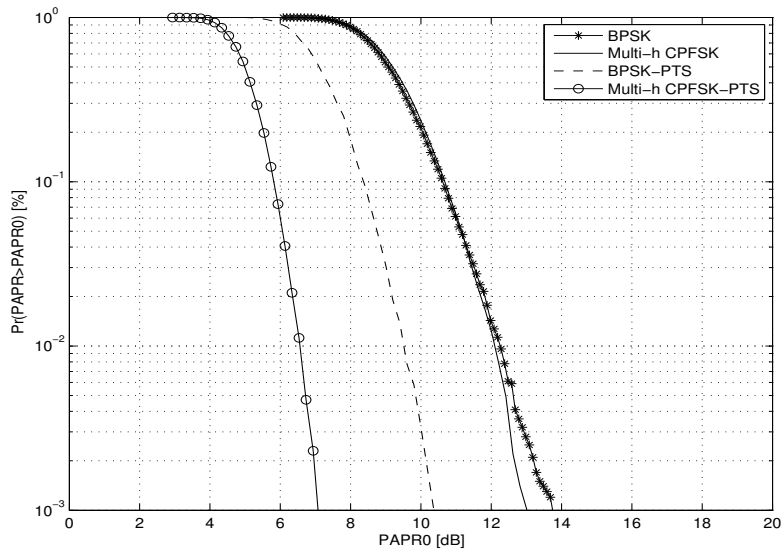


Figure 5.12: CCDFs of PAPR of an OFDM system with multi- h CPFSK mapper $(\{\frac{2}{4}, \frac{3}{4}\})$ with PTS technique ($N = 128$)

($H_{+i} = \{\frac{2}{4}, \frac{3}{4}\}$ and $H_{-i} = \{\frac{3}{4}, \frac{2}{4}\}$) for $N = 64, 128, 256,$ and $512,$ respectively. The phase rotating vectors that minimize PAPR are $b^{(55)}, b^{(98)}, b^{(671)},$ and $b^{(3290)}$ for $N = 64, 128, 256,$ and $512,$ respectively. A comparison of PAPR performance of this mapper relative to BPSK mapper as a function of number of subcarriers of the system is given in

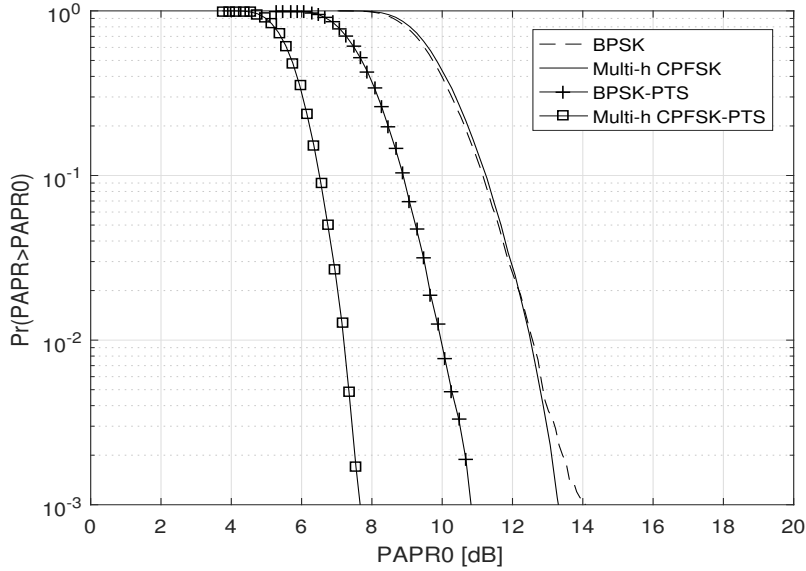


Figure 5.13: CCDFs of PAPR of an OFDM system with multi- h CPFSK mapper $(\{\frac{2}{4}, \frac{3}{4}\})$ with PTS technique ($N = 256$)

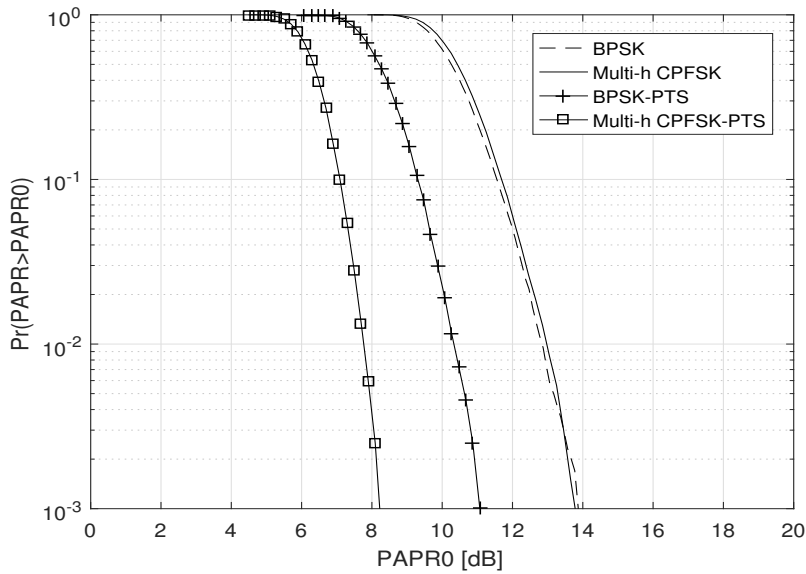


Figure 5.14: CCDFs of PAPR of an OFDM system with multi- h CPFSK mapper $(\{\frac{2}{4}, \frac{3}{4}\})$ with PTS technique ($N = 512$)

Table 5.5. It is observed that the amount of reduction in PAPR in the case of asymmetric multi- h CPFSK mapper ($H_{+i} = \{\frac{2}{4}, \frac{3}{4}\}$ and $H_{-i} = \{\frac{3}{4}, \frac{2}{4}\}$) with the use of PTS technique relative to corresponding system without PTS technique is nearly 5.8 dB, for $N = 64$. Single- h CPFSK mapper ($h = 1/2$) on the other hand, provides only 4.8 dB reduction in

Table 5.5: Comparison of PAPR performance of asymmetric multi- h CPFSK mapper ($H_{+i} = \{\frac{2}{4}, \frac{3}{4}\}$ and $H_{-i} = \{\frac{3}{4}, \frac{2}{4}\}$) as a function of number of subcarriers

Number of Subcarriers	Mapper			
	BPSK		asy multi- h CPFSK	
	Without PTS (dB)	With PTS (dB)	Without PTS (dB)	With PTS (dB)
64	13.1	10.0	10	5.2
128	13.2	10.3	10.3	6.0
256	13.5	10.7	10.7	6.1
512	14.1	10.9	11.0	6.3

going from a system without PTS technique to a system with PTS technique. In general, PTS technique is more effective with asymmetric multi- h CPFSK mapper compared to single- h CPFSK mapper.

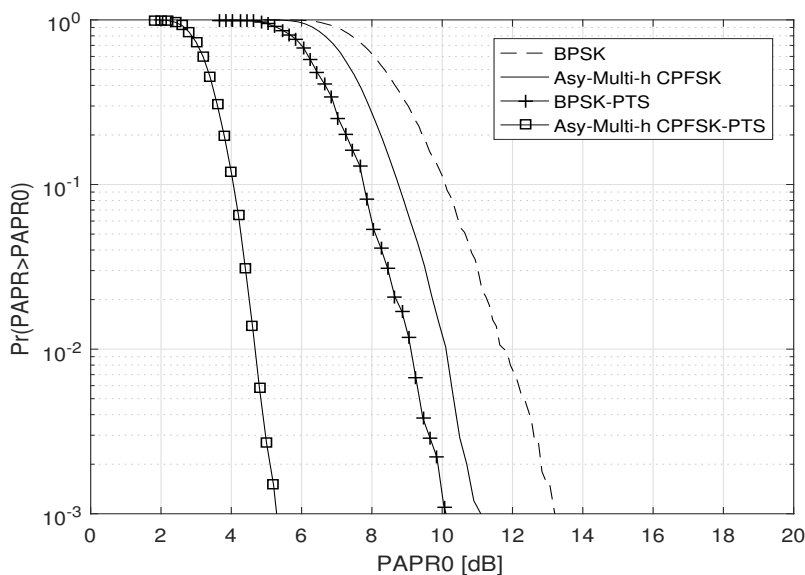


Figure 5.15: CCDFs of PAPR of an OFDM system with asymmetric multi- h CPFSK mapper ($H_{+i} = \{\frac{2}{4}, \frac{3}{4}\}$ and $H_{-i} = \{\frac{3}{4}, \frac{2}{4}\}$) with PTS technique ($N = 64$)

5.4 Conclusions

In this Chapter PTS technique is applied to an OFDM system with g-CPFSK mapper to examine possible reductions in PAPR of the system. A method is suggested to narrow

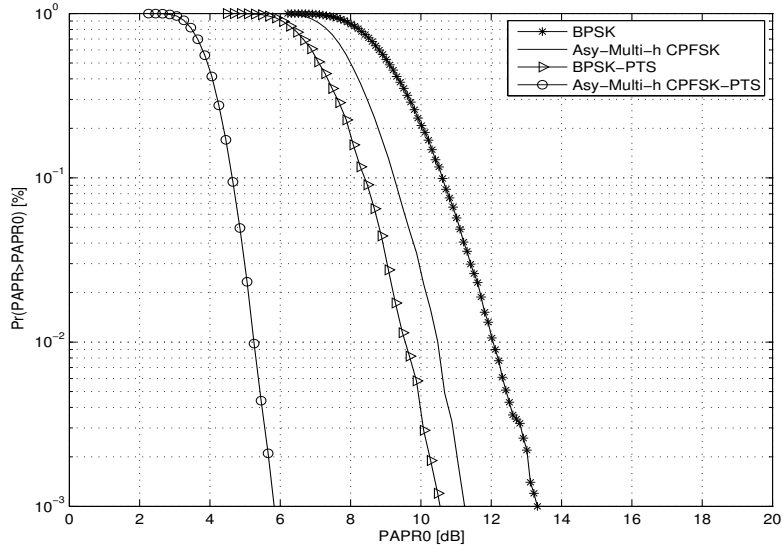


Figure 5.16: CCDFs of PAPR of an OFDM system with asymmetric multi- h CPFSK mapper ($H_{+i} = \{\frac{2}{4}, \frac{3}{4}\}$ and $H_{-i} = \{\frac{3}{4}, \frac{2}{4}\}$) with PTS technique ($N = 128$)

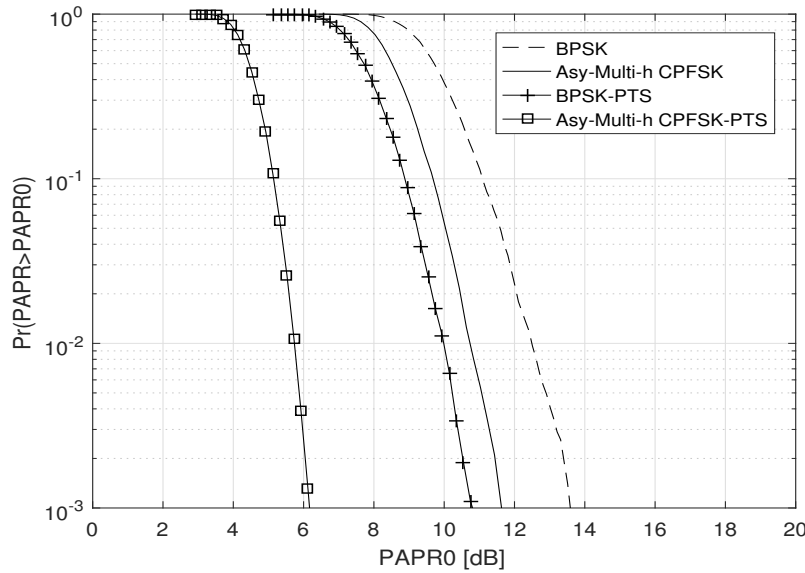


Figure 5.17: CCDFs of PAPR of an OFDM system with asymmetric multi- h CPFSK mapper ($H_{+i} = \{\frac{2}{4}, \frac{3}{4}\}$ and $H_{-i} = \{\frac{3}{4}, \frac{2}{4}\}$) with PTS technique ($N = 256$)

down search space in finding best phase rotating vectors in PTS technique that can be applied to any arbitrary OFDM system with arbitrary number of subcarriers. The g-CPFSK mapper, in general, in conjunction with PTS technique in an OFDM system can be very attractive from the viewpoint of PAPR reduction; however, at the cost of

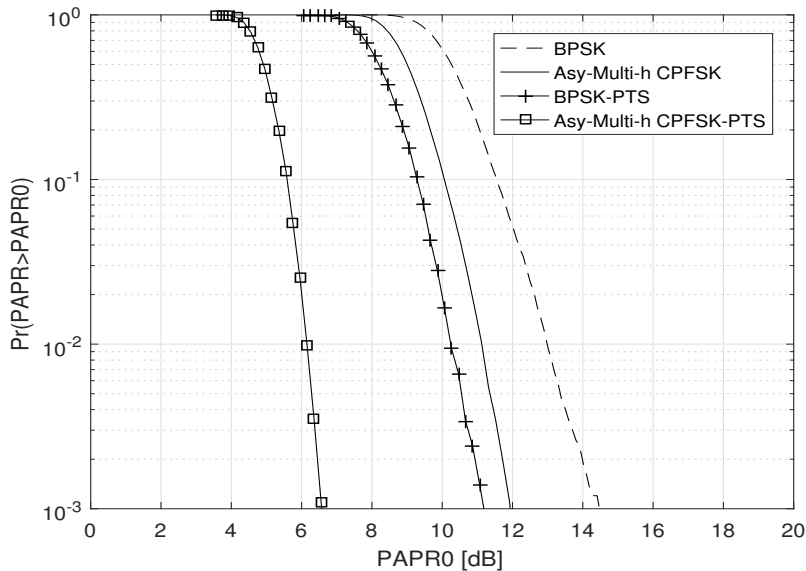


Figure 5.18: CCDFs of PAPR of an OFDM system with asymmetric multi- h CPFSK mapper ($H_{+i} = \{\frac{2}{4}, \frac{3}{4}\}$ and $H_{-i} = \{\frac{3}{4}, \frac{2}{4}\}$) with PTS technique ($N = 512$)

increased side information to be conveyed to the receiver. This, of course, will decrease the spectral efficiency of the system. Although, it is demonstrated that PTS technique in an OFDM system with g-CPFSK mapper is attractive for specific examples, more research is required to find best g-CPFSK mapper by expanding its parameter space, which, of course, will be computationally intensive.

Chapter 6

PAPR Reduction using CF Technique for OFDM System with g-CPFSK Mapper^{1,2}

6.1 Introduction

An OFDM system with g-CPFSK mapper is examined for PAPR reduction using Clipping and Filtering (CF) technique. The ability of the system to reduce PAPR is assessed as a function of parameters of the mapper, the number of subcarriers in the system, and parameters of CF block used. Three specific mappers, single- h CPFSK, multi- h CPFSK, and asymmetric multi- h CPFSK mappers, are considered in the OFDM system with CF technique and their PAPR performances are examined. A comparison of the PAPR reduction capability of g-CPFSK mapper with CF technique relative to memoryless BPSK mapper in an OFDM system is presented.

6.2 CF Technique and g-CPFSK Mapper

One of the simple and effective PAPR reduction techniques is clipping. However, clipping results in amplitude distortion, which in term expands the transmitted signal spectrum. Clipping is a nonlinear process and causes in-band and out-of-band distortion; resulting

-
1. E. Shafter and R. K. Rao, "CF technique with CPFSK mappers in OFDM systems for reduction of PAPR," IEEE Canadian Conference on Electrical and Computer Engineering (CCECE), Vancouver, BC, pp. 1-5, 2016.
 2. E. Shafter, and R. RK. Rao. "A Comparison between SLM, PTS, and CF Schemes for the Reduction of PAPR of OFDM System with CPFSK Mappers," IAENG International Journal of Computer Science 43.2, 2016.

in decreased spectral efficiency [8]. Clipping followed by Filtering technique is effective in removing components of expanded spectrum. This can be done by passing the clipped signal through a low pass filter. However, the low pass filter used after clipping operation marginally increases the value of the PAPR of the signal. Filtering after clipping can reduce out-of-band radiation but may also cause some peak regrowth so that the signal after clipping and filtering will exceed the clipping level at some points. To reduce peak regrowth caused by filtering recursive/iterative clipping and filtering technique is used. For a single iteration two FFT/IFFT plus one extra IFFT operations are required. In the case of W number of iterations $2W+1$ FFT/IFFT operations are required. The in-band distortion cannot be reduced by filtering and results in an error performance degradation, while out-of-band radiation reduces spectral efficiency of the system. In CF technique, amplitude clipping is used and is characterized by the Clipping Ratio (CR), which is defined as the ratio of clipping level and Root Mean Square (RMS) value of the OFDM signal. It is typically expressed as:

$$(CR)dB = 10 \log_{10} \left(\frac{A}{\rho} \right) dB \quad (6.1)$$

where A is the clipping level and ρ is the RMS value. Clipping is a non linear process and causes in-band distortion, which degrades in the BER performance of OFDM system and also introduces out-of-band noise, thereby decreasing the spectral efficiency of the system [8]. The OFDM signal is clipped in time domain and can be written as

$$B(S) = \begin{cases} S, & |S| \leq A \\ Ae^{j\phi(S)}, & |S| > A, \end{cases} \quad (6.2)$$

where ϕ represents the phase of OFDM signal $S(t)$, and A is the clipping level. The clipped signal $B(S)$ is then converted back into the frequency domain using FFT block to apply filtering to minimize out-of-band noise. Subsequently, transmitted signal in time domain is generated using IFFT operation. Filtering is applied to the baseband signals in the frequency domain using a rectangular window [68]. The filtering eliminates out-of-band spectral regrowth, without affecting the time domain peak after the IFFT operation. As a result, repeated CF operations can be used before achieving the desired level of PAPR. This technique is shown in Fig 6.1. In Fig 6.1 H_1 represents the low-pass

filter. The characteristics of this filter is well-documented and can be found in [69].

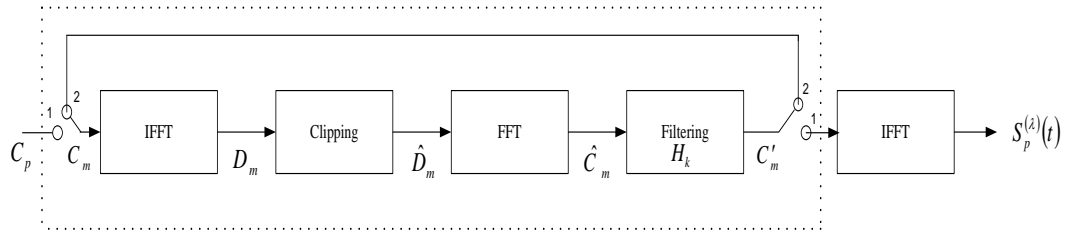


Figure 6.1: Block diagram of the repeated CF technique

6.3 Numerical Results and Discussion

In this Section numerical results are presented using CCDFs of PAPR of OFDM system with g-CPFSK mapper with and without CF technique, as a function of number of subcarriers ($N=64, 128, 256, 512$). In the computation of PAPR, an oversampling factor $L = 4$ is used and simulation results have been obtained using MATLAB. For each CCDF plot 10,000 random OFDM symbols are considered. Fig. 6.2 shows the flow-chart used for finding transmitted signal using repeated CF technique.

6.3.1 Single- h CPFSK Mapper

The CCDFs of PAPR of an OFDM system with and without CF technique for $h = \frac{1}{2}$ are shown in Figs. 6.3 to 6.6 for $N = 64, 128, 256, \text{ and } 512$, and $CR = 0.25$. It is observed that the OFDM system with single- h CPFSK ($h = \frac{1}{2}$) mapper has a PAPR that exceeds 11.1 dB for less than 0.1 percent of data blocks and for BPSK mapper it is 13.8 dB. However, when CF is used with these mappers the PAPR reduces to 4.2 dB and 8.8 dB for single- h CPFSK and BPSK mappers, respectively. The CCDFs of PAPR of an OFDM system with single- h CPFSK ($h = 2/3$) mapper for $N = 64, 128, 256, \text{ and } 512$, with and without CF technique, are shown in Figs. 6.7, 6.8, 6.9, and 6.10, respectively. It is observed that single- h CPFSK mapper with CF can offer an improvement in PAPR of nearly 9.6 dB relative to corresponding system without CF. Also, it is noted that the improvement in PAPR by using CF in these two systems are 6.8 dB and 5 dB for single- h CPFSK and BPSK mappers, respectively. A comparison of PAPR reductions for both

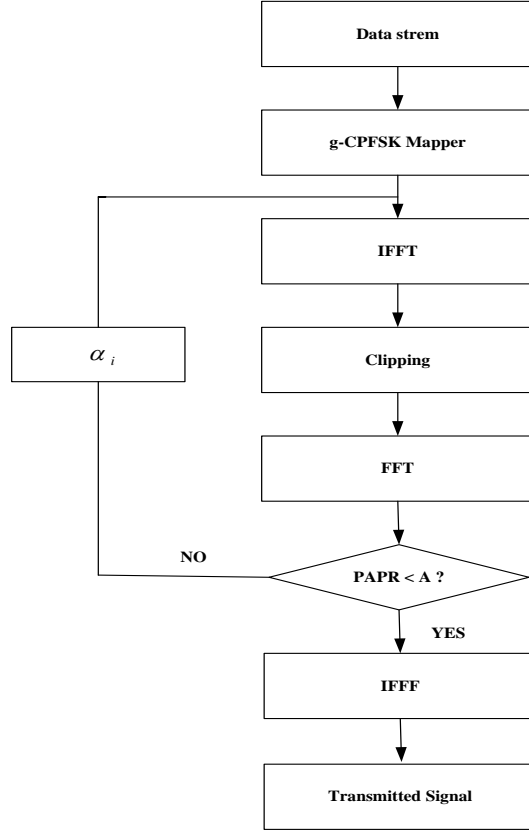


Figure 6.2: Flow-chart for finding an OFDM signal with a specific value of PAPR using repeated CF technique

BPSK and single- h CPFSK ($h = \frac{1}{2}$) mappers before and after applying CF technique for single- h CPFSK and BPSK mappers $CR = 0.25$ and $N = 128$ is given in Table 6.1.

The CCDFs of PAPR of an OFDM system with BPSK mapper, with CF technique applied three times, for $N = 64, 128, 256$, and 512 , are shown in Figs. 6.11, 6.12, 6.13, and 6.14, respectively. It is noted that in the first iteration the PAPR is reduced by 5.5 dB, in the second and third iterations PAPR reduced further by 6 dB and 6.2 dB, respectively. Also, The CCDFs of PAPR of an OFDM system with CPFSK ($h = 1/2$) mapper with three CF iterations for $N = 64, 128, 256$, and 512 , are shown in Figs.6.15,

Table 6.1: PAPR performance of single- h CPFSK ($\frac{1}{2}$) and BPSK mappers with and without CF technique ($N = 128, CR = 0.25$)

Description	PAPR (dB)	
	BPSK	Single-h CPFSK
Before CF	13.8	11
After CF	8.8	4.2

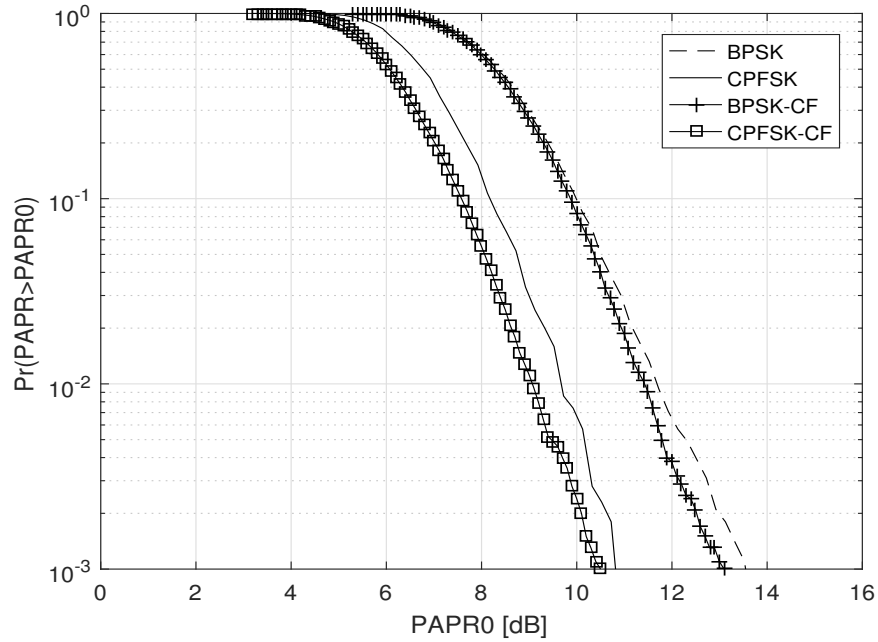


Figure 6.3: CCDFs of PAPR of an OFDM system with single- h CPFSK mapper ($h = \frac{1}{2}$) with and without CF technique ($N = 64, CR = 0.25$)

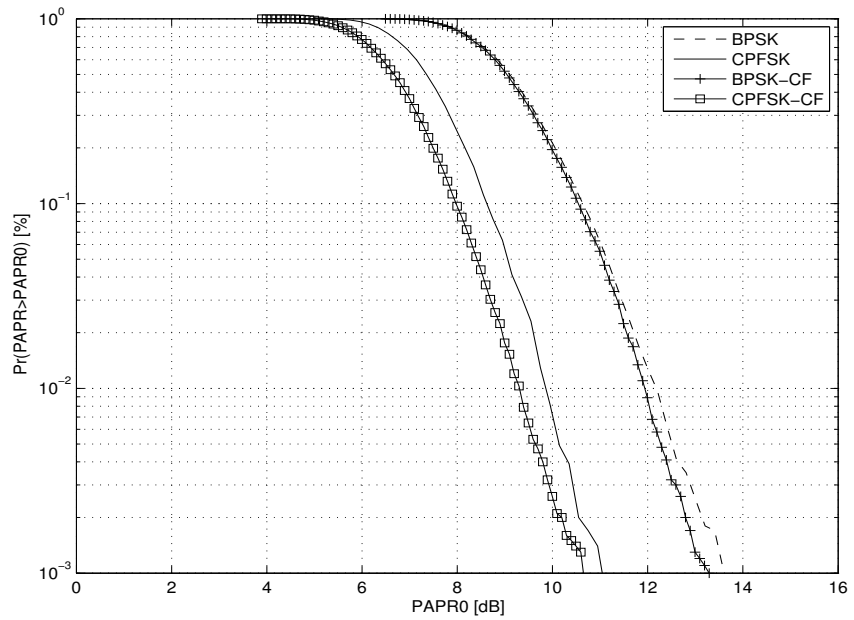


Figure 6.4: CCDFs of PAPR of an OFDM system with single- h CPFSK mapper ($h = \frac{1}{2}$) with and without CF technique ($N = 128, CR = 0.25$)

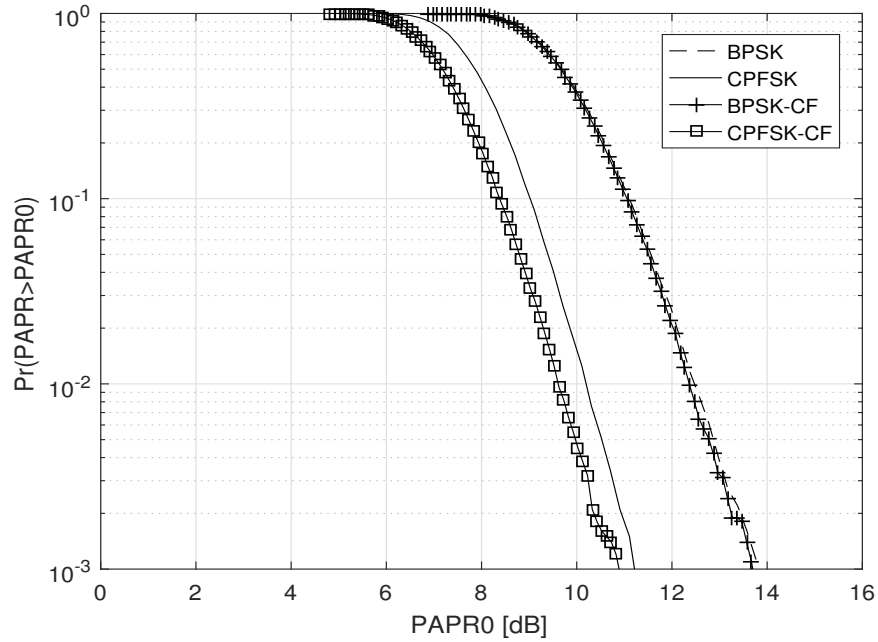


Figure 6.5: CCDFs of PAPR of an OFDM system with single- h CPFSK mapper ($h = \frac{1}{2}$) with and without CF technique ($N = 256, CR = 0.25$)

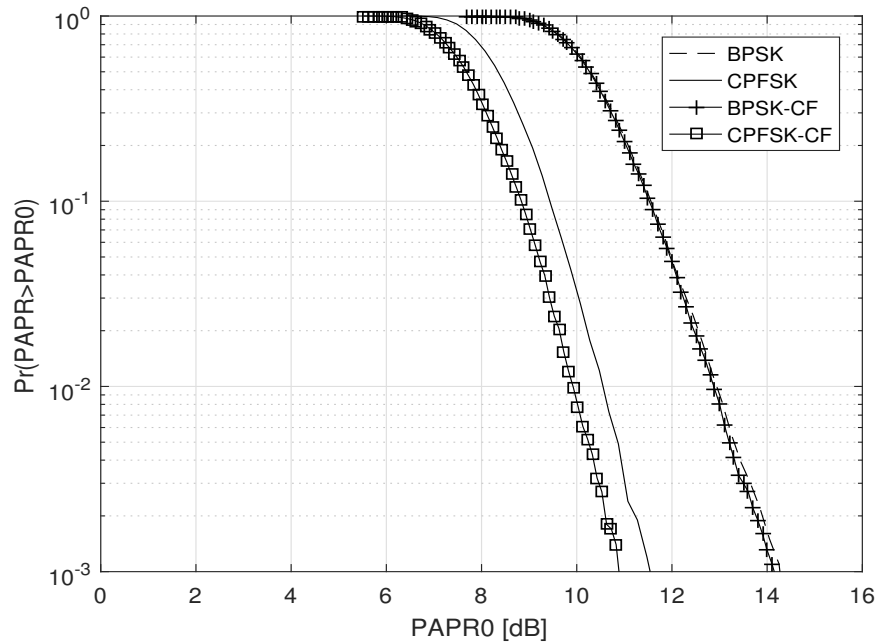


Figure 6.6: CCDFs of PAPR of an OFDM system with single- h CPFSK mapper ($h = \frac{1}{2}$) with and without CF technique ($N = 512, CR = 0.25$)

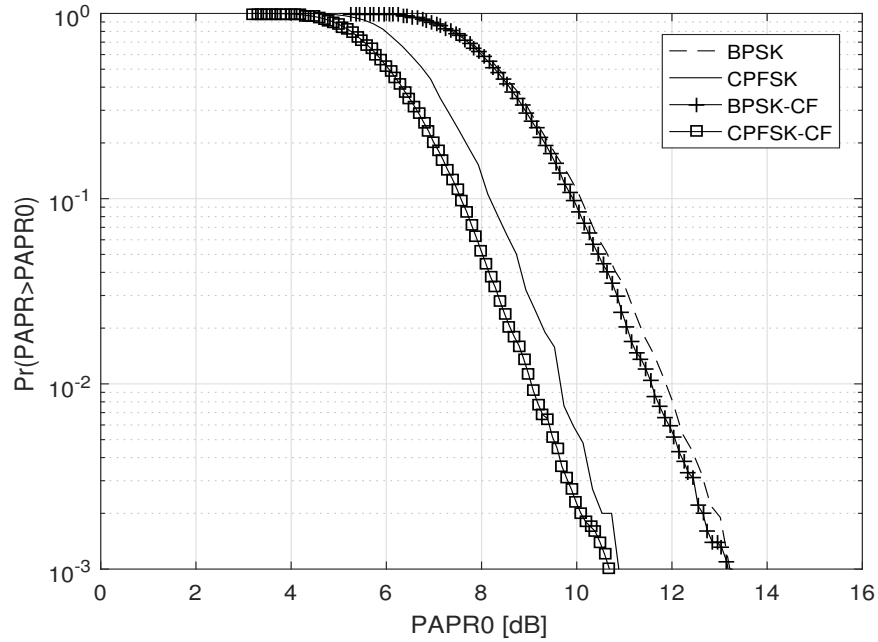


Figure 6.7: CCDFs of PAPR of an OFDM system with single- h CPFSK mapper ($h = \frac{2}{3}$) with and without CF technique ($N = 64, CR = 0.25$)

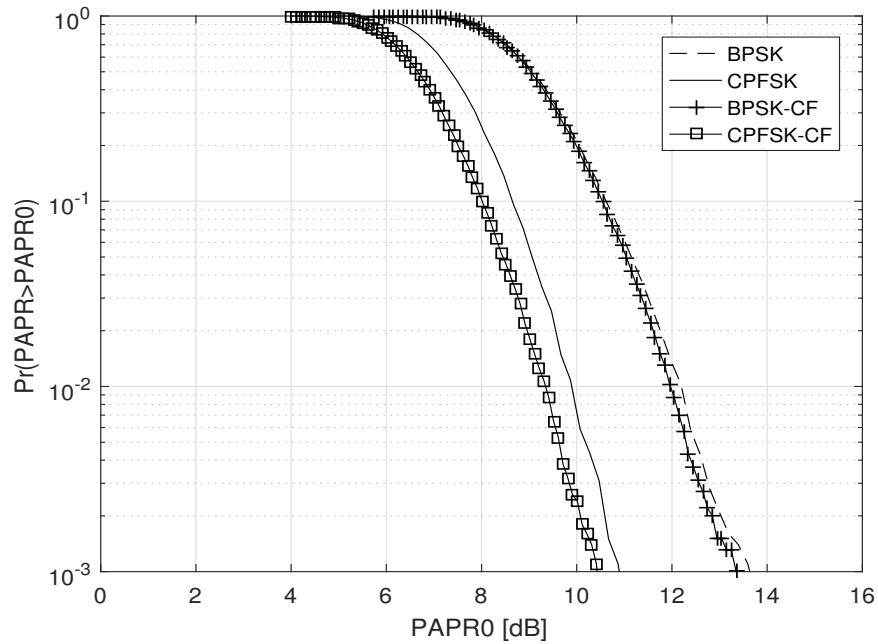


Figure 6.8: CCDFs of PAPR of an OFDM system with single- h CPFSK mapper ($h = \frac{2}{3}$) with and without CF technique ($N = 128, CR = 0.25$)

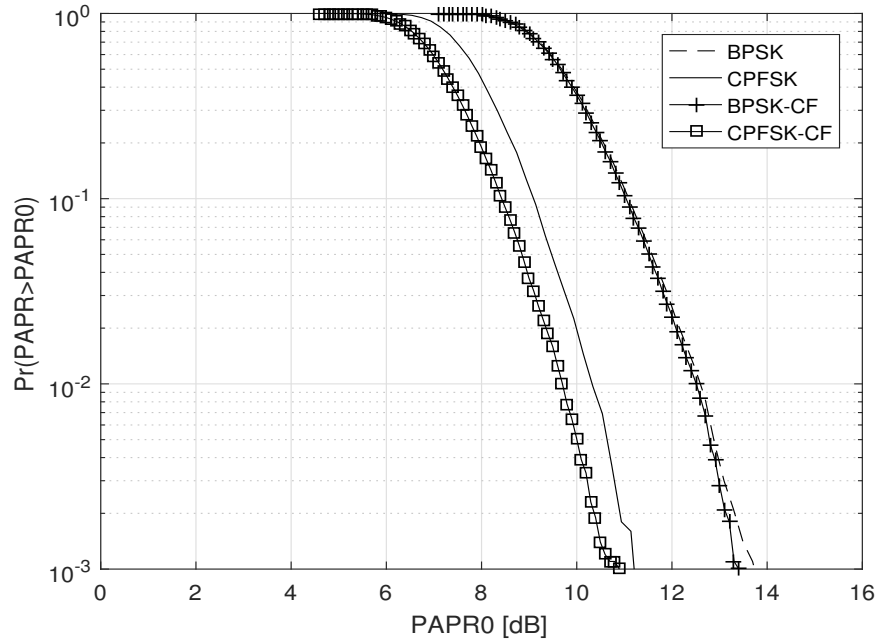


Figure 6.9: CCDFs of PAPR of an OFDM system with single- h CPFSK mapper ($h = \frac{2}{3}$) with and without CF technique ($N = 256, CR = 0.25$)

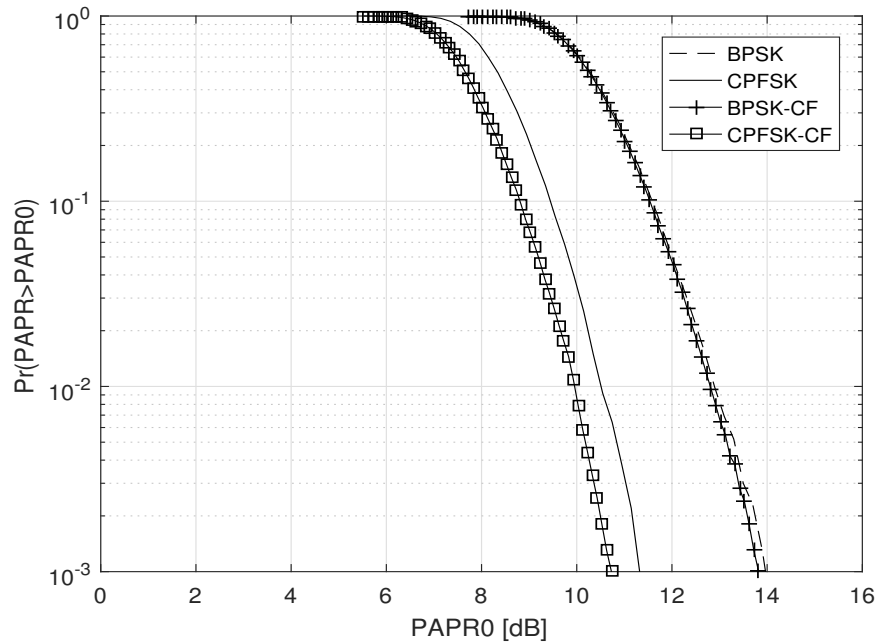


Figure 6.10: CCDFs of PAPR of an OFDM system with single- h CPFSK mapper ($h = \frac{2}{3}$) with and without CF technique ($N = 512, CR = 0.25$)

6.16, 6.17, and 6.18, respectively. It is observed that the first iteration reduced the PAPR by 4.3 dB and in second and third iterations PAPR reduced by 3.7 dB and 3.5 dB, respectively.

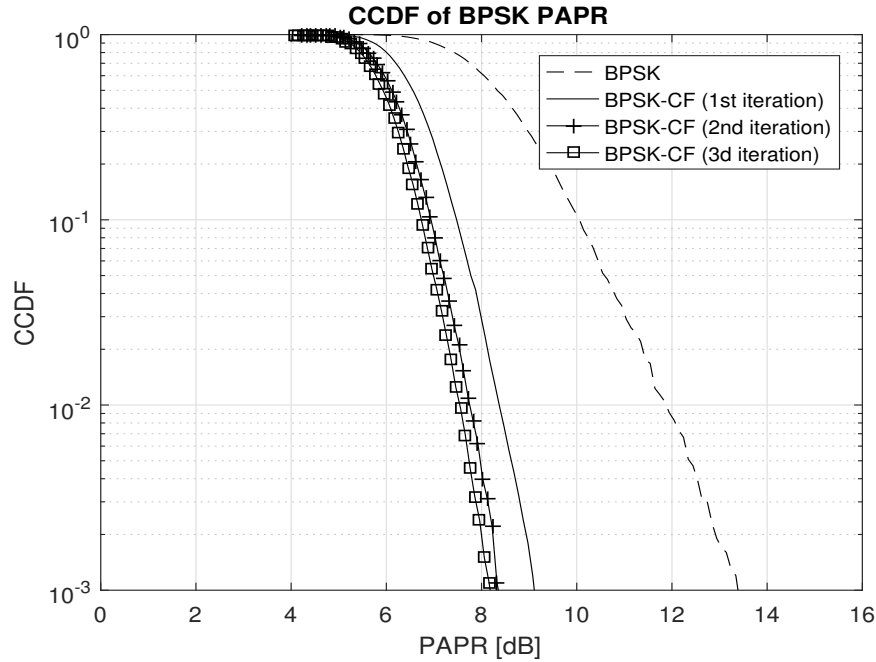


Figure 6.11: CCDFs of PAPR of an OFDM system with BPSK mapper and repeated CF technique ($N = 64, CR = 0.25$)

6.3.2 Multi- h CPFSK Mapper

To illustrate the PAPR performance of multi- h CPFSK mapper, the set of mapper parameters $\left\{\frac{2}{4}, \frac{3}{4}\right\}$ is used. In Figs. 6.19, 6.20, 6.21, and 6.22 are shown CCDFs of PAPR of an OFDM system with multi- h CPFSK mapper ($\left\{\frac{2}{4}, \frac{3}{4}\right\}$) for $N = 64, 128, 256$, and 512, respectively. It is noted that this specific multi- h CPFSK mapper performs nearly same as that of BPSK mapper. However, when CF is used with these systems, multi- h CPFSK outperforms BPSK by more than 2 dB. A comparison of PAPR reductions for both BPSK and multi- h CPFSK mappers before and after applying CF technique for multi- h CPFSK $\left\{\frac{2}{4}, \frac{3}{4}\right\}$ and BPSK mappers for $CR = 0.25$ and $N = 128$ is given in Table 6.2.

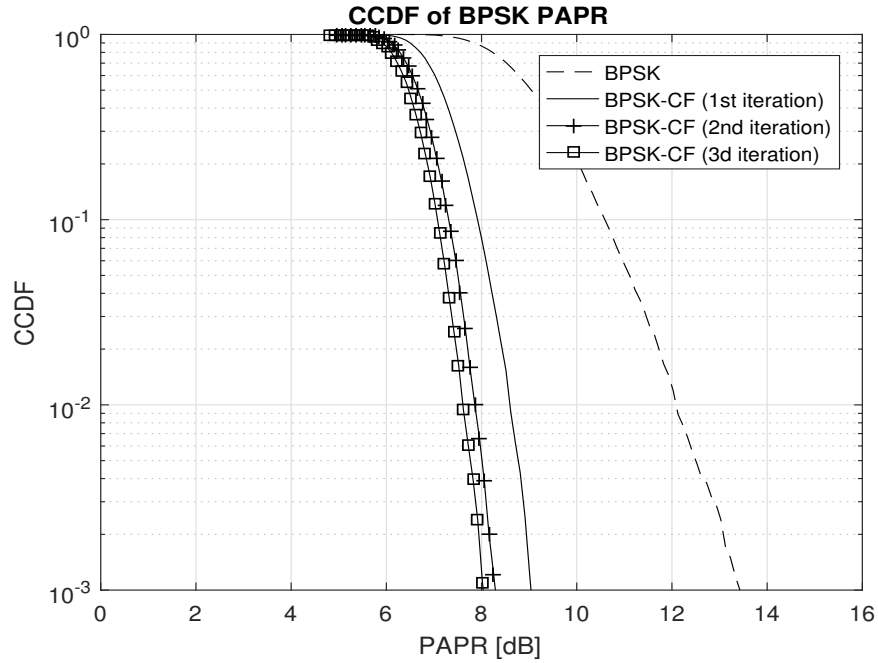


Figure 6.12: CCDFs of PAPR of an OFDM system with BPSK mapper and repeated CF technique ($N = 128, CR = 0.25$)

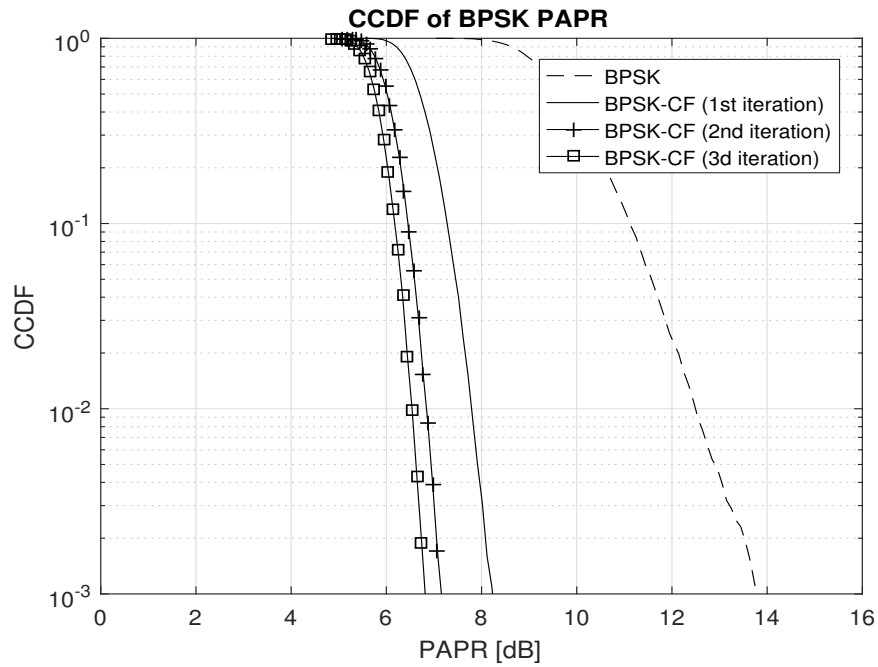


Figure 6.13: CCDFs of PAPR of an OFDM system with BPSK mapper and repeated CF technique ($N = 256, CR = 0.25$)

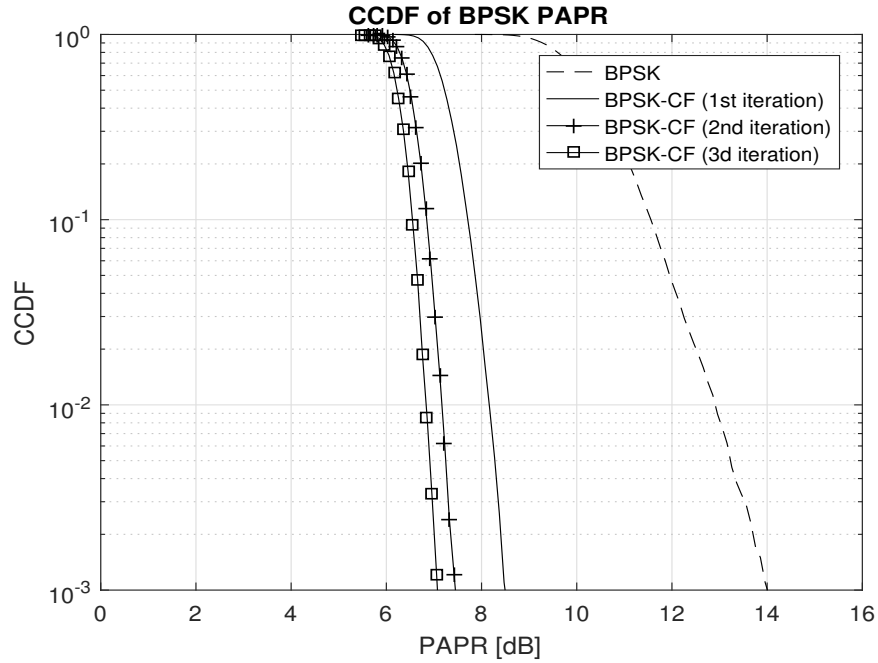


Figure 6.14: CCDFs of PAPR of an OFDM system with BPSK mapper and repeated CF technique ($N = 512, CR = 0.25$)

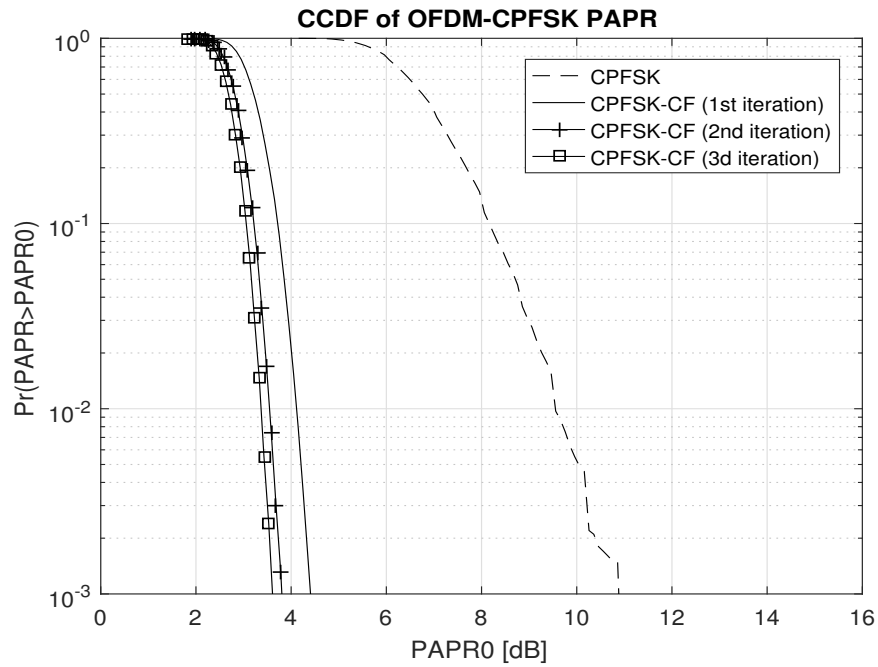


Figure 6.15: CCDFs of PAPR of an OFDM system with single- h CPFSK mapper ($h = \frac{1}{2}$) and repeated CF technique ($N = 64, CR = 0.25$)

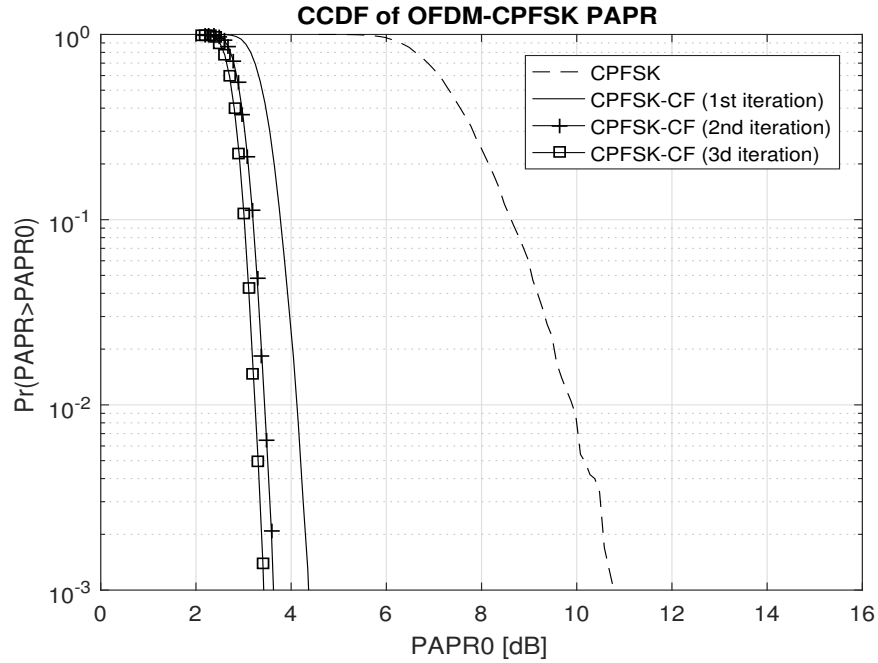


Figure 6.16: CCDFs of PAPR of an OFDM system with single- h CPFSK mapper ($h = \frac{1}{2}$) and repeated CF technique ($N = 128, CR = 0.25$)

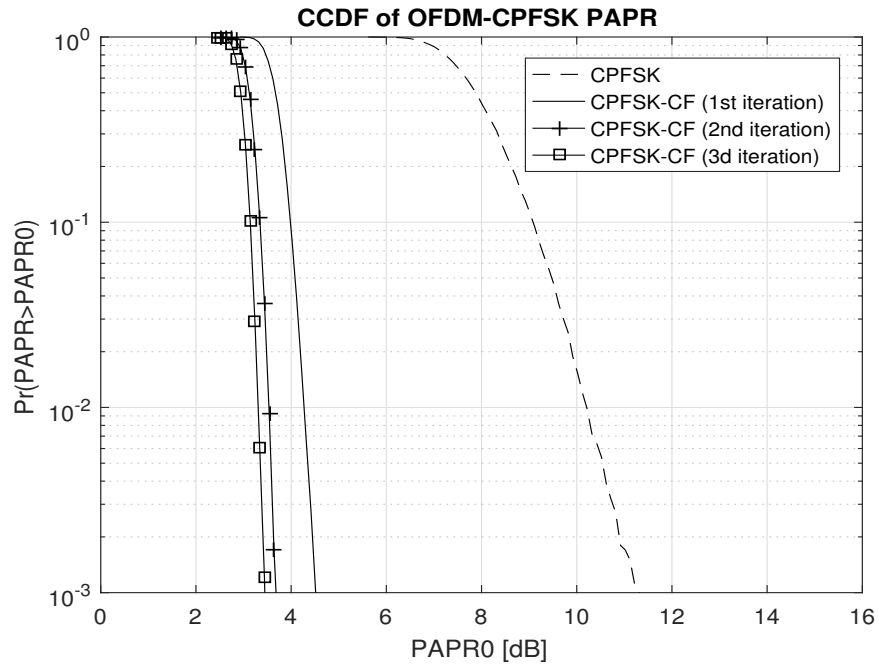


Figure 6.17: CCDFs of PAPR of an OFDM system with single- h CPFSK mapper ($h = \frac{1}{2}$) and repeated CF technique ($N = 256, CR = 0.25$)

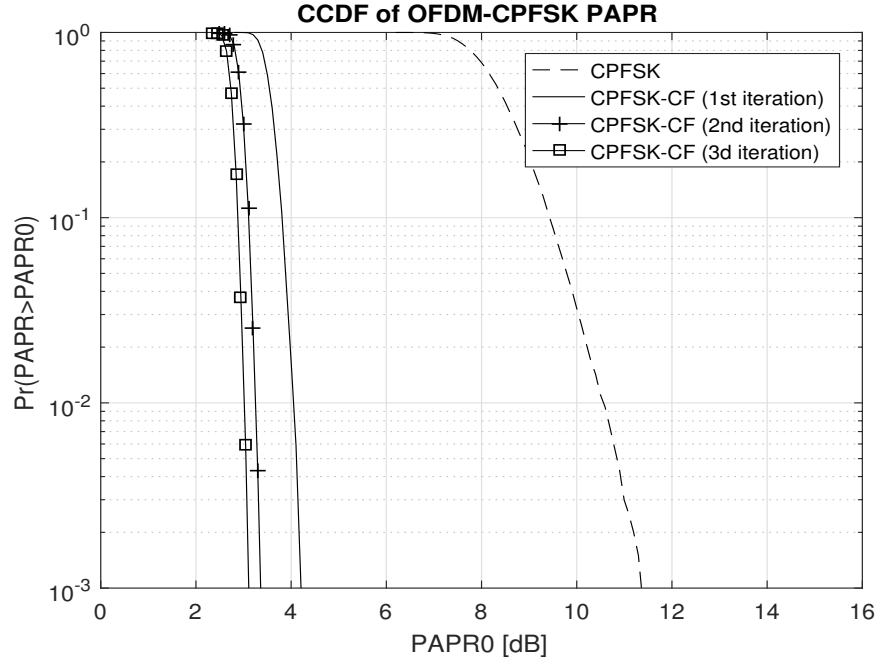


Figure 6.18: CCDFs of PAPR of an OFDM system with single- h CPFSK mapper ($h = \frac{1}{2}$) and repeated CF technique ($N = 512, CR = 0.25$)

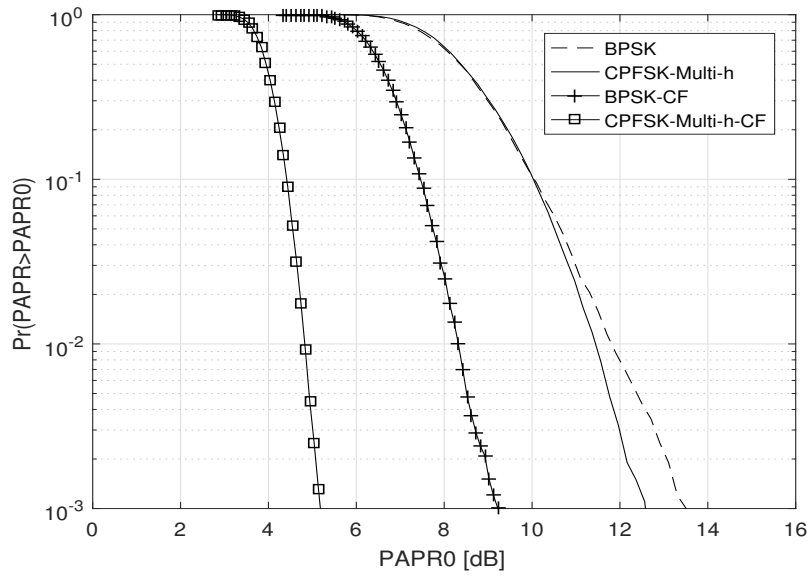


Figure 6.19: CCDFs of PAPR of an OFDM system with multi- h CPFSK mapper ($\{\frac{2}{4}, \frac{3}{4}\}$) with and without CF technique ($N = 64, CR = 0.25$)

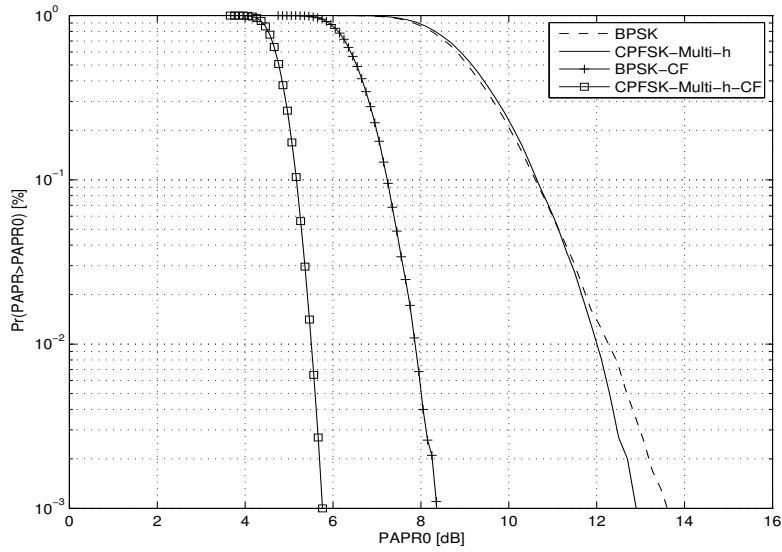


Figure 6.20: CCDFs of PAPR of an OFDM system with multi- h CPFSK mapper ($\{\frac{2}{4}, \frac{3}{4}\}$) with and without CF technique ($N = 128, CR = 0.25$)

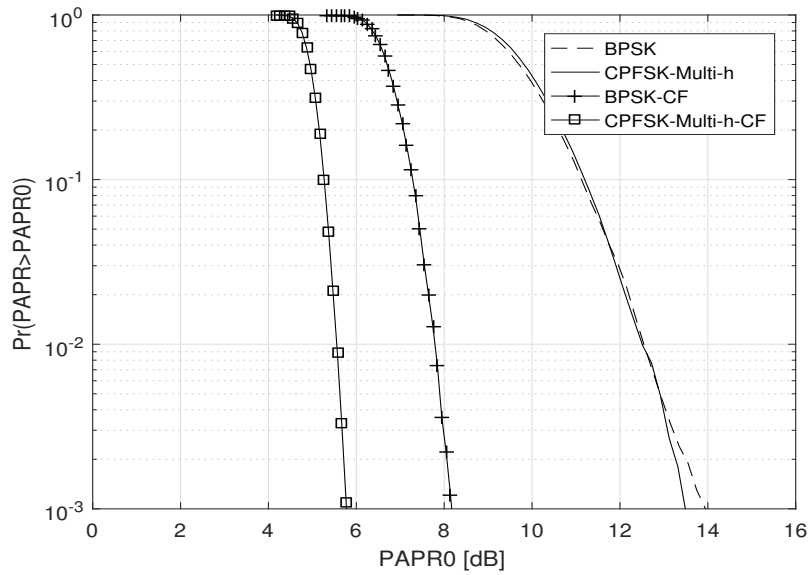


Figure 6.21: CCDFs of PAPR of an OFDM system with multi- h CPFSK mapper ($\{\frac{2}{4}, \frac{3}{4}\}$) with and without CF technique ($N = 256, CR = 0.25$)

Table 6.2: PAPR performance of multi- h CPFSK $\{\frac{2}{4}, \frac{3}{4}\}$ and BPSK mappers with and without CF technique ($N = 128, CR = 0.25$)

Description	PAPR (dB)	
	BPSK	multi- h CPFSK
Before CF	13.8	13
After CF	8.3	5.8

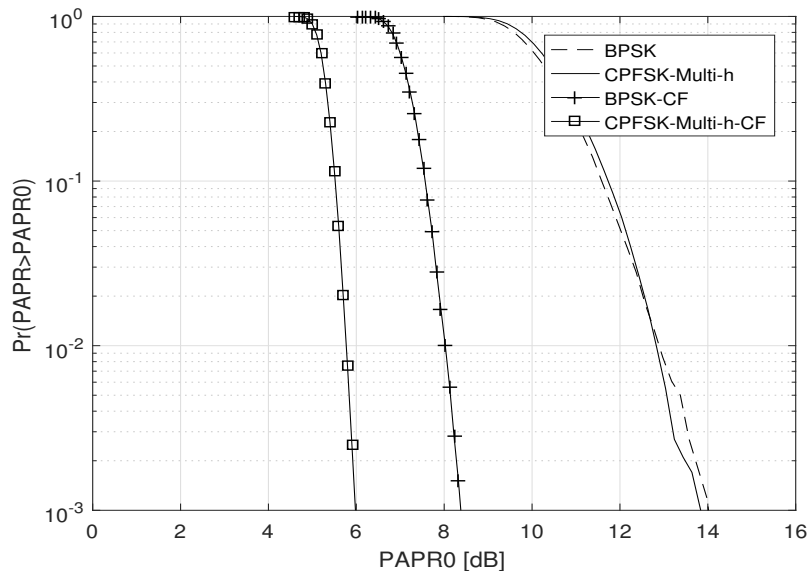


Figure 6.22: CCDFs of PAPR of an OFDM system with multi- h CPFSK mapper ($\{\frac{2}{4}, \frac{3}{4}\}$) with and without CF technique ($N = 512, CR = 0.25$)

6.3.3 Asymmetric multi- h CPFSK Mapper

Figs. 6.23, 6.24, 6.25, and 6.26 show CCDFs of PAPR for asymmetric multi- h CPFSK mapper ($H_{+i} = \{\frac{2}{4}, \frac{3}{4}\}$ and $H_{-i} = \{\frac{3}{4}, \frac{2}{4}\}$) for $N = 64, 128, 256$, and 512 , respectively. These CCDFs show PAPR performances for $CR = 0.25$. It is noted that the difference in PAPR performance between asymmetric multi- h CPFSK with and without CF technique is more than 6 dB. The difference in PAPR performance between multi- h CPFSK and asymmetric multi- h CPFSK mappers is approximately 2 dB, for an OFDM system with 128 subcarriers. The PAPR performance of asymmetric multi- h CPFSK and BPSK mappers before and after CF technique is summarized in Table 6.3, for $CR = 0.25$ and $N = 128$.

Table 6.3: PAPR performance of asymmetric multi- h CPFSK and BPSK mappers with and without CF technique ($N = 128, CR = 0.25$)

Description	PAPR (dB)	
	BPSK	asy multi- h CPFSK
Before CF	13.8	11.2
After CF	8.8	4.7

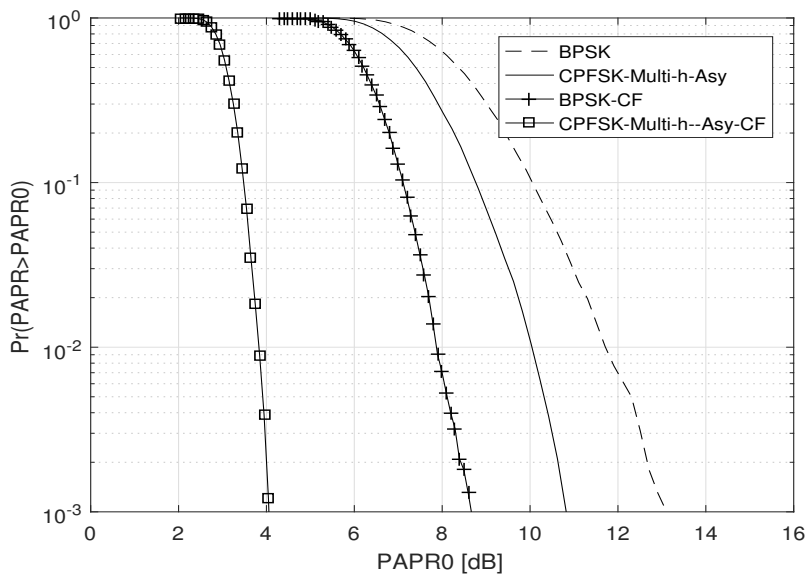


Figure 6.23: CCDFs of PAPR of an OFDM system with asymmetric multi- h CPFSK mapper ($H_{+i} = \{\frac{2}{4}, \frac{3}{4}\}$ and $H_{-i} = \{\frac{3}{4}, \frac{2}{4}\}$) with CF technique ($N = 64, CR = 0.25$)

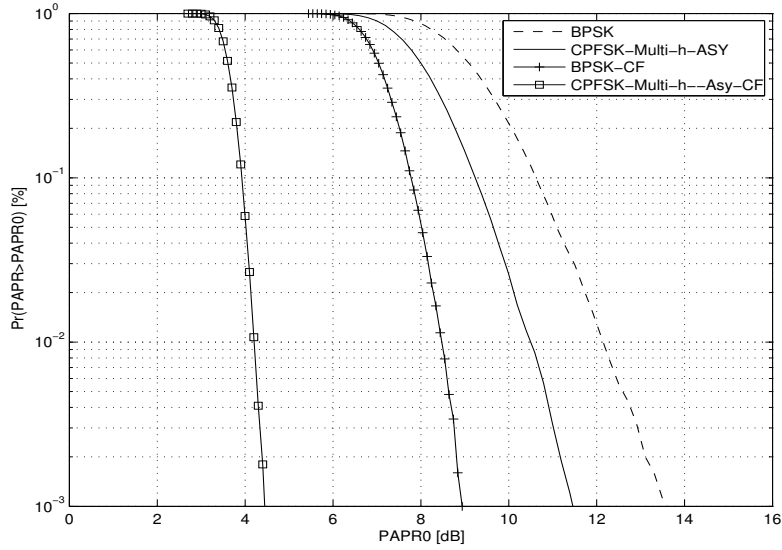


Figure 6.24: CCDFs of PAPR of an OFDM system with asymmetric multi- h CPFSK mapper ($H_{+i} = \{\frac{2}{4}, \frac{3}{4}\}$ and $H_{-i} = \{\frac{3}{4}, \frac{2}{4}\}$) with CF technique ($N = 128, CR = 0.25$)

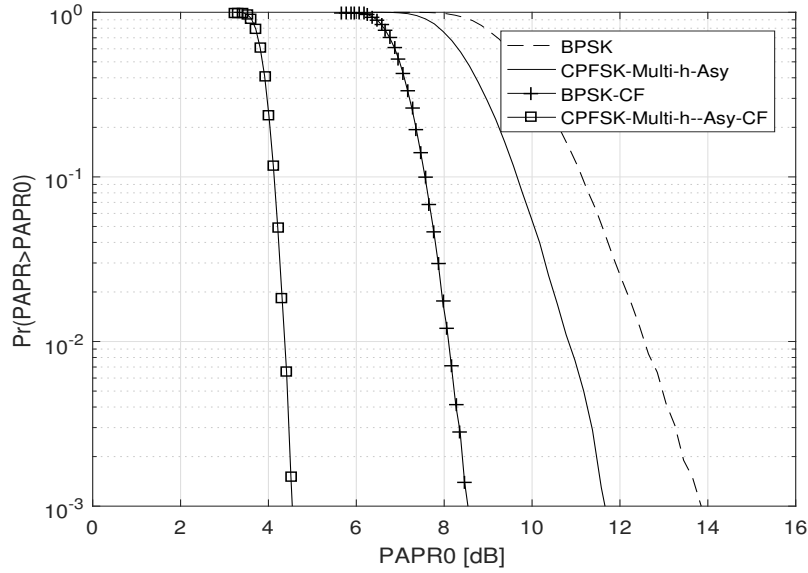


Figure 6.25: CCDFs of PAPR of an OFDM system with asymmetric multi- h CPFSK mapper ($H_{+i} = \{\frac{2}{4}, \frac{3}{4}\}$ and $H_{-i} = \{\frac{3}{4}, \frac{2}{4}\}$) with CF technique ($N = 256, CR = 0.25$)

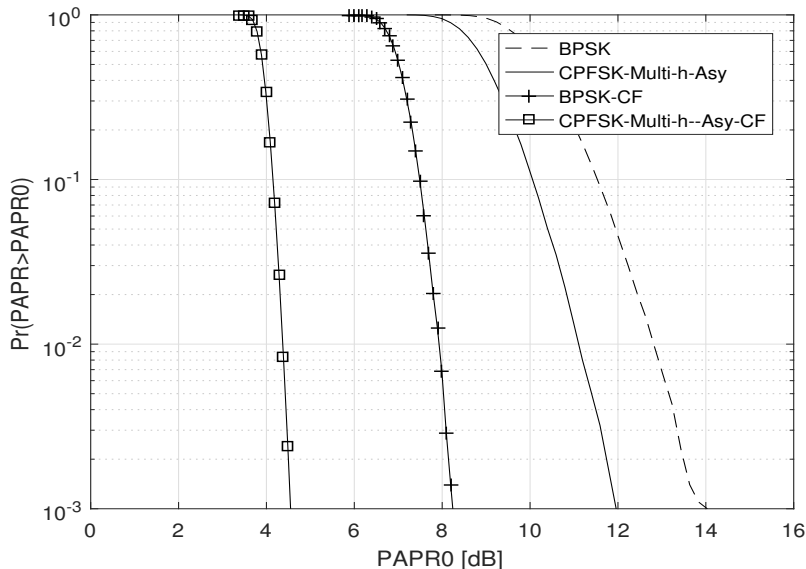


Figure 6.26: CCDFs of PAPR of an OFDM system with asymmetric multi- h CPFSK mapper ($H_{+i} = \{\frac{2}{4}, \frac{3}{4}\}$ and $H_{-i} = \{\frac{3}{4}, \frac{2}{4}\}$) with CF technique ($N = 512, CR = 0.25$)

6.4 Conclusions

In this Chapter, g -CPFSK mapper in an OFDM system with CF technique is investigated for PAPR performance. Three subclasses of g -CPFSK mapper, single- h CPFSK, multi- h CPFSK, and asymmetric multi- h CPFSK, are considered and their PAPR reduction abilities relative to conventional BPSK mapper are assessed using extensive simulations. It is observed that the amount of reduction in PAPR in the case of asymmetric multi- h CPFSK mapper outperforms better than in multi- h CPFSK and single- h CPFSK mappers.

Chapter 7

Performance of OFDM System with g-CPFSK Mapper in AWGN Channel¹

7.1 Introduction

The signals in an OFDM system with g-CPFSK mapper have inherent memory and this feature can be exploited to enhance the error probability performance of the system. The multiple symbol detection of signals in three subclasses of g-CPFSK mapper, single- h , multi- h , and asymmetric multi- h CPFSK mappers, in an OFDM system, over AWGN channel is addressed. The structure of optimum g-CPFSK demapper is derived and an expression for its error probability performance, that is optimum at high SNR, is presented, and the performance of OFDM system is illustrated as a function of modulation parameters of g-CPFSK mapper, E_b/N_0 , and the observation length of demapper.

7.2 Structure and Performance of Receiver

The structure of the receiver of an OFDM system with g-CPFSK mapper is shown in Fig. 7.1. The received signal during the p^{th} OFDM symbol can be written as

$$r(t) = S_p(t) * h(t) + w(t) \quad (p-1)T \leq t \leq pT, \quad (7.1)$$

1. E. Shafter, A. M. Hamed and K. R. Rao, "PAPR and BER performance analysis of OFDM system with multi-h CPFSK mapper," IEEE 30th Canadian Conference on Electrical and Computer Engineering (CCECE), Windsor, pp. 1-4, 30 Apr-3 May, 2017.

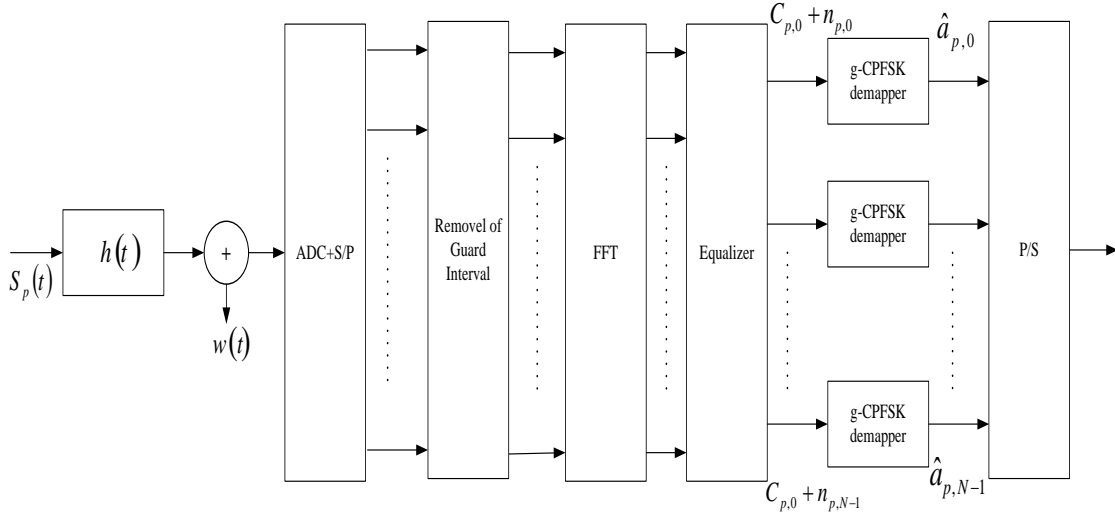


Figure 7.1: Block diagram of structure of receiver in an OFDM system with g-CPFSK mapper

where $S_p(t)$ is the transmitted OFDM signal during the p^{th} symbol interval, $h(t)$ is impulse response of the channel, and $w(t)$ is the zero mean AWGN with two-sided PSD of $\frac{N_0}{2}$ watts/Hz, and $T = nT_b$ is the OFDM symbol duration. In this Chapter, the channel impulse response is assumed equal to $h(t) = \alpha \delta(t)$ with $\alpha = 1$. Thus, the received signal can be written as

$$r(t) = S_p(t) + w(t), \quad (p-1)T \leq t \leq pT, \quad p = 1, 2, \dots \quad (7.2)$$

which is sampled every T_b sec and converted to parallel form and after removal of guard interval is fed to the FFT demodulator. Since the channel is known no equalization is needed. The input to the g-CPFSK demappers are simply AWGN corrupted transmitted data symbols. The g-CPFSK demappers in Fig. 7.1 are Maximum Likelihood Demappers (MLDs). In every OFDM symbol one sample is fed to each of the g-CPFSK mappers. Using the notation used in Chapter 3, eqn. (3.6), the inputs to N g-CPFSK demappers during the p^{th} OFDM symbol can be written as a vector given by:

$$r_p = \begin{bmatrix} C_{p,0} + n_{p,0} \\ C_{p,1} + n_{p,1} \\ \vdots \\ C_{p,N-1} + n_{p,N-1} \end{bmatrix}, p = 1, 2, \dots \quad (7.3)$$

where $n_{p,i}$ are, $i = 0, 1, \dots, N - 1$ the outputs of FFT block due to input $w_{p,i}, i = 0, 1, \dots, N - 1$. With the knowledge of modulation parameters of g-CPFSK mapper and the starting phase, $a_{p,i}$ can be estimated, which is then passed through P/S block to obtain serial stream of data transmitted. The maximum likelihood g-CPFSK demapper, and its detection strategy is presented next.

7.3 Maximum Likelihood g-CPFSK Demapper

The strategy used by the j^{th} of N g-CPFSK demapper is to observe n AWGN corrupted data $[C_{1,j} + n_{1,j}, C_{2,j} + n_{2,j}, \dots, C_{n,j} + n_{n,j}]$ and arriving at an optimum decision on the data, $a_{1,j}$, transmitted during the first ($0 \leq t \leq T$) OFDM symbol. Since $[C_{1,j}, C_{2,j}, \dots, C_{n,j}]$ is related to input data $[a_{1,j}, a_{2,j}, \dots, a_{n,j}]$ along the j^{th} subcarrier, and noting that $a_{p,j} = \pm 1, p = 1, 2, \dots, n$, there are 2^{n-1} input data vectors with $a_{1,j} = +1$ and equal number of data vector with $a_{1,j} = -1$. Modeling the input of j^{th} g-CPFSK demapper as:

$$\mathbb{R}_j = C + N \quad (7.4)$$

where

$$\mathbb{R}_j = \begin{bmatrix} r_1 \\ r_2 \\ \vdots \\ r_n \end{bmatrix}, C = \begin{bmatrix} C_{1,j} \\ C_{2,j} \\ \vdots \\ C_{n,j} \end{bmatrix}, N = \begin{bmatrix} n_{1,j} \\ n_{2,j} \\ \vdots \\ n_{n,j} \end{bmatrix} \quad (7.5)$$

Denoting the data sequence along the j^{th} subcarrier over n symbols as

$$A = [a_{1,j}, a_{2,j}, \dots, a_{n,j}] = [a_{1,j}, B] \quad (7.6)$$

where B represents $(n - 1)$ -tuple $[a_{2,j}, a_{3,j}, \dots, a_{n,j}]$. The demapper is then required differentiate between the two hypotheses:

$$\begin{aligned} H_0 : \mathbb{R}_j &= C_B^{+1} + N \\ H_1 : \mathbb{R}_j &= C_B^{-1} + N \end{aligned} \quad (7.7)$$

where C_B^{+1} represents complex data sequence corresponding to $A = [a_{j,1} = +1, B]$ and C_B^{-1} represents complex data sequence corresponding to $A = [a_{j,1} = -1, B]$. The demapper strategy is to decide on $a_{j,1} = \pm 1$ is the likelihood ratio test given by:

$$\Lambda = \frac{\int_B p(\mathbb{R}_j | H_0, B) p(B) dB}{\int_B p(\mathbb{R}_j | H_1, B) p(B) dB} \quad (7.8)$$

where

$$p(B) = p(a_{2,j}) \cdots p(a_{n,j}) \quad (7.9)$$

$$\int_B dB = \int \int \cdots \int da_{2,j} \cdots da_{n,j} \quad (7.10)$$

and

$$p(a_{k,j}) = \frac{1}{2} [\delta(a_{k,j} + 1) + \delta(a_{k,j} - 1)], k = 2, 3, \dots, n \quad (7.11)$$

Nothing that \mathbb{R}_j in (7.5) is Gaussian, using (7.9) to (7.11) in (7.8), we get

$$\Lambda = \frac{\sum_{j=1}^m \exp \left[\frac{1}{N_0} \text{Re} \left\{ \mathbb{R}_j^T \left(C_{B_j}^{+1} \right)^* \right\} \right]}{\sum_{j=1}^m \exp \left[\frac{1}{N_0} \text{Re} \left\{ \mathbb{R}_j^T \left(C_{B_j}^{-1} \right)^* \right\} \right]} \underset{-1}{\overset{+1}{\geq}} 0 \quad (7.12)$$

where $*$ denotes complex conjugation. The structure of the demapper dictated by (7.12) is shown in Fig. 7.2. Using high SNR approximation in (7.12), we get

$$\max_{l=1,2,\dots,m} \text{Re} \left\{ \mathbb{R}_j^T \left(C_{B_l}^{+1} \right)^* \right\} \underset{-1}{\overset{+1}{\geq}} \max_{l=1,2,\dots,m} \text{Re} \left\{ \mathbb{R}_j^T \left(C_{B_l}^{-1} \right)^* \right\} \quad (7.13)$$

where $m = 2^{n-1}$. The high SNR suboptimum g-CPFSK demapper is shown using dotted line in Fig. 7.2. The high-SNR g-CPFSK mapper correlates the received noise corrupted data vector with all possible data vectors (2^n) and arrives at an estimate of the data transmitted during the first OFDM symbol. Next, the window of demapper is moved to $T \leq t \leq (n+1)T$ to decide about the symbol transmitted during the second OFDM symbol. The process is continued to obtain estimates of symbols transmitted during subsequent OFDM symbols. Viterbi demapper can be employed as the optimum g-CPFSK demapper and such a demapper is referred to as the Maximum Likelihood Sequence

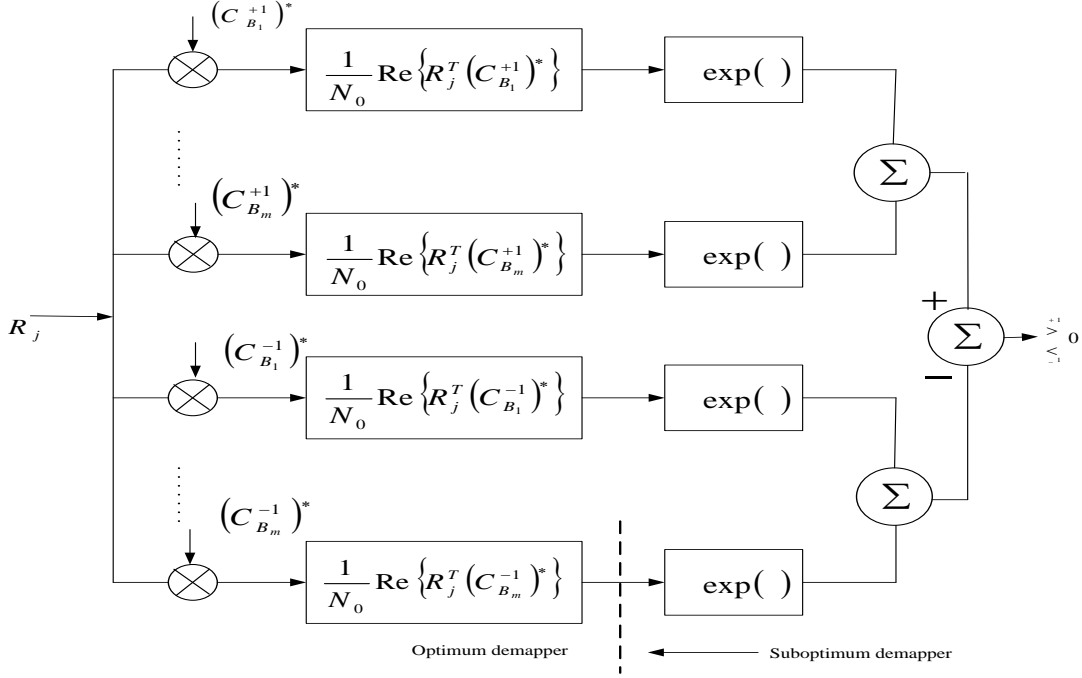


Figure 7.2: Structure of optimum and high-SNR suboptimum g-CPFSK demapper

Demapper (MLSD). The performance of optimum demapper shown in Fig. 7.2 and that of the MLSD are the same at high SNR [53]. The performance can be union bounded and a closed-form expression for BER for g-CPFSK demapper can be derived and is given by:

$$P_e = \frac{1}{K 2^{n-1}} \sum_{l=1}^{2^n-1} \sum_{j=1}^{2^n-1} \sum_{v=1}^K Q \left(\sqrt{\frac{nE_b}{N_0}} [1 - \rho_v(l, j)] \right) \quad (7.14)$$

where $\rho_v(l, j)$ is the normalized correlation coefficient and is given by:

$$\rho_v(l, j) = \frac{1}{nE_b} \int_0^{nT_b} S^{(v)}(t, -1, B_l) S^{(v)}(t, +1, B_j) dt \quad (7.15)$$

For multi- h CPFSK demapper, the $\rho_v(l, j)$ is obtained as

$$\rho_v(l, j) = \text{Sinc} \left(\frac{1}{2} h_{[i]}^{(v)} \eta_i \right) \cos \left(\frac{\pi}{2} h_{[i]}^{(v)} \eta_i + \theta_i \right) \quad (7.16)$$

where $\theta_i = \pi \sum_{r=1}^{i-1} \eta_r h_{[r]}^{(v)}$ is the accumulated phase, $\eta_i = a_{i,j}^l - a_{i,j}^j$ is the difference

sequence between data bits, taking values from the set $-2, 0, +2$. The cyclic arrangements of the K modulation indexes are given as $\{h_{[i]}^{(v)}; i = 1, \dots, n\}$, $v = 1, \dots, K$. For instance, $\{h_{[i]}^{(1)}\} = (h_1, \dots, k_K, h_1, \dots)$. The lower bound on probability of bit error can be obtained by assuming that for each transmitted sequence, the demapper needs only decide between this sequence and its closest neighbour; this means $\rho_v^*(l) = \max_j \varrho_v(l, j)$. The expression for lower bound on probability bit error can then be written as

$$P_e = \frac{1}{K2^{n-1}} \sum_{l=1}^{2^{n-1}} \sum_{v=1}^K Q \left\{ \sqrt{\frac{nE_b}{N_o} (1 - \rho_v^*(l))} \right\} \quad (7.17)$$

7.4 Numerical Results and Analysis

The error probability upper and lower bounds on the performance of optimum g-CPFSK mapper are functions of: i) E_b/N_o , Signal-to-Noise Ratio (SNR); ii) parameters of the g-CPFSK mapper; iii) n , observation length of the demapper; and iv) M , number of modulation levels. In this thesis $M = 2$ is used to illustrate BER result. The set of mapper parameters that should be selected is the one that minimizes the bit error probability upper bound for the three subclasses of g-CPFSK mapper. In Fig 7.3 bounds are plotted for single- h CPFSK mapper with $h = 0.715$ for $n = 2$ and $n = 3$. The value of $h = 0.715$ is the optimum value that minimizes BER. In the same figure performance of BPSK mapper is also shown. It can be observed that single- h CPFSK ($h = 0.715$) demapper with $n = 3$ is better than the corresponding mapper with $n = 2$ by 1 dB.

The BER performance of multi- h CPFSK mapper is also investigated. The error probability upper and lower bounds are plotted in Fig.7.4 for $H_2 = \{0.77, 0.62\}$ and $n = 2, 3$, as a function of E_b/N_o . It is noted that this H_2 is optimum and minimizes BER. The bit error rate for the BPSK mapper is also plotted in the same figure. It is noted that the multi- h CPFSK mapper performs better than the BPSK mapper by 1 dB on average. Also, it is noted that the bit error probability for $n = 3$ is slightly better than for $n = 2$; however, the receiver will be more complex as n increases. Fig.7.5 show plots of upper and lower bounds for asymmetric multi- h CPFSK mapper with A-type $H_3 = \{6/8, 4/8, 5/8\}$ for $n = 4$ and $n = 6$ as a function of E_B/N_o . The bit error rate for the BPSK mapper is also plotted for comparison purpose. It is clearly seen that asymmetric multi- h

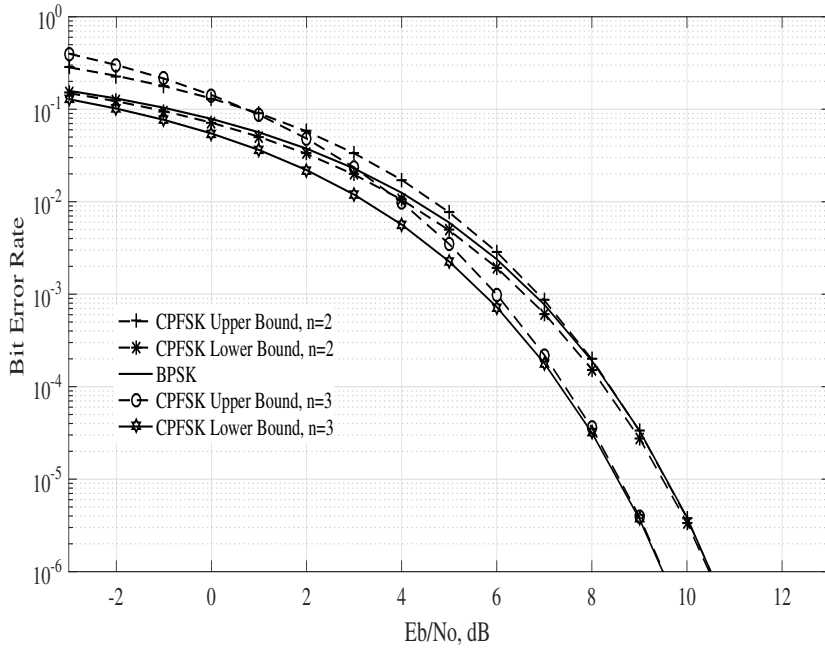


Figure 7.3: BER performance of single- h CPFSK mapper ($h = 0.715$) over AWGN for $n = 2, 3$

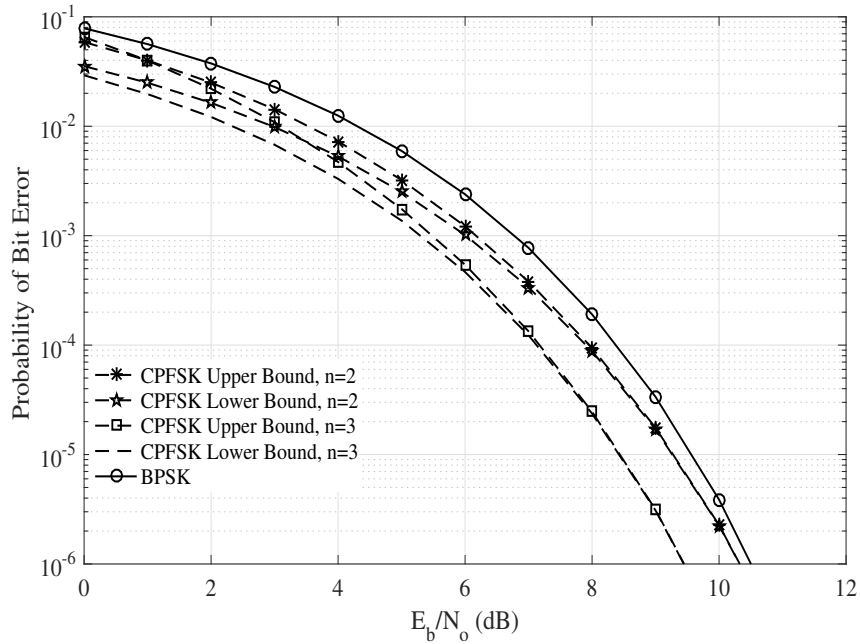


Figure 7.4: BER performance of multi- h CPFSK demapper ($H_2 = \{0.77, 0.62\}$) over AWGN for $n = 2, 3$

CPFSK mapper performs better than multi- h CPFSK mapper for both $n = 4$ and $n = 6$. It is evident that asymmetric multi- h CPFSK mapper achieves better performance as n increases. This is due to the fact that memory introduced lasts over several OFDM symbols compared to single- h and multi- h CPFSK mappers.

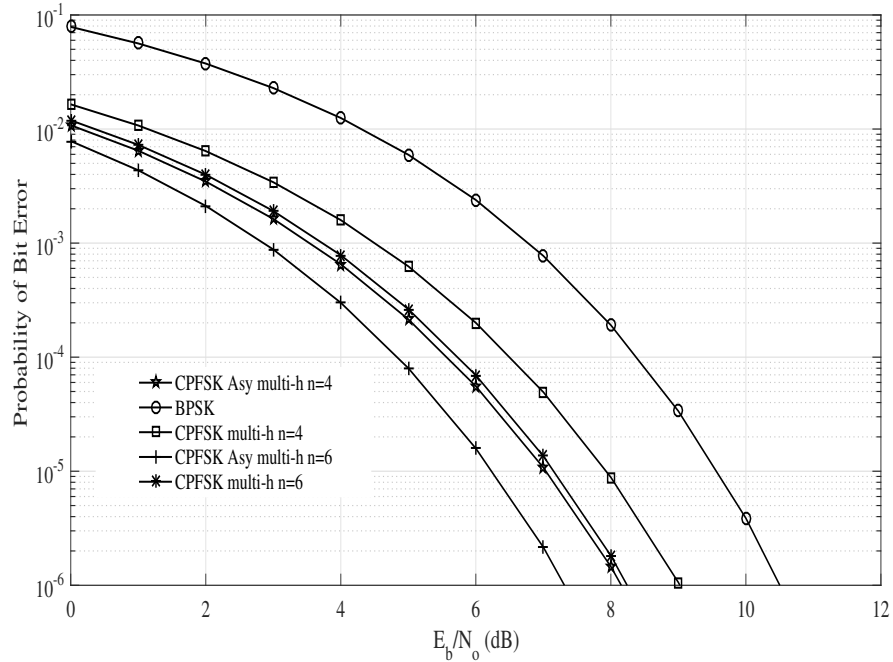


Figure 7.5: BER performance of asy multi- h CPFSK demapper ($H_3 = \{6/8, 4/8, 5/8\}$, A-type) over AWGN for $n = 4$ and $n = 6$

The receiver complexity of OFDM system with g-CPFSK mapper is mainly dependent on the observations length, n , of the receiver and the modulation parameters of mapper. The receiver consists of M^n branches and each branch includes a multiplier and a correlator as shown in Fig.7.2. It can be observed from Fig.7.6, that the length plays an important role for improving the system performance. It is observed that lower error probability can be achieved by increasing the number of observation intervals of the demapper. However, the system complexity increases exponentially as n . For example, in case of single- h CPFSK demapper for $n = 6$ requires 64 correlators and 64 multipliers. There exist, trade off between observation length and system complexity and this must be considered in the system design.

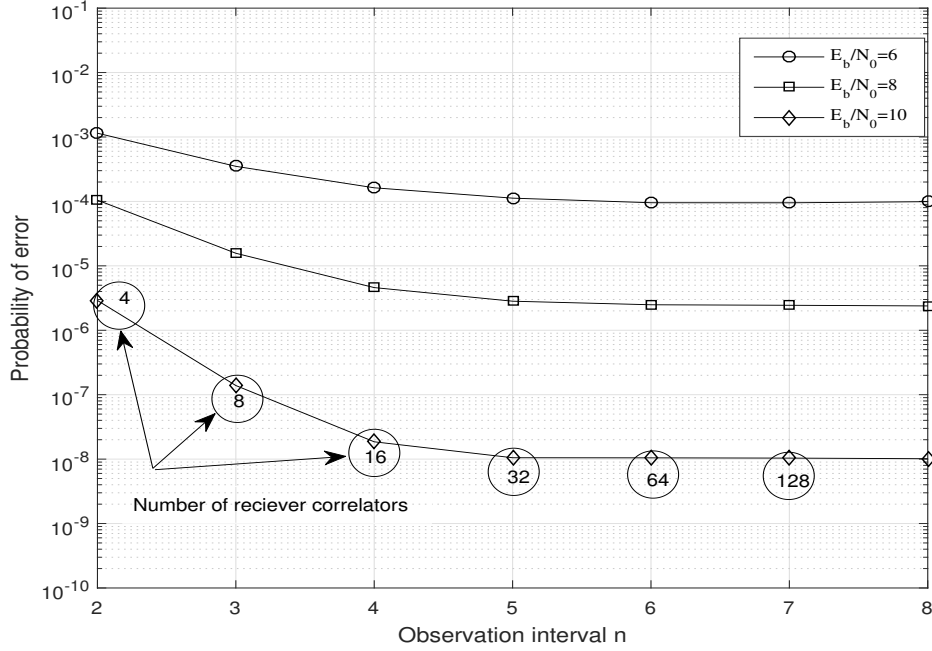


Figure 7.6: Probability of error as a function of observation length of receiver for single- h CPFSK demapper, n , at $E_b/N_o = 6, 8$, and 10 dB.

7.5 Conclusions

In this Chapter, detection of signals in an OFDM system with g-CPFSK mapper over AWGN channel is addressed. The structures of optimum and suboptimum g-CPFSK demapper are presented and expressions for high-SNR upper and lower bounds on BER of the system are given and illustrated. Optimum parameters that minimize BER for single- h and multi- h CPFSK demapper in the system are determined. It is noted that asymmetric multi- h CPFSK demappers can offer superior BER performance compared to single- h and multi- h CPFSK mappers. However, this superiority in performance comes with increased complexity of the system.

Chapter 8

Performance of OFDM System with g-CPFSK Mapper over Fading Channels¹

8.1 Introduction

In Chapter 7, OFDM system with g-CPFSK mapper is analyzed for BER performance over AWGN channel. The aims of this Chapter is to examine the performance of such a system over fading channels. In particular, closed-form expressions for bit error rate of OFDM system with g-CPFSK mapper are derived over: i) Rayleigh and ii) Nakagami- m , fading environments.

8.2 Fading Channel Models

The wireless communication environment is highly susceptible to fading effects due to multi-path propagation. These effects cause major degradation in SNR, which impacts the system error rate performance. Two models for small scale fading are considered in this thesis, specifically, the Rayleigh and the Nakagami- m distributions. The fading is assumed to be flat during the entire observation length ($0 \leq t \leq nT$) of the demapper. The received signal from an OFDM system with g-CPFSK mapper over the fading channel can be expressed as

1. E. Shafter, A. M. Hamed and K. R. Rao, "PAPR and BER performance analysis of OFDM system with multi-h CPFSK mapper," IEEE 30th Canadian Conference on Electrical and Computer Engineering (CCECE), Windsor, pp. 1-4, 30 Apr-3 May, 2017.

$$r(t) = h(t) * S(t, a, A_l) + n(t) \quad 0 \leq t \leq nT, \quad (8.1)$$

where $h(t) = \alpha\delta(t)$ and α is a random variable representing channel gain and $n(t)$ is the AWGN. The instantaneous SNR and average SNR can be expressed as $\gamma = \alpha^2(E_b/N_o)$ and $\bar{\gamma} = \Omega(E_b/N_o)$, respectively, where $\Omega = \overline{\alpha^2}$. The average bit error probability P_{av} over the fading channel can be determined by averaging bit error probability conditioned on α over the probability density function (pdf) of α [70],[71]. That is

$$P_{av} = \int_0^{\infty} P_{e|\alpha} P(\alpha) d\alpha \quad (8.2)$$

The probability densities of α , Rayleigh and Nakagami- m channel models are given by (2.18) and (2.22), respectively. The bit error rate expression for OFDM system with g-CPFSK mapper is given by (7.17).

8.3 Error Rate Expressions for OFDM System with g-CPFSK mapper over Fading Channels

8.3.1 Rayleigh Fading Channel

A closed-form expression for BER of OFDM system with g-CPFSK mapper over Rayleigh fading channel be evaluated using (7.14) and (2.18) in (8.2). Using $Q(x) = \frac{1}{\pi} \int_0^{\frac{\pi}{2}} \exp\left(-\frac{x^2}{2 \sin^2(\theta)}\right) d\theta$ [72] and nothing that when α is Rayleigh α^2 is exponential, the BER, $P_{av,R}$, is obtained as

$$P_{avR} = \frac{1}{NK2^n} \sum_{l=1}^{2^{n-1}} \sum_{v=1}^K \sum_{k=1}^N \left[1 - \sqrt{\frac{\bar{\gamma}\beta(h,n)}{\bar{\gamma}\beta(h,n) + 1}} \right] \quad (8.3)$$

where $\beta(h,n) = \frac{n}{2}[1 - \rho_v(h,n)]$. This expression applies to all subclasses of g-CPFSK mapper. where $\bar{\gamma} = \Omega(E_b/N_o)$ is the average SNR.

8.3.2 Nakagami- m Fading Channel

The average lower bound bit error probability for the case of Nakagami- m fading channel can then be derived by using (7.14) and (2.22) in (8.2). Using [eq. (8.4.15/1),(2.24.1/1)] [73], the BER, $P_{av,N}$, can be shown to be given by:

$$P_{av,N} = \frac{1}{NK2^n\sqrt{\pi}\Gamma(m)} \sum_{l=1}^{2^{n-1}} \sum_{v=1}^K \sum_{k=1}^N G_{2,2}^{2,1} \left(\beta(n,h) \frac{\bar{\gamma}}{m} \left| \begin{matrix} 1, 1-m \\ 0, 1/2 \end{matrix} \right. \right) \quad (8.4)$$

where $G_{q,p}^{a,b}(x)$ is the Meijer G-function [73].

8.4 Numerical Results and Discussion

The BER expressions for OFDM system with g-CPFSK mapper over Rayleigh and Nakagami- m channels are given by (8.3) and (8.4), respectively. These can be used to estimate BER for any g-CPFSK mapper in an OFDM system. The P_{avR} and P_{avN} for single- h , multi- h , and asymmetric multi- h demapper are plotted in Fig.8.1- Fig.8.6 for $m = 1, 3, 6$, and $n = 2, 3, 4, 6$.

Fig.8.2 shows that BER for Nakagami- m ($m = 1$) and Rayleigh channels are the same. It is noted that by using $m = 1$ in density given by (2.22) one gets density in (2.12) which Rayleigh. The bit error rate bound of the OFDM system for Nakagami- m improves as m increases, and it approaches AWGN performance as $m \rightarrow \infty$. The power penalty (PP) versus m are plotted for various values of E_b/N_0 in Fig.8.3, where the PP is the difference between SNR required for the fading channel and that required for AWGN channel [55]. The probability of bit error rate as a function of average SNR for asymmetric multi- h CPFSK mapper ($H_3 = \{6/8 \ 4/8 \ 5/8\}$, A-type) is plotted in Fig.8.4.

The performance of OFDM system with asymmetric multi- h CPFSK mapper ($H_3 = \{6/8 \ 4/8 \ 5/8\}$, A-type) over Rayleigh and Nakagami- m are plotted in Fig.8.5 and Fig.8.6 for $m = 1, 3, 6$, and $n = 4, 6$.

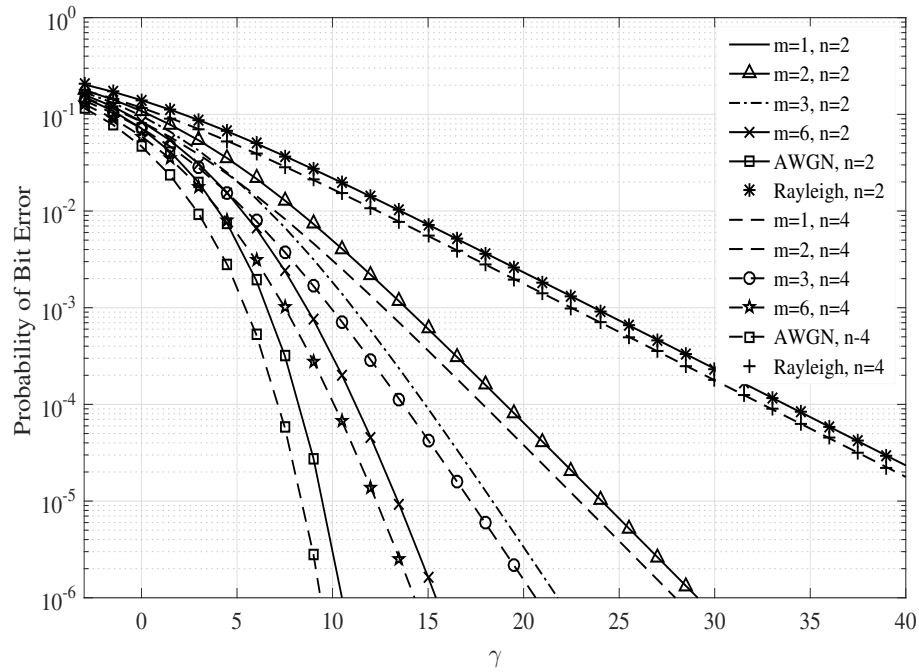


Figure 8.1: BER performance of OFDM system with single- h CPFSK ($h = 0.715$) over Rayleigh and Nakagami- m for $n = 2, 4$

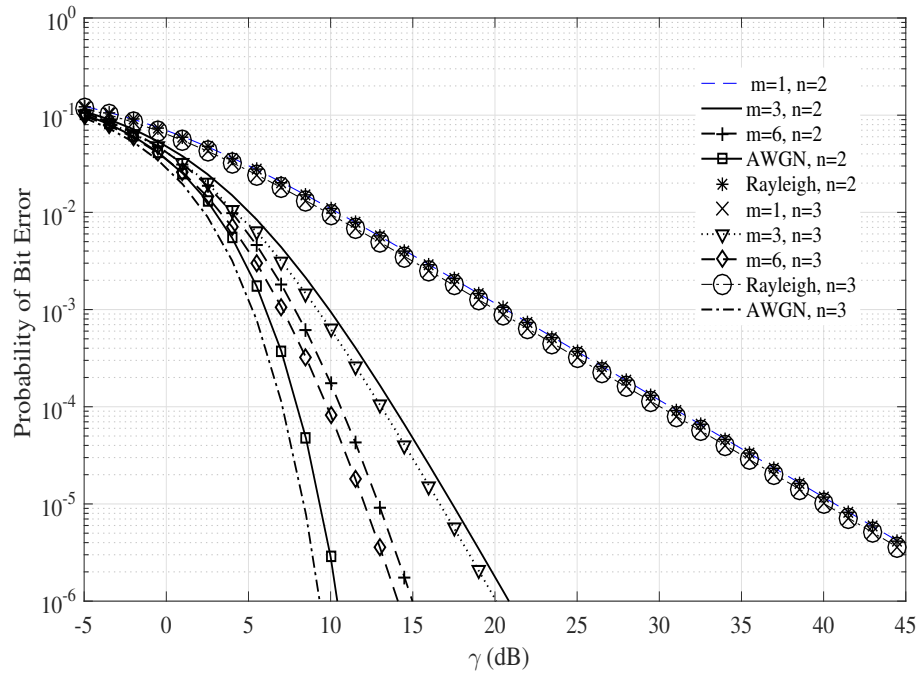


Figure 8.2: BER performance of OFDM system with multi- h CPFSK mapper ($H_2 = \{0.77, 0.62\}$) over Rayleigh and Nakagami- m channel for $n = 2, 3$

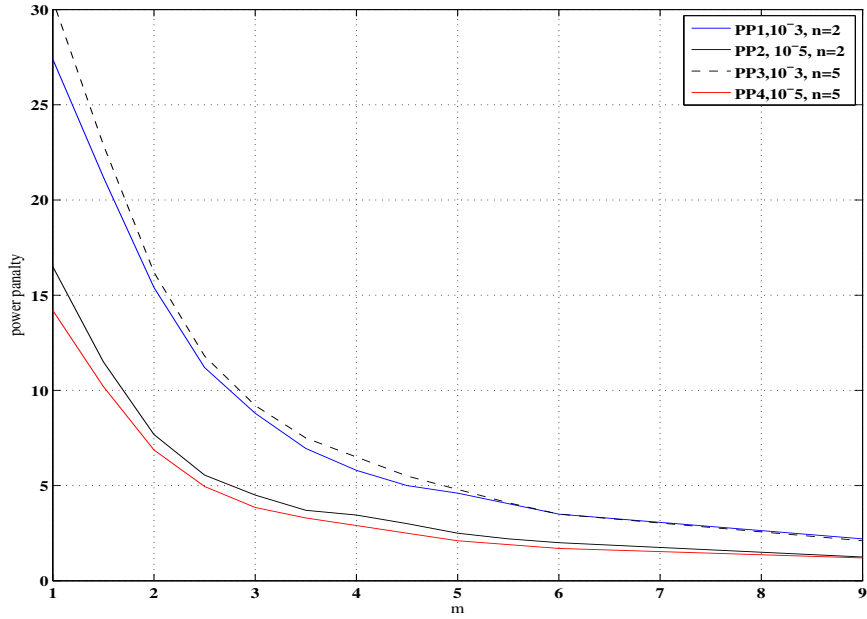


Figure 8.3: BER versus m for OFDM system with multi- h CPFSK $H_2 = \{0.77, 0.62\}$ mapper as a function of SNR

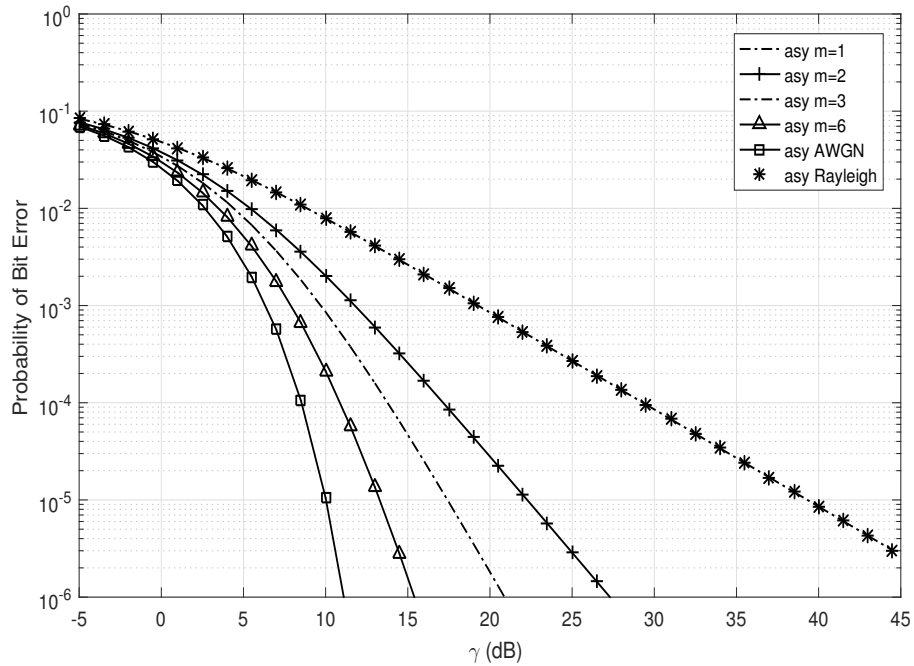


Figure 8.4: BER performance of OFDM system with asymmetric multi- h CPFSK ($H_3 = \{6/8 4/8 5/8\}$, A-type) mapper over Rayleigh and Nakagami- m channels for $n = 2$

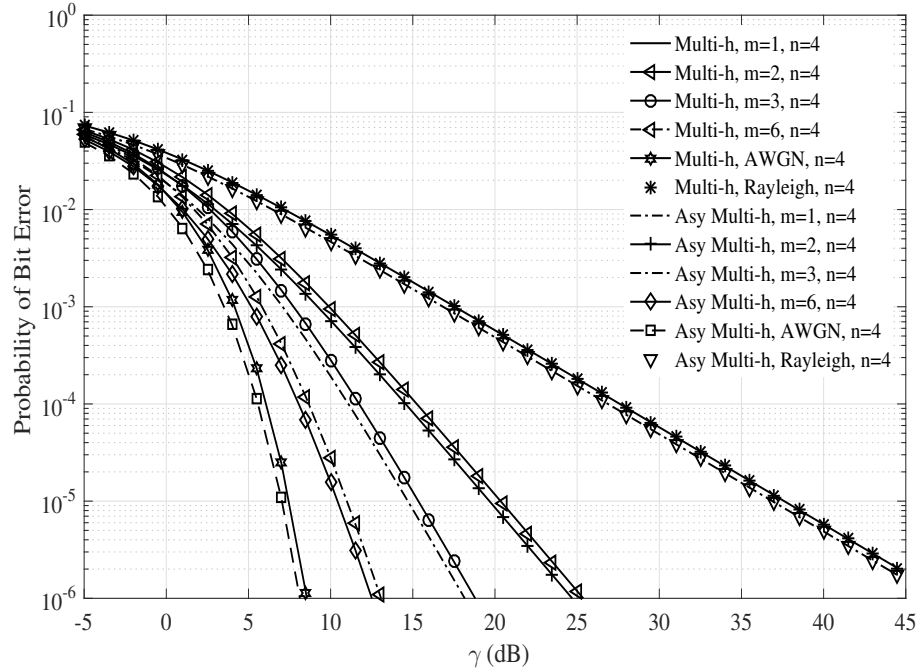


Figure 8.5: BER performance of OFDM system with multi- h $H_2 = \{0.77, 0.62\}$ and asy multi- h ($H_3 = \{6/8, 4/8, 5/8\}$, A-type) CPFSK mappers over Rayleigh and Nakagami- m for $n = 4$

8.5 Conclusions

The Performance of OFDM system with g-CPFSK mapper over fading channels have been introduced and illustrated. The three subclasses of g-CPFSK mapper namely; i) single- h CPFSK; ii) multi- h CPFSK and iii) asymmetric multi- h CPFSK mappers are examined for BER performance over Rayleigh and Nakagami- m fading channels as a function of average SNR, length of observation interval of demapper, and parameters of mapper. Asymmetric multi- h CPFSK mapper achieves better performance than single- h CPFSK and multi- h CPFSK mappers in terms of error probability. The power penalty required over fading channels are determined and illustrated.

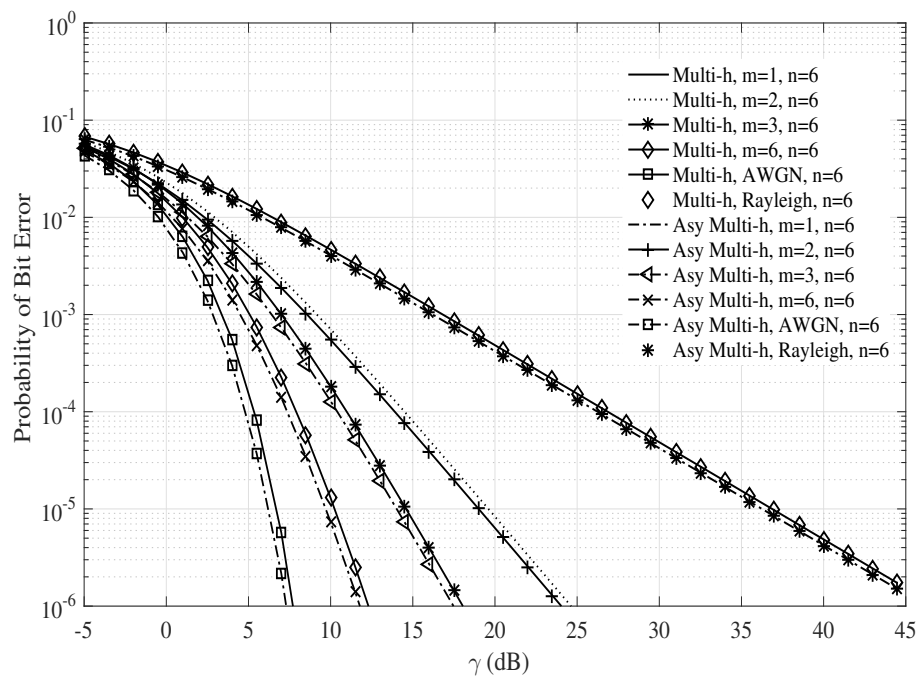


Figure 8.6: BER performance of OFDM system with multi- h CPFSK $H_2 = \{0.77, 0.62\}$ and asymmetric multi- h CPFSK ($H_3 = \{6/8, 4/8, 5/8\}$, A-type) mappers over Rayleigh and Nakagami- m channels for $n = 6$

Chapter 9

Concluding Remarks and Suggesting for Further Research^{1,2,3}

9.1 Introduction

This Chapter provides a summary of contributions of the thesis and offers suggestion for future research in the light of the results obtained.

9.2 Summary of contributions

The concept of correlated symbols is introduced in an OFDM system using mapper with memory referred to as generalized CPFSK (g-CPFSK) mapper. The properties of such a mapper are presented using a state, trellis and tree diagrams. Three subclasses of g-CPFSK mapper namely single- h , multi- h , and asymmetric multi- h mappers are described in terms of a set of parameters and the effects of this on the properties of mappers are identified. Mathematical expressions of signals in an OFDM system with g-CPFSK

-
1. E. Shafter, A. Noorwali and R. K. Rao, "OFDM systems with CPM mappers for smart grid applications," IEEE Electrical Power and Energy Conference (EPEC), London, ON, pp. 424-428, 2015.
 2. E. Shafter, A. Noorwali and R. K. Rao. "Peak-to-Average Power Ratio of OFDM Systems with CPM Mappers using PTS for Smart Grid Applications," Proceedings of the International Conference on Communications Computer Science and Information Technology (ICCCSIT), International conference on, Dubai, pp. 2-6, Mar. 2016.
 3. E. Shafter, and R. K. Rao. "A Comparison between SLM, PTS, and CF Schemes for the Reduction of PAPR of OFDM System with CPM Mappers," IAENG International Journal of Computer Science 43.2, 2016.

mapper are developed and given. The various blocks of such a system are presented and described.

The problem of PAPR in OFDM system with g-CPFSK mapper is addressed and three techniques are presented for reduction of PAPR in such a system. These techniques are SLM, PTS, and CF and are used in conjunction with the OFDM system with g-CPFSK mapper. Each technique has its own complexity, PAPR reduction capability, and the amount of side information required to be communicated to the receiver. The PAPR reduction abilities of these three techniques with single- h , multi- h , and asymmetric multi- h mappers in an OFDM system are extensively studied. Low-complexity methods are suggested for the use of SLM and PTS techniques in an OFDM system with g-CPFSK mapper. In general, it is observed that SLM technique is quite effective with asymmetric multi- h CPFSK mapper. An OFDM system with multi- h CPFSK mapper can be designed with PTS technique for up to 6 dB reduction in PAPR. The CF technique can be used g-CPFSK mapper for PAPR reductions up to 4 dB; however, at the cost of decreased BER performance of the system due to information loss due to clipping.

The maximum Likelihood multiple-symbol detection of signals in an OFDM system with g-CPFSK mapper in AWGN, Rayleigh, and Nakagami- m channels is addressed and structure of optimum g-CPFSK mapper is derived and its BER performance in terms of high SNR upper and lower bounds of maximum likelihood sequence demapper is given and illustrated. It is observed that while improved error rate performance can be achieved by increasing the length of observation of the demapper, the complexity of demapper increases exponentially. Asymmetric multi- h CPFSK mapper in an OFDM system can be attractive from the viewpoint of BER performance of the system, as memory introduced lasts over several symbols compared to single- h and multi- h CPFSK mappers. The performance of OFDM system over Rayleigh and Nakagami- m fading channels is also illustrated. The power penalty required over fading channels to achieve the same error rate as in AWGN channel is assessed and illustrated for Rayleigh and Nakagami- m channels.

9.3 Suggestions for Further Research

One of the major concerns of this research was to reduce PAPR in an OFDM systems with g-CPFSK mapper, it is noted that, further investigations are needed to thoroughly examine g-CPFSK parameters space to assess ultimate capability of PAPR reductions. Smart grid is used to provide end-to-end wireless communication services between consumers and control station in a power grid. Smart grid can be thought of as a network of interconnected wireless networks of Home Area Network (HAN), Neighbourhood Area Network (NAN) and Wide Area Network (WAN) as shown in Fig. (9.1) [74]. In smart grids if OFDM system is used it is possible to achieve higher spectral efficiency with lower energy consumption. Therefore, OFDM system with g-CPFSK mapper can be highly attractive in smart grid applications.

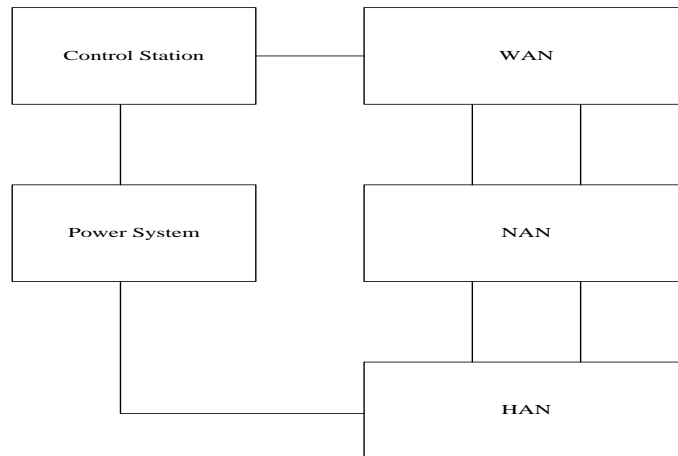


Figure 9.1: Conceptual model of smart grid.

In this thesis it is demonstrated that g-CPFSK mapper can be gainfully employed in an OFDM systems. A study of OFDM system with CPFSK mappers for smart grid applications is given in [75].

The other suggestions for further research are:

1. Constant Envelope OFDM systems are attractive as they eliminate the need for PAPR reduction. It is attractive to examine such systems with g-CPFSK mapper.
2. It is worthwhile considering OFDM system with g-CPFSK mapper with channel coding over fading channels to reduce power penalty.

3. It is important to examine the implementation of OFDM system with g-CPFSK mapper using VLSI.

References

- [1] B. P. Lathi, *Modern Digital and Analog Communication Systems*. 2nd ed. New York: Oxford University Press, 1995.
- [2] J. M. Cioff, *Course notes for Digital Communication: Signal Processing*. <http://www.stanford.edu/group/cioffi/book/>.
- [3] R. K. Martin and C. R. Johnson, "Adaptive equalization: transitioning from single-carrier to multicarrier systems," *IEEE Signal Process. Mag.*, vol. 22, pp. 108–122, Nov. 2005.
- [4] M. Tomlinson, "New automatic equaliser employing modulo arithmetic," *Elect. Lett.*, vol. 7, no. 5, pp. 138-139, Mar. 1971.
- [5] J. A. Davis and J. Jedwab, "Peak-to-mean power control in OFDM, Golay complementary sequences, and Reed-Muller codes," *IEEE Trans. On Inform. Theory*, vol. 45, pp. 2397-2417, Nov. 1999.
- [6] J. Yang, L. Chen, Q. Liu, and D. Chen, "A modified selected mapping technique to reduce the peak-to-average power ratio of OFDM signals," *IEEE Trans. Consumer Electron.*, vol. 53, no. 3, pp. 846-851, Aug. 2007.
- [7] Xin-chun Wu and Jin-xiang Wang and Zhi-gang Mao, "A novel PTS architecture for PAPR reduction of OFDM signals," *Proc. IEEE Int. Conf. Commun. Syst. (ICCS)*, China, pp. 1055–1060, 19-21 Nov. 2008.
- [8] Xiaodong Li and L. J. Cimini, "Effects of clipping and filtering on the performance of OFDM," *IEEE Commun. Lett.*, vol. 2, no. 5, pp. 131-133, May. 1998.
- [9] R. J. Baxley and G. T. Zhou, "Comparing Selected Mapping and Partial Transmit Sequence for PAR Reduction," *IEEE Trans. Broadcast.*, vol. 53, no. 4, pp. 797-803, Dec. 2007.

- [10] S. H. Han and J. H. Lee, "An overview of peak-to-average power ratio reduction techniques for multicarrier transmission," *IEEE Wireless Commun.*, vol. 12, no. 2, pp. 56-65, Apr. 2005.
- [11] Chin-Liang Wang and Yuan Ouyang, "Low-complexity selected mapping schemes for peak-to-average power ratio reduction in OFDM systems," *IEEE Trans. Signal Processing*, vol. 53, no. 12, pp. 4652–4660, Dec. 2005.
- [12] C. Tellambura, "Computation of the continuous-time PAR of an OFDM signal with BPSK subcarriers," *IEEE Commun. Lett.*, vol. 5, no. 5, pp. 185-187, May 2001.
- [13] J. A. C. Bingham, "Multicarrier modulation for data transmission: an idea whose time has come," *IEEE Commun. Mag.*, vol. 28, no. 5, pp. 5-14, May. 1990.
- [14] Y. H. Kim, I. Song, H. G. Kim, T. Chang, and H. M. Kim, "Performance analysis of a coded OFDM system in time-varying multipath Rayleigh fading channels," *IEEE Trans. Veh. Technol.*, vol. 48, no. 5, pp. 1610–1615, Sep. 1999.
- [15] J. Lu, T. T. Tjhung, F. Adachi, and C. L. Huang, "BER performance of OFDM-MDPSK system in frequency-selective Rician fading with diversity reception," *IEEE Trans. Veh Technol*, vol. 49, no. 4, pp. 1216-1225, Jul. 2000.
- [16] J. G. Proakis, *Digital communications*, McGraw-Hill, New York, 1995.
- [17] B. Sklar, *Digital Communications: Fundamentals and Applications*. Upper Saddle River, NJ, USA: Prentice-Hall, Inc., 1988.
- [18] S. C. Thompson, A. U. Ahmed, J. G. Proakis and J. R. Zeidler, "Constant envelope OFDM phase modulation: spectral containment, signal space properties and performance," *Proc. of IEEE MILCOM*, Vol. 2, pp. 1129-1135, Nov. 2004.
- [19] I. A. Tasadduq and R. K. Rao, "PAPR reduction of OFDM signals using multi-amplitude CPM," *Elect. Lett.*, vol.38, no.16, pp.915-917, Aug. 2002.
- [20] S. C. Thompson, "Constant envelope OFDM phase modulation," Ph.D. dissertation, Univ. of California, San Diego, CA, 2005.

- [21] S. C. Thompson, A. U. Ahmed, J. G. Proakis, J. R. Zeidler and M. J. Geile, "Constant Envelope OFDM," *IEEE Trans. Commun*, vol. 56, no. 8, pp. 1300-1312, Aug. 2008.
- [22] T. Aulin and C. Sundberg, "Continuous Phase Modulation-Part I: Full Response Signaling," *IEEE Trans. on Communications* , vol. 29, pp. 196–209, Mar. 1981.
- [23] J. Anderson, T. Aulin, and C. Sundberg, *Digital Phase Modulation*. ser. Applications of Communications Theory. Springer US, 1986.
- [24] G. D. Forney, "Principles of digital communications II," lecture notes, available from MIT Opencourseware (2005).
- [25] R. G. Gallager, *Principles of digital communication*. Cambridge, UK, Cambridge University Press, 2008.
- [26] T. Starr, M. Sorbara, J. M. Cioffi and P. J. Silverman., *DSL advances*. Prentice Hall Professional, 2003.
- [27] J. M. Cioffi, *Course notes for Digital Communication: Signal Processing*. <http://www.stanford.edu/group/cioffi/book/>.
- [28] B. A. Dave and R. K. Rao, "Generalized asymmetric multi-h phase-coded modulation for M-ary data transmission," *Proc. Canadian Conf. Elect. and Comp. Engr.*, vol. 1, pp. 559-562, May 2004.
- [29] A. Ferreol, P. Chevalier and L. Albera, "Second-order blind separation of first- and second-order cyclostationary sources-application to AM, FSK, CPFSK, and deterministic sources," *IEEE Trans. Signal Process.*, vol. 52, no. 4, pp. 845–861, Apr. 2004.
- [30] W. Osborne and M. Luntz, "Coherent and Noncoherent Detection CPFSK," *IEEE Trans on Commun*, vol. 22, no. 8, pp. 1023-1036, Aug. 1974.
- [31] T. Schonhoff, "Symbol Error Probabilities for M-ary CPFSK: Coherent and Noncoherent Detection," *IEEE Trans on Commun*, vol. 24, no. 6, pp. 644-652, Jun. 1976.

- [32] I. A. Tasadduq, *Novel OFDM-CPM Signals for Wireless Communications: Properties, Receivers and Performanc.* Ph.D. Thesis, Faculty of Graduate Studies, University of Western Ontario, 2002.
- [33] E. Hassan, “Performance enhancement of continuous-phase modulation based OFDM systems using chaotic interleaving,” WSEAS Transactions on Systems, pp. 1-10, 2013.
- [34] I. Baig and V. Jeoti, “DCT precoded SLM technique for PAPR reduction in OFDM systems,” Proc. of International Conference on Intelligent and Advanced Systems, Kuala Lumpur, Malaysia, pp. 1-6, Jun. 2010.
- [35] I. A. Tasadduq and R. K. Rao, “OFDM-CPM signals for wireless communications,” Proc. IEEE Int. Conf. Communications (ICC’2002), vol. 3, pp. 1651-1655, Apr. 2002.
- [36] A. D. S. Jayalath and C. Tellambura, “Reducing the peak-to-average power ratio of orthogonal frequency division multiplexing signal through bit or symbol interleaving,” Proc. of Elect Lett, vol. 36, no. 13, pp. 1161-1163, Jun. 2000.
- [37] L. Wang and C. Tellambura, “An Overview of Peak-to-Average Power Ratio Reduction Techniques for OFDM Systems,” Proc. IEEE Int’l Symp. on Signal Processing and Information Tech., pp. 840-845, Aug. 2006.
- [38] J. Tellado, *Multicarrier modulation with low PAR: applications to DSL and wireless.* Vol. 587. Springer Science & Business Media, 2006.
- [39] J. Armstrong, “Peak-to-average power reduction for OFDM by repeated clipping and frequency domain filtering,” IEEE Elect. Lett., vol. 38, no. 8, pp. 246-247, Feb. 2002.
- [40] Y. Rahmatallah and S. Mohan, “Peak-To-Average Power Ratio Reduction in OFDM Systems: A Survey And Taxonomy,” IEEE Commun. Surveys Tuts., vol. 15, no. 4, pp. 1567–1592, Dec. 2013.

- [41] A. E. Jones, T. A. Wilkinson and S. K. Barton, "Block coding scheme for reduction of peak to mean envelope power ratio of multicarrier transmission schemes," *Elect Lett*, vol. 30, no. 25, pp. 2098-2099, Dec. 1994.
- [42] H. Chen and A. M. Haimovich, "Iterative estimation and cancellation of clipping noise for OFDM signals," *IEEE Commun. Lett.*, vol. 7, pp. 305–307, Jul. 2003.
- [43] R. J. Baxley and G. T. Zhou, "MAP metric for blind phase sequence detection in selected mapping," *IEEE Trans. Broadcast.*, vol. 51, no. 4, pp. 565–570, Dec. 2005.
- [44] Y. Hassan and M. El-Tarhuni, "A comparison of SLM and PTS peak-to-average power ratio reduction schemes for OFDM systems," *Proc. of Fourth International Conference on Modeling, Simulation and Applied Optimization*, Kuala Lumpur, pp. 1-4, Apr. 2011.
- [45] D. W. Lim, S. J. Heo and J. S. No, "An overview of peak-to-average power ratio reduction schemes for OFDM signals," *J. Communications and Networks*, vol. 11, no. 3, pp. 229–239, Jun. 2009.
- [46] S. H. Muller and J. B. Huber, "A comparison of peak power reduction schemes for OFDM," *Proc. of GLOBECOM'97*, pp. 1-5, Nov. 1998.
- [47] R. W. Bauml, R. F. H. Fischer and J. B. Huber, "Reducing the peak-to-average power ratio of multicarrier modulation by selected mapping," *Elect. Lett*, vol. 32, no. 22, pp. 2056-2057, Oct. 1996.
- [48] A. D. S. Jayalath and C. Tellambura, "SLM and PTS peak-power reduction of OFDM signals without side information," *IEEE Trans. Wireless Commun.*, vol. 4, pp. 2006–2013, Sep. 2005.
- [49] L. J. Cimini and N. R. Sollenberger, "Peak-to-average power ratio reduction of an OFDM signal using partial transmit sequences," *IEEE Commun Lett*, vol. 4, no. 3, pp. 86-88, Mar. 2000.
- [50] S. Weinstein and P. Ebert, "Data Transmission by Frequency-Division Multiplexing Using the Discrete Fourier Transform," *IEEE Trans. Commun.*, vol. COM-19, pp. 628–634, Oct. 1971.

- [51] M. K. Simon and M. S. Alouini, *Digital Communication Over Fading Channels*. Hoboken, New Jersey: John Wiley & Sons, Inc., 2005.
- [52] L. Cimini, "Analysis and Simulation of a Digital Mobile Channel Using Orthogonal Frequency Division Multiplexing," *IEEE Trans. on Comm.*, Vol. 33, No. 7, Jul. 1985.
- [53] A. Vahlin and N. Holte, "Maximum-likelihood sequence estimation for OFDM," *Proc. of the 7th Int'l Thyrrhenian Workshop on Digital Communcations, Viareggio.*, pp. 207–219, Nov. 1994.
- [54] Y. H. Kim, I. Song, H. G. Kim, T. Chang, and H. M. Kim, "Performance analysis of a coded OFDM system in time-varying multipath Rayleigh fading channels," *IEEE Trans. Veh. Technol*, vol. 48, pp. 1610-1615, Sep. 1999.
- [55] P. M. Shankar, *Fading and Shadowing in Wireless Systems*, NewYork, NY, USA: Springer Science Business Media, 2012.
- [56] Jonhson, N. L. Kotz, S. Balakrishnan, "Chi-Squared Distributions including Chi and Rayleigh". *Continuous Univariate Distributions*. John Willey and Sons. pp. 415–493, 1994.
- [57] Forbes, Catherine, et al, *Chi Squared Distribution*. *Statistical Distributions*, Fourth Edition, (2010).
- [58] Chi-Tsong Chen, *Digital Signal Processing*. Oxford University Press, New York, 2003.
- [59] J. Mitola, " Software radios-survey, critical evaluation and future directions," *National Telesystems Conference*, pp. 13-23, 1992.
- [60] R. O'Neill and L. B. Lopes, "Envelope Variations and Spectral Splatter in Clipped Multicarrier Signals," *Proc. IEEE PIMRC '95, Toronto, Canada*, pp. 71–75, 1995.
- [61] J. Heiskala and J. Terry, *OFDM Wireless LANs: A Theoretical and Practical Guid*. Sams Publishing, 2002.

- [62] H. Saeedi, M. Sharif, and F. Marvasti, "Clipping Noise Cancellation in OFDM Systems Using Oversampled Signal Reconstruction," *IEEE Commun. Lett.*, vol. 6, no. 2, pp. 73–75, Feb. 2002.
- [63] R. W. Bäuml, R. F. H. Fisher, and J. B. Huber, "Reducing the Peak-to-Average Power Ratio of Multicarrier Modulation by Selected Mapping," *Elect. Lett.*, vol. 32, no. 22, pp. 2056–57, Oct. 1996.
- [64] S. H. Muller and J. B. Huber, "OFDM with Reduced Peak-to-Average Power Ratio by Optimum Combination of Partial Transmit Sequences," *Elect. Lett.*, vol. 33, no. 5, pp. 368–69, Feb. 1997.
- [65] S. H. Muller and J. B. Huber, "A Novel Peak Power Reduction Scheme for OFDM," *Proc. IEEE PIMRC 97*, Helsinki, Finland, pp. 1090–94, 1997.
- [66] A. D. S. Jayalath and C. Tellambura, "Adaptive PTS Approach for Reduction of Peak-to-Average Power Ratio of OFDM Signal," *Elect. Lett.*, vol. 36, no. 14, pp. 1226–28, 2000.
- [67] J. B. Anderson and D. P. Taylor, "A bandwidth-efficient class of signals space codes," *IEEE Trans. Inform. Theory*, vol. IT-24, pp. 703-712, 1978.
- [68] C. Wang and Z.-Q. Luo, "Optimized iterative clipping and filtering for PAPR reduction of OFDM signals," *IEEE Trans. Commun.* vol.59, no. 1, pp. 33–37, Jan. 2011.
- [69] A. V. Oppenheim and R. W. Schaffer., *Discrete-Time Signal Processing* . New Jersey, U.S.A. Prentice-Hall International, 1989.
- [70] A. M. Hamed, M. Alsharef and R. K. Rao, "Bit error probability performance bounds of CPFSK over fading channels," *IEEE CCECE*, Halifax, NS, pp. 1329-1334, May 2015.
- [71] E. Shafter, A. M. Hamed and R. K. Rao, "PAPR and BER performance analysis of OFDM system with multi-h CPFSK mapper," *IEEE 30th Canadian Conference on Electrical and Engineering (CCECE)*, Windsor, pp. 1-4, 30 Apr-3 May, 2017.

- [72] I. S. Gradshteyn and I. M. Ryzhik, *Table of Integrals, Series, and Products*. 7th ed. Amsterdam: Elsevier/Academic Press, 2007.
- [73] A. Prudnikov, I. Brychkov, and O. Marichev, “Integrals and Series: Special functions,” ser. Integrals and Series. Gordon and Breach Science Publishers, 1998.
- [74] N. L. S. da Fonseca, “Fourth quarter 2009 IEEE communications surveys and tutorials,” *IEEE Commun Surveys & Tutorials*, vol. 11, no. 4, pp. 1-2, Fourth Quarter 2009.
- [75] E. Shafter, A. Noorwali and R. K. Rao, “OFDM systems with CPM mappers for smart grid applications,” *IEEE Electrical Power and Energy Conference (EPEC)*, London, ON, pp. 424-428, Oct. 2015.

Curriculum Vitae

Name: Emammer Shafter

Date of Birth: Mar 30, 1975

Education:

Ph.D. Candidate Western University, London, Ontario, Canada
2011 - 2017 Department of Electrical and Computer Engineering
Major Communication Systems and Data Networks

M.S. University Utara Malaysia, Kedah, Sintok, Malaysia
2003 - 2005 Information Communication Technology,
Major Information Communication Technology

B.S. College of Engineering Technology, Tripoli-Janzour, Libya
1997- 2000 Department of Electrical Engineering
Major Electrical Engineering

Publications:

- [1] E. Shafter and R. K. Rao, "CF technique with CPM mappers in OFDM systems for reduction of PAPR," IEEE Canadian Conference on Electrical and Computer Engineering (CCECE), Vancouver, BC, pp. 1-5, 15-18 May 2016.
- [2] E. Shafter, and R. K. Rao. "The Reduction of PAPR using CPM Mappers and Partial Transmit Sequence (PTS) Scheme in OFDM Systems" Lecture Notes in Engineering and Computer Science: Proceedings of The World Congress on Engineering and Computer Science, WCECS, San Francisco, USA, pp. 707-710, Vol. 2, Oct. 2015.
- [3] E. Shafter, and R. K. Rao. "PAPR Reduction using CPM Mappers and SLM in OFDM Systems." Proceedings of the World Congress on Engineering and Computer Science (WCECS), Vol. 2, Oct. 2015.
- [4] E. Shafter, and R. K. Rao. "A Comparison between SLM, PTS, and CF Schemes for the Reduction of PAPR of OFDM System with CPM Mappers." International Journal of Computer Science (IAENG) 43.2, pp. 1-9, May 2016.

- [5] E. Shafter, et al. "A Wireless Framework for Lecturers' Attendance System with Automatic Vehicle Identification (AVI) Technology." *Compusoft 3.1*, pp. 457-460, Jan. 2014.
- [6] E. Shafter, A. Noorwali and R. K. Rao, "OFDM systems with CPM mappers for smart grid applications," *IEEE Electrical Power and Energy Conference (EPEC)*, London, ON, pp. 424-428, Jan. 2016 .
- [7] E. Shafter, A. Noorwali and R. K. Rao, "Peak-to-Average Power Ratio of OFDM Systems with CPM Mappers using PTS for Smart Grid Applications," *Proc. of the International Conference on Communications, Computer Science and Information Technology (ICCCSIT)*, pp. 2-6. Mar. 2016.
- [8] E. Shafter, M. Alsharif and R. K. Rao, "Detection of M-ary OFDM systems with CPM mapper over multipath channels," *IEEE 21st International Workshop on Computer Aided Modelling and Design of Communication Links and Networks (CAMAD)*, Toronto, ON, pp. 107-111, Oct. 2016.
- [9] E. Shafter, A. M. Hamed and R. K. Rao, "PAPR and BER performance analysis of OFDM system with multi-h CPFSK mapper," *IEEE 30th Canadian Conference on Electrical and Computer Engineering (CCECE)*, Windsor, pp. 1-4, 30 Apr-3 May, 2017 .